NASA CR-134494
ASRL TR 154-8

APPLICATION OF THE COLLISION-IMPARTED VELOCITY METHOD FOR ANALYZING THE RESPONSES OF CONTAINMENT AND DEFLECTOR STRUCTURES TO ENGINE ROTOR FRAGMENT IMPACT

Thomas P. Collins
Emmett A. Witmer

Aeroelastic and Structures Research Laboratory
Department of Aeronautics and Astronautics
Massachusetts Institute of Technology
Cambridge, Massachusetts 02139

August 1973

Prepared for
AEROSPACE SAFETY RESEARCH AND DATA INSTITUTE
LEWIS RESEARCH CENTER
NATIONAL AERONAUTICS AND SPACE ADMINISTRATION
CLEVELAND, OHIO 44135

NASA Grant NGR 22-009-339

1. Report No	2. Government Accession No.	3. Recipient's Catalog No.
NASA CR -134494		

4 Title and Subtitle	5 Report Date
Application of the Collision-Imparted Velocity Method for Analyzing the Responses of Containment and Deflector Structures to Engine Rotor Fragment Impact	August 1973
	6. Performing Organization Code
7. Author(s) Thomas P. Collins and Emmett A. Witmer	8 Performing Organization Report No ASRL TR 154-8
	10 Work Unit No
9. Performing Organization Name and Address Massachusetts Institute of Technology Aeroelastic and Structures Research Laboratory Cambridge, Massachusetts 02139	11. Contract or Grant No NGR 22-009-339
	13. Type of Report and Period Covered Contractor Report
12 Sponsoring Agency Name and Address National Aeronautics and Space Administration Washington, D.C. 20546	14 Sponsoring Agency Code

15 Supplementary Notes

Technical Monitors: Patrick T. Chiarito and Solomon Weiss, Aerospace Safety Research and Data Institute

Technical Advisor: Richard H. Kemp, Materials and Structures Division
NASA Lewis Research Center, Cleveland, Ohio

16 Abstract

An approximate analysis termed the collision imparted velocity method (CIVM) has been employed for predicting the transient structural responses of containment rings or deflector rings which are subjected to impact from turbojet-engine rotor burst fragments. These 2-d structural rings may be initially circular or arbitrarily curved and may have either uniform or variable thickness; elastic, strain hardening, and strain rate material properties are accommodated. Also these rings may be free or supported in various ways. The fragments have been idealized, for convenience, as being circular and non-deformable with appropriate mass and pre-impact velocity properties for each of the one to n fragments considered. The effects of friction between each fragment and the impacted ring are taken into account.

This approximate analysis utilizes kinetic energy and momentum conservation relations in order to predict the after-impact velocities of the fragment and the impacted ring segment. This information is then used in conjunction with a finite element structural response computation code to predict the transient, large deflection responses of the ring. Similarly, the equations of motion for each fragment are solved in small steps in time.

The effects of varying certain geometric and mechanical property parameters upon the structural ring responses and upon the fragment motions have been explored briefly for both free complete containment rings and for partial-ring fragment deflectors which are supported in each of several ways. Also, some comparisons of predictions with experimental data for fragment-impacted free containment rings are presented.

17. Key Words (Suggested by Author(s))		18. Distribution Statement
Turbojet Rotor Containment	Large Deflections	Unclassified, Unlimited
Aircraft Hazards	Elastic-Plastic Behavior	
Aircraft Safety	Strain Analysis	
Structural Mechanics	Computer Program	
Finite Element Method		
Transient Structural Response		

19. Security Classif (of this report)	20. Security Classif (of this page)	21 No of Pages	22 Price*
Unclassified	Unclassified	~~249~~ 250	14.50

* For sale by the National Technical Information Service, Springfield, Virginia 22151

NASA-C-168 (Rev 6-71)

/

FOREWORD

This report has been prepared by the Aeroelastic and Structures Research Laboratory (ASRL), Department of Aeronautics and Astronautics, Massachusetts Institute of Technology, Cambridge, Massachusetts under NASA Grant No. NGR 22-009-339 from the Lewis Research Center, National Aeronautics and Space Administration, Cleveland, Ohio 44135. Mr. Patrick T. Chiarito and Mr. Solomon Weiss of the Lewis Research Center served as technical monitors and Mr. Richard H. Kemp served as technical advisor. The valuable cooperation and advice received from these individuals is acknowledged gratefully.

We are indebted to Messrs. G.J. Mangano and R. DeLucia of the Naval Air Propulsion Test Center, Phila., Pa. for supplying pertinent rotor fragment data and 4130 cast steel uniaxial static stress-strain data.

The authors especially wish to acknowledge the careful reviewing of this report and the many constructive suggestions from their colleagues Dr. R. W-H. Wu and Dr. John W. Leech. Mr. R.P. Yeghiayan of the MIT-ASRL also provided valuable advice and discussion during the conduct of these studies.

The use of SI units (NASA Policy Directive NPD 2220.4, September 14, 1970) was waived for the present document in accordance with provisions of paragrph 5d of that Directive by the authority of the Director of the Lewis Research Center.

CONTENTS

CONTENTS Continued

CONTENTS Continued

LIST OF ILLUSTRATIONS

CONTENTS Continued

CONTENTS Concluded

SUMMARY

Arguments are presented supporting the proposition that the development and the selective utilization of prediction methods which are restricted to two-dimensional (2-d) transient large-deflection elastic-plastic responses of engine rotor burst fragment containment/deflector structures are useful and advisable for parametric and trends studies. In conjunction with properly-selected experimental studies of rotor-burst fragment interaction with actual containment and/or deflector structure -- wherein three-dimensional effects occur -- one may be able to develop convenient rules-of-thumb to estimate certain actual 3-d containment/deflection structural response results from the use of the very convenient and more efficient but simplified 2-d response prediction methods.

Accordingly, the collision-imparted velocity method (CIVM) for predicting the collision-interaction behavior of a fragment which impacts containment/deflector structures has been combined with a modified version of the JET 3C two-dimensional structural response code to predict the transient large-deflection, elastic-plastic responses and motions of containment/deflector structures subjected to impact by one or more idealized fragments. Included are the effects of friction between each fragment and the attacked structure. A single type of fragment geometry has been selected for efficiency and convenience in these fragment/structure interaction and response calculations, but the most important fragment parameters, it is believed, have been retained; n fragments each with its own m_f, I_f, V_f, ω_f, r_f, and r_{cg} may be employed.

Calculations have been carried out and reported illustrating the application of the present CIVM-JET analysis and program for predicting 2-d containment ring large-deflection elastic-plastic transient responses to (a) single-fragment impact and (b) to impacts by three equal-size fragments. The influence of containment ring thickness, axial length, and strain-rate dependence, as well as friction between the fragment and the impacted structure have been explored.

Similar illustrative calculations have been performed and reported for the responses of (a) ideal hinged-fixed/free and (b) elastic-foundation-supported fragment-deflector rings of uniform thickness to impact by a single idealized fragment. With respect to the latter more-realistic and yet-idealized model, it was found that plausible increases in the values for the stiffnesses of the "elastic foundation" was a more effective means for changing the path of the attacking fragment than by plausible increases in the thickness of the deflector ring itself.

Although calculations were of very limited scope, some interesting response trends were noted. More extensive calculations in which more of the problem variables accommodated in the CIVM-JET-4A analysis and program are included and in which each of certain quantities are varied over plausible ranges would provide a more illuminating picture of the roles and effectiveness of these parameters with respect to fragment-containment and/or fragment-deflection protection.

It is believed that the present analysis method and program (CIVM-JET-4A) provides a convenient, versatile, and efficient means for estimating the effects of numerous problem variables upon the severe nonlinear 2-d responses of variable-thickness containment/deflector structures to engine-rotor-fragment impact. Although a limited number of comparisons of predictions with appropriate experimental data show encouraging agreement, more extensive comparisons are required to establish a firmer assessment and confidence level in the accuracy and the adequacy of the present prediction method, consistent with its inherent 2-d limitations.

SECTION 1

INTRODUCTION

1.1 Outline of the Engine Rotor Fragment Problem

As pointed out in Refs. 1 through 6, for example, there has been a not-insignificant number of failures of rotor blades and/or disks of turbines and compressors of aircraft turbojet engines of both commercial and military aircraft each year, with essentially no improvement in the past 10 years in the number of uncontained failures. The resulting uncontained fragments, if sufficiently energetic, might injure personnel occupying the aircraft or might cause damage to fuel lines and tanks, control systems, and/or other vital components, with the consequent possibility of a serious crash and loss of life. It is necessary, therefore, that feasible means be devised for protecting (a) on-board personnel and (b) vital components from such fragments.

Two commonly recognized concepts for providing this protection are evident. First, the structure surrounding the "failure-prone" rotor region could be designed to contain (that is, prevent the escape of) rotor burst fragments completely. Second, the structure surrounding this rotor could be designed so as to prevent fragment penetration in and to deflect fragments away from certain critical regions or directions, but to permit fragment escape readily in other "harmless" regions or directions. These two concepts are illustrated schematically in Figs. 1 and 2. In certain situations, the first scheme (complete containment) may be required, while in other cases either scheme might be acceptable. For the latter situation, one seeks the required protection for the least weight and/or cost penalty. A definitive comparative weight/cost assessment of these two schemes is not available at this time because of (a) inadequate knowledge of the fragment/structure interaction phenomena and (b) incomplete analysis/design tools, although much progress has been made in these two areas in the past several years; however, this question is explored in a limited preliminary fashion in the present report.

Studies reported in Refs. 1 through 3 of rotor burst incidents in commerical aviation from the Federal Aviation Administration (FAA), the National Transportation Safety Board (NTSB), and other sources, indicate that uncontained-fragment incidences occur at the rate of about 1 for every 10^6 engine flight hours. In 1971, for example, 124 fragment-producing rotor failures were reported in U.S. commercial aviation (Ref. 2); in 35 of these incidents, uncontained rotor fragments were reported. The total number of failures and the number of uncontained failures are classified as to fragment type in three broad categories as follows (Ref. 2):

Fragment Type	Total No. of Failures	No. of Uncontained Failures
Disk Segment	13	13
Rim Segment	6	4
Rotor Blades	105	18

The sizes and the kinetic energies of the attacking fragments, however, are not reported.

From a detailed study of NTSB and industrial records, Clarke (Ref. 3) was able to find 32 case histories with descriptive and photographic information sufficient to permit a reasonable determination of the type and size of the largest fragment and the associated kinetic energy. His assessment is that these data are sufficient to define trends for disk bursts. According to Clarke, the disk breakup modes for the 11,000 to 19,000-lb thrust range of engines studied are classified into four categories: (1) rim segment failures, (2) rim/web failures, (3) hub or sector failures, and (4) shaft-type failures; these and other types of engine rotor fragments are illustrated in Fig. 3. Rim failures contain only rim sections or serrations. Rim/web failures include rim and web sections but do not include hub structure. Hub or sector fragments result when the rotor fails from the rim to the hub, thus nullifying the disk hoop strength and allowing the disk to separate into several large sections. The shaft-type failure mode usually occurs as a result of a bearing failure or a disk unbalance that fails the disk shaft or the attaching tie rods; this mode can release more than one engine stage from the nacelle. Accordingly, the 32 cases of failure are divided into these four categories as follows; with the number of failures and percent of total failures shown in parentheses (number/percent): rim (15/47), rim/web (3/9), sector (10/31), and shaft (4/13). Thus the rim and the sector failures comprise the lion's share of the failure modes for these 32 cases. Although in one case there were 10 major fragments, in about 80 percent of the cases there were 4 or fewer fragments, with an overall mean of 3 major fragments. A major fragment is defined as one which contains a section of the rotor disk whose largest dimension is greater than 20 per cent of the disk diameter and also contains more kinetic energy than a single blade from the same stage. In that report, blade failures are not included as major fragments. Failed blades (excluding fan blades) tend to be contained in accordance with Federal Aviation Regulations (FAR) Part 33. In only about 15 to 20 per cent of rotor blade failures does casing penetration occur. These "escaped single-blade fragments" possess reduced kinetic energy; thus, their potential for further damage is limited.

In the Ref. 3 study, the size of the largest major rotor fragment as a cumulative percentage of the 32 cases analyzed is reported. Also, it is deduced that the largest translational kinetic energy of a major fragment will not exceed 40 per cent of the total rotational kinetic energy of the unfailed rotor. For a large majority of rotor burst fragments, the kinetic energy possessed by each fragment will be substantially less than this 40 per cent value.

The studies of Refs. 1 through 3 and 6 through 11 indicate that for disk fractures, a 120° sector is a good candidate as a "maximum-size fragment and danger" criterion. If one examines the translational and rotational energy content of rotor disk fragments as a function of sector-angle size, it is found that a sector of about 120° contains the maximum translational kinetic energy. However, in view of the fragment-size and type statistics available, the choice of a smaller and less energetic "criterion fragment" for fragment containment/deflector design appears to be much more sensible for obtaining a reasonable and feasible improvement in the "safety index" of aircraft turbojet engine/airframe installations with respect to rotor-burst damage effects. Also, fragments of this class apparently occur much more frquently than do those of the 120-degree sector type. In this vein, Clarke suggests that enhanced safety would be achieved by requiring the complete containment of a fragment consisting of a rim segment (serration) with 3 blades attached; the authors of the present report concur in this judgment.

Despite intensive conscientious effort through the use of improved materials, design, fabrication, and inspection, the annual number of aircraft engine rotor bursts remains at a too-high level -- with little or no improvement in the past decade. With the large increase of wide-body and jumbo jets, the potential for a large-life-loss accident from this cause grows monthly. In order to assist the FAA (and industry) to achieve improved safety in this respect, NASA has been sponsoring a research effort with the following long-range objectives:

(1) to improve the understanding of the phenomena attending engine rotor fragment attack upon and the transient structural response of engine casing fragment-containment and/or fragment-deflection structure via an integrated program of appropriate experiments and theoretical analysis,

(2) to develop and verify theoretical methods for predicting the interaction behavior and the transient structural responses of containment/deflection structure to engine-rotor fragment attack, and

(3) to develop (a) an engine rotor fragment test capability to accommodate reasonably foreseeable needs, (b) experimental containment/deflection data in limited pertinent parametric studies, (c) experimental techniques and high quality experimental data for evaluating and guiding the development of theoretical-analysis methods, and (d) a "proof test" capability for conducting test fragment and structure combinations which are too complex to be analyzed reliably by available methods.

Hopefully, useful theoretical analysis tools of limited complexity could be devised, verified, demonstrated, and transmitted to both the FAA and industry to assist via parametric design calculations and appropriate experiments the development of improved protection without imposing excessive weight penalties.

Starting about 1964, the Naval Air Propulsion Test Center (NAPTC) under NASA sponsorship has constructed and employed a spin-chamber test facility wherein rotors of various sizes can be operated at high rpm, failed, and the interactions of the resulting fragments with various types of containment and/or deflection structures can be studied with high-speed photography and transient strain measurements, in addition to post-mortem studies of the containment/ deflection structure and the fragments. Many such tests involving single fragments or many complex fragments impinging upon containment structures of various types and materials have been conducted (Refs. 6 through 11) and have substantially increased the body of knowledge of the attendant phenomena. Since mid-1968 NASA has sponsored a research effort at the MIT Aeroelastic and Structures Research Laboratory (ASRL) to develop methods for predicting theoretically the interaction behavior between fragments and containment-deflection structures, as well as the transient deformations and responses of containment/deflection structures -- the principal objective being to devise reliable prediction/ design procedures and containment/deflection techniques. Important cross-fertilization has occurred between the NAPTC experimental and the MIT-ASRL theoretical studies, with special supportive-diagnostic experiments and detailed measurements being designed jointly by NASA, NAPTC, and MIT personnel and conducted at the NAPTC. Subsequent analysis and theoretical-experimental correlation work has been increasing both the understanding of the phenomena involved and the ability to predict these interaction/structural-response phenomena quantitatively.

1.2 Review of Some Analysis Options

Because of the multiple complexities involved in the very general case wherein the failure of one blade leads to impact against the engine casing, rebound, interaction with other blades and subsequent cascading rotor-failures and multiple-impact interactions of the various fragments with the casing, and with each other, it is necessary to focus attention initially upon a much simpler situation in order to develop an adequate understanding of these collision-interaction processes. Accordingly, rather than considering the general <u>three-dimensional</u> large deformations of actual engine casings under multiple rotor-fragment attack (see Fig. 4, for example), the simpler problem of planar structural response of containment structures has been scrutinized. That is, the containment structure is regarded simply as a structural ring lying in a plane; the ring may undergo large deformations but these deformations are confined essentially to that plane. For such a case, numerical finite-difference

(Refs. 12 and 13) and finite element (Ref. 14) methods of analysis to predict the transient large-deformation responses of such structures to known impulsive and/or transient external loading and/or to a known distribution, magnitude, and time history of velocities imparted to the structure have been developed at the MIT-ASRL and have been verified by evaluative comparison with high-quality experimental data to provide reliable predictions.

In the present context, therefore, the crucial information which needs to be determined (if the structural response of a containment ring is to be predicted reliably) concerns the magnitude, distribution, and time history of either the loading or the impact-induced velocities which the ring experiences because of fragment impact and interaction with the ring. Two means for supplying this information have been considered:

(1) The TEJ concept (Refs. 15 and 16) which utilizes measured experimental ring position-time data during the ring-fragment interaction process in order to deduce the external forces experienced by the ring. This concept has been pursued. An important merit of this approach is that it can be applied with equal facility to ring problems involving simple single fragments such as one blade, or to cases involving a complex multi-bladed-disk fragment. The central idea here is that if the TEJ-type analysis were applied to typical cases of, for example, (a) single-blade impact, (b) disk-segment impact, and/or (c) multi-bladed disk fragment impact, one could determine the distribution and time history of the forces applied to the containment ring for each case. Such forces could then be applied tentatively in computer code response-prediction-and-screening studies for similar types of ring-fragment interaction problems involving various other materials, where guidance in the proper application of these forces or their modification could be furnished by dimensional-analysis considerations and selected spot-check experiments. It remains, however, to be demonstrated whether adequate rules can be devised to "extrapolate" this

forcing function information to represent similar types of fragment attack (with perhaps different fragment material properties) against containment vessels composed of material different from that used in the aforementioned experiments.*

On the other hand, this approach suffers from the fact that experimental transient structural response data of high quality must be available; the forcing function is not determined from basic material property, geometry, and initial impact information.

(2) The second approach, however, utilizes basic material property, geometry, and initial impact information in an approximate analysis. If the problem involves only a single fragment, this method can be carried out and implemented without undue difficulty, but can become complicated if complex fragments and/or multiple fragments must be taken into account. However, measured transient structural response data are not required in order to employ this method successfully.

Approach 1 is explained in detail in Refs. 14 and 15. The present report deals with one version of approach 2; other versions of approach 2 (denoted by CIVM and/or CFM) are discussed in Refs. 14 and 17.

Various levels of sophistication may be employed in approach 2. One could, for example, utilize a finite-difference shell-structure analysis such as PETROS 3 (Ref. 18) or REPSIL (Refs. 19 and 20), or similar finite-element codes, to predict the large general transient deformations of engine casing containment/deflection structure to engine rotor fragment impact. For even more general behavior, one could employ 3-d solid-continuum finite-difference

---

*It is to circumvent this tenuous extrapolation problem and to eliminate the necessity for making detailed transient response measurements now required in the TEJ concept that effort has been devoted to developing alternate methods of analysis (see the next approach in item 2).

codes such as HEMP (Ref. 21), STRIDE (Ref. 22), or HELP (Ref. 23) wherein both the containment ring and fragment may be represented by a suitably fine three-dimensional mesh, and the conservation equations can be solved in time in small time increments; these latter codes can handle only a limited number of simple configurations. Both the 3-d shell codes and the 3-d solid codes take into account elastic, plastic, strain hardening, and strain-rate behavior of the material. Such computations (especially the 3-d solid type) while vital for certain types of problems are very lengthy and expensive, and are not well suited for the type of engineering analysis/design purposes needed in the present problem; for complicated or multiple fragments, such calculations would be prohibitively complicated, lengthy, and expensive. A simpler, less complicated, engineering-analysis attack with this general framework is needed; namely, the 2-d structural response analysis method (see Fig. 5).

Two categories of such an engineering analysis in the approach 2 classification may be identified and are termed: (a) the collision-imparted velocity method (CIVM) and (b) the collision-force method (CFM). The essence of each method follows:

(a) Collision-Imparted Velocity Method (CIVM)

In this approach (Ref. 14), the local deformations of the fragment or of the ring at the collision interface do not enter explicitly, but the containment ring can deform in an elastic-plastic fashion by membrane and bending action as a result of having imparted to it a collision-induced velocity at the contact region via (a) a perfectly-elastic, (b) perfectly-inelastic, or (c) intermediate behavior. Since the collision analysis provides only collision-imparted velocity information for the ring and the fragment (not the collision-induced interaction forces themselves), this procedure is called the collision-imparted velocity method.

(b) Collision-Force Method (CFM)

In this method (Ref. 17) the motion of the fragment and the motion of the containment/deflection ring (2-d idealized structure) is predicted and followed in small increments Δt in time. If fragment/ring collision occurs during such a Δt increment, a collision-interaction calculation is performed. This calculation provides an estimate of the force experienced by the ring at the contact region during an appropriate portion of this Δt time period; an equal and opposite force is experienced by the (rigid or deformable) fragment. The calculation advances similarly during the next Δt increment.

In practice the TEJ, CIVM, and CFM procedures are employed in intimate conjunction with one or more of the 2-d structural response ring codes*:JET 1 (Ref. 15), JET 2 (Ref. 16), or JET 3 (Ref. 24). These ring codes have various different capabilities but each permits one to predict reliably the 2-d, large-deflection, elastic-plastic, transient deformations of structural rings for either (1) transient external forces of prescribed distribution, magnitude, and time history or (2) locally-imparted velocities of prescribed distribution, magnitude, and time history. Accordingly, these respective fragment/ring response analyses are termed TEJ-JET, CIVM-JET, and CFM-JET. These procedures are indicated in the information flow diagram on page 10.

Finally, it is useful to note that these three approaches to analyzing the transient structural responses of two-dimensional containment/deflection structure subjected to engine rotor fragment attack play useful complementary roles rather than duplicatory roles. In cryptic self-explanatory form, these complementary roles are summarized on page 11.

---

*A concise summary of the capabilities of the computer codes JET 1, JET 2, and JET 3 is given in Appendix B.

EFFECTS ON CONTAINMENT RINGS
FROM ROTOR-DISK FRAGMENT IMPACT

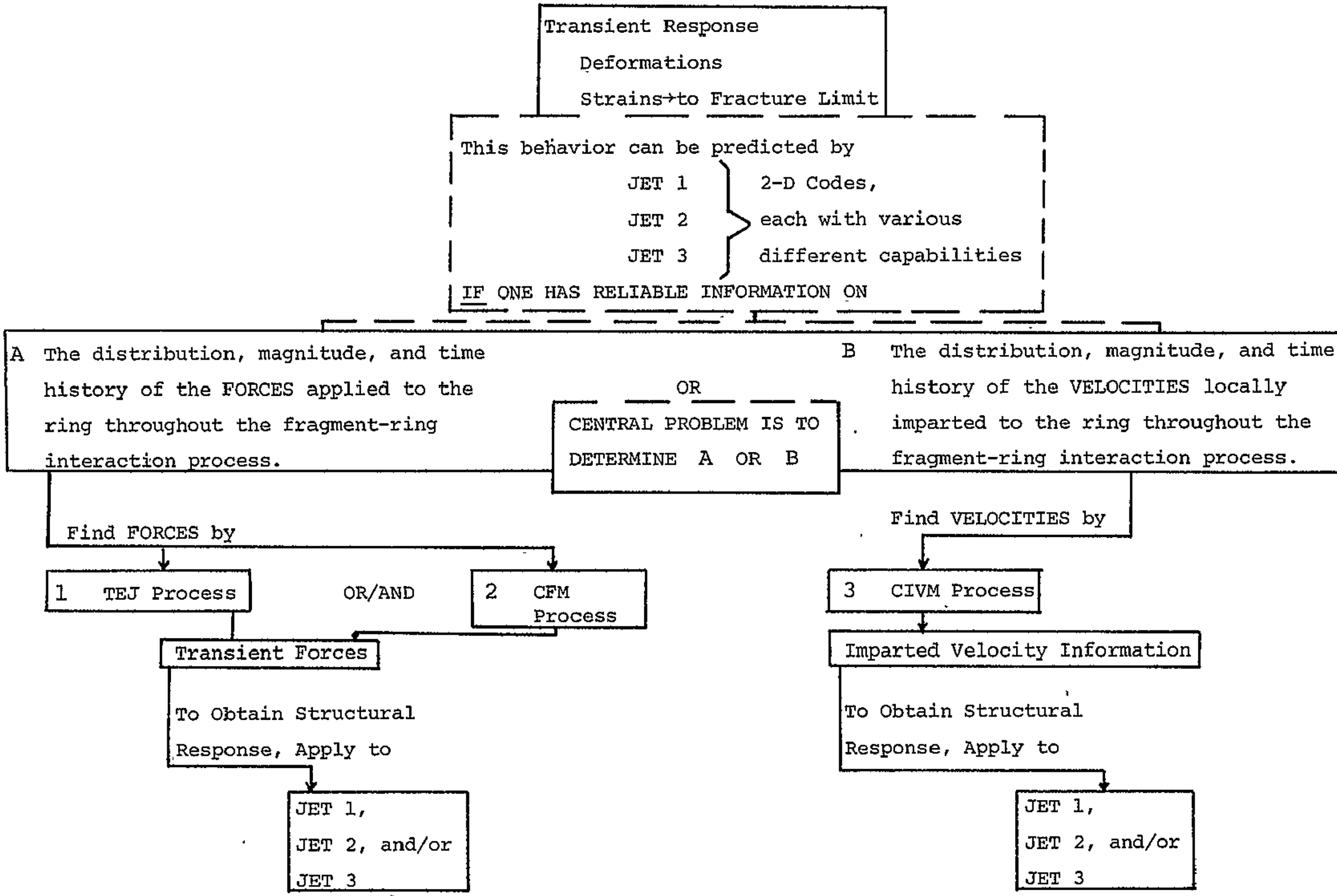

COMPLEMENTARY ROLES OF

TEJ-JET , CIVM-JET , CFM-JET

- TEJ-JET
  - Applicable to Simple Single as well as Complex Multiple Fragments
  - Must have <u>Measured</u> Structural Response Data
  - Predicted Transient Externally-Applied Loads are Useful for Preliminary Design
    - Use as Unchanged in Screening Calculations for Various Containment Vessel Materials

      or

    - Conduct Spot Check Tests and TEJ-JET Analysis for One or Two Other Materials to Guide Forcing Function Modification

- CIVM-JET AND/OR CFM-JET
  - Does <u>Not</u> Require Measured Transient Response Data
  - Uses Basic Geometry, Material Property, and Initial Condition Data
  - Readily Applied to Single Fragments
  - Multiple or Complex Fragments
    - More Difficult to Apply
    - Needs Further Development; Complex Logic
  - Complex but has Much Potential for Future

1.3 Current Status of the Fragment/Ring Collision-Interaction and Response Analyses

Having chosen for engineering convenience and simplicity to restrict initial theoretical prediction method developments to two-dimensional* structural response behavior of containment and/or deflector structures, the development of the analyses TEJ-JET, CIVM-JET, and CFM-JET have been pursued to the extent permitted by the available time and funds. In this context the plan of action included the following elements (see Fig. 5):

1. Use TEJ-JET, CIVM-JET, etc. for materials screening studies, parametric calculations, and thickness estimates for 2-d containers and/or deflector structure.
2. Conduct experiments to determine the structural thickness required for fragment containment or fragment deflection, as desired:
   (a) conduct such experiments on axially short (2d) containment/deflection structure to evaluate and verify the 2-d predictions for the required structural thickness h_{2d}, and
   (b) conduct such experiments on containment/deflection structure of various axial lengths in order to determine the smallest wall thickness h_{opt} required (and the associated shortest axial length) for fragment containment or deflection for realistic three-dimensional deformation behavior.
3. Next, carry out 2-d calculations and correlations with experiments in order to seek convenient rules of thumb for relating h_{2d} to the desired h_{opt}.

Therefore, the first task to be carried out was the development of TEJ-JET, CIVM-JET, and/or the CFM-JET analyses for idealized 2-d structural models

---

*While the present (initial) analysis has been restricted to idealized containment/deflection structures undergoing two-dimensional behavior for convenience and simplicity, more comprehensive structural modeling and analysis could be employed later if found to be necessary.

for containment and/or deflector structure. Schematics of "actual" and idealized 2-d models of, respectively, containment structure and deflector structure are shown in Figs. 6 and 7.

1.3.1 TEJ-JET Status

References 15 and 16 document the early studies of the TEJ-JET concept and its feasibility. The theoretical feasibility of the TEJ-JET concept has been verified. This has been carried out by predicting the large-deflection elastic-plastic transient response of an initially-circular, uniform-thickness, containment ring subjected to a prescribed circumferential distribution and time history of externally-applied forces via the JET 1 computer program; this provided position-time data for many mass points (typically 72) around the circumference of the ring. In order to simulate the effects of experimental and data conversion uncertainties upon this position-time information, these data were perturbed by random numbers with a mean of zero but with various plausible levels of probable error. The resulting "simulated experimental position-time data" were then subjected to TEJ processing in order to "extract" predictions of the externally-applied forces which produced these "modified structural response data"; the resulting predicted external forces were in very good agreement with the original known prescribed external forces.

Analysis of an early set of high-speed photographic measurements carried out by the NAPTC of the transient response of a containment ring subjected to impact from a single rotor blade from a T58 turbine rotor revealed certain data deficiencies. Subsequently, the effects upon the TEJ-JET prediction process of various uncertainty factors have been studied, and means for reducing the prediction uncertainty, including both analysis improvements and improvements in measurement precision and accuracy, are in progress. Improved NAPTC experimental data are expected to be received shortly for use in a more definitive evaluation of the TEJ-JET analysis method.

It should be noted that the success of this method depends crucially upon the availability of very high quality experimental data to define the time history of the motion of the containment/deflection structure and of the fragments and/or other moving structure which strikes the containment-deflection structure. The feasibility and accuracy of the TEJ-JET method for estimating the impact forces applied to the containment ring in an actual experimental situation have been verified only in part and then only for the simplest case: a single blade impacting a free circular containment ring. These forces have been deduced (it is believed successfully) from the analysis of the CG motion of the ring, but another independent estimate involved in the TEJ-JET scheme is obtained from analyzing the motion of <u>individual</u> mass points of the ring. The latter estimate has not yet been carried out successfully -- this work utilizing recent experimental data of improved quality is still in progress.

If this TEJ-JET method (especially the second scheme) turns out to be successful for this simplest of all cases, serious consideration could then be given to the further development of this method in order to predict the fragment/ring collision forces for more complex problems such as (a) an n-fragment burst of a rotor, (b) a single blade failure from a fully-bladed rotor, (c) a rim chunk with a few blades attached, etc. If successful for these cases of more practical interest (such as case (c), for example), the attendant predicted external forces could then be employed as first-approximation forcing function information in 2-d JET codes to predict the transient structural responses of various candidate containment/deflection rings and materials. For a given type of fragment attack for which one presumes the availability of the above-noted forcing-function information, one will need to develop some means of estimating how these forces would be altered if radically different containment/deflection structural materials, thicknesses, etc. from those used in the "source experiment are used in parametric/design studies.

1.3.2 CFM-JET Status

A study of the collision force method (CFM) is reported in Ref. 17. This method was applied successfully to predict the transient structural response of a simply-supported steel beam subject to impact by a steel ball; comparisons of CFM-JET predictions for this case were in good agreement with independent predictions.

The CFM-JET method was also applied to analyze the impact interaction and transient response of an aluminum containment ring to impact from a single blade from a T58 engine turbine rotor; experimental transient response photographic data were available from NAPTC experiments for comparison. In these CFM-JET studies, the rotor blade was modeled in three different ways: (1) the blade was prescribed to remain straight and to experience purely-elastic behavior, (2) the blade was permitted to shorten and to experience elastic-plastic behavior but to remain straight, and (3) the blade was permitted to undergo a plausible curling deformation behavior over a region near the impacted end and to behave in an elastic-plastic fashion. In all cases, the free initially-circular aluminum containment ring was permitted to experience large-deflection, elastic-plastic bending and stretching behavior. For all three blade-behavior cases, the predicted containment ring transient responses were very similar, with type (3) providing the best theoretical-experiment agreement. Also, the type (3) prediction demonstrated the best agreement between the predicted and the observed fragment motion. For the type (3) model, impact between the blade and the ring was treated as either frictionless or as involving various fixed values of the friction coefficient μ.

For plausible combinations of the curling-blade-model parameters and the frictional coefficient, the CFM-JET predictions for both the transient response of the ring, and the motion and the final deformed configuration of the blade were in very good agreement with experimental observations.

As is made clear in Refs. 14 and 17, the CIVM-JET method is more readily extendable than is the CFM-JET method to more complex types of fragments and fragment-attack situations. Hence, future development effort has favored the CIVM-JET method.

1.3.3 CIVM-JET Status

Initial studies of the CIVM-JET method of analysis are reported in Ref. 14. In analyzing containment and deflection ring responses to impact from a single blade, the blade is modeled in the analysis as being nondeformable (remains straight rather than deforming as observed experimentally). However, the effect of neglecting this type of blade deformation, and its attendant changing moment of inertia, has a very minor influence on the transient response of the containment/deflection structure. Another simplification used in that initial CIVM-JET study was to ignore the effects of friction between the ring and the impacting blade. As a result of these two simplifications, one finds a fair discrepancy between predictions and observations of the motion of the blade after initial impact with the ring. However, one observes very good agreement between predictions and measurements of the transient large deformations of the containment ring.

Also reported in Ref. 14 are some illustrative CIVM-JET calculations to predict the responses of 90-degree sector partial rings (fragment deflectors) to impact by a single blade. One end of the partial ring was either ideally clamped or pinned-fixed while the other end was free. Frictionless impact and a non-deformable blade were assumed also in these cases. There were, however, no appropriate experimental data available for comparison.

1.4 Purposes and Scope of the Present Study

Experience gained in these initial CIVM-JET studies and in the subsequent CFM-JET investigations suggested that the former approach would be more readily extendable than the latter to analyze containment/deflection structural responses to impact from more complex types of fragments. Accordingly, it was decided to extend the CIVM-JET analysis and to carry out some illustrative calculations.

Specifically, the tasks undertaken and discussed in this report follow:

1. To include the effects of friction between the fragment and the impacted structure.
2. To combine the resulting CIVM collision-interaction analysis with the JET 3 structural response computer program in order to make available a convenient CIVM-JET computer code for interested users, together with a user's manual and example problems.
3. To include an approximate means of accounting for the "restraint effects" of adjacent structure upon the responses of fragment-impacted 2-d containment and/or deflector structures.
4. To illustrate the utilization of this updated CIVM-JET

analysis and program for predicting

(a) containment ring responses to single-fragment and multiple-fragment attack and

(b) deflector ring responses to single-fragment attack.

Section 2 is devoted to describing the CIVM-JET method including the updating features cited in tasks 1 through 3. Illustrative containment ring response studies are discussed in Section 3, while illustrative fragment deflector response calculations are described in Section 4. A summary of the present studies, pertinent conclusions, and suggestions for further research are presented in Section 5.

Appendix A contains a description and a listing of the resulting CIVM-JET-4A computer program together with input and output instructions. Included are example problems, the associated proper input, and solution data which may aid the user in adapting this program to his computer facility.

Appendix B contains a concise summary of the capabilities of the two-dimensional, elastic-plastic, large-deflection, transient structural response computer codes JET 1, JET 2, and JET 3.

SECTION 2

COLLISION-IMPARTED VELOCITY METHOD

2.1 Outline of the Method

For present purposes, attention is restricted to analyzing the transient responses of two-dimensional containment and/or deflector rings which are subjected to fragment impact; examples of these types of structural models are indicated schematically in Figs. 6 and 7. Accordingly, these structures may undergo large elastic-plastic bending and stretching deformations but those deformations as well as the fragment motions are assumed to lie in one plane; namely, the Y,Z plane as shown in Fig. 8.

Using this ring-fragment problem as an illustrative example, this section is devoted to a description of the general procedure used to calculate the transient motions of the ring and the fragment in accordance with the process called the collision-imparted velocity method (CIVM). An information flow schematic of this procedure is shown in Fig. 9. Briefly, the analysis procedure indicated in Fig. 9 consists of the following principal steps:

1. Motions and Positions of Bodies
The motions of the fragment and of the containment ring are predicted and the (tentative) region of space occupied by each body at a given instant in time is determined.

2. Collision Inspection
Next, an inspection is performed to determine whether a collision has occurred during the small increment (Δt) in time from the last instant at which the body locations were known to the present instant in time at which body-location data are sought. If a collision has not occurred during this Δt, one follows the motion of each body for another Δt, etc. However, if a collision has occurred, one proceeds to carry out a collision-interaction calculation.

3. Collision-Interaction Calculation
In this calculation energy and momentum conservation relations are

employed in an approximate analysis to compute the collision-induced changes (a) in the velocities V_f (translation) and ω_f (rotational) of the fragment and (b) nodal velocities of the ring segment which has been struck by the fragment. The coordinates which locate the positions of the fragment and of this particular ring segment are thereby corrected from their tentative uncorrected-for-impact locations.

One then returns to step 1, and the process is repeated for as many time increments as desired.

The details of this analysis procedure as well as various considerations and simplifying assumptions employed are discussed in the remainder of this section.

2.2 Fragment-Idealization Considerations

Consistent with the decision to idealize containment and deflector structure as behaving in a two-dimensional fashion, a similar decision has been reached to idealize the various types of rotor-burst fragments in a way which is both versatile and convenient for analysis. Further, it was desired to include from 1 to n fragments, where these fragments may have either identical or different masses, velocities, kinetic energies, etc. Some of the considerations which led to the selected fragment idealization are discussed in the following.

In the initial theoretical studies reported in Refs. 14 and 17, only a single rotor blade fragment was utilized. Various types of blade fragment behavior were assumed and the consequences investigated. The assumed types of behavior included:

(a) straight non-deforming blade
(b) elastically-deforming straight blade
(c) elastic-plastic straight blade
(d) elastic-plastic curling blade

In all cases before initial impact, these blades had identical masses, mass moment of inertia about the CG, translation velocities, and rotational velocities. Although the motion of the blade fragment after initial impact differed from model to model, the large-deflection elastic-plastic transient responses of the fragment-impacted containment rings exhibited only small differences for the various blade-fragment models. Thus, the effect of the changing geometry of the deforming blade fragment during impact-interaction with the ring is of distinctly secondary importance with respect to containment ring response. Accordingly, the most important fragment quantities requiring duplication in the idealized fragment model are its mass and translational kinetic energy; of lesser importance are its rotational kinetic energy, mass moment of inertia, and "geometric size".

Therefore, one may idealize the fragment geometry in order to reduce the complexity of determining at successive instants of time during predictions whether or not the fragment has collided with the ring. However, it is possible to analyze and follow in detail the deforming configuration of a rotor-blade fragment (or even of a bladed disk fragment) during impact-interaction with a containment ring if one is willing to pay the price in complexity and in computational expense. At the present stage of study, this degree of complexity is considered to be unjustified. Hence, the "severe" but convenient and reasonable idealization that a single rotor blade, a bladed-rim segment, or bladed rim-web segments, for example, may be represented as a non-deformable circular configuration of appropriate diameter, mass, and mass moment of inertia has been adopted. This decision also greatly simplifies the matter of determining at a given instant in time whether or not a given fragment has collided with the ring because the space occupied by the fragment is readily defined by the Y,Z coordinates of its center, and its radius. The space occupied is compared with the space instantaneously occupied by the ring in order to determine whether or not a fragment/ring collision has occurred.

Shown schematically in Fig. 10 are pre-impact and final-deformed configurations of a single rotor blade, a one-sixth bladed disk segment, and a one-third bladed disk segment from a T58 turbine rotor. These fragments were employed in containment ring experiments conducted at the NAPTC; information on intermediate states of typical fragment deformation are also available (Refs. 10 and 25). Also depicted in Fig. 10 are certain fragment idealizations, including the currently adopted non-deformable circular configuration used in the present 2-d analysis. It is seen that a circle of appropriate diameter may be chosen to circumscribe each type of undeformed and deformed fragment. Since for a given type of fragment these diameters do not vary greatly (up to about 30 per cent or less typically), one may choose the diameter of the idealized non-deformable fragment to be either "extreme" or some intermediate value because these fragment-size extremes produce very little effect upon the predicted transient deformation of the ring and the maximum circumferential strains experienced by an impacted containment ring.

2.3 Collision-Interaction Analysis, Including Friction

The collision-interaction analysis employed is described in the following in the context of two-dimensional behavior of both the containment/deflection structure* and the fragment. Further, the analysis will be described for a case in which only a single idealized fragment is present; similar relations are employed for the individual impacts of each of n fragments when n fragments are present.

For the CIVM approach, the following simplifying assumptions are invoked:

1. Only the fragment and the ring segment or element struck by that fragment are affected by the "instantaneous collision" (see Fig. 8).
2. In an overall sense, the fragment is treated as being rigid but at the "immediate contact region" between the fragment and the struck object (termed "target" for convenience), the collision process is regarded as acting in a perfectly elastic ($e = 1$), perfectly inelastic ($e = 0$), or an intermediate fashion ($0<e<1$), where e represents the coefficient of restitution.

---

*A similar procedure could be employed if one were to model the containment/deflection structure in a more comprehensive and realistic way by using shell finite elements or the spatial finite difference method.

(3) The colliding surfaces of both the fragment and the target may be either perfectly smooth ($\mu=0$) or may be "rough" ($\mu\neq0$), where μ denotes the coefficient of sliding friction. Hence, respectively, force and/or momentum (or velocities) are transmitted only in the normal-to-surface direction or in both the normal and the tangential direction.

(4) During the collision, the contact forces are the only ones considered to act on the impacted ring segment and in an anti-parallel fashion on the fragment. Any forces which the ring segment on either side of the impacted ring segment may exert* on that segment as a result of this instantáneous collision are considered to be negligible because this impact duration is so short as to preclude their "effective development".

(5) To avoid unduly complicating the analysis and because of the smallness of the arc length of the ring element being impacted, the ring element is treated as a straight beam (see Fig. 11) in the derivation of the impact inspections and equations. However, for modeling of the ring itself for transient response predictions, the ring is treated as being arbitrarily curved and of variable thickness.

As indicated in Fig. 11a the curved variable-thickness (or uniform thickness) containment/deflector ring is represented by straight-line segments:

(1) to identify in a simple and approximate way the space occupancy of the beam segment under imminent impact attack and
(2) to derive the impact equations.

The ends of ring segment or element i are bounded by nodal stations i and i+1 at which the ring thickness is h_i and h_{i+1}, respectively; these nodes are located in Y,Z inertial space by Y_i, Z_i, and Y_{i+1}, Z_{i+1}, respectively.

---

*Such forces are termed "internal forces" as distinguished from the "external impact-point forces".

In the CIVM-JET studies reported in Ref. 14, the inertial effects of the impacted segment were taken into account by means of two different models: a consistent-mass model and a lumped-mass model. It was found that the lumped mass collision model provides more convenient and reliable collision-interaction predictions. Accordingly, only the lumped-mass collision model is employed in the present studies. With respect to the inertia forces of the structural ring itself, the studies of Ref. 14 have shown that lumped-mass modeling is somewhat more efficient than consistent-mass modeling of the ring insofar as transient response prediction accuracy is concerned. Hence, lumped mass modeling of the ring is employed in the present work.

For the lumped-mass collision model, the impacted beam segment is represented, as depicted in the exploded line schematic of Fig. 12, by concentrated masses m_1 and m_2 at nodes 1 (or i) and 2(or i+1), respectively. Also, for the impacted segment indicated in Fig. 11b, it is assumed that the two surfaces of this variable-thickness element are close enough to being parallel that the cosine of one half of the angle between them is essentially unity. Accordingly, it is assumed that the direction normal to the impacted surface is the same as the perpendicular to a straight line joining nodes 1 and 2. For the collision analysis, it is convenient to resolve and discuss velocities, impulses, etc., in directions normal (N) and tangential (T) to the straight line joining nodes 1 and 2; the positive normal direction is always taken from the inside toward the outside of the ring, while the positive-tangential direction is along the straight line from node 1 toward node 2 (see Figs. 11b and 11c) -- a clockwise numbering sequence is used (for all impacted ring segments). Hence, the impacted ring segment lumped-mass velocities and the idealized-fragment velocities are expressed with respect to this local, N,T inertial coordinate system as V_{1N}, V_{1T}, V_{2N}, V_{2T}, V_{fN}, and V_{fT} in the exploded schematic shown in Fig. 12.

As shown in Fig. 12, the center of gravity of the idealized impacted beam (ring) segment is located at a distance $\gamma_L s$ from mass m_1, and a distance $\delta_L s$ from mass m_2, where s is the distance from m_1 to m_2. The "point of fragment impact" between masses m_1 and m_2 is given by the distances αs and βs, respectively; at this location, it is assumed that the fragment applies a normally-directed impulse p_N and a tangentially directed impulse p_T to the impacted idealized ring segment. Denoting by primes the "after-impact" translational and/or rotational velocities, the impulse-momentum law may be written to characterize the "instantaneous impact behavior" of this system, as follows:

Normal-Direction Translation Impulse-Momentum Law

$$m_1\left[V_{1N}' - V_{1N}\right] + m_2\left[V_{2N}' - V_{2N}\right] = p_N \qquad \text{(ring segment)} \qquad (2.1)$$

$$m_f\left[V_{fN}' - V_{fN}\right] = -p_N \qquad \text{(fragment)} \qquad (2.2)$$

Tangential-Direction Translational Impulse-Momentum Law

$$m_1\left[V_{1T}' - V_{1T}\right] = \beta p_T \qquad (2.3)$$

(ring segment)

$$m_2\left[V_{2T}' - V_{2T}\right] = \alpha p_T \qquad (2.4)$$

$$m_f\left[V_{fT}' - V_{fT}\right] = -p_T \qquad \text{(fragment)} \qquad (2.5)$$

Rotational Impulse-Momentum Law

$$-m_1\left[V_{1N}' - V_{1N}\right]\gamma_L s + m_2\left[V_{2N}' - V_{2N}\right]\delta_L s = -p_N(\gamma_L - \alpha)s + p_T\left(\frac{h_I}{2}\right) \qquad \text{(ring segment)} \qquad (2.6)$$

$$I_f\left[\omega_f' - \omega_f\right] = p_T r_f \qquad \text{(fragment)} \qquad (2.7)$$

where

p_N = normal-direction impulse

p_T = tangential-direction impulse

$\gamma_L = m_2/(m_1 + m_2)$

$\delta_L = m_1/(m_1 + m_2)$

h_I = ring thickness at the immediate "impact point"

m_f = mass of the fragment

I_f = mass moment of inertia of the fragment about its CG

The relative velocity of sliding S' and the relative velocity of approach A' at the immediate "contact points" between the fragment (at A) and the ring segment (at C) are defined by

$$S' = \left[V_{fT}' - \omega_f' r_f\right] - \left[\left(\beta V_{1T}' + \alpha V_{2T}'\right) + \left(\frac{h_I}{2}\right)\left(\frac{V_{2N}' - V_{1N}'}{s}\right)\right] \tag{2.8}$$

$$A' = V_{fN}' - \left(\beta V_{1N}' + \alpha V_{2N}'\right) \tag{2.9}$$

Substituting Eqs. 2.1 through 2.7 into Eqs. 2.8 and 2.9, one obtains

$$S' = S_o - B_3 p_N - B_1 p_T \tag{2.10}$$

$$A' = A_o - B_2 p_N - B_3 p_T \tag{2.11}$$

where the initial (pre-impact) relative velocity of sliding S_o, the initial relative velocity of approach A_o, and the geometrical constants B_1, B_2, and B_3 are given by

$$S_o = \left[V_{fT} - \omega_f r_f\right] - \left[\left(\beta V_{1T} + \alpha V_{2T}\right) + \left(\frac{h_I}{2}\right)\left(\frac{V_{2N} - V_{1N}}{s}\right)\right] \tag{2.12}$$

$$A_o = V_{fN} - \left(\beta V_{1N} + \alpha V_{2N}\right) \tag{2.13}$$

$$B_1 = \frac{1}{m_f} + \frac{r_f^2}{I_f} + \frac{\beta^2}{m_1} + \frac{\alpha^2}{m_2} + \left(\frac{h_I}{2s}\right)^2\left(\frac{1}{m_1} + \frac{1}{m_2}\right) \tag{2.14}$$

$$B_2 = \frac{1}{m_f} + \frac{\beta^2}{m_1} + \frac{\alpha^2}{m_2} \tag{2.15}$$

$$B_3 = \left(\frac{h_I}{2s}\right)\left(\frac{\alpha}{m_2} - \frac{\beta}{m_1}\right) \tag{2.16}$$

where in Eqs. 2.12 and 2.13, by definition $A_o \geq 0$; otherwise, the two bodies will not collide with each other. Also, if $S_o \geq 0$, the fragment slides initially along the ring segment. It perhaps should be noted that sliding of the bodies on each other is assumed to occur at the value of "limiting friction" which requires that $p_T = |\mu p_N|$, and when $p_T < |\mu p_N|$, only rolling (i.e., no sliding) exists. For a given value of e and a given value of μ which, respectively, describes the degree of "plasticity" of the collision process, and accounts for the frictional properties (roughness) of the contact surfaces, nine equations (Eqs. 2.1 - 2.7 and Eqs. 2.10 - 2.11) can be solved to obtain the post-impact quantities V'_{1N}, V'_{1T}, V'_{2N}, V'_{2T}, V'_{fN}, V'_{fT}, and ω'_f, as well as p_N and p_T; these are nine "unknowns".

The graphic technique which provides a convenient way to obtain the values of p_N and p_T at the instant of the termination of impact as described in Ref. 26 is employed in the present collision-interaction analysis. In this technique, the trajectory of an "image" point $\overline{P}$ in the plane formed by the impulse coordinates p_N and p_T (Fig. 13) represents the state of the colliding bodies at each instant of the contact interval. The image print $\overline{P}$ which is initially located at the origin and is denoted by P_o ($p_N = 0$, $p_T = 0$) will always proceed in the upper half-plane with increasing p_N. The locations of the line of no sliding $S' = 0$ and the line of maximum approach $A' = 0$ are determined by the system constants B_1, B_2, and B_3. From Eqs. 2.10 through 2.16, it is noted that B_1 and B_2 are positive; also since $B_1B_2 > B_3^2$, the acute angle between the p_N axis and the line $A' = 0$ is greater than the corresponding acute angle formed by the line $S' = 0$ with the p_N axis; hence, the line $A' = 0$ and the line $S' = 0$ cannot intersect with each other in the third quadrant of the p_N,p_T plane. Depending on the values of the coefficient of sliding friction μ, the coefficient of restitution e, the system constants B_1, B_2, and B_3, and the initial conditions S_o, and A_o, several variations of the impact process may occur and will be discussed in the following.

First, the cases in which the coefficient of sliding friction μ range from $0<\mu<\infty$ will be considered; the two special cases with $\mu = 0$ (perfectly-smooth contact surfaces) and $\mu = \infty$ (completely rough surfaces) will be discussed shortly thereafter.

<u>Case I</u>: If $0 < \mu < \infty$ and $B_3 \leq 0$, both the slope of line $S' = 0$ and the slope of line $A' = 0$ are non-negative (when $B_3 = 0$, lines $S' = 0$ and $A' = 0$ are parallel to the p_N axis and the p_T axis, respectively). The two lines $S' = 0$ and $A' = 0$ intersect with each other at point P_3 as shown in Figs. 13a and 13b, where the friction angle ν and the angle Λ formed with the p_N axis by the line connecting points P_o and P_3 and are defined by

$$\nu = \mathrm{TAN}^{-1}\mu \tag{2.17}$$

and

$$\Lambda = \mathrm{TAN}^{-1}\left(\frac{B_2 S_o - B_3 A_o}{B_1 A_o - B_3 S_o}\right) \tag{2.18}$$

Initially, the image point $\overline{P}$ travels from point P_o along the path P_oL which subtends an angle ν with the P_N axis because the limiting friction impulse $p_T = \mu p_N$ is developed during the initial stage of impact. Subsequently:

(a) if $\mu = \tan\nu < \tan\Lambda$ (Fig. 13a), line P_oL will intersect the line of maximum approach $A' = 0$ at point P_1, before reaching the line of no sliding $S' = 0$. The intersection point P_1 represents the state at the instant of the termination of the approach period. This is followed by the restitution period; the impact process ceases at point P' (path $P_o - P_1 - P'$). The coordinates of P' are

$$p_N = (1+e)\,p_{N1} \tag{2.19}$$

$$p_T = \mu p_N = \mu(1+e)\,p_{N1} \tag{2.20}$$

where p_{N1}, the ordinate of point P_1 is determined from the simultaneous solution of equations $p_T = \mu p_N$ and $A' = 0$, and is given by

$$p_{N1} = \frac{A_o}{B_2 + \mu B_3} \tag{2.21}$$

(b) However, if $\mu = \tan\nu > \tan\Lambda$ (Fig. 13b), line P_oL will intersect the line of no sliding $S' = 0$ first at the intersection point P_2 which marks the end of the initial sliding phase. The image point $\overline{P}$ then will continue to proceed along the line of no sliding $S' = 0$ through the intersection point P_3 with line $A' = 0$ to the end of impact at point P' (path $P_o - P_2 - P_3 - P'$). The final values of p_N and p_T are:

$$p_N = (1+e)\,p_{N3} \tag{2.22}$$

$$p_T = \frac{S_o - B_3 p_N}{B_1} = \frac{S_o - B_3 (1+e)\,p_{N3}}{B_1} \tag{2.23}$$

where p_{N3}, the ordinate of point P_3 which represents the end of the approach period, is given by

$$p_{N3} = \frac{B_1 A_o - B_3 S_o}{B_1 B_2 - B_3^2} \tag{2.24}$$

<u>Case II:</u> If $0 < \mu < \infty$ and $B_3 > 0$, both the lines $S' = 0$ and $A' = 0$ have negative slopes as shown in Figs. 13c, 13d, and 13e. By following the same argument as in Case I, one has:

(a) If $\mu = \tan\nu < \tan\Lambda$ (Fig. 13c), line P_oL will intersect the line $A' = 0$ first, before reaching the line $S' = 0$, and the impact process ends at point P' (path $P_o - P_1 - P'$), whose coordinates are

$$p_N = (1+e)\,p_{N1} \tag{2.25}$$

$$p_T = \mu\,(1+e)\,p_{N1} \tag{2.26}$$

where

$$p_{N1} = \frac{A_o}{(B_2 + \mu B_3)} \tag{2.27}$$

(b) If $\mu = \tan\nu > \tan\Lambda$ (Figs. 13d and 13e), the image point $\overline{P}$ moves first along line P_oL to the intersection with line $S' = 0$ at point P_2; up to that point, the two bodies will slide along each other. However, beyond point P_2, only as much friction will act as is necessary to prevent sliding, provided that this is less than the value of the limiting friction (Ref. 26). Let the angle Ω formed by the line $S' = 0$ with the p_N axis be defined as

$$\Omega = \tan^{-1}\left(\frac{B_3}{B_1}\right) \tag{2.28}$$

(bi) If $\Omega < \nu$ (Fig.13d), the maximum friction is not required to prevent sliding; hence, $\bar{P}$ will continue to move along line $S' = 0$, through the end of approach period at point P_3, which is the intersection point with line $A' = 0$, to the termination of impact at point P' (path $P_o - P_2 - P_3 - P'$) whose coordinates are

$$p_N = (1+e)\, p_{N3} \tag{2.29}$$

$$p_T = \frac{S_o - B_3(1+e)\, p_{N3}}{B_1} \tag{2.30}$$

where

$$p_{N3} = \frac{B_1 A_o - B_3 S_o}{B_1 B_2 - B_3^2} \tag{2.31}$$

(bii) On the other hand, if $\Omega > \nu$(Fig. 13e), more friction than available is required to prevent sliding. Thus, the friction impulse will change its direction beyond P_2, and maintain its limiting value; the point $\bar{P}$ moves along line P_2M which is the line of reversed limiting friction and is defined as

$$p_T = \mu\,(2p_{N2} - p_N) \tag{2.32}$$

where

$$p_{N2} = \frac{S_o}{\mu B_1 + B_3} \tag{2.33}$$

Through the intersection with line $A' = 0$ at point P_4 to its final state P' at the end of impact (path $P_o - P_2 - P_4 - P'$). The coordinates of P' are

$$p_N = (1+e)\, p_{N4} \tag{2.34}$$

$$p_T = \mu \left[2 p_{N2} - (1+e)\, p_{N4}\right] \tag{2.35}$$

where p_{N2} is defined in Eq. 2.33 and

$$p_{N4} = \frac{A_o - 2\mu B_3\, p_{N2}}{B_2 - \mu\, B_3} \tag{2.36}$$

The above solution process can be specialized to represent the cases with $\mu = 0$ and $\mu = \infty$.

Case III: If $\mu = 0$ (perfectly smooth contact surfaces), line P_oL coalesces with the p_N axis. The image point $\bar{P}$ will move along the p_N axis to the end of impact. Thus

$$p_N = (1+e)\, \frac{A_o}{B_2} \tag{2.37}$$

$$p_T = 0 \tag{2.38}$$

Case IV: If $\mu = \infty$ (completely rough contact surface), point $\bar{P}$ moves initially along the p_T axis.

(a) If $\frac{S_o}{B_1} < \frac{A_o}{B_3}$ or if $\frac{A_o}{B_3} < 0$, point $\bar{P}$ will move along the p_T axis to the intersection with $S' = 0$, then will follow the line $S' = 0$ to the end of impact. The post-impact value of p_N and p_T are

$$p_N = (1+e)\, p_{N3} \tag{2.39}$$

$$p_T = \frac{S_o - B_3 (1+e)\, p_{N3}}{B_1} \tag{2.40}$$

where

$$p_{N3} = \frac{B_1 A_o - B_3 S_o}{B_1 B_2 - B_3^2} \tag{2.41}$$

(b) However, if $\frac{S_o}{B_1} > \frac{A_o}{B_3} > 0$, point $\overline{P}$ moves along the p_T axis and ceases at the intersection with line $S' = 0$. Thus the final value of p_N and p_T are

$$p_N = 0 \tag{2.42}$$

$$p_T = \frac{S_o}{B_1} \tag{2.43}$$

Knowing the values of p_N and p_T at the end of impact for the above discussed various impact processes, the corresponding post-impact velocities then can be determined from Eqs. 2.1 through 2.7 as follows:

$$V_{1N}' = V_{1N} + \frac{\beta s\, p_N - \left(\frac{h_I}{2}\right) p_T}{m_1 s} \tag{2.44}$$

$$V_{1T}' = V_{1T} + \frac{\beta\, p_T}{m_1} \tag{2.45}$$

$$V_{2N}' = V_{2N} + \frac{\alpha s\, p_N + \left(\frac{h_I}{2}\right) p_T}{m_2 s} \tag{2.46}$$

$$V_{2T}' = V_{2T} + \frac{\alpha\, p_T}{m_2} \tag{2.47}$$

$$V_{fN}' = V_{fN} - \frac{p_N}{m_f} \tag{2.48}$$

$$V_{fT}' = V_{fT} - \frac{p_T}{m_f} \tag{2.49}$$

$$\omega_f' = \omega_f + \frac{p_T r_f}{I_f} \tag{2.50}$$

Thus, this approximate analysis provides the post-impact velocity information for the impacted ring segment and for the fragment so that the timewise step-by-step solution of this ring/fragment response problem may proceed. Note that these post-impact velocity components are given in directions N and T at each end of the idealized impacted ring segment; as explained later, these velocity components are then transformed to (different) directions appropriate for the curved-ring dynamic response analysis.

2.4 Prediction of Containment/Deflector Ring-Motion and Position

The motion of a complete containment ring or of a partial-ring fragment deflector may be predicted conveniently by means of the finite-element method of analysis described in Ref. 14 and embedded in the JET 3 series of computer programs described in Ref. 24. These structures may be of either uniform or of variable thickness, with various types of support conditions. Large deflection transient Kirchhoff-type* responses including elastic, plastic, strain hardening, and strain-rate sensitive material behavior may be accommodated.

In this method, the ring is represented by an assemblage of discrete (or finite) elements joined compatibly at the nodal stations (see Fig. 8). The behavior of each finite element is characterized by a knowledge of the four generalized displacements q at each of its nodal stations, referred to the η,ζ local coordinates (see Fig. 14). The displacement behavior within each finite element is represented by a cubic polynomial for the normal displacement w and a cubic polynomial for the circumferential displacement v, anchored to the four generalized displacements q_1, q_2, q_3, and q_4 or v, w, ψ, and χ at each node of the element (see Refs. 14 and 24 for further details).

For present purposes, it suffices to note that the resulting equations of motion for the "complete assembled discretized structure (CADS)", for which the independent generalized nodal displacements are denoted by q*, are (Ref. 14):

*Transverse shear deformation is excluded.

$$[M]\{\ddot{q}^*\} + \{P\} + [H]\{q^*\} + [K_s]\{q^*\} = \{F^*\} \quad (2.51)$$

where

$\{q^*\}$, $\{\ddot{q}^*\}$ represent the generalized displacements and generalized accelerations, respectively

$[M]$ is the mass matrix for the CADS

$\{P\}$ is an "internal force matrix" which replaces the "conventional stiffness terms" $[K]\{q^*\}$ for small displacements but now also includes some plastic behavior contributions

$[H]$ represents a "new" stiffness matrix which arises because of large deflections and also plastic behavior

$[K_s]$ represents the global effective stiffness supplied by an elastic foundation and/or other "restraining springs"

$\{F^*\}$ denotes the externally-applied generalized forces acting on the CADS

Further, it is assumed that all appropriate boundary conditions have already been taken into account in Eq. 2.51.

The timewise solution of Eq. 2.51 may be accomplished by employing an appropriate timewise finite-difference scheme such as the central difference method. Accordingly, for the cases of CIVM fragment impact or of prescribed externally-applied forces, Eq. 2.51 at time instant j may be written in the following form:

$$[M]\{\ddot{q}^*\}_j = \left(\{F^*\} - [K_s]\{q^*\} - \{P\} - [H]\{q^*\}\right)_j \quad (2.52)$$

Let it be assumed that all quantities are known at any given time instant t_j. Then one may determine the generalized displacement solution at time t_{j+1} (i.e., $\{q^*\}_{j+1}$) by the following procedure. First, one employs the timewise central-difference expression for the acceleration $\{\ddot{q}^*\}_j$:

$$\{\ddot{q}^*\} \cong \frac{1}{(\Delta t)^2}\left(\{q^*\}_{j+1} - 2\{q^*\}_j + \{q^*\}_{j-1}\right) \tag{2.53}$$

It follows that one can solve for $\{q^*\}_{j+1}$ since $\{\ddot{q}^*\}_j$ is already known from Eq. 2.52 and all other quantities in Eq. 2.53 are known. However, a fragment-ring collision may occur between time instants t_j and t_{j+1}; this would require a "correction" to the $\{q^*\}_{j+1}$ found from Eq. 2.53. Thus, one uses and rewrites Eq. 2.53 to form a <u>trial</u> value (overscript T):

$$\{\Delta \overset{T}{q}{}^*\}_{j+1} = \{\Delta q^*\}_j + (\Delta t)^2 \{\ddot{q}^*\}_j \tag{2.54}$$

where

$$\{\Delta q^*\}_j = \{q^*\}_j - \{q^*\}_{j-1}$$

$$\{\Delta \overset{T}{q}{}^*\}_{j+1} = \{\overset{T}{q}{}^*\}_{j+1} - \{q^*\}_j \qquad = \text{trial increment} \tag{2.55}$$

$$\{q^*\}_j = \{q^*\}_0 + \{\Delta q^*\}_1 + \ldots\ldots + \{\Delta q^*\}_j$$

$$\Delta t \qquad = \text{time increment step}$$

Note that $t_j = j(\Delta t)$ where $j = 0, 1, 2, \ldots$, and $\{\Delta q^*\}_0 \equiv 0$. Also, no such trial value is needed if only <u>prescribed</u> external forces were applied to the containment/deflection ring.

Let it be assumed that one prescribes at $t = t_0 = 0$ ($j=0$) values for the initial velocities $\{\dot{q}^*\}_0$ and external forces $\{F^*\}_0$, and that the initial stresses and strains are zero. The increment of displacement between time t_0 and time t_1 is then given by:

$$\{\Delta q^*\}_1 = \{\dot{q}^*\}_0 (\Delta t) + \{\ddot{q}^*\}_0 \frac{(\Delta t)^2}{2} \tag{2.56}$$

where $\{\ddot{q}^*\}_0$ can be calculated from

$$[M]\{\ddot{q}^*\}_0 = \{F^*\}_0 \tag{2.57}$$

wherein it is assumed that no ring-fragment collision occurs between t_0 and t_1 (accordingly, overscript T is not used on $\{\Delta q^*\}_1$ in Eq. 2.56).

2.5 Prediction of Fragment Motion and Position

In the present analysis, the fragment is assumed to be undeformable and, for analysis convenience to be circular; hence, its equations of motion for the case of no externally-applied forces are:

$$m_f \ddot{Y}_f = 0 \tag{2.58}$$

$$m_f \ddot{Z}_f = 0 \tag{2.59}$$

$$I_f \ddot{\theta} = 0 \tag{2.60}$$

where (Y_f, Z_f) and $(\ddot{Y}_f, \ddot{Z}_f)$ denote, respectively, the global coordinates and acceleration components of the center of gravity of the fragment (see Figs. 8 and 12)

θ represents the angular displacement of the fragment in the $+\omega_f$ direction (Fig. 12).

In timewise finite-difference form, Eqs. 2.58 through 2.60 become

$$(\Delta \overset{T}{\dot{Y}}_f)_{j+1} = (\Delta \dot{Y}_f)_j \tag{2.61}$$

$$(\Delta \overset{T}{\dot{Z}}_f)_{j+1} = (\Delta \dot{Z}_f)_j \tag{2.62}$$

$$(\Delta \overset{T}{\dot{\theta}})_{j+1} = (\Delta \dot{\theta})_j \tag{2.63}$$

where overscript "T" signifies a trial value which requires modification, as explained later, if ring-fragment collision occurs between t_j and t_{j+1}.

By an inspection procedure to be described shortly, the instant of ring-fragment collision is determined, and the resulting collision-induced velocities which are imparted to the fragment and to the affected ring segment are determined in accordance with the analysis of Subsection 2.3.

2.6 Collision Inspection and Solution Procedure

2.6.1 One-Fragment Attack

The collision inspection and solution procedure will be described first for the case in which only one idealized fragment is present. With minor modifications this procedure can also be applied for an n-fragment attack as discussed in Subsection 2.6.2.

The following procedure indicated in the flow diagram of Fig. 9 may be employed to predict the motions of the ring and the rigid fragment, their possible collision, the resulting collision-imparted velocities experienced by each, and the subsequent motion of each body:

Step 1: Let it be assumed at instant t_j that the coordinates $\{q^*_j\}$, Y_{f_j}, and Z_{f_j}, and coordinate increments $\{\Delta q^*\}_j$, ΔY_{f_j}, and ΔZ_{f_j} are known. One can then calculate the strain increments $\Delta\varepsilon_j$ at all Gauss stations j along and through the thickness of the ring (see Ref. 14).

Step 2: Using a suitable constitutive relation for the ring material, the stress increments $\Delta\sigma_j$ at corresponding Gaussian stations within each finite element can be determined from the now-known strain increments $\Delta\varepsilon_j$. Since the σ_{j-1} are known at time instant t_{j-1}, the stresses at t_j are given by $\sigma_j = \sigma_{j-1} + \Delta\sigma_j$. This information permits determining all quantities on the right-hand side of Eq. 2.52, where for the present CIVM problem $\{F^*\}_j$ is regarded as being zero.

Step 3: Solve Eq. 2.52 for the trial ring displacement increments $\{\overset{T}{\Delta q^*}\}_{j+1}$. Also, use Eqs. 2.61, 2.62, and 2.63 for the trial fragment displacement increments $(\overset{T}{\Delta Y}_f)_{j+1}$, $(\overset{T}{\Delta Z}_f)_{j+1}$, and $(\overset{T}{\Delta\theta})_{j+1}$.

Step 4: Since a ring-fragment collision may have occurred between t_j and t_{j+1}, the following sequence of substeps may be employed to determine whether or not a collision occurred and, if so, to effect a correction of the coordinate increments of the affected ring segment and of the fragment.

Step 4a: To check the possibility of a collision between the fragment and ring element i (approximated as a straight beam) as depicted in Figs. 11, 12, and 14, compute the trial projection $(\overset{T}{p}_i)_{j+1}$ of the line from ring node i+1 to point A at the center of the fragment, upon the straight line connecting ring nodes i and i+1, as follows, at time instant t_{j+1}:

$$(\overset{T}{p}_i)_{j+1} = \left[\overset{T}{Y}_{i+1} - \overset{T}{Y}_f\right]_{j+1} \cos(\overset{T}{\alpha})_{j+1} + \left[\overset{T}{Z}_{i+1} - \overset{T}{Z}_f\right]_{j+1} \sin(\overset{T}{\alpha})_{j+1} \tag{2.64}$$

where the Y,Z are inertial Cartesian coordinates. Now, examine $(\overset{T}{p}_i)_{j+1}$; three cases are illustrated in Fig. 15a.

Step 4b: If $(\overset{T}{p}_i)_{j+1} <$ or if $(\overset{T}{p}_i)_{j+1} > s_i$ where $s_i > 0$, a collision between the fragment and ring element i is impossible. Proceed to check ring element i+1, etc. for the possibility of a collision of the fragment with other ring elements.

Step 4c: If $0 \leq (\overset{T}{p}_i)_{j+1} \leq s_i$, a collision with ring element i is possible, and further checking is pursued. Next, calculate the fictitious "penetration distance" $(\overset{T}{a}_i)_{j+1}$ of the fragment into ring element i at point C by (see Fig. 15b):

$$(\overset{T}{a}_i)_{j+1} = \left[\frac{1}{2} h_{1i} + \frac{\alpha}{2}(h_{2i} - h_{1i}) + r_f\right]_{j+1} - \left[\overset{T}{d}_i\right]_{j+1} \tag{2.65}$$

where

$[\frac{1}{2} h_{1i} + \frac{\alpha}{2} (h_{2i} - h_{1i})]$ = local semi-thickness of the ring element which is approximated as a straight beam in this "collision calculation".

r_f = radius of the fragment

$$\alpha_{j+1} = 1 - \left(\frac{\overset{T}{p}_i}{s_i}\right)_{j+1}$$ = fractional distance of s_i from node i to where the collision occurs (recall: $\alpha + \beta = 1$, and α_{j+1} should not be confused with the angle $(\alpha_i)_{j+1}$).

$$(\overset{T}{d}_i)_{j+1} = -\left[\overset{T}{Y}_{i+1} - \overset{T}{Y}_f\right] \sin (\overset{T}{\alpha}_i)_{j+1} + \left[\overset{T}{Z}_{i+1} - \overset{T}{Z}_f\right] \cos (\overset{T}{\alpha}_i)_{j+1} \tag{2.66}$$

= the projection of the line connecting node i+1 with the center of the fragment upon a line perpendicular to the line joining nodes i and i+1.

Next, examine $(\overset{T}{a}_i)_{j+1}$ which is indicated schematically in Fig. 15b and is given by Eq. 2.65.

<u>Step 4d</u>: If $(\overset{T}{a}_i)_{j+1} \leq 0$, no collision of the fragment upon element i has occurred during the time interval from t_j to t_{j+1}. Hence, one can proceed to check element i+1, etc. for the possibility of a collision of the fragment with other ring elements.

<u>Step 4e</u>: If $(\overset{T}{a}_i)_{j+1} > 0$, a collision has occurred; corrected coordinate increments (overscipt "C") may be determined approximately by (see Figs. 14 and 15b):

$$(\Delta \overset{C}{Y}_f)_{j+1} = (\Delta \overset{T}{Y}_f)_{j+1} + (\Delta t^*)\Big[(V_{fN}' - V_{fN}) \sin (\overset{T}{\alpha}_i)_{j+1} - (V_{fT}' - V_{fT}) \cos (\overset{T}{\alpha}_i)_{j+1}\Big] \tag{2.67a}$$

$$(\Delta \overset{C}{Z}_f)_{j+1} = (\Delta \overset{T}{Z}_f)_{j+1} + (\Delta t^*)\Big[-(V_{fN}' - V_{fN}) \cos (\overset{T}{\alpha}_i)_{j+1} - (V_{fT}' - V_{fT}) \sin (\overset{T}{\alpha}_i)_{j+1}\Big] \tag{2.67b}$$

$$(\Delta \overset{C}{\theta}) = (\Delta \overset{T}{\theta})_{j+1} + (\Delta t^*)(\omega_f' - \omega_f) \tag{2.67c}$$

$$(\Delta \overset{C}{V}_i)_{j+1} = (\Delta \overset{T}{V}_1)_{j+1} + (\Delta t^*)\Big[(V_{1N}' - V_{1N}) \sin(\phi_i - \overset{T}{\alpha}_i)_{j+1} + (V_{1T}' - V_{1T}) \cos(\phi_i - \overset{T}{\alpha}_i)_{j+1}\Big] \quad (2.67d)$$

$$(\Delta \overset{C}{W}_i)_{j+1} = (\Delta \overset{T}{W}_1)_{j+1} + (\Delta t^*)\Big[(V_{1N}' - V_{1N}) \cos(\phi_i - \overset{T}{\alpha}_i)_{j+1} - (V_{1T}' - V_{1T}) \sin(\phi_i - \overset{T}{\alpha}_i)_{j+1}\Big] \quad (2.67e)$$

$$(\Delta \overset{C}{V}_{i+1})_{j+1} = (\Delta \overset{T}{V}_2)_{j+1} + (\Delta t^*)\Big[(V_{2N}' - V_{2N}) \sin(\phi_{i+1} - \overset{T}{\alpha}_i)_{j+1} + (V_{2T}' - V_{2T}) \cos(\phi_{i+1} - \overset{T}{\alpha}_i)_{j+1}\Big] \quad (2.67f)$$

$$(\Delta \overset{C}{W}_{i+1})_{j+1} = (\Delta \overset{T}{W}_2)_{j+1} + (\Delta t^*)\Big[(V_{2N}' - V_{2N}) \cos(\phi_{i+1} - \overset{T}{\alpha}_i)_{j+1} - (V_{2T}' - V_{2T}) \sin(\phi_{i+1} - \overset{T}{\alpha}_i)_{j+1}\Big] \quad (2.67g)$$

where the after-impact (primed) quantities be found from Eqs. 2.44 through 2.50 and where time interval from <u>actual</u>

$$\Delta t^* = \frac{(\overset{T}{a}_i)_{j+1}}{(V_{Ri})_j} \quad (2.68a)$$

= impact on ring element i until t_{j+1}

$$(V_{Ri})_j = V_{fN} - (\beta V_{1N} + \alpha V_{2N}) \quad (2.68b)$$

= preimpact relative velocity of point A on the fragment and point C on the ring.

The terms, in Eqs. 2.67a through 2.67g, which are multiplied by (Δt^*) represent corrections to the trial incremental quantities for the (Δt^*) time interval. Also, since Δt is small, one may use either angle $(\overset{T}{\alpha}_i)_{j+1}$ or angle $(\overset{T}{\alpha}_i)_j$ in Eqs. 2.67a through 2.67g.

Step 5: Having determined the corrected coordinate increments[+] for the impacted ring element, this time cycle of calculation is now complete. One then proceeds to calculate the ring nodal coordinate increments and the fragment coordinates for the time step from t_{j+1} to t_{j+2}, starting with Step 1. The process proceeds cyclically thereafter for as many time increments as desired.

This solution procedure may be carried out for as many time steps as desired or may be terminated by invoking the use of a termination criterion such as, for example, the reaching of a critical value of the strain at the inner surface or the outer surface of the ring. Appropriate modifications of this approximate analysis could be made, if desired, to follow the behavior of the ring and the fragment after the initiation and/or completion of local fracturing of the ring has occurred.

Finally, note that it is possible for the fragment to have impacted more than one ring segment during the Δt time step in question. The collision inspection process reveals this. Then, the quantities noted in Step 4e are corrected in sequence starting with the ring segment experiencing the "largest penetration", the next largest penetration, etc.

2.6.2 N-Fragment Attack

In the case of "attack" by n idealized fragments each with its individual m_f, I_f, r_f, ω_f, V_{fN}, and V_{fT}, a similar procedure is used. During each Δt, the collision-inspection procedure is carried out for every fragment; none, some, or all of these n fragments may have collided with one or more ring segments. The penetration distance is computed (see Eq. 2.65, for example) for each impacted segment; this penetration information is then ordered from the largest to the smallest. Then the corrected quantities indicated in Step 4e of Subsection 2.6.1 are determined in succession, starting with the largest penetration combination, the next largest, etc. After all of the corrections have been carried out for the present Δt time interval, the calculation process of Fig. 9 proceeds similarly for the next Δt.

[+] It should be noted that in this approximate calculation, only the coordinate increments of the fragment and of the impacted ring segment are corrected. Those for all other ring segments are regarded as already being correct. The time increment Δt is regarded as being sufficiently small to make these approximations acceptable.

SECTION 3

CONTAINMENT RING RESPONSE PREDICTIONS

In order to illustrate the application of the present CIVM-JET analysis for predicting the transient responses of 2-d containment structures, two types of problems have been investigated and are described in this section. These types involve the responses of containment rings to attack either (1) by a single fragment or (2) by three equal-size fragments. For convenience and simplicity, initially circular 4130 cast steel containment rings of uniform thickness* and fixed inner-surface radius are employed.

For the single-fragment-attack cases, it was desired to explore in a preliminary fashion, if possible, the "effectiveness" of complete containment as compared with combined containment-and-deflection (to achieve a desired fragment trajectory path) for the identical single-fragment attack. Accordingly, a plausible candidate for such comparisons was believed to be either a rotor rim segment with a number of attached blades or perhaps a disk segment with a number of attached blades. Thus, since the NAPTC had conducted numerous rotor burst experiments on T58 turbine rotors which were caused to fail in 2, 3, 4, or 6 equal-size fragments and since high-speed photographic data were available to show the behavior of these fragments as well as of the containment rings which were subjected to attack by these fragments, an example single fragment having the properties of one sixth of a T58 turbine rotor was selected for the present CIVM-JET prediction studies. Similarly, for illustrative CIVM-JET studies of the response of containment rings subjected to 3-fragment attack, the NAPTC fragments for tri-hub T58 rotor bursts were chosen. In each case these selected fragments were idealized to be "rigid circular fragments" for use in the CIVM-JET calculations, as depicted in Figs. 16a and 16b.

---

*Two dimensional containment/deflection "rings" which are arbitrarily curved and/or of variable thickness can be analyzed by the CIVM-JET program; such cases, however, introduce many more variables than time and funds permitted studying in the present investigation.

The main objectives of the studies discussed in Sections 3 and 4 are (a) to demonstrate an illustrative utilization of the present approximate analysis capability included in the CIVM-JET program and (b) to display typical response behavior and the influence of varying a limited number of geometric and material parameters which can be used to characterize 2-d containment/deflector structures.

3.1 Single Fragment Examples

The selected single fragment represented by a one-sixth T58 turbine rotor fragment is shown in Fig. 16a together with its mass, m_f, mass moment of inertia I_f about its CG, translational velocity V_f, rotational velocity ω_f, and its general dimensions. This fragment is idealized for CIVM-JET analysis purposes as being a circular disk with duplicate properties, m_f, I_f, V_f, and ω_f; its fixed radius (non-deformable fragment) was chosen to be r_f = 3.37 inches, as a reasonable size-compromise between that for a circle circumscribing the undeformed pre-impact fragment and an "effective radius" of the deformed fragment as revealed from NAPTC high-speed photographs. The chosen r_f is, however, nearly the same as one would select based upon physical considerations in the absence of such photographs. With these properties, the pre-impact fragment possesses a translational kinetic energy $(KE)_{ot}$ of 9.6×10^4 in-lb and a rotational kinetic energy $(KE)_{or}$ of 5.4×10^4 in-lb or a total kinetic energy $(KE)_o$ of 15×10^4 in-lb.

Listed below are the characterizing quantities which remained fixed and those that were varied in the present calculations:

CONTAINMENT RING	FRAGMENT
Fixed Quantities	Fixed Quantities
Material	Material
Inner Surface Radius, r	m_f, I_f, V_f, ω_f, r_f, r_{cg}
Variables	Variables
Radial Thickness, h	None
Axial Length, L	

where r_{cg} is the distance from the fragment CG to the rotor axis. For most of the calculations, frictionless impact (μ=0) was assumed; in a few cases the effects of $\mu \neq 0$ were explored.

In the present containment-structure response calculations, the quantity of primary interest was the maximum transient circumferential strain $(\varepsilon_{\theta\theta})_{max}$ produced on the containment ring during its response to fragment attack, since $\varepsilon_{\theta\theta}$ may be a convenient indicator of imminent containment ring fracture; in all cases this maximum occurred at the outer surface of the containment ring.

According to well-established principles of dimensional analysis, one may express the dimensionless response parameter $(\varepsilon_{\theta\theta})_{max}$ as a function of the following dimensionless variables:

$$\underbrace{(\varepsilon_{\theta\theta})_{MAX}}_{\text{RESULT}} = f\,\underbrace{\left(h/r,\ L/r,\ wr/(KE)_o,\ \mu \right)}_{\text{VARIABLES}} \tag{3.1}$$

where w denotes the weight of the containment ring. Alternatively, if one assumes that a known critical value of $\varepsilon_{\theta\theta}$ can be used to define the limit of fragment containment, one can represent the <u>containment threshold</u> by the following dimensionless characterization:

$$(wr)/(KE)_o = g\left(h/r,\ L/r,\ \mu \right) \tag{3.2}$$

In Eqs. 3.1 and 3.2, f and g, respectively, denotes an unknown but experimentally and/or theoretically determinable functional dependence of the left-hand side "result" upon the dimensionless <u>variables</u> on the right-hand side.

Although dimensionless representation of the type given by Eqs. 3.1 and 3.2 provide the most systematic and orderly way to present $(\varepsilon_{\theta\theta})_{max}$ or containment threshold results, it may be more graphic and clear to show (for the latter condition) simply containment ring weight w instead of only $(wr)/(KE)_o$ since in the present example both r and $(KE)_o$ are held fixed. Other dimensional-result displays will be presented for similar reasons.

For the present CIVM-JET calculations, the free containment ring was modeled by means of 40* uniform length finite elements or segments in the

*It has been shown in Ref. 14 that about 9 or more finite elements per 90-degree sector of a ring produce converged transient response results.

the circumferential direction as indicated in Fig. 17a; shown also is the nodal numbering of the ring, the attacking fragment, and the point of initial impact. The uniaxial static stress-strain properties of the 4130 cast steel ring material used in these calculations were approximated by a piecewise straight-line-segment fit of static test data furnished by the NAPTC (Ref. 25), defined by the following stress-strain pairs (σ,ε): σ,ε = 0,0; 80,950 psi, .00279 in/in; 105,300 psi, .02250 in/in; and 121,000 psi, 0.20 in/in. All of the calculations discussed in this section have utilized these static stress-strain properties; later, strain-rate effects are discussed briefly. The central-difference-operator time-step value used in all cases considered in this illustrative study was one microsecond. This value was found to yield stable, convergent fragment/ring interaction and response results*. In all cases, the inner surface radius of the ring was held constant at 7.50 inches. The density of this steel ring material was taken to be 0.283 lb/cu in.

Shown in Fig. 17b is the outer surface strain $\varepsilon_{\theta\theta}$ at the midlength location of elements 4, 5, and 6 as a function of time for cases of μ=0 and μ=0.5 for a containment ring with an axial length L = 2.50 in. and a radial thickness h = 0.40 in; the sequential locations of fragment-ring impact as a function of time are shown in Fig. 17c. One observes that for this rather extreme value (μ= 0.5) of friction coefficient used, the effect on $\varepsilon_{\theta\theta}$ compared with that for frictionless impact/interaction (μ=0) is small; hence, most of the subsequent results in this report are for μ=0. Also, the peak strain response (see Fig. 17b has occurred by about 450 microseconds after initial impact. Figure 17d illustrates the distribution of the energy of the system among fragment kinetic energy, ring plastic work, ring kinetic energy, and ring elastic energy as a function of time for the case μ = 0.5, L = 2.50 in, and h = 0.40 in; it is seen

*Note that the "critical time increment criterion" $\Delta t \approx 0.8(2/\omega_{max})$ which amounts to about 4.5 microseconds and is sufficiently small to provide converged transient response predictions of an impulsively-loaded ring is, however, too large to provide converged results for the fragment/ring impact interaction and response cases. Hence, numerical experiments were conducted with various Δt values, and it was determined that a Δt of 1 μsec was adequate for these cases.

that by about 600 microseconds after initial impact, these energies have reached essentially an "equilibrium" state.

The effect of $\mu = 0$ vs. $\mu = 0.5$ on the maximum circumferential normal strain $(\varepsilon_{\theta\theta})_{max}$ is shown in Fig. 18 as a function of both the ring thickness h and the thickness ratio h/r for containment rings of 2.50-inch axial length. It is seen that the value of friction coefficient μ has only a small effect upon the predicted $(\varepsilon_{\theta\theta})_{max}$. Hence, to minimize computing time, the results produced and discussed in this section are for cases of $\mu = 0$.

Predictions of containment ring responses to impact by the single idealized fragment shown in Fig. 16a for rings of axial lengths L = 5/8 in, 5/4 in, and 10/4 in (each axial length is increased by a factor of 2) were carried out for various ring thicknesses h and for $\mu = 0$.

Shown in Fig. 19 is $(\varepsilon_{\theta\theta})_{max}$ as a function of h (and h/r) for fixed values of L (and L/r); $(\varepsilon_{\theta\theta})_{max}$ is seen to decrease rapidly with increasing ring thickness for each given ring axial length ratio.

Instead of plotting $(\varepsilon_{\theta\theta})_{max}$ versus h/r for given values of L/r one can plot with equal validity the implied ring weight w and/or $(wr)/(KE)_o$. This is shown in Fig. 20. As expected on physical grounds, $(\varepsilon_{\theta\theta})_{max}$ decreases essentially monotonically with ring weight for each given value of L or L/r.

A further interesting way to depict these maximum strain predictions as a function of the problem variables is to plot ring weight w (or $(wr)/(KE)_o$) versus ring axial length L (or L/r) for fixed value of $(\varepsilon_{\theta\theta})_{max}$ as shown in Fig. 21. If one assumes that ring fracture might occur at various fixed values of the normal strain $\varepsilon_{\theta\theta}$, these curves could be regarded as giving an estimate of the containment ring weight as a function of ring axial length. Thus, one notes that these predictions indicate that (assuming that a known fixed value of $\varepsilon_{\theta\theta}$ denotes the containment threshold) the containment ring weight decreases monotonically as the axial length (or length ratio) of the ring increases. However, the present predictions lose their validity as L increases too much because the actual structural response to attack by a fragment of given axial-direction dimensions becomes three dimensional whereas, in the present 2-d model this added axial direction ring material is treated as behaving in a 2-d fashion. The result is that the present predictions tend to underestimate the structural response compared with the actual 3-d behavior. Hence, as pointed out in Subsection 1.3, one may employ the present CIVM-JET analysis to do parametric calculations, to study trends, and to compare various potential containment-structure materials;however, it remains essential as of now to develop selected experimental containment-threshold data to bridge the gap between the present simplified, convenient 2-d predictions and the actual behavior.

3.2 Three Fragment Examples

To illustrate the use of the CIVM-JET-4A analysis and program to predict containment ring responses to multiple fragment attack, it was decided to analyze NAPTC Test No. 67 in which a 4130 cast steel containment ring of $L = 1.501$ in, $h = .339$ in, and inner surface radius = 7.50 in. was subjected to a trihub burst of a T58 turbine rotor operating at 18,830 rpm. It appears from the high-speed movies and from post-test inspection that the ring did succeed in containing these fragments.

Shown in Fig. 16b is a schematic of one pre-impact trihub burst fragment together with the idealized fragment model selected for use in the present calculations. Each fragment has $m_f = 0.932 \times 10^{-2}$ lb-sec^2/in, $I_f = 0.666 \times 10^{-1}$ lb-sec-in, $V_f = 5515$ in/sec, $\omega_f = 1918$ rad/sec, and $(KE)_o = 27.1 \times 10^4$ in-lb. For the idealized model r_f is taken to be 2.42 in.

Because of time and funding constraints, only two illustrative calculations have been carried out for this problem -- both assuming frictionless impact interaction ($\mu=0$). In one case the 4130 cast steel ring material was assumed to behave in an elastic, strain hardening (EL-SH) fashion without strain-rate effects. In the other case, this behavior was modified to include strain-rate effects by assuming this material to behave like "mild steel" with strain-rate constants $p = 5$ and $D = 40.4$ sec^{-1} (Ref. 27) where the rate-dependent mechanical sublayer yield stress σ_y is related to the corresponding static yield stress σ_o by

$$\sigma_y = \sigma_o\left[1 + \left|\frac{\dot{\varepsilon}}{D}\right|^{1/p}\right] \tag{3.3}$$

For these calculations the ring was modeled by a total of 36 finite elements (segments) so that convenient impact symmetry would occur.

Deformed ring profiles observed experimentally as well as those predicted in these two calculations are shown in Fig. 22 at the following times after initial impact (TAII): 0, 350, 700, and 1400 microseconds. It is seen that these two predictions exhibit small differences; in turn, these predictions compare favorably with the photographic observations (Ref. 25). Since there are uncertainties in the "proper modeling" of this fragment (i.e., r_f) and fragment/ring interactions (value or values for $\mu \neq 0$) as well as for the strain-rate material properties of 4130 cast steel, these comparisons should be regarded only as tentative. Further modeling and calculation studies should be carried out; also, more detailed and precise experimental data for such a case should be obtained by using the recently improved experimental techniques, as well as including transient strain measurements.

Although no transient strain measurements are available for comparison with predictions, it is interesting to examine the predicted outer-surface strains at several locations on a "lobe" of the deformed ring as a function of time for both the EL-SH and the EL-SH-SR calculations. These transient strains are shown in Fig. 23. It is seen that the "effective material stiffening" associated with the increased yield stress arising from strain-rate dependence results in significantly smaller peak transient strains.

Finally, by an inspection of the outer surface mid-element circumferential strains of all elements throughout each calculation*, the maximum $\varepsilon_{\theta\theta}$ was determined for each case. It was found for this "lobe" that $(\varepsilon_{\theta\theta})_{max}$ was 17.74% and 12.40% for the EL-SH and the EL-SH-SR calculation, respectively.

*The response time studied ranged to about 1400 microseconds after initial impact.

SECTION 4

DEFLECTOR RING RESPONSE PREDICTIONS

The primary purpose of this section is to illustrate via some simple examples the application of the CIVM-JET method for predicting the responses of idealized 2-d fragment-deflector structures subjected to impact by a single idealized fragment. Predicted also is the (changed) path of the attacking fragment. As depicted in Fig. 2, one seeks to prevent the attacking fragment from entering the "protected zone" but to permit or perhaps even encourage, if feasible, fragment escape from the engine casing, and penetration into the "unprotected zone", since this condition might define a minimum-weight design.

In order to apply the present 2-d transient structural response analysis method to this fragment/structure interaction problem, it is useful and convenient for present purposes to view the deflector structure as consisting of an integral locally-thickened portion of the engine casing as shown schematically in Figs. 2, 7, and 24. Further, one may account approximately for the "restraining effect" of the adjacent portion of the engine casing upon the (thick) "deflector structure" by regarding the non-thickened engine casing as consisting of a very long cylindrical shell of uniform thickness as depicted in Fig. 24a; section views through the "standard" casing and through the deflector region are shown in Figs. 24b and 24c, respectively. Hence, one is led to the idealized elastic-foundation-supported deflector model shown in Fig. 24d, where the uniformly distributed elastic foundation stiffnesses per unit circumferential length are denoted by k_N and by k_T, in the normal and in the tangential direction, respectively.

As perhaps a reasonable first estimate, these elastic foundation constants k_N and k_T may be estimated from (a) the stiffness of this casing in a uniform radial expansion mode for k_N, and (b) the torsional first mode stiffness for k_T. In the limit of an infinitely long cylindrical shell, one may readily show from free-body equilibrium of a circumferential portion of length $d\eta$, the strain-displacement equations, and the stress-strain relations for isotropic material that dk_N is given by

$$dK_N = \left[\frac{E_c h_c}{r_{mc}^2 (1-\nu^2)}\right] d\eta \qquad (4.1a)$$

or, for a short cylindrical shell by

$$dK_N = \left[\frac{E_c h_c}{r_{mc}^2}\right] d\eta \qquad (4.1b)$$

where subscript c pertains to the engine casing (cylindrical), E_c is the elastic modulus, ν_c is the Poisson ratio, and h_c is the thickness and r_{mc} is the midsurface radius of the engine casing. Hence, the foundation stiffness k_N per unit circumferential length ($d\eta = 1$) is given by the quantity in square brackets in Eq. 4.1a or Eq. 4.1b. Similarly, from St. Venant's torsion theory for a cylindrical shell element of dx axial length, one can show that dk_T is given by

$$dK_T = \frac{1}{dx}\left[G_c h_c\right] \qquad (4.2)$$

where G_c is the shear modulus of the engine casing material. Since the torsional stiffness is independent of the axial length of the cylindrical shell, one may employ $k_T = G_c h_c$.

Because of the many geometric, mechanical, and impact variables present in fragment/deflector interaction and response problems, it is instructive to utilize some even simpler, more approximate idealizations for such problems as indicated, for example, in Fig. 24e. After studying the responses of such simpler models in various impact situations, one can more effectively select the more interesting and illuminating conditions for study in conjunction with the more realistic modeling depicted in Fig. 24d. Accordingly, studies involving the use of the simpler model shown in Fig. 24e are discussed in Subsection 4.1. This is followed in Subsection 4.2 by a description of a more restricted set of calculations carried out utilizing the more realistic model of Fig. 24d. In both of these studies because of time and funding constraints, only uniform-thickness deflector structures were analyzed although variable-thickness deflectors as indicated schematically in Figs. 2 and 7 might very well be of interest in practical applications and can be analyzed by the

CIVM-JET-4 program described in Appendix A. Also, for similar reasons, only deflectors with an included angle ψ of 90 degrees, an inner surface radius of 7.50 in, and conditions of frictionless impact (μ = 0) were analyzed. In all cases, the deflector structure was assumed, for illustration, to consist of 4130 cast steel, the physical and mechanical properties of which have been cited in Subsection 3.1.

For both types of idealized deflectors (Figs. 24d and 24e), these studies employed a single idealized fragment with the following properties:

$m_f = 4.6 \times 10^{-3}$ (lb-sec^2)/in $\quad r_f = 3.37$ in $\quad V_f = 6400$ in/sec

$I_f = 2.61 \times 10^{-2}$ lb-sec^2-in $\quad r_{cg} = 3.05$ in $\quad \omega_f = 2100$ rad/sec

$(KE)_{ot} = 9.6 \times 10^4$ in-lb $\quad (KE)_{or} = 5.4 \times 10^4$ in-lb $\quad (KE)_o = 15 \times 10^4$ in-lb

A structural response quantity of interest with respect to preventing deflector structure rupture (along the to-be-protected zone) might be the maximum circumferential tensile strain $(\varepsilon_{\theta\theta})_{max}$ which occurs at either the outer surface or the inner surface of the deflector ring at some to-be-determined circumferential station for each case. Similarly, the determination (see Fig. 24e) of the quantities $z_d{}^*$, $\alpha_d{}^*$, and β^* <u>at the instant of fragment escape</u> from the deflector structure should be adequate to define whether or not the deflector has changed the path of the attacking fragment sufficiently to prevent its entering the "protected region"+. Therefore, these four quantities $(\varepsilon_{\theta\theta})_{max}$, $z_d{}^*$, $\alpha_d{}^*$, and β^* (or their dimensionless counterparts) are of primary interest in the studies reported in Subsections 4.1 and 4.2.

Finally, for these studies each deflector ring was modeled by 10 equal-length segments or finite elements (see Fig. 24e, for example).

4.1 Hinged-Fixed/Free Deflector Examples

As shown in Fig. 24e, the idealized fragment deflector structure has a hinged-fixed support at one end but is free at the other. Thus under fragment

---

+At time prior to fragment escape, the "fragment diversion quantities" are denoted by z_d, α_d, and β (i.e., without the asterisk).

attack, this structure experiences impact/interaction forces (or velocity increments), inertial forces, internal elastic and plastic forces, and "translational support forces" at its hinged-fixed end. The initial point of fragment impact against the structure is identified in Fig. 24e by the angle θ_I. By applying the CIVM-JET analysis and computer program, one can predict the motion and path of the fragment as well as the large-deflection elastic-plastic transient response of the deflector structure.

Summarized concisely in the following tabulation are the characterizing quantities which were held fixed and those which were varied in the present studies:

HINGED-FIXED/FREE DEFLECTOR EXAMPLES

DEFLECTOR RING	FRAGMENT	OTHER CONDITIONS
	Fixed Quantities	
Material Inner Surface Radius, r Subtended Angle, ψ	Material m_f, I_f, V_f, ω_f, r_f, r_{cg}	$\mu = 0$
	Variables	
Thickness, h_d Axial Length, L	None	θ_I (for some cases)

Utilizing dimensional analysis, one may, in principle, express the "dimensionless response parameters" $(\varepsilon_{\theta\theta})_{max}$, α_d^*, z_d^*/r, and β^* as a function of the dimensionless variables, as follows for somewhat more general cases than indicated in the above tabulation:

$$(\varepsilon_{\theta\theta})_{MAX} = f_1\left(h_d/r,\ L/r,\ \psi,\ \theta_I,\ (wr)/(KE)_o,\ \mu\right) \tag{4.3a}$$

$$\alpha_d^* = f_2\left(h_d/r,\ L/r,\ \psi,\ \theta_I,\ (wr)/(KE)_o,\ \mu\right) \tag{4.3b}$$

$$Z_d^*/r = f_3(h_d/r, L/r, \psi, \theta_I, (Wr)/(KE)_o, \mu) \qquad (4.3c)$$

$$\beta^* = f_4(h_d/r, L/r, \psi, \theta_I, (Wr)/(KE)_o, \mu) \qquad (4.3d)$$

where a single idealized fragment with the previously-defined geometric parameters is assumed to be employed in all cases. For the present studies, however, μ, ψ, r, $(KE)_o$, and the deflector ring material are held fixed. Thus, Eqs. 4.3a through 4.3d reduce to

$$(\varepsilon_{\theta\theta})_{MAX} = f_1(h_d/r, L/r, \theta_I) \qquad (4.4a)$$

$$\alpha_d^* = f_2(h_d/r, L/r, \theta_I) \qquad (4.4b)$$

$$Z_d^*/r = f_3(h_d/r, L/r, \theta_I) \qquad (4.4c)$$

$$\beta^* = f_4(h_d/r, L/r, \theta_I) \qquad (4.4d)$$

Geometric similarity is assumed to be maintained.

In order to make a limited assessment of the effects of initial impact location θ_I upon the fragment-deflector responses, calculations were carried out by varying θ_I for L = 1.25 in. and h = 0.40 in. These results are summarized below for θ_I vs. $(\varepsilon_{\theta\theta})_{max}$:

θ_I (deg)	16	27.5	39	61
$(\varepsilon_{\theta\theta})_{max}$ (percent)	12.6	10.6	7.2	4.9

and in Figs. 25a and 25b for α_d and z_d (and z_d/r), respectively, as a function of time after initial impact (TAII); β is of lesser interest and is not shown.

For this highly-idealized configuration, it is seen that the response quantities are largest when θ_I is the smallest. However, the closer the point of initial impact is to the hinged-fixed support, the less valid is this model for approximating the behavior of deflector structures such as that depicted in Fig. 2. Further, the CIVM-JET-4A program which was utilized for these calculations has in it the restriction that proper predictions will not result if the attacking fragment impacts the finite element whose one end is located at the hinged-fixed support+; fragment impact/interaction is handled

+This same restriction applies for any other "fixed" type of support such as ideally clamped, etc.

properly when impact occurs with any of the other finite elements with which the deflector structure is modeled for analysis. In subsequent calculations it was decided to keep θ_I fixed at 16 degrees, and to vary h for each of several fixed values of L. The resulting predictions for $(\varepsilon_{\theta\theta})_{max}$ are shown in Fig. 26 as a function of h_d (or h_d/r) for various fixed values of L (or L/r). Alternatively, one may display $(\varepsilon_{\theta\theta})_{max}$ as a function of ring weight w or $(wr)/(KE)_o$ for various fixed values of L (or L/r); see Fig. 27. Further, one may display the deflector ring weight w or $wr/(KE)_o$ as a function of L (or L/r) for various fixed values of $(\varepsilon_{\theta\theta})_{max}$ as shown in Fig. 28. If one assumes that some given $(\varepsilon_{\theta\theta})_{max}$ will insure the avoidance of deflector ring fracture, Fig. 28 indicates that the attendant deflector ring weight decreases monotonically as the axial length L of the fragment-deflector structure is increased; of course if L becomes too large, the actual behavior will deviate from the 2-d behavior which the present CIVM-JET analysis and program requires. All of these trends are consistent with the behavior that is expected on physical grounds.

A similar effectiveness trend may be observed by examining the effect upon the path of the fragment from its impact and interaction with the deflector structure. Shown in Figs. 29a and 29b are, respectively, α_d and z_d (or z_d/r) at TAII = 650 microseconds as a function of h_d (or h_d/r) for various fixed values of L (or L/r). Here again it is seen that an increase of L for otherwise fixed conditions leads to larger fragment path deviations. Note that Figs. 29a and 29b show fragment path information at TAII = 650 microseconds rather than at the fragment-escape point (defining α_d* and z_d*); the latter occurs somewhat later for most of the cases shown, and would have required longer computer runs to obtain. For present illustrative and comparative purposes, however, the α_d and z_d data shown at TAII = 650 microseconds are believed to be informative and (from spot check examinations) to differ little from α_d* and z_d*.

4.2 Elastic-Foundation-Supported Deflector Examples

The influence of "support structure" upon the response and effectiveness of deflector structure has been explored in a brief approximate fashion by employing the idealized elastic-foundation-supported deflector model shown in Fig. 24d. A single idealized fragment with the same properties as defined in Subsection 4.1 was the "attacking fragment".

Summarized in the following are the fixed quantities and the variables employed:

ELASTICALLY-SUPPORTED DEFLECTOR EXAMPLES

DEFLECTOR RING	SUPPORT STRUCTURE	FRAGMENT	OTHER CONDITIONS
Fixed Quantities			
Material Inner Surface Radius, r Axial Length, L Subtended Angle, ψ	Material Inner Surface Radius, r	Material m_f, I_f V_f, ω_f r_f, r_{CG}	$\mu = 0$ θ_I
Variables			
Thickness, h_d	Thickness, h_c	None	None

For the previously-discussed elastic-foundation modeling (Fig. 24d) and for somewhat more general situations than indicated in the above tabulation, one may express the dimensionless response quantities $(\varepsilon_{\theta\theta})_{max}$, $\alpha_d{}^*$, $z_d{}^*/r$, and β^* as a function of appropriate dimensionless variables as follows:

$$(\varepsilon_{\theta\theta})_{MAX} = g_1\left(h_d/r,\ L/r,\ \psi,\ h_c/r,\ \theta_I,\ (Wr)/(KE)_o,\ \mu\right) \quad (4.5a)$$

$$\alpha_d{}^* = g_2\left(h_d/r,\ L/r,\ \psi,\ h_c/r,\ \theta_I,\ (Wr)/(KE)_o,\ \mu\right) \quad (4.5b)$$

$$z_d{}^*/r = g_3\left(h_d/r,\ L/r,\ \psi,\ h_c/r,\ \theta_I,\ (Wr)/(KE)_o,\ \mu\right) \quad (4.5c)$$

$$\beta^* = g_4\left(h_d/r,\ L/r,\ \psi,\ h_c/r,\ \theta_I,\ (Wr)/(KE)_o,\ \mu\right) \quad (4.5d)$$

In Eqs. 4.5a through 4.5d, it is assumed that geometric similarity is maintained and that the deflector structure and the engine casing (support) structure consist of the same[+] given material. Also, a single idealized fragment having the previously-defined geometric properties is assumed to be used in all cases[+].

[+]Otherwise, many more dimensionless variables would be present.

In addition, since ψ, r, L, $(KE)_o$, θ_I, and μ are held fixed in the present studies, Eqs. 4.5a through 4.5d reduce to:

$$(\varepsilon_{\theta\theta})_{MAX} = g_1 (h_d/r,\ h_c/r) \tag{4.6a}$$

$$\alpha_d^* = g_2 (h_d/r,\ h_c/r) \tag{4.6b}$$

$$Z_d^*/r = g_3 (h_d/r,\ h_c/r) \tag{4.6c}$$

$$\beta^* = g_4 (h_d/r,\ h_c/r) \tag{4.6d}$$

where the above-noted fixed values are

ψ = 90 deg	$(KE)_o = 15 \times 10^4$ in-lb
r = 7.50 in	θ_I = 16 deg
L = 1.25 in	μ = 0

Thus it is seen that the "retained variables" are h_d and h_c.

For time-and-economy reasons only two values of casing thickness, h_c, were explored: 0.1 in and 0.6 in; three values of deflector-ring thickness, h_d, were used: 0.20, 0.40, and 0.80 in. Assuming the engine casing to consist of steel with $E = 29 \times 10^6$ psi and $G = 11.5 \times 10^6$ psi, the elastic foundation stiffnesses were estimated to be:

CASE	A	B
h_c(in)	0.10	0.60
k_N(lb/in^2)	$.544 \times 10^5$	3.07×10^5
k_T(lb/in^2)	1.15×10^6	6.90×10^6

Here, in accordance with the estimates furnished by Eqs. 4.1a and 4.2, the thicker (0.60 in) engine casing (or foundation support) provides increased normal-direction and increased tangential-direction elastic stiffness compared with that for the thinner (0.10 in) casing structure.

Shown in Fig. 30 is $(\varepsilon_{\theta\theta})_{max}$ as a function of deflector structure thickness h_d (or h_d/r) for the two sizes of support structure thickness*:

---

*For present purposes, one is interested primarily in the effect of various sets of support stiffnesses (k_N, k_T) -- not in h_c values themselves; thus, one should pay no attention to the h_c values themselves.

Case A for $h_c = 0.1$ in. and Case B for $h_c = 0.6$ in. Note that $L = 1.25$ in, $\theta_I = 16$ deg, and $\mu = 0$ have been used. It is seen that the more rugged Case B support structure reduces $(\varepsilon_{\theta\theta})_{max}$ for all values of deflector structure thickness h_d. However, for either Case A or Case B, the dependence of $(\varepsilon_{\theta\theta})_{max}$ upon the deflector thickness h_d is somewhat unexpected in that the "expected monotonic decrease" of $(\varepsilon_{\theta\theta})_{max}$ with increasing h_d is not observed. The curious behavior seen in Fig. 30 may be the result of having "inspected" the $\varepsilon_{\theta\theta}$ value at the inner and the outer surface only at the midspan station of each finite element. It should be expected that the location of $(\varepsilon_{\theta\theta})_{max}$ may very well be at some other spanwise location. Hence, a more thorough "inspection" of $\varepsilon_{\theta\theta}$ should reveal a more "sensible" trend of $(\varepsilon_{\theta\theta})_{max}$ with increasing h_d. For example, one could feasibly make such evaluations at the inner and the outer surface at each of the three spanwise Gaussian stations of each finite element. Such more thorough studies will be conducted in the near future. Finally, for all of the cases shown in Fig. 30, $(\varepsilon_{\theta\theta})_{max}$ was found to have occurred on the outer surface of the ring, but not necessarily in the same deflector-ring finite element.

The influence of support-structure thickness h_c upon diverting the attacking fragment from its pre-impact path is shown in Fig. 31a for α_d and β, and in Fig. 31b for z_d (or z_d/r) as a function of time for a deflector structure with $L = 1.25$ in and $h_d = 0.40$ in. It is seen, as expected, that the more rugged support structure increases the amount by which the fragment is caused to deviate from its pre-impact path. On the other hand, the amount of fragment-path deviation changes only slightly as a function of deflector ring thickness h_d for a fixed value of engine casing (or support) thickness h_c as seen from Figs. 32a and 32b for α_d and z_d (or z_d/r), respectively, at TAII = 650 μsec which is close to but not at the fragment escape point for all cases. Thus, Figs. 31a through 32b suggest that the ruggedness of the (linear elastic) support structure is much more effective in changing the path of the attacking fragment than is achieved by simply increasing the thickness h_d of the deflector structure itself for a given set of support stiffness values k_N, k_T.

In Figs. 31a and 32a, both the fragment location angle α_d and the fragment path angle β(angle between the original and the current direction of the translational velocity vector of the fragment) are shown. Note that while the slope of the β curve is zero, no fragment-ring impacts are occurring (see β for Case B in Fig. 31a); at later times one would observe further fragment-ring impacts.

4.3 Comments

Since these parametric calculations have been of very limited scope, one must use caution so as to avoid coming to premature conclusions. More extensive studies of this type together with carefully posed "protection criteria" are recommended in order to assemble enough "trends predictions" to permit making more soundly based conclusions. Further, one should remember that the effect of support structure upon the behavior of deflector structure has been approximated as that of a linear elastic foundation. This approximation is believed to be a good one for small deformations but clearly degenerates when the deflections become larger and larger. Further effort to develop a better (nonlinear) approximation for the "foundation stiffness" may be advisable -- preferably either concurrent with or following the recommended more extensive parametric studies.

It is apparent that the circumferential extent of fragment-deflector structures required for most prospective situations would most likely be about 180 degrees, more or less, in order to insure protection for all critical directions of possible "fragment release"; hence further studies of fragment-deflector performance involving ψ = 180 degrees appear to be advisable. Also, the effectiveness of variable thickness deflector structure should be explored.

With these more extensive and realistic calculations* together with experimental fragment deflector performance data for verification and to assess 3-d response effects, it should then be possible to reach a reasonable judgment as to whether complete fragment containment or fragment deflection will be the more efficient approach for those cases for which either alternative is, basically, permissible.

*Including varying also at least θ_I, μ, k_T/E and k_N/E.

SECTION 5

SUMMARY AND COMMENTS

Arguments are presented supporting the proposition that the development and the selective utilization of prediction methods which are restricted to two-dimensional (2-d) transient large-deflection elastic-plastic responses of engine rotor burst fragment containment/deflector structures are useful and advisable for parametric and trends studies. In conjunction with properly-selected experimental studies of rotor-burst fragment interaction with actual containment and/or deflector structure -- wherein three-dimensional effects occur -- one may be able to develop convenient rules-of-thumb to estimate certain actual 3-d containment/deflection structural response results from the use of the very convenient and more efficient but simplified 2-d response prediction methods.

Accordingly, the collision-imparted velocity method (CIVM) for predicting the collision-interaction behavior of a fragment which impacts containment/deflector structures has been combined with a modified version of the JET 3C two-dimensional structural response code to predict the transient large-deflection, elastic-plastic responses and motions of containment/deflector structures subjected to impact by one or more idealized fragments. Included are the effects of friction between each fragment and the attacked structure. A single type of fragment geometry has been selected for efficiency and convenience in these fragment/structure interaction and response calculations, but the most important fragment parameters, it is believed, have been retained; n fragments each with its own m_f, I_f, V_f, ω_f, r_f, and r_{cg} may be employed.

Calculations have been carried out and reported illustrating the application of the present CIVM-JET analysis and program for predicting 2-d containment ring large-deflection elastic-plastic transient responses to (a) single-fragment impact and (b) to impacts by three equal-size fragments. The influence of containment ring thickness, axial length, and strain-rate dependence, as well as friction between the fragment and the impacted structure have been explored.

Similar illustrative calculations have been performed and reported for the responses of (a) ideal hinged-fixed/free and (b) elastic-foundation-supported fragment-deflector rings of uniform thickness to impact by a single idealized fragment. With respect to the latter more-realistic and yet-idealized model, it was found that plausible increases in the values for the stiffnesses of the "elastic foundation" was a more effective means for changing the path of the attacking fragment than by plausible increases in the thickness of the deflector ring itself.

Because of time and funding constraints, these calculations were of very limited scope; some interesting response trends, however, were noted. More extensive calculations in which more of the problem variables accommodated in the CIVM-JET-4A analysis and program are included and in which each of certain quantities are varied over plausible ranges would provide a more illuminating picture of the roles and effectiveness of these parameters with respect to fragment-containment and/or fragment-deflection protection.

It is believed that the present analysis method and program (CIVM-JET-4A) provides a convenient, versatile, and efficient means for estimating the effects of numerous problem variables upon the severe nonlinear 2-d responses of variable-thickness containment/defelctor structures to engine-rotor-fragment impact. Although a limited number of comparisons of predictions with appropriate experimental data show encouraging agreement, more extensive comparisons are required to establish a firmer assessment and confidence level in the accuracy and the adequacy of the present prediction method, consistent with its inherent 2-d limitations.

Finally, in addition to carrying out more extensive parametric calculations and comparisons with appropriate experiments (both containment and deflector type), it is recommended that the following CIVM-JET analysis matters be investigated:

(1)* The development of an improved model for accounting for the restraint effects of structure attached to

*The advisability of effecting these improvements will be to an extent dependent upon the outcome of the recommended additional theoretical-experimental correlation studies.

or located adjacent to the containment and/or the deflector structure; this may involve defining an appropriate nonlinear hardening-type elastic or elastic-plastic "foundation model".

(2) The feasibility of CIVM-JET-type analyses of situations wherein engine rotor-burst fragments strike the containment/deflector structure and then are struck by remaining rotor structure attached to the shaft, and then once again strike the C/D structure, etc.

(3)* The necessity for including transient deformation effects of the attacking fragments.

(4) The feasibility of employing the CIVM scheme in conjunction with finite-difference or finite-element shell-structure codes in order to represent the actual 3-d transient large-deflection elastic-plastic structural response behavior of shell structures subjected to fragment attack.

---

*Ibid, page 59.

REFERENCES

1. Chiarito, P.T., "Status of Engine Rotor Burst Protection Program for Aircraft." NASA Aircraft Safety and Operating Problems Conference, Volume 1. Langley Research Center, NASA SP-270, May 4-6, 1971, pp. 75-88. Also see AIAA Journal of Aircraft, Vol. 9, No. 7, July 1972, pp. 449-450)

2. DeLucia, R.A.; and Mangano, G.J.: "Rotor Burst Protection Program: Statistics on Aircraft Gas Turbine Engine Failures that Occurred in Commercial Aviation during 1971." NAPTC-PE-12, U.S. Navy, Feb. 1973. (Available as NASA CR-121151.)

3. Clarke, R.B., "Rotor Disk Burst Characteristics Data Analysis." Report No. S & A 73-1, Boeing Commercial Airplane Company, Feb. 28, 1973.

4. --- "Eastern Grounds Nine L-1011s for Inspection." Aviation Week & Space Technology, Vol. 98, No. 3, January 15, 1973, p. 24.

5. --- "Disk Plating Cited in 747 Engine Incident." Aviation Week & Space Technology, Vol. 96, No. 9, February 28, 1972, p. 50-51.

6. Martino, Albert A., "Turbine Disk Burst Protection Study. Phase I - Final Report on Problem Assignment NASA DPR R-105." NAEC-AEL-1973, U.S. Navy, Mar. 1965. (Available as NASA CR-80962.)

7. Martino, A.A.; and Mangano, G.J., "Turbine Disk Burst Protection Study. Phases II-III - Final Report on Problem Assignment NASA DPR R-105." NAEC-AEL-1848, U.S. Navy, Feb. 1967. (Available as NASA CR-84967.)

8. Martino, A.A.; and Mangano, G.J., "Rotor Burst Protection Program Initial Test Results. Phase IV - Final Report [on Problem Assignment] NASA DPR R-105." NAPTC-AED-1869, U.S. Navy, Apr. 1968. (Available as NASA CR-95967.)

9. Martino, A.A.; and Mangano, G.J., "Rotor Burst Protection Program. Phase V - Final Report [on] Problem Assignment NASA DPR R-105." NAPTC-AED-1901, U.S. Navy, May 1969. (Available as NASA CR-106801.)
10. Mangano, G.J., "Rotor Burst Protection Program. Phases VI & VII - Exploratory Experimentation to Provide Data for the Design of Rotor Burst Fragment Containment Rings." NAPTC-AED-1968, U.S. Navy, Mar. 1972. (Available as NASA CR-120962.)
11. --- "Rotor Burst Protection Program." (Study for NASA Lewis Research Center on NASA DPR R-105 and NASA Interagency Agreement C-41581-B), Naval Air Propulsion Test Center, Phila., Pa., Progress Reports, September 1969 to April 1973.
12. Balmer, H.A. and Witmer, E.A., "Theoretical-Experimental Correlation of Large Dynamic and Permanent Deformations of Impulsively-Loaded Simple Structures." Massachusetts Institute of Technology, AFFDL-TDR-64-108, July 1964.
13. Balmer, H.A., "Improved Computer Program -- DEPROSS 1, 2, and 3 -- to Calculate the Dynamic Elastic-Plastic Two-Dimensional Responses of Impulsively-Loaded Beams, Rings, Plates, and Shells of Revolution." Massachusetts Institute of Technology, ASRL TR 128-3, August 1965.
14. Wu, R.W.-H.; and Witmer, E.A., "Finite-Element Analysis of Large Transient Elastic-Plastic Deformations of Simple Structures, with Application to the Engine Rotor Fragment Containment/Deflection Problem." ASRL TR 154-4, Aeroelastic and Structures Research Laboratory, Massachusetts Institute of Technology, January 1972. (Available as NASA CR-120886.)
15. McCallum, R.B.; Leech, J.W.; and Witmer, E.A., "Progress in the Analysis of Jet Engine Burst-Rotor Containment Devices." ASRL TR 154-1, Aeroelastic and Structures Research Laboratory, Massachusetts Institute of Technology, August 1969. (Available as NASA CR-107900.)
16. McCallum, R.B.; Leech, J.W.; and Witmer, E.A., "On the Interaction Forces and Responses of Structural Rings Subjected to Fragment Impact." ASRL TR 154-2, Aeroelastic and Structures Research Laboratory, Massachusetts Institute of Technology, Sept. 1970. (Available as NASA CR-72801.)

17. Zirin, R.M. and Witmer, E.A., "Examination of the Collision Force Method for Analyzing the Responses of Simple Containment/Deflection Structures to Impact by One Engine Rotor Blade Fragment." ASRL TR 154-6, Aeroelastic and Structures Research Laboratory, Massachusetts Institute of Technology, May 1972. (Available as NASA CR-120952.)

18. Atluri, S., Witmer, E.A., Leech, J.W., and Morino, L., "PETROS 3: A Finite-Difference Method and Program for the Calculation of Large Elastic-Plastic Dynamically-Induced Deformations of Multilayer Variable-Thickness Shells." BRL CR-60 (also MIT-ASRL TR 152-2), November 1971.

19. Huffington, N.J., Jr., "Blast Response of Panels." U.S. Army Ballistic Research Laboratories, Technical Note No. 1702, August 1968.

20. Santiago, J.M., "Formulation of the Large Deflection Shell Equations for Use in Finite Difference Structural Response Computer Codes." U.S. Army Ballistic Research Laboratories, Report BRL R1571, February 1972.

21. Wilkins, M.L., "Calculation of Elastic-Plastic Flow." Lawrence Radiation Laboratory, Livermore, UCRL-7322, Rev. I, Jan. 1969.

22. Kreyenhagen, K.N., Read, H.E., Rosenblatt, M., and Moore, W.C., "Hardening Technology Studies -- III, STRIDE Code Solutions and Extension to Multimaterial Systems." SAMSO-TR-69-16, December 1968.

23. Hageman, L.J. and Walsh, J.M., "HELP: A Multimaterial Eulerian Program for Compressible Fluid and Elastic-Plastic Flows in Two Space Dimensions and Time." (Vol. I - Formulation; Vol. II - Fortran Listing of HELP), BRL CR No. 39, Systems, Science, and Software, La Jolla, Calif., May 1971.

24. Wu, R.W.-H. and Witmer, E.A., "Computer Program - JET 3 - to Calculate the Large Elastic-Plastic Dynamically-Induced Deformations of Free and Restrained, Partial and/or Complete Structural Rings." ASRL TR 154-7, Aeroelastic and Structures Research Laboratory, Massachusetts Institute of Technology, August 1972. (Available as NASA CR-120993.)

25. Private communications from G.J. Mangano, Naval Air Propulsion Test Center, Phila., Pa., 1972 to August 1973.

26. Goldsmith, W., Impact: The Theory and Physical Behaviour of Colliding Solids, Edward Arnold (Publishers) Ltd., London, 1960.

27. Ting, T.C.T., "The Plastic Deformation of a Cantilever Beam with Strain Rate Sensitivity under Impulsive Loading." Brown University, TR 70, ONR Contract 562(10), July 1961.

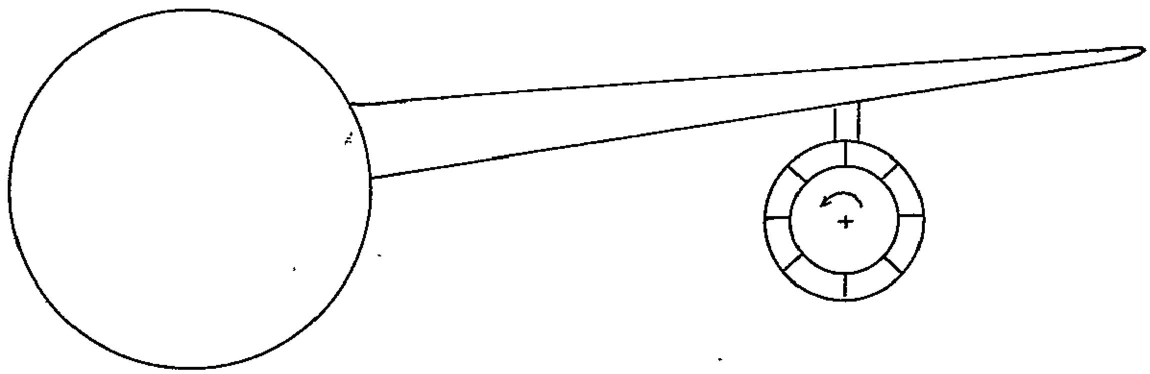

(a) Before Rotor Burst

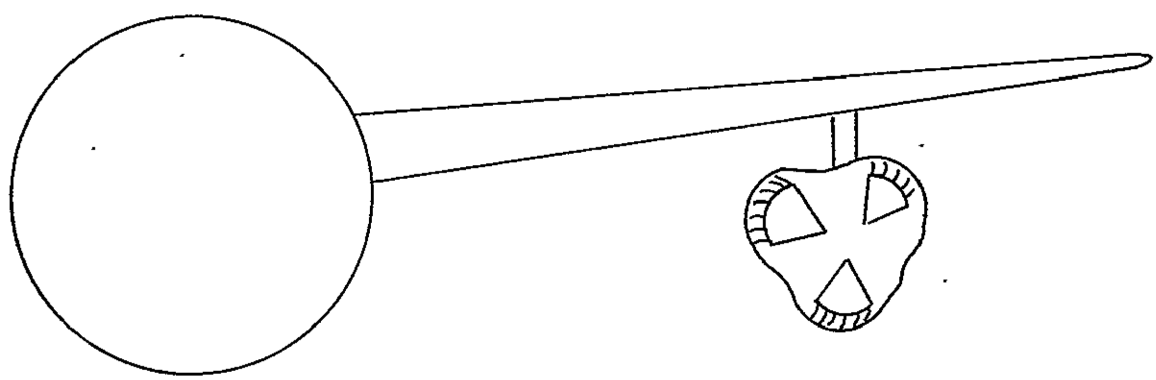

(b) After: Fragments Contained Within Casing

FIG. 1 ROTOR BURST CONTAINMENT SCHEMATIC

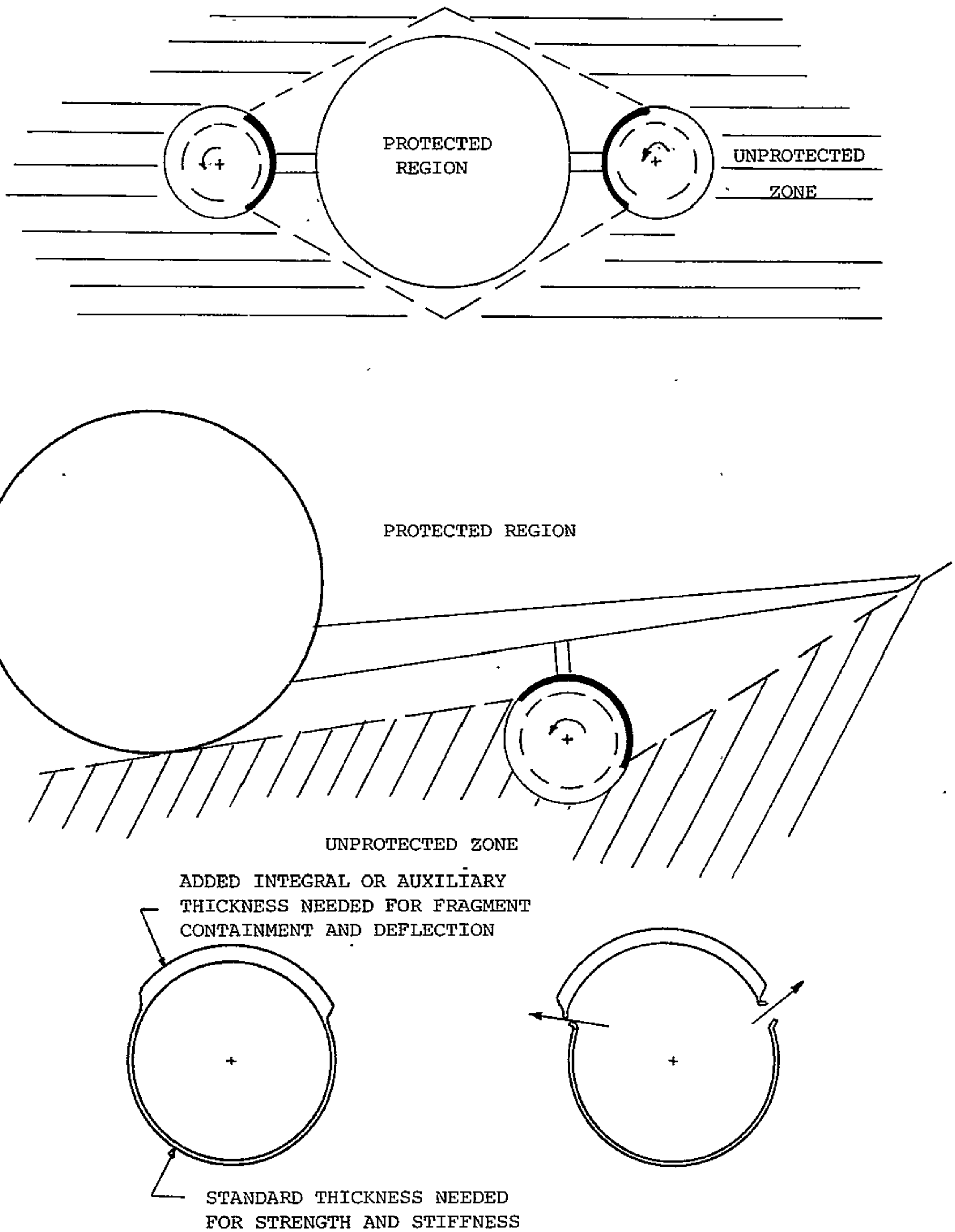

FIG. 2 SCHEMATICS OF THE ROTOR BURST FRAGMENT-DEFLECTION CONCEPT

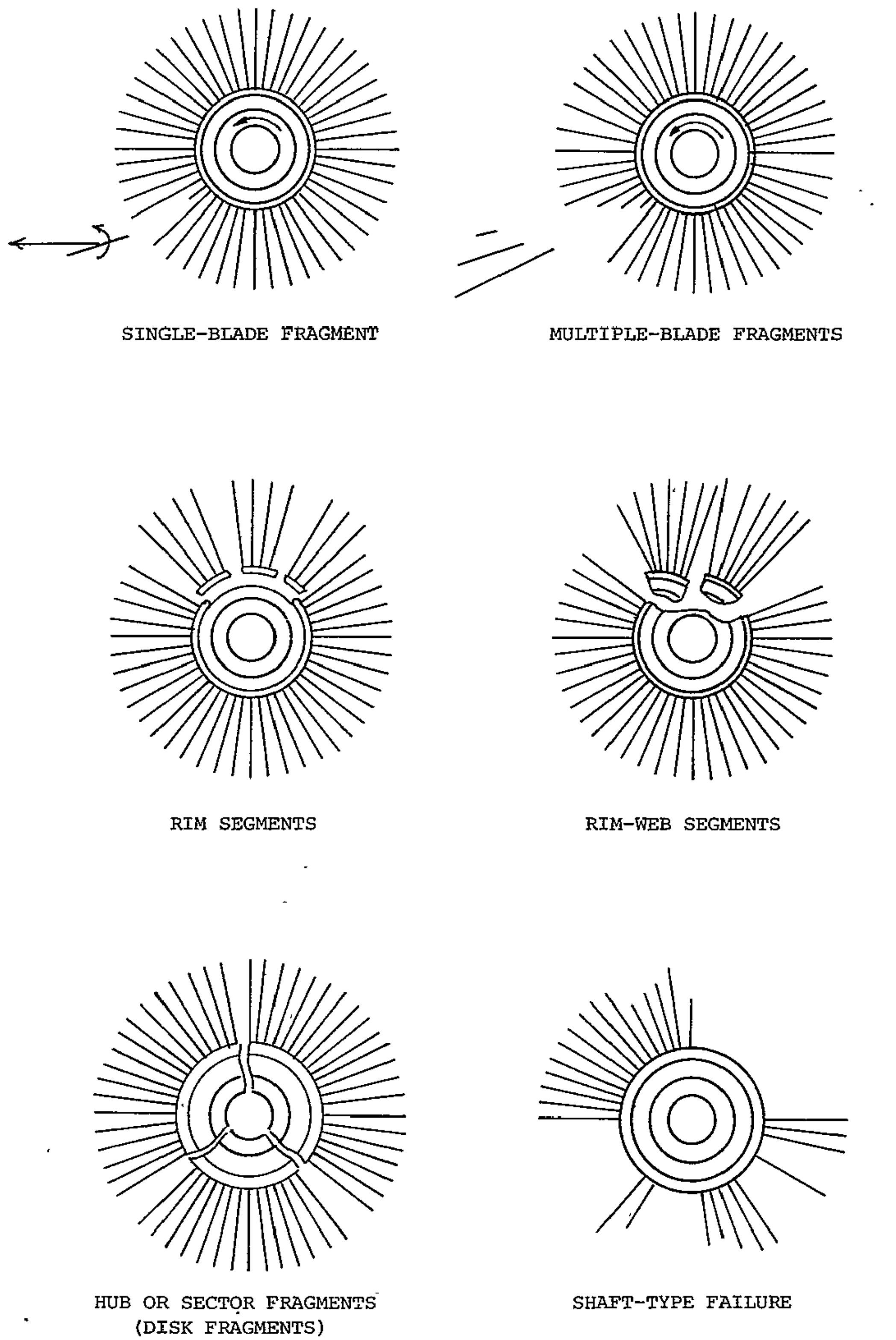

FIG. 3 SCHEMATICS OF VARIOUS TYPES OF ROTOR-BURST FRAGMENTS AND FAILURES

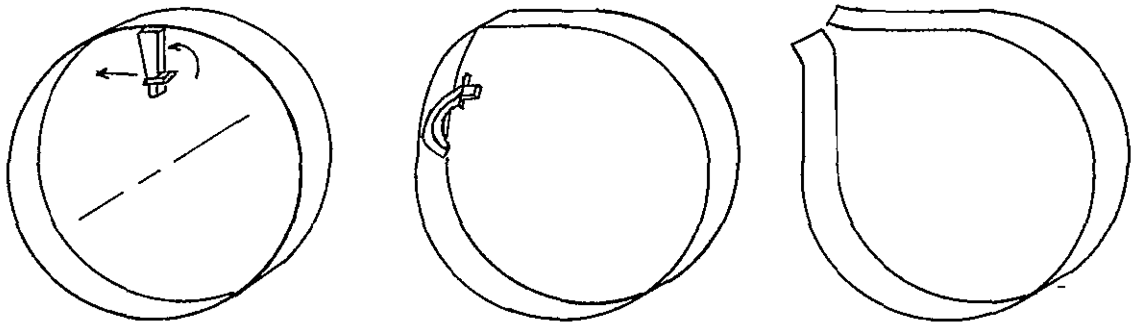

(a) 2D: Short Cylindrical Container

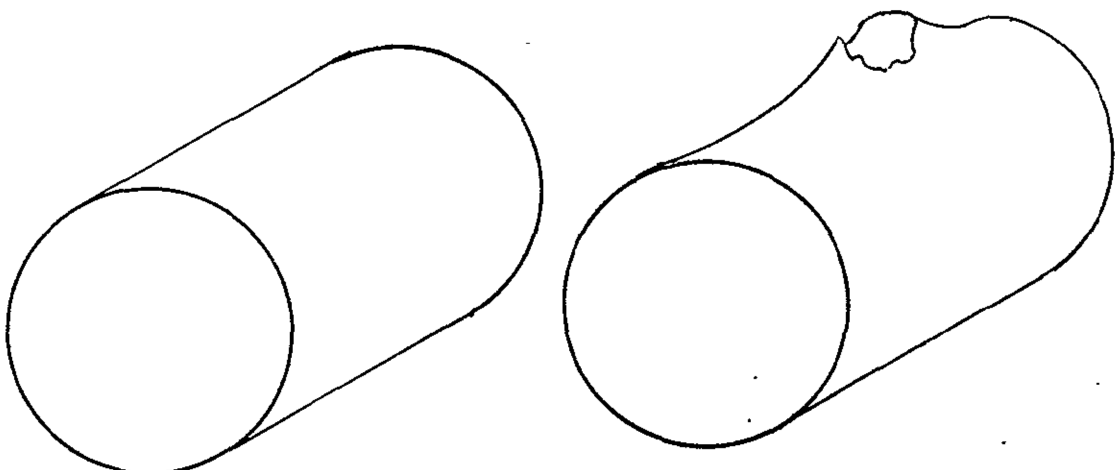

(b) 3D: Long Cylindrical Container

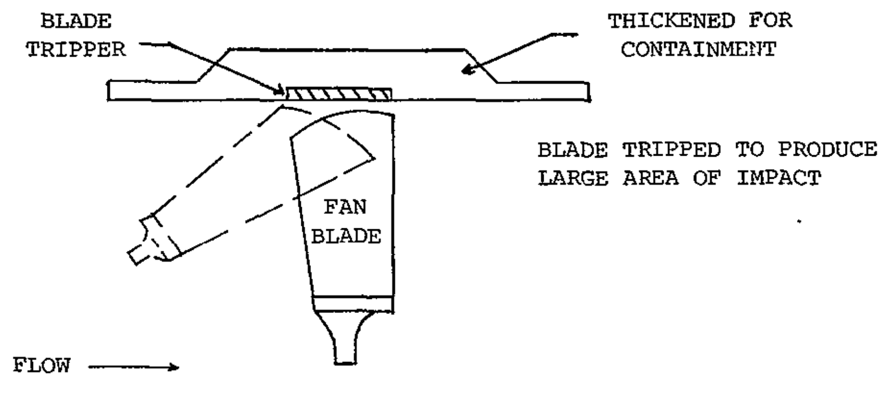

(c) Schematic Fan Blade Containment Concept

FIG. 4 SCHEMATICS OF TWO-DIMENSIONAL AND THREE-DIMENSIONAL ENGINE CASING STRUCTURAL RESPONSE TO ENGINE ROTOR FRAGMENT IMPACT

CHOICE OF TRANSIENT STRUCTURAL RESPONSE ANALYSIS METHOD

2D RINGS, BEAMS	3D SHELLS	3D SOLIDS
RESTRICTED TYPE OF DEFORMATION	MORE GENERAL DEFORMATIONS	EVEN MORE GENERAL TYPE OF DEFORMATION
INCLUDES MAIN TYPES OF EXPECTED BEHAVIOR	CAPABLE OF PHYSICALLY MORE REALISTIC SIMULATION	LIMITED NUMBER OF CONDITIONS READY FOR IMMEDIATE ANALYSIS
CALCULATIONS ARE RELATIVELY SIMPLE, SHORT, AND INEXPENSIVE	MORE COMPLEX AND EXPENSIVE TO USE	MUCH MORE EXPENSIVE TO USE
JET	PETROS, REPSIL	HEMP, HELP, STRIDE

CHOICE FOR ENGINEERING CONVENIENCE AND SIMPLICITY

PLAN OF ACTION

- USE JET, CIVM-JET, ETC. (2D CODES) FOR
  - MATERIALS SCREENING
  - PARAMETRIC CALCULATIONS
  - THICKNESS ESTIMATES FOR CONTAINERS AND DEFLECTORS: h_{2D}
- CONDUCT EXPERIMENTS TO DETERMINE THICKNESS NEEDED FOR CONTAINMENT/DEFLECTION
  - 2D SHORT STRUCTURES
  - 3D LONGER STRUCTURES → FIND MIN. REQUIRED THICKNESS: h_{OPT}
- CORRELATE 2D CALCULATIONS WITH EXPERIMENT TO FIND RULE-OF-THUMB CONVERSION FOR ESTIMATING h_{OPT}

FIG. 5 SUMMARY OF CHOICE OF TRANSIENT STRUCTURAL RESPONSE ANALYSIS METHOD AND PLAN OF ACTION FOR THE ENGINE ROTOR FRAGMENT CONTAINMENT/DEFLECTION PROBLEM

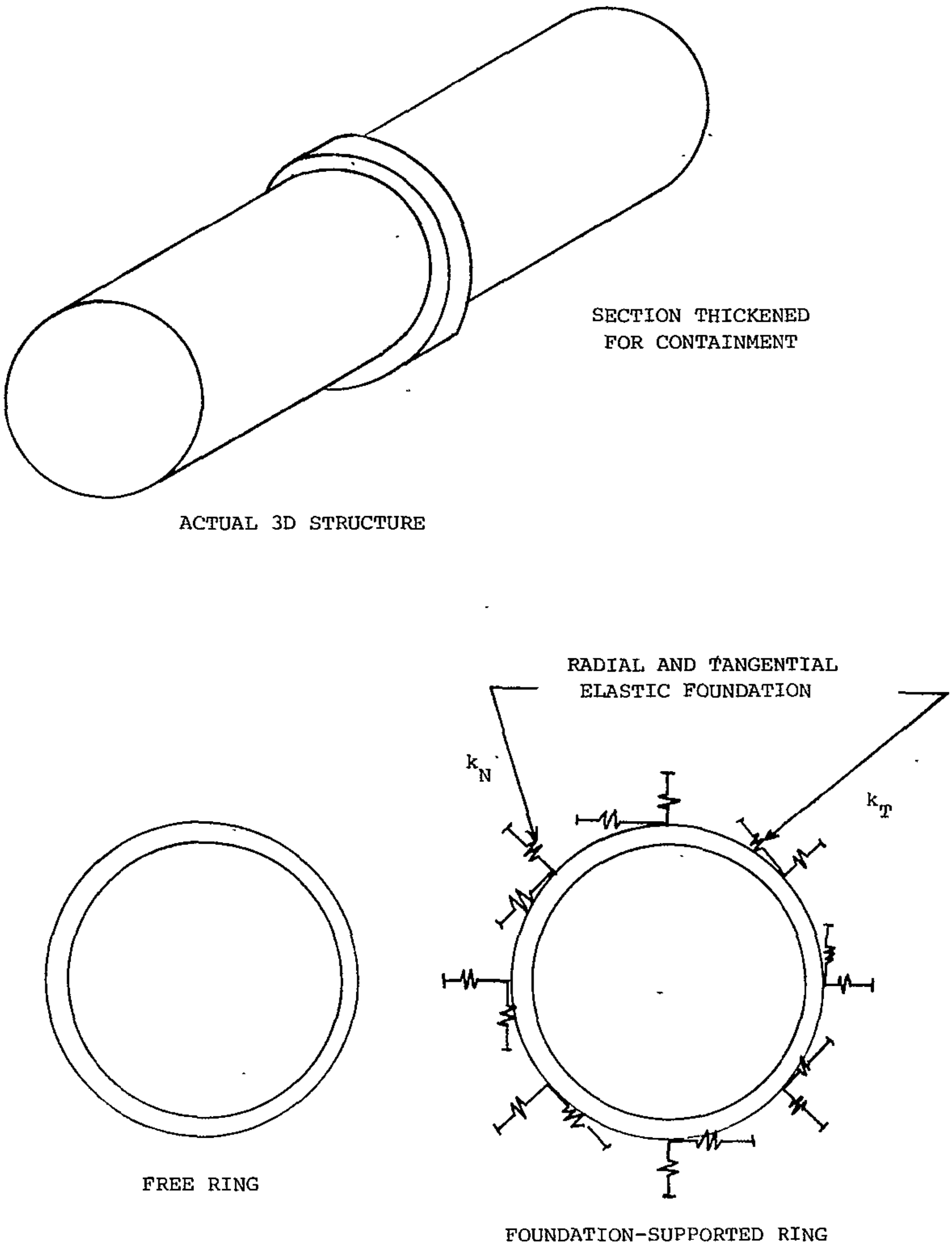

IDEALIZED 2D MODELS

FIG. 6 CONTAINMENT-STRUCTURE SCHEMATICS

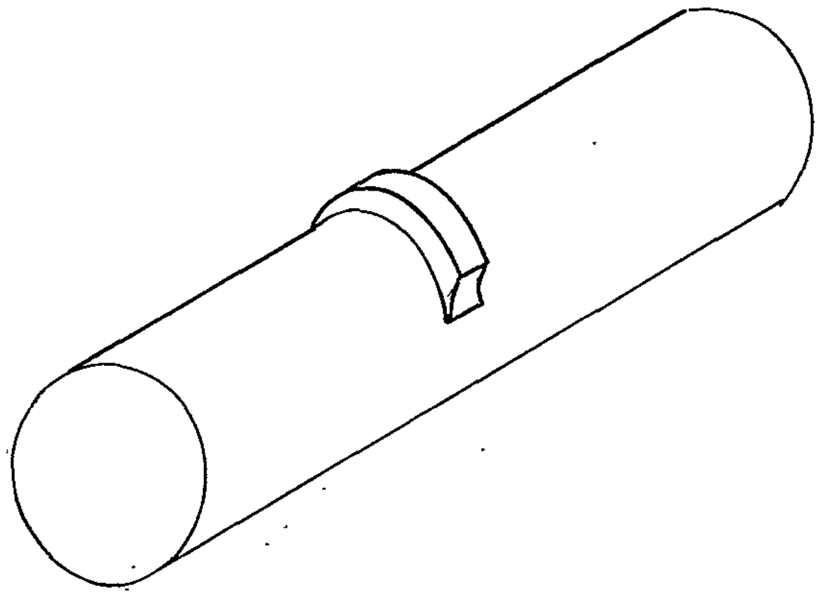

ACTUAL 3D STRUCTURE

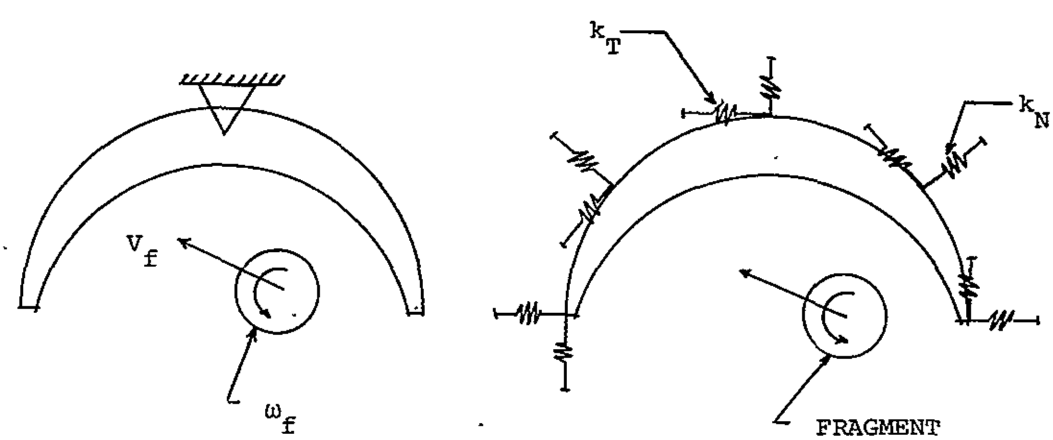

IDEALIZED 2D MODELS

FIG. 7 DEFLECTOR STRUCTURE SCHEMATICS

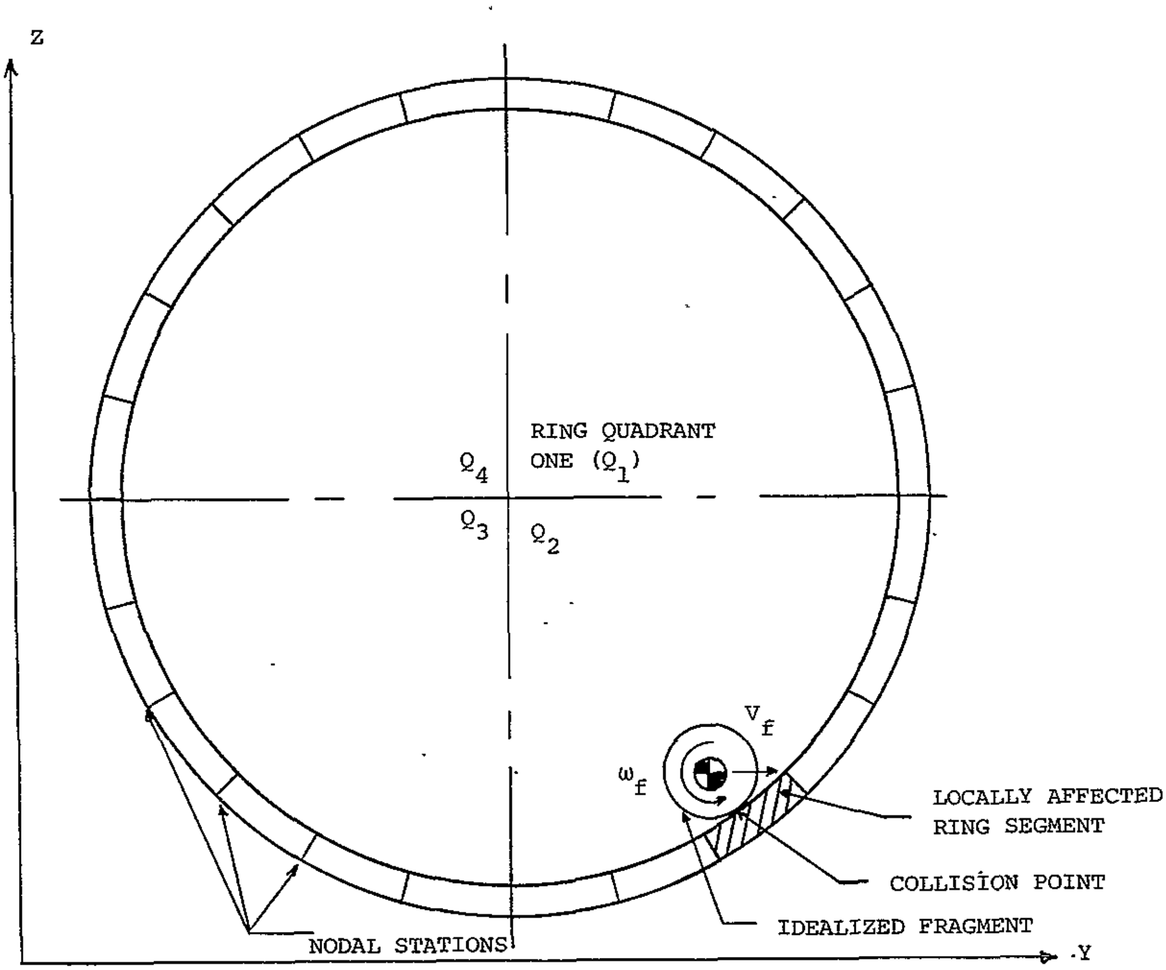

<u>NOTE</u>: Ring is divided into discrete segments (or finite elements) for analysis.

Y,Z represents a Cartesian inertial reference frame.

FIG. 8 SCHEMATIC OF A 2D CONTAINMENT RING SUBJECTED TO FRAGMENT IMPACT

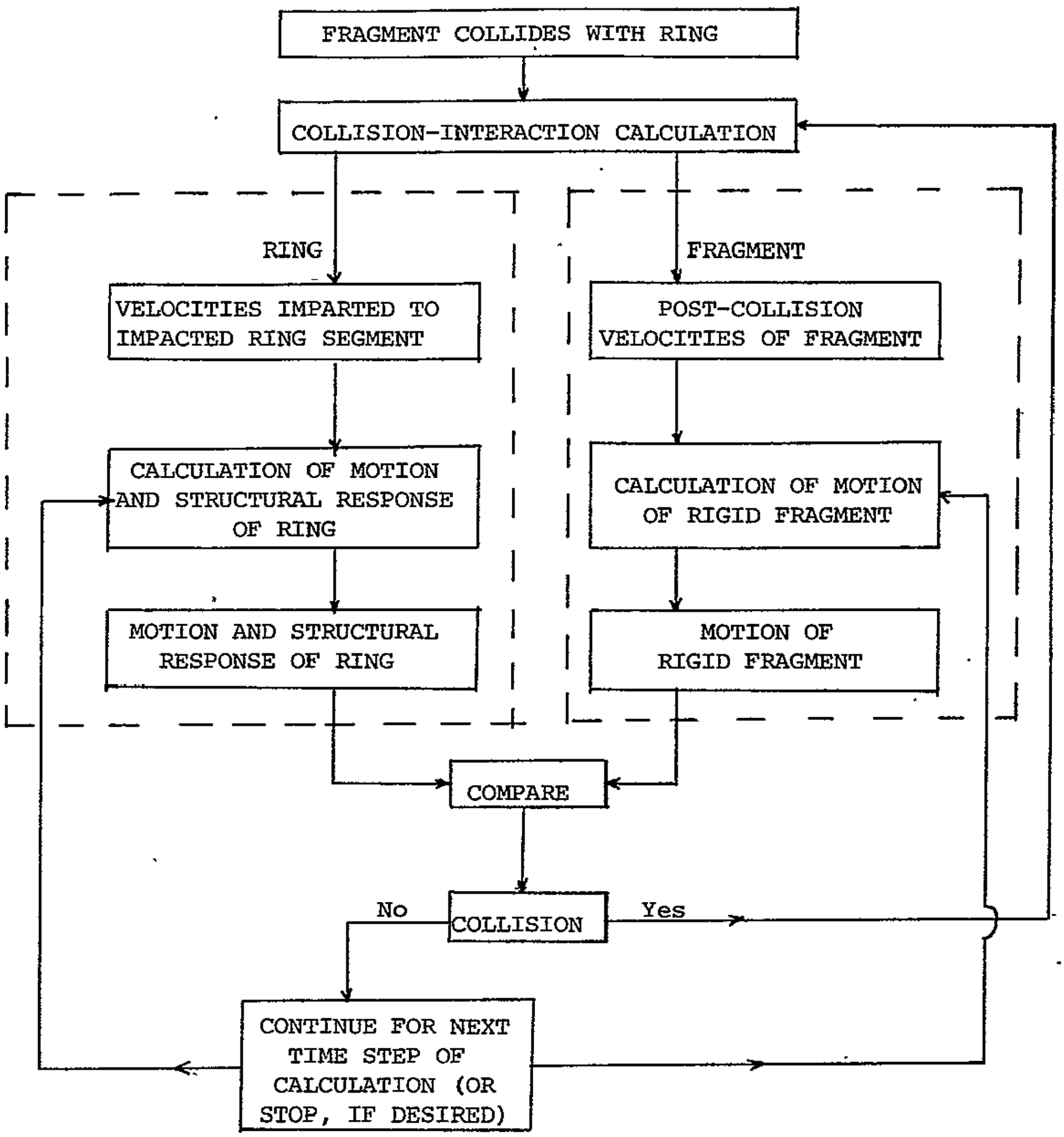

FIG. 9 INFORMATION FLOW SCHEMATIC FOR PREDICTING RING AND FRAGMENT MOTIONS IN THE COLLISION-IMPARTED VELOCITY METHOD

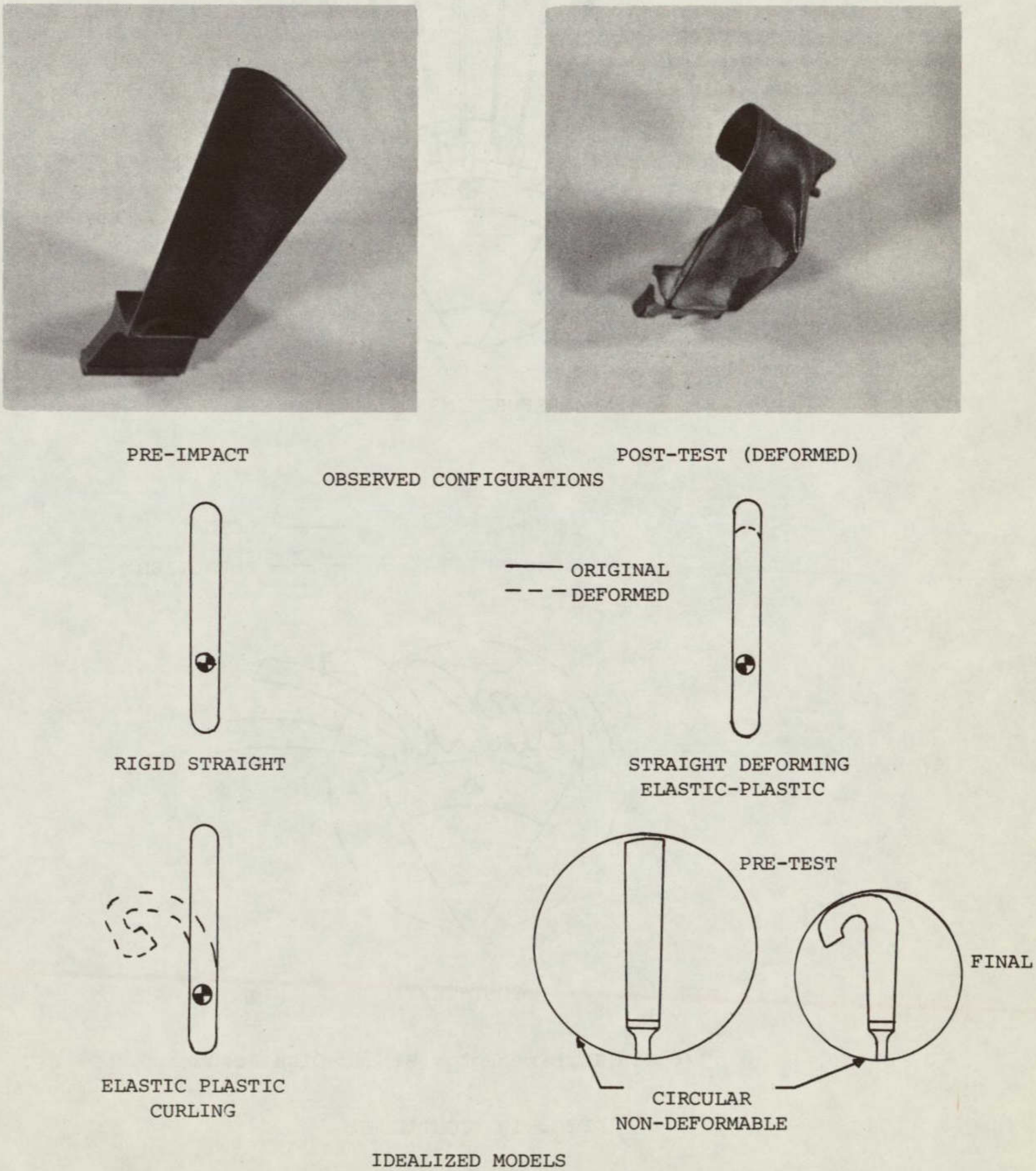

(a) Single Blade Fragment

FIG. 10 SCHEMATICS OF ACTUAL AND IDEALIZED FRAGMENTS

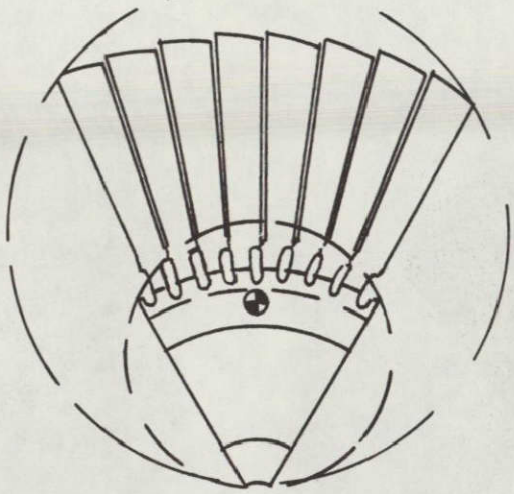

BEFORE IMPACT

——— ACTUAL

– – – IDEALIZED

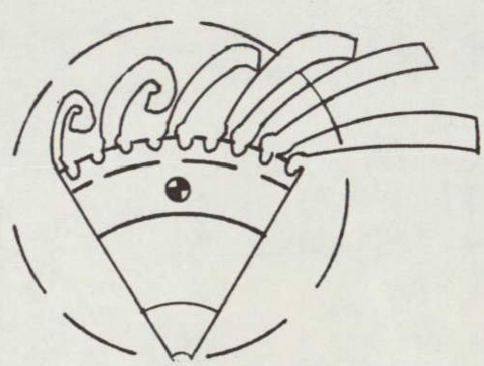

POST-TEST

(b) 1/6 T58 Turbine Rotor Bladed-Disk Fragment

FIG. 10 CONTINUED

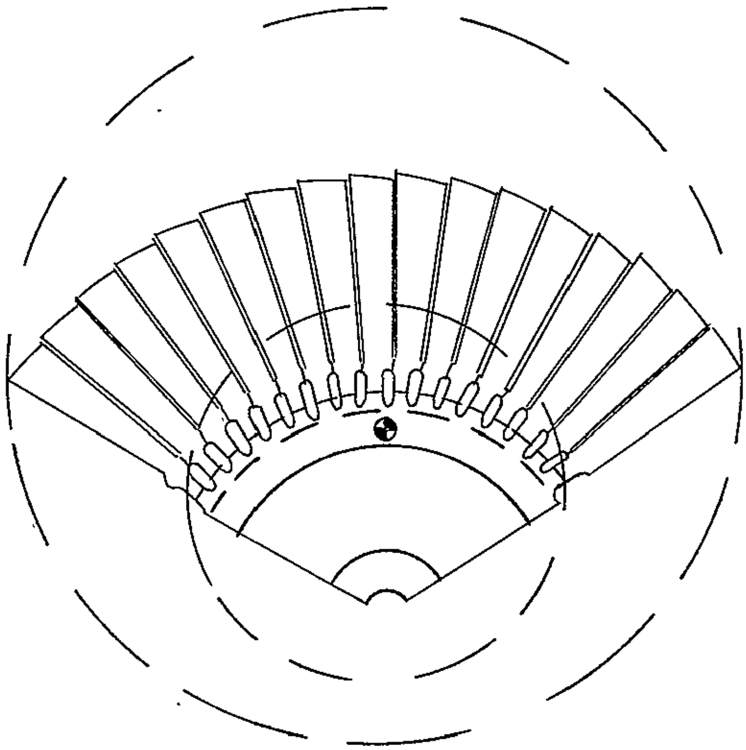

BEFORE IMPACT

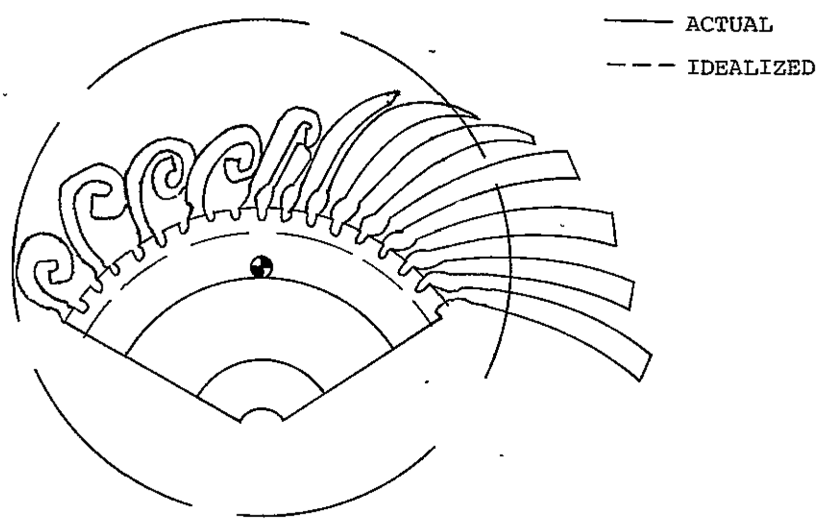

POST-TEST

(c) 1/3 T58 Turbine Rotor Bladed-Disk Fragment

FIG. 10 CONCLUDED

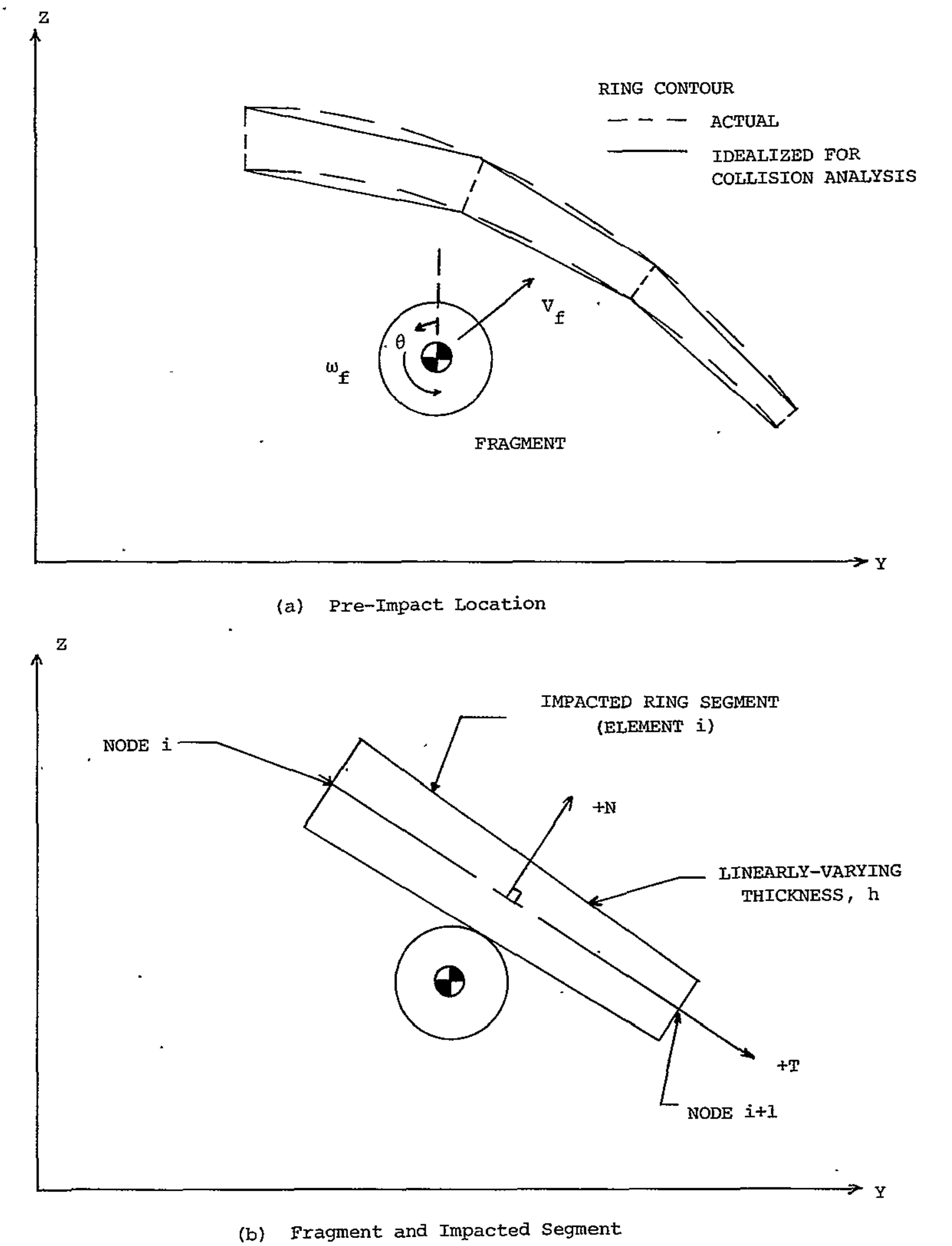

FIG. 11 IDEALIZATION OF RING CONTOUR FOR COLLISION ANALYSIS

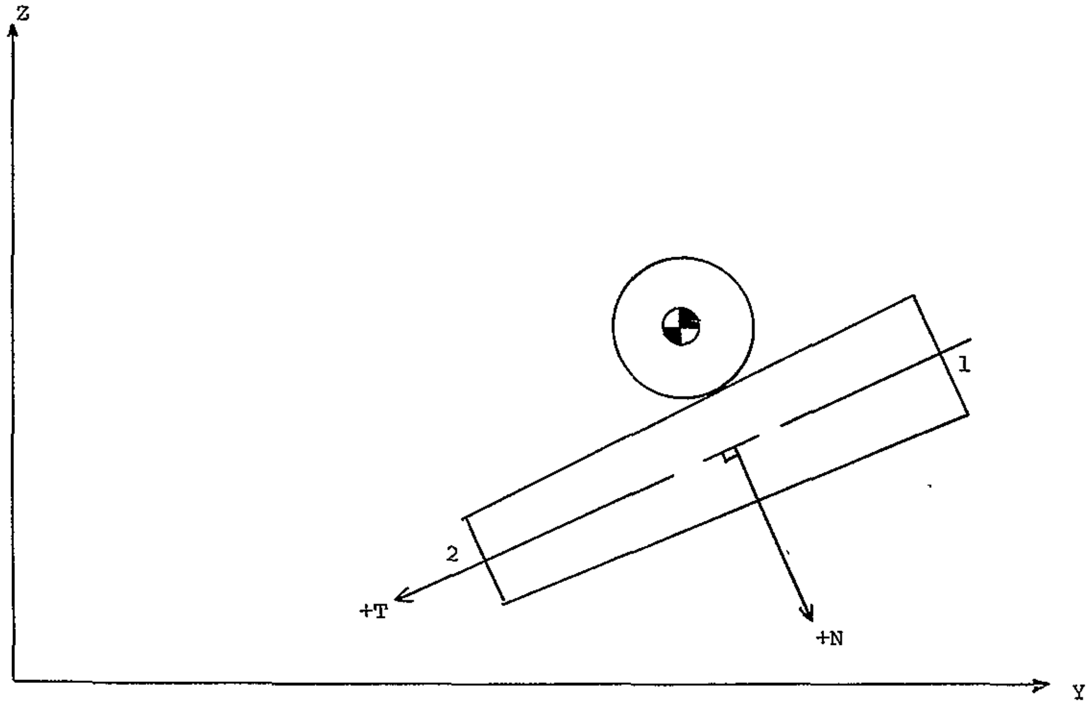

(c) Directions +N and +T

FIG. 11 CONCLUDED

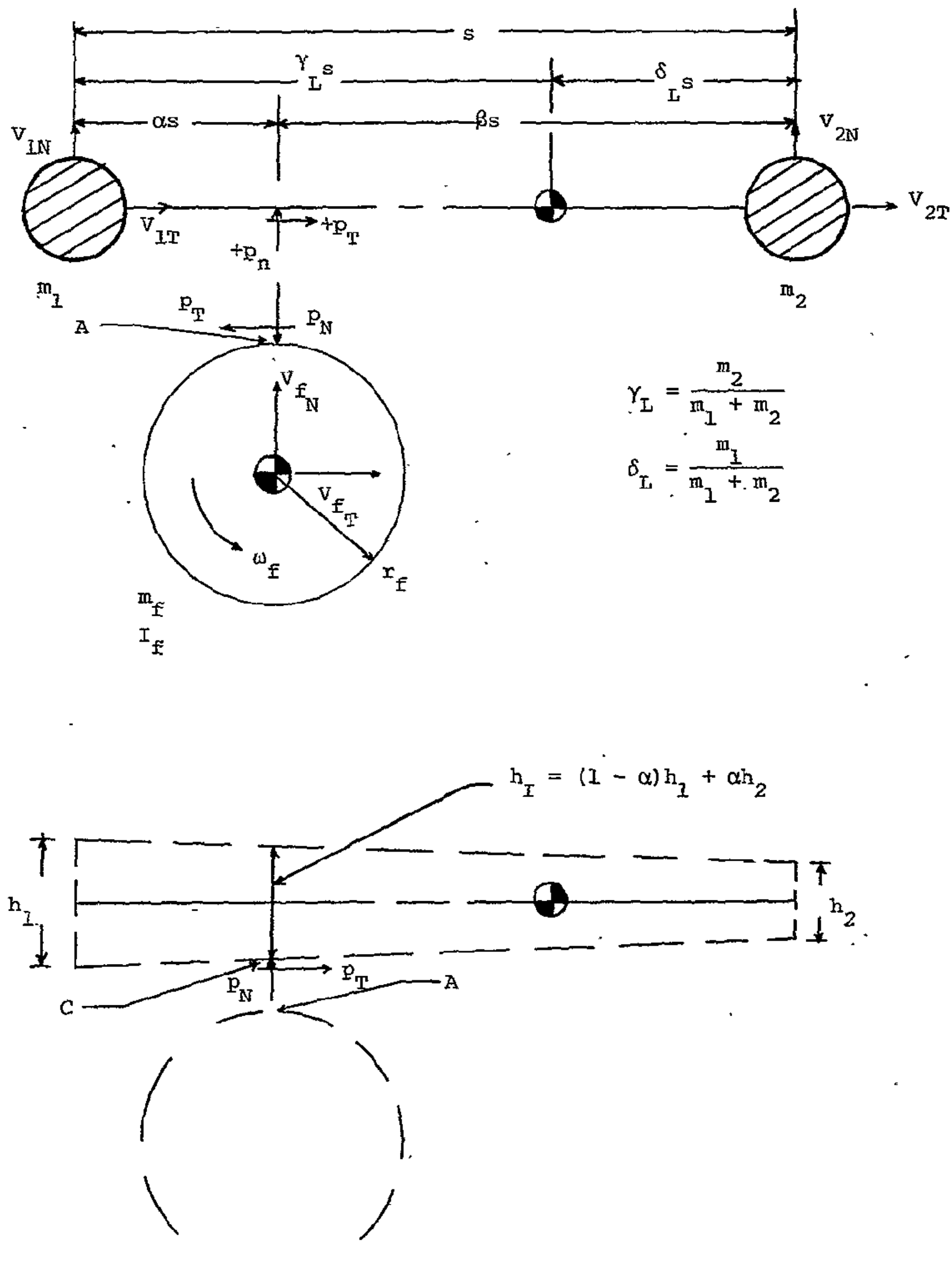

FIG. 12 EXPLODED SCHEMATIC OF THE LUMPED MASS COLLISION MODEL AT THE INSTANT OF IMPACT

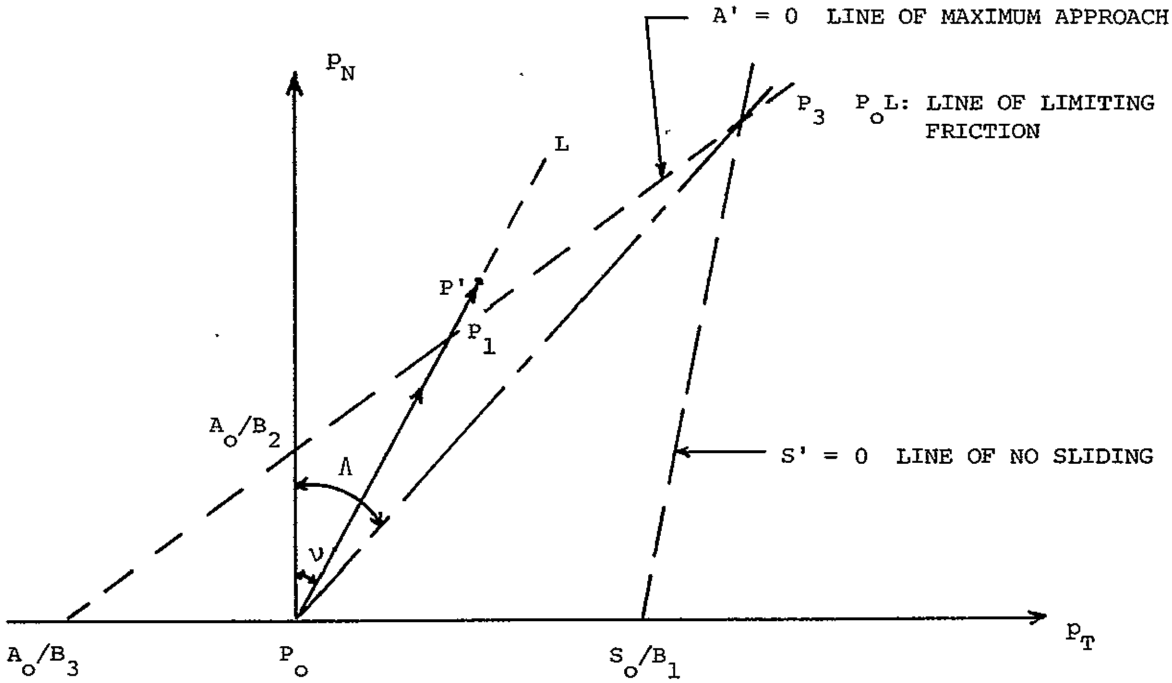

(a) $B_3 < 0, \quad \nu < \Lambda$

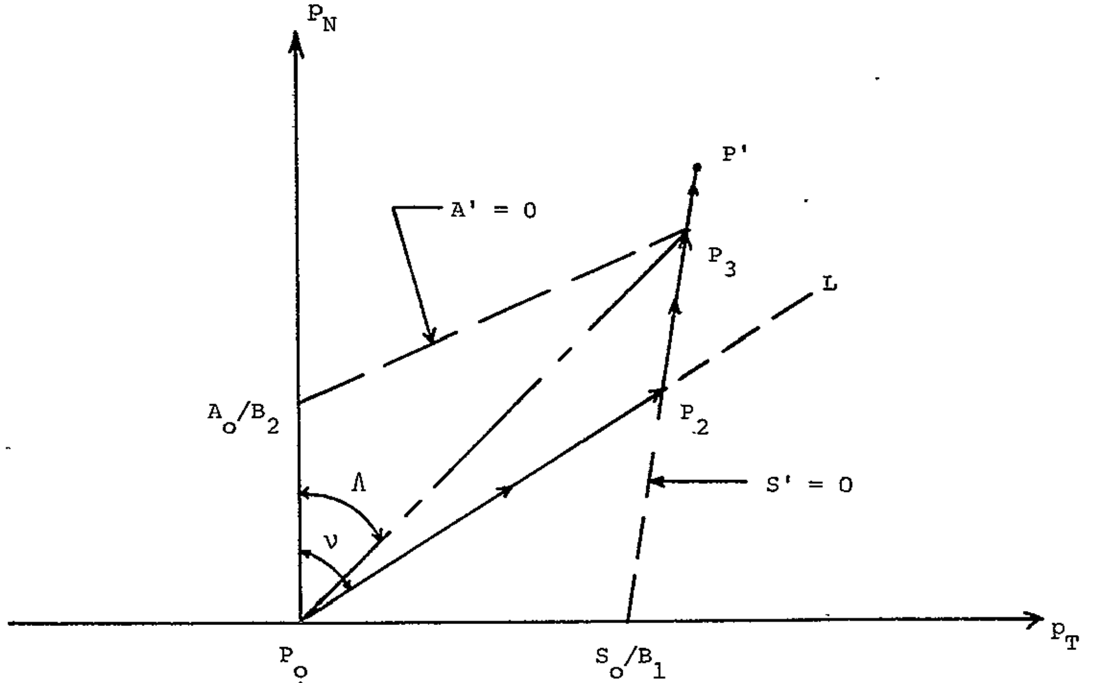

(b) $B_3 < 0, \quad \nu > \Lambda$

FIG. 13 THE TRAJECTORY OF THE IMAGE POINT $\overline{P}$ IN THE $p_N - p_T$ PLANE TO DESCRIBE THE STATE AT EACH CONTACT INSTANT FOR VARIOUS IMPACT PROCESSES

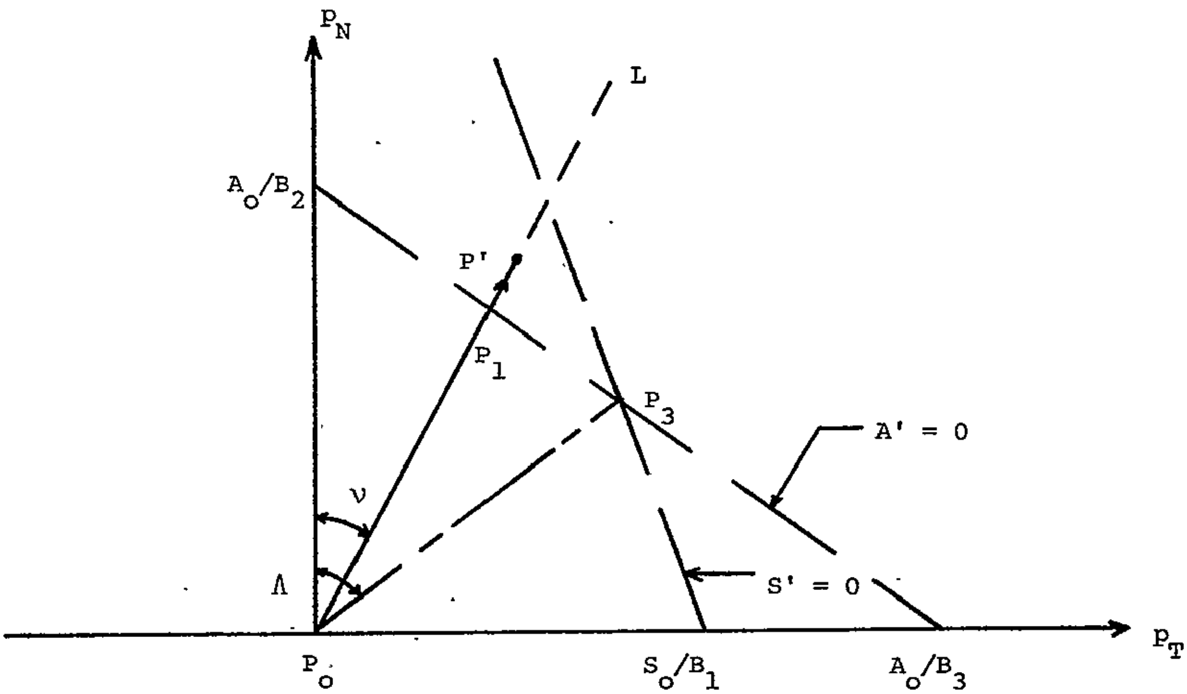

(c) $B_3 > 0, \nu < \Lambda$

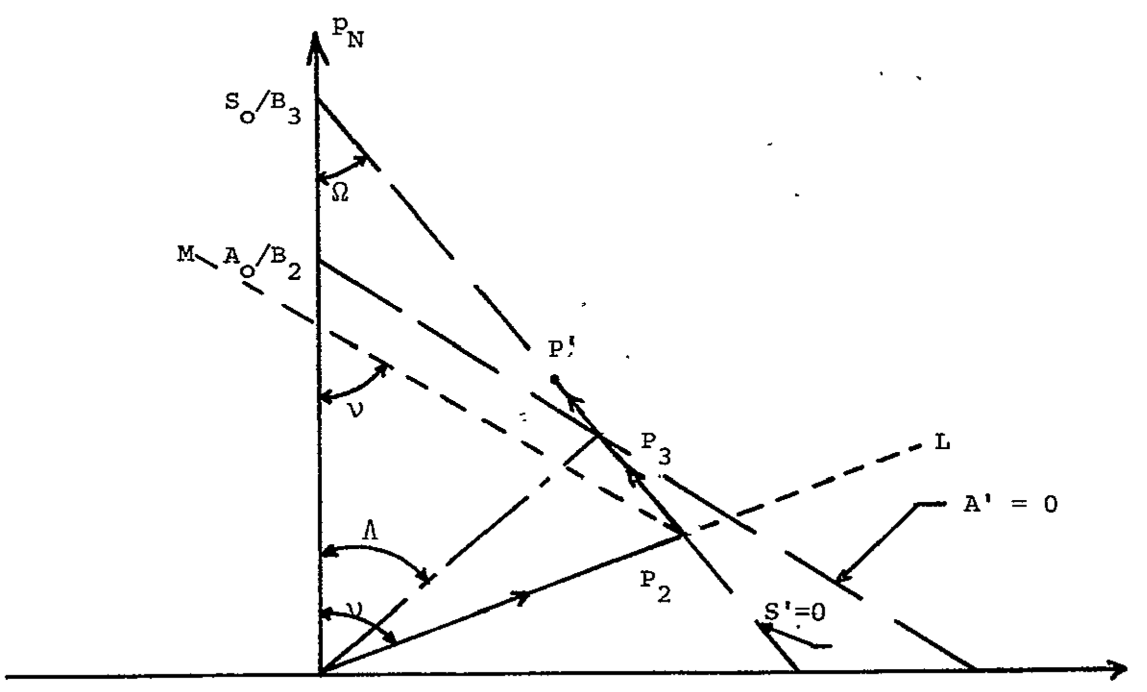

(d) $B_3 > 0, \nu > \Lambda, \nu > \Omega$

FIG. 13 CONTINUED

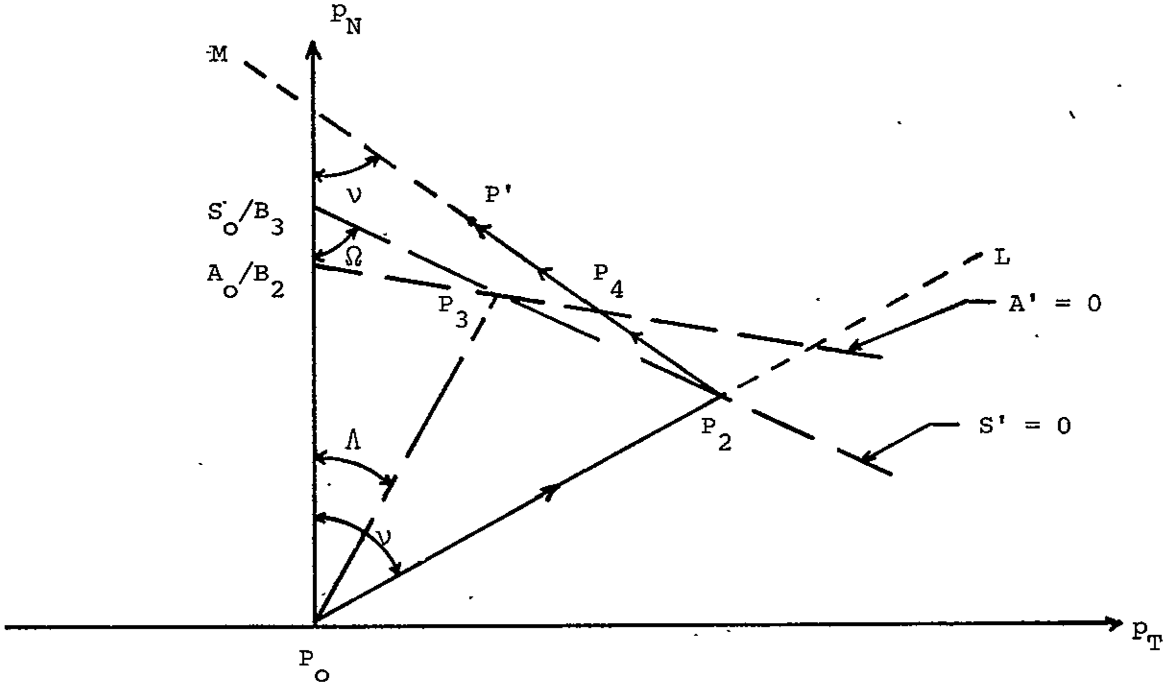

(e) $B_3 > 0$, $\nu > \Lambda$, $\nu < \Omega$

FIG. 13 CONCLUDED

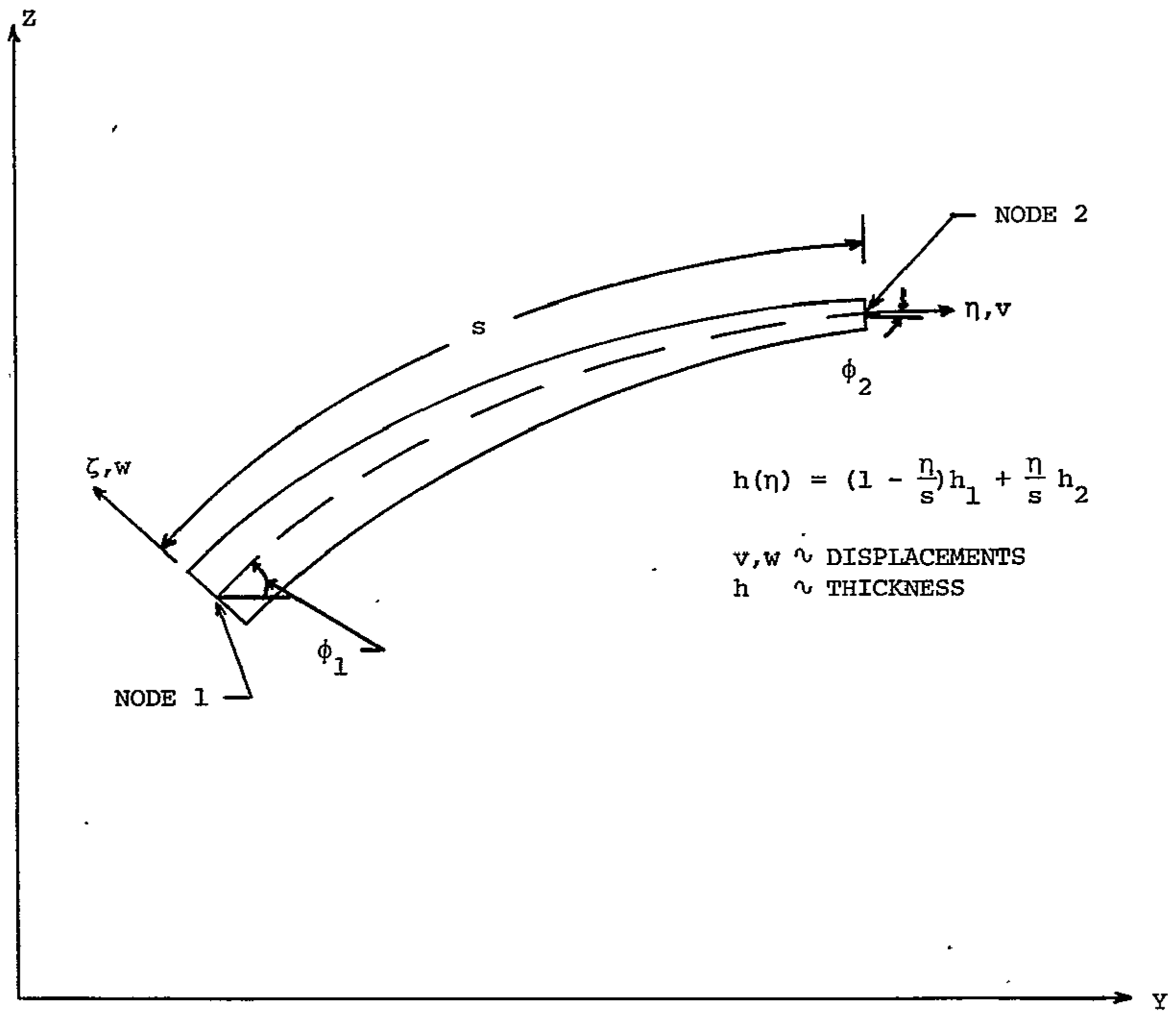

LOCAL SYSTEM		CARTESIAN REFERENCE
η, ζ	∿ COORDINATES	Y, Z ∿ COORDINATES
v, w, ψ χ	∿ DISPLACEMENTS	
q_1, ..., q_8	∿ ELEMENT GENERALIZED DISPLACEMENTS	

FIG. 14 COORDINATES, GENERALIZED DISPLACEMENTS, AND NOMENCLATURE FOR A 2D ARBITRARILY-CURVED-RING FINITE ELEMENT

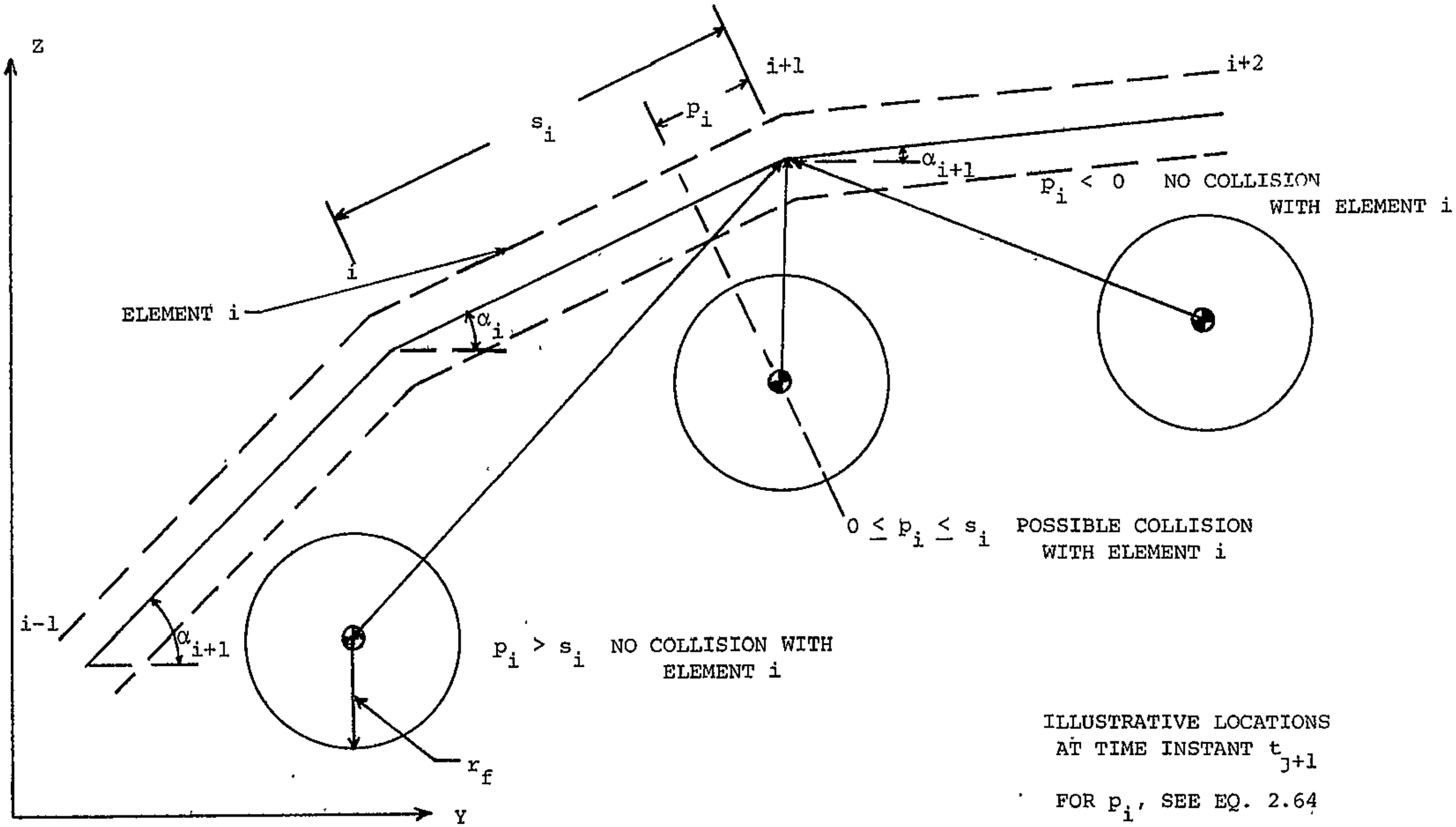

(a) Projection Inspection

FIG. 15 INSPECTION FOR DETERMINING A COLLISION OF THE FRAGMENT WITH THE RING

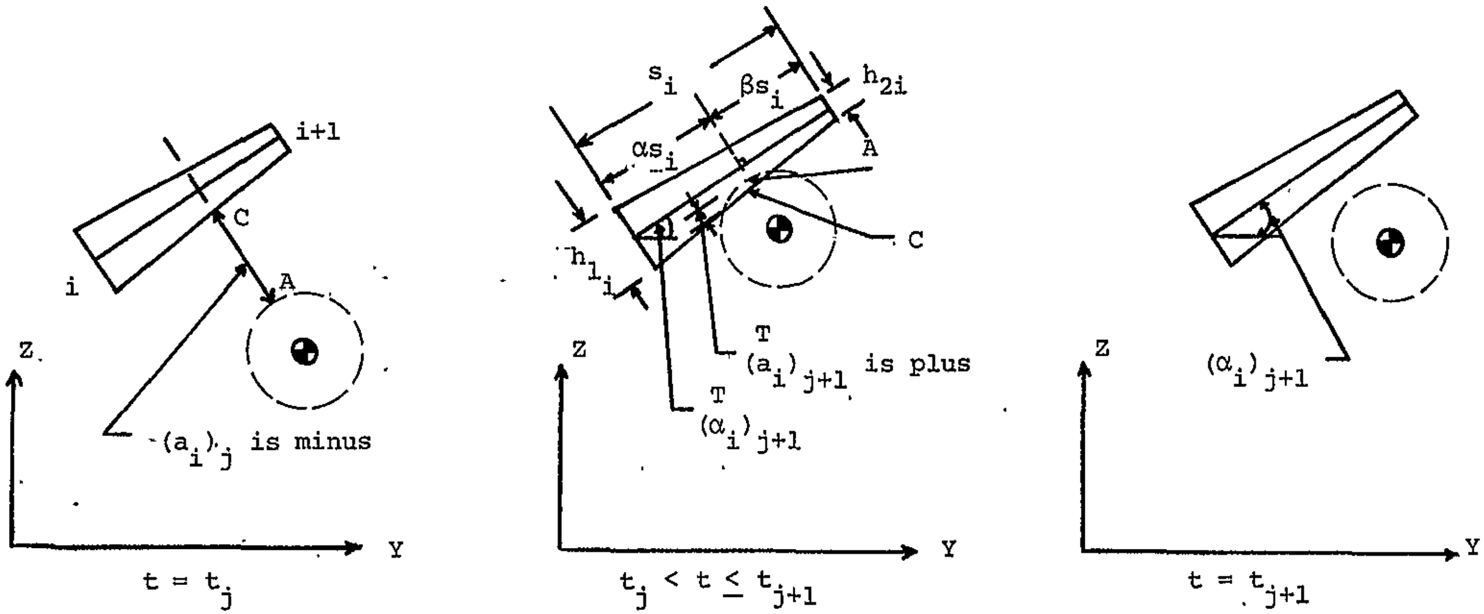

"MAXIMUM PENETRATION CONDITION"

NOTE: 1. $(p_i)^T_{j+1} = (\alpha s_i)_{j+1}$

2. $(a_i)^T_{j+1} = (V_{A_N} - V_{C_N})_j (\Delta t^*) \equiv [V_{R_i}]_j (\Delta t^*)$

Δt^* is the time interval from actual impact until t_{j+1} (see Eq. 2.68a)

(b) Penetration Inspection

FIG. 15 CONCLUDED

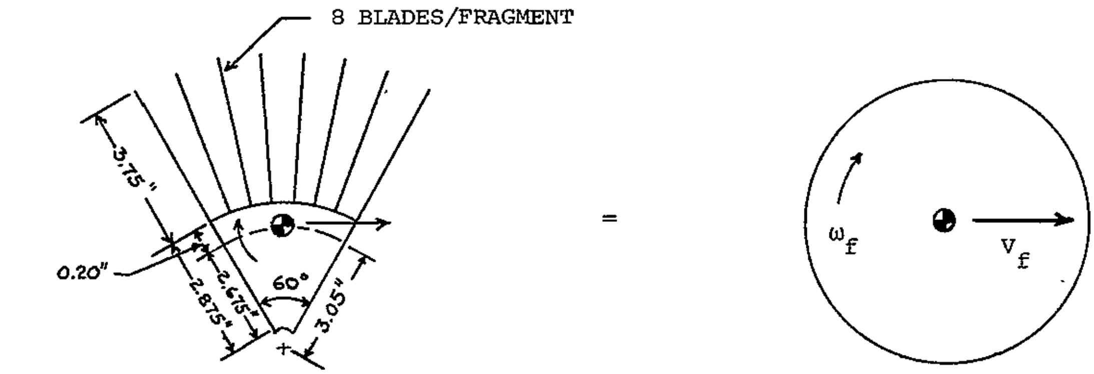

1/6 T58 TURBINE ROTOR FRAGMENT

m_f = 4.6 x 10^{-3} LB-SEC^2/IN
I_f = 2.61 x 10^{-2} LB-SEC^2-IN
ω_f = 20,000 RPM
(2100 RAD/SEC)
V_f = 6400 IN/SEC

CIRCULAR DISK IDEALIZED MODEL

m_f = 4.6 x 10^{-3} LB-SEC^2/IN
I_f = 2.61 x 10^{-2} LB-SEC^2-IN
ω_f = 20,000 RPM
(2100 RAD/SEC)
V_f = 6400 IN/SEC
r_f = 3.37 IN

(a) Circular Disk Representation of a 1/6 T58 Turbine Rotor Fragment

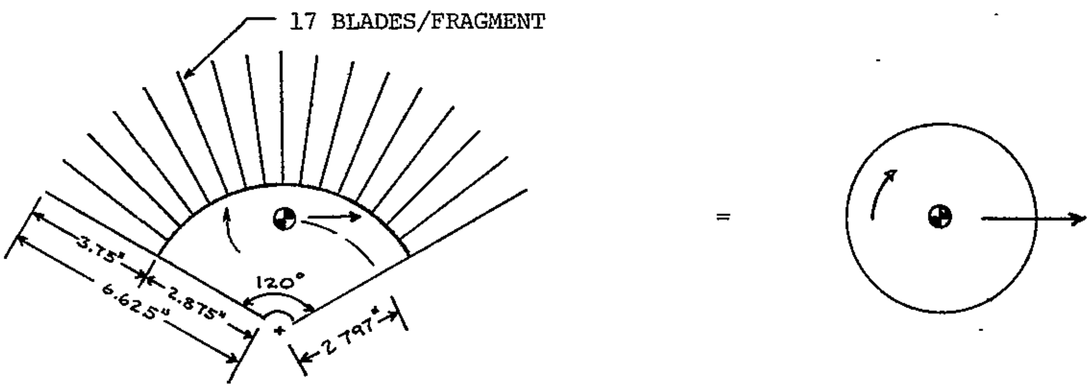

1/3 T58 TURBINE ROTOR FRAGMENT

m_f = 9.32 x 10^{-3} LB-SEC^2/IN
I_f = 6.66 x 10^{-2} LB-SEC^2-IN
ω_f = 18,830 RPM
(1972 RAD/SEC)
V_f = 5515 IN/SEC

CIRCULAR DISK IDEALIZED MODEL

m_f = 9.32 x 10^{-3} LB-SEC^2/IN
I_f = 6.66 x 10^{-2} LB-SEC^2-IN
ω_f = 18,830 RPM
(1972 RAD/SEC)
V_f = 5515 IN/SEC
r_f = 2.42 IN

(b) Circular Disk Representation of a 1/3 T58 Turbine Rotor Fragment

FIG. 16 FRAGMENT IDEALIZATIONS USED IN THE PRESENT STUDY

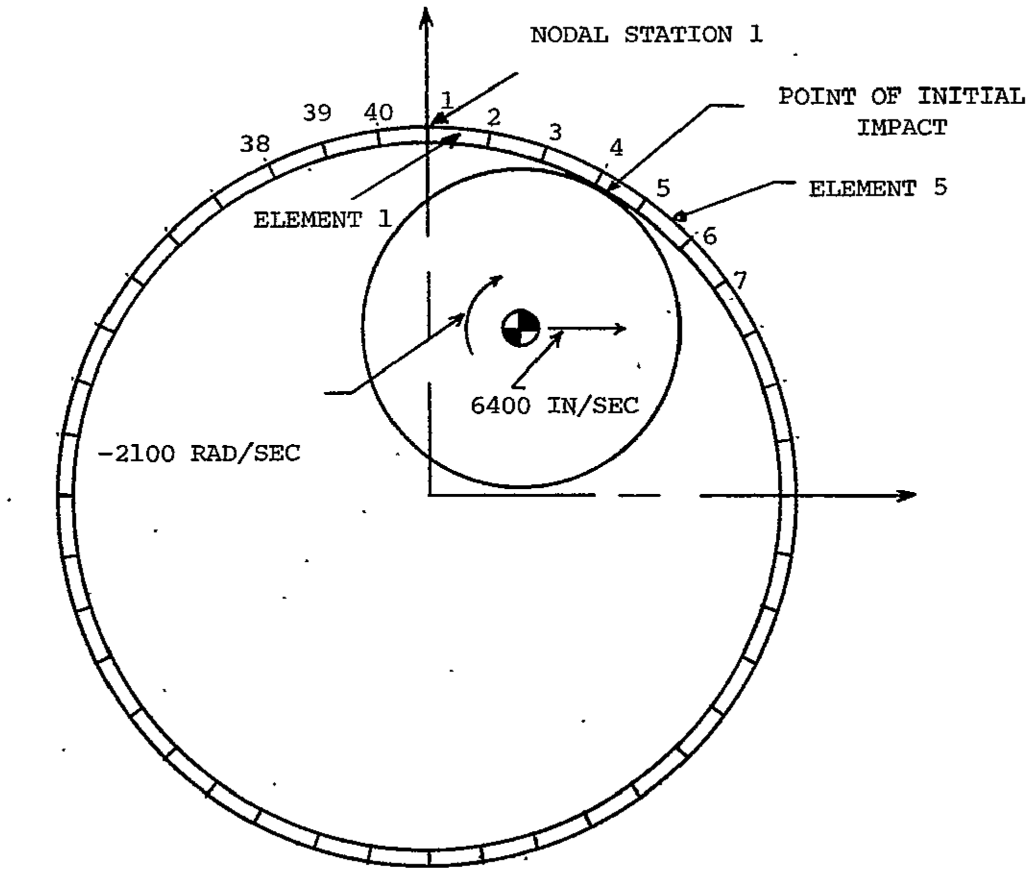

RING	FRAGMENT
4130 CAST STEEL	r_f = 3.37 in
r = 7.5 IN	$m_f = 4.6 \times 10^{-3}$ LB-SEC^2/IN
L = 2.50 IN	$I_f = 2.61 \times 10^{-2}$ LB-SEC^2-IN
h = 0.40 IN	V_f = 6400 IN/SEC
ρ = 0.283 LB/CU.IN	ω_f = - 2100 RAD/SEC

(a) Ring/Fragment Modeling and Nomenclature

FIG. 17 RING/FRAGMENT MODELING AND RESPONSE DATA FOR CONTAINMENT RINGS SUBJECTED TO SINGLE-FRAGMENT ATTACK

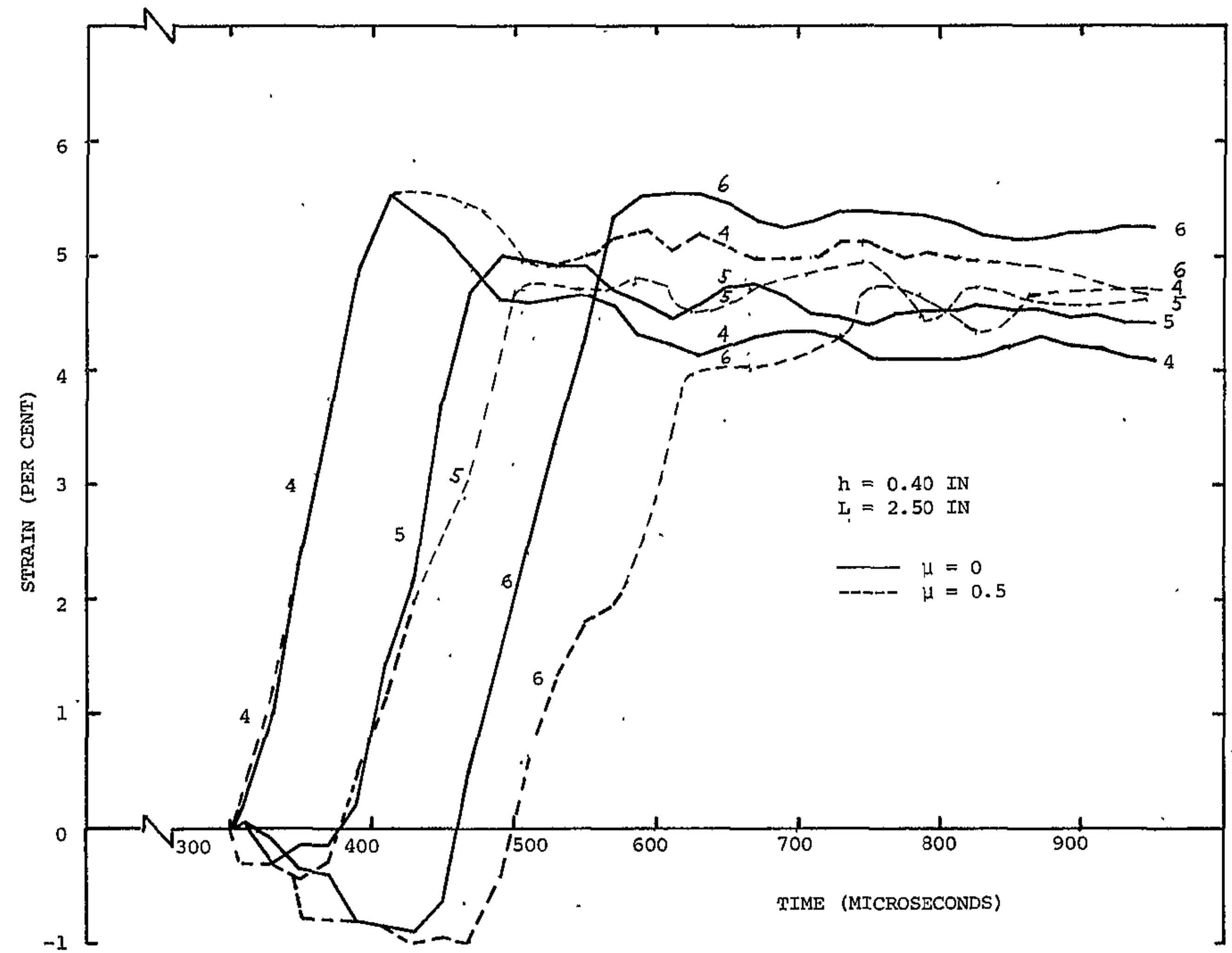

(b) Ring Element Midlength Outer Surface Circumferential Strain Histories

FIG. 17 CONTINUED

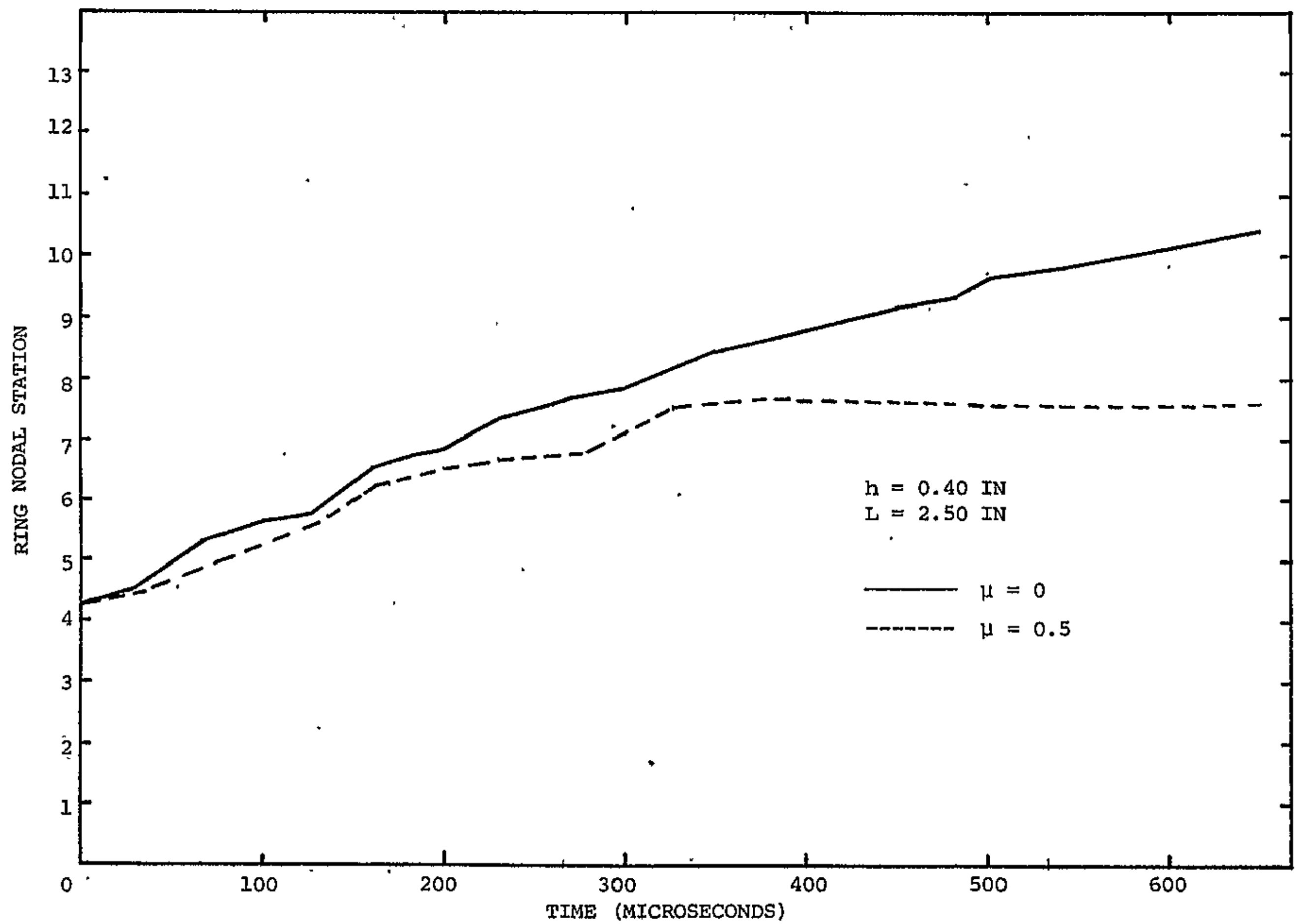

(c) Fragment Impact Position as a Function of Time After Initial Impact for Frictional and Frictionless Impact Cases for a Ring of Constant Thickness

FIG. 17 CONTINUED

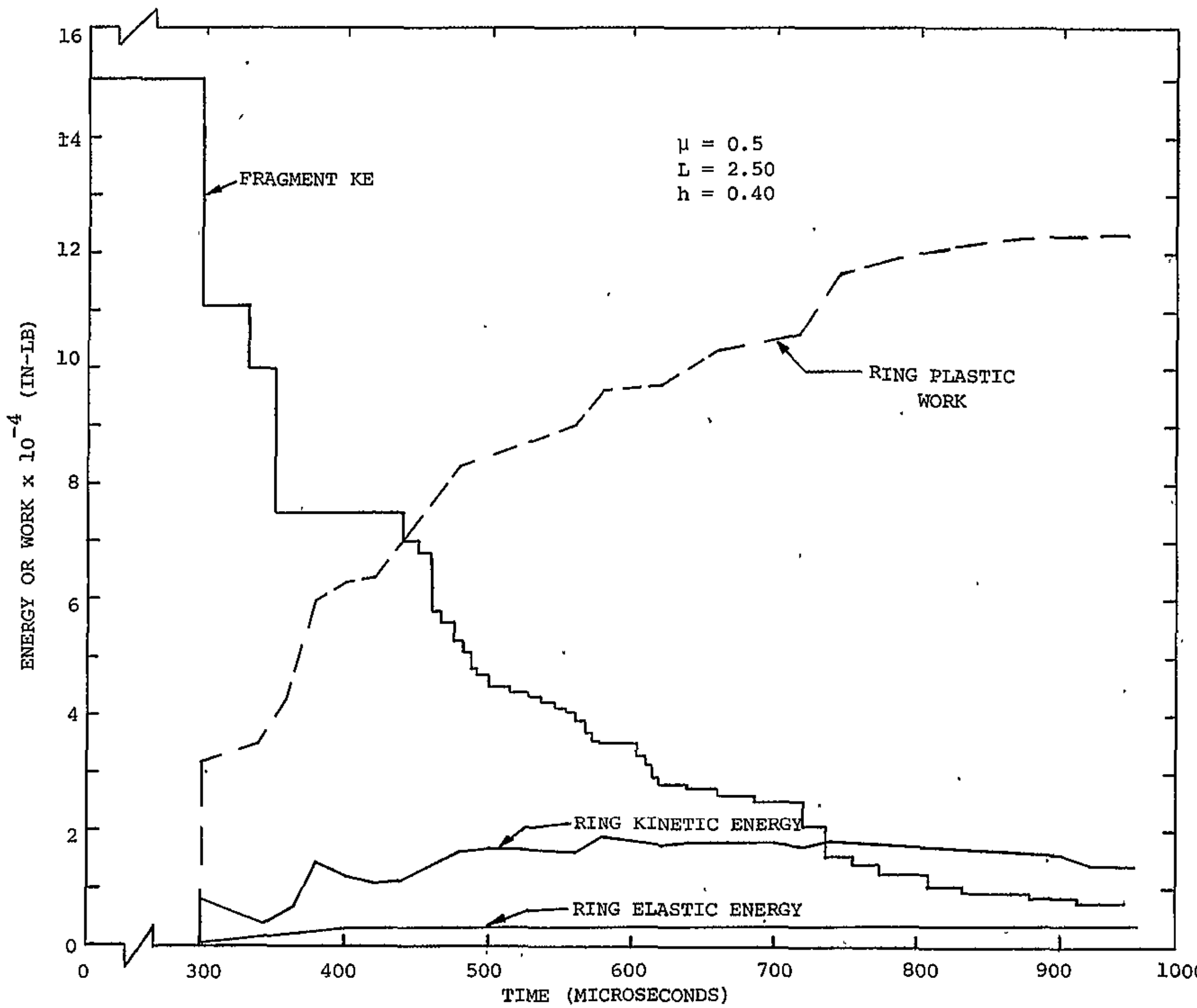

(d) Illustration of the Time Histories of Fragment Kinetic Energy, and Containment Ring Elastic Energy, Kinetic Energy, and Plastic Work

FIG. 17 CONCLUDED

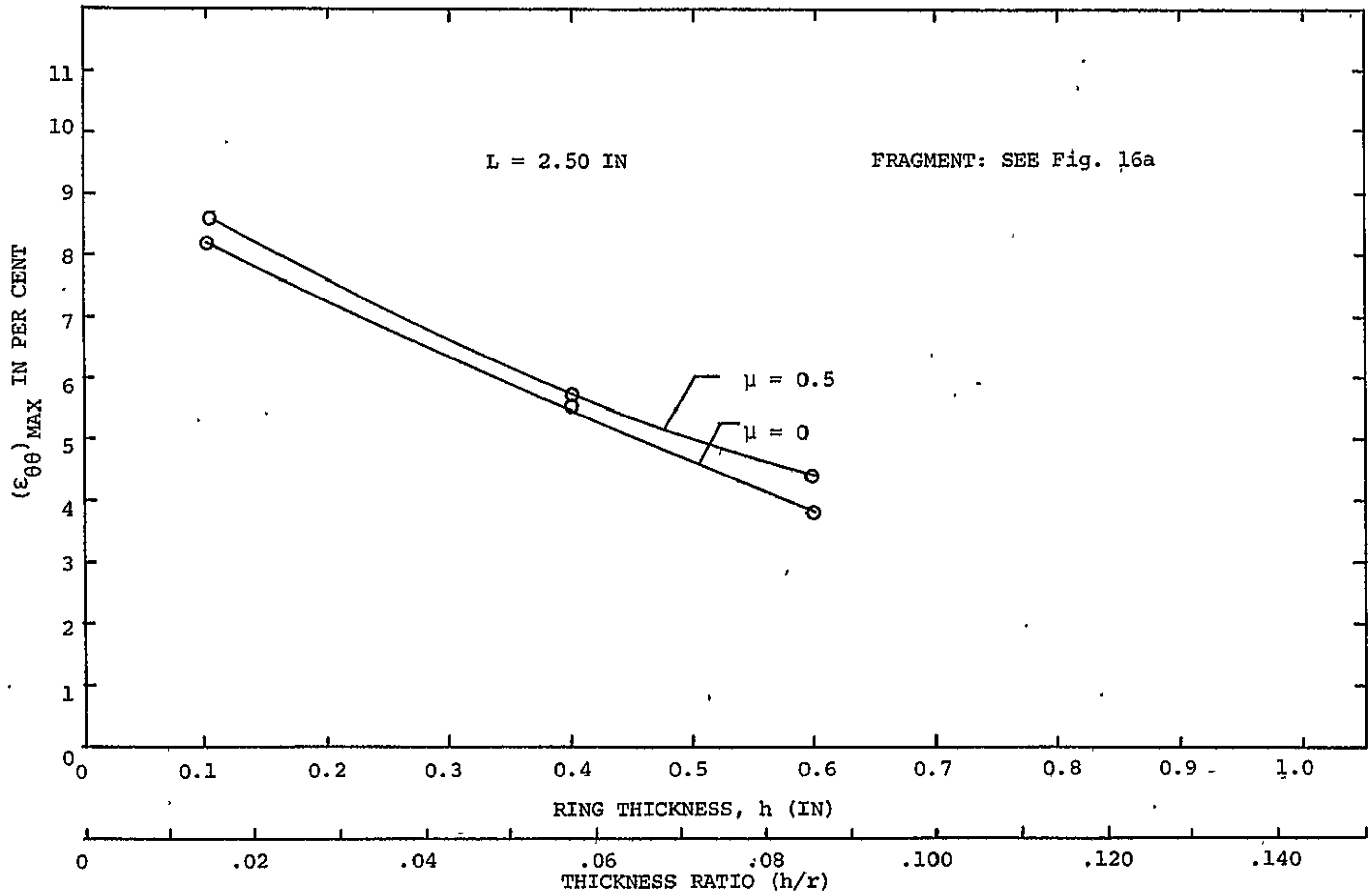

FIG. 18 EFFECT OF FRICTION ON THE PREDICTED MAXIMUM CIRCUMFERENTIAL STRAIN PRODUCED ON 4130 CAST STEEL CONTAINMENT RINGS BY SINGLE FRAGMENT IMPACT

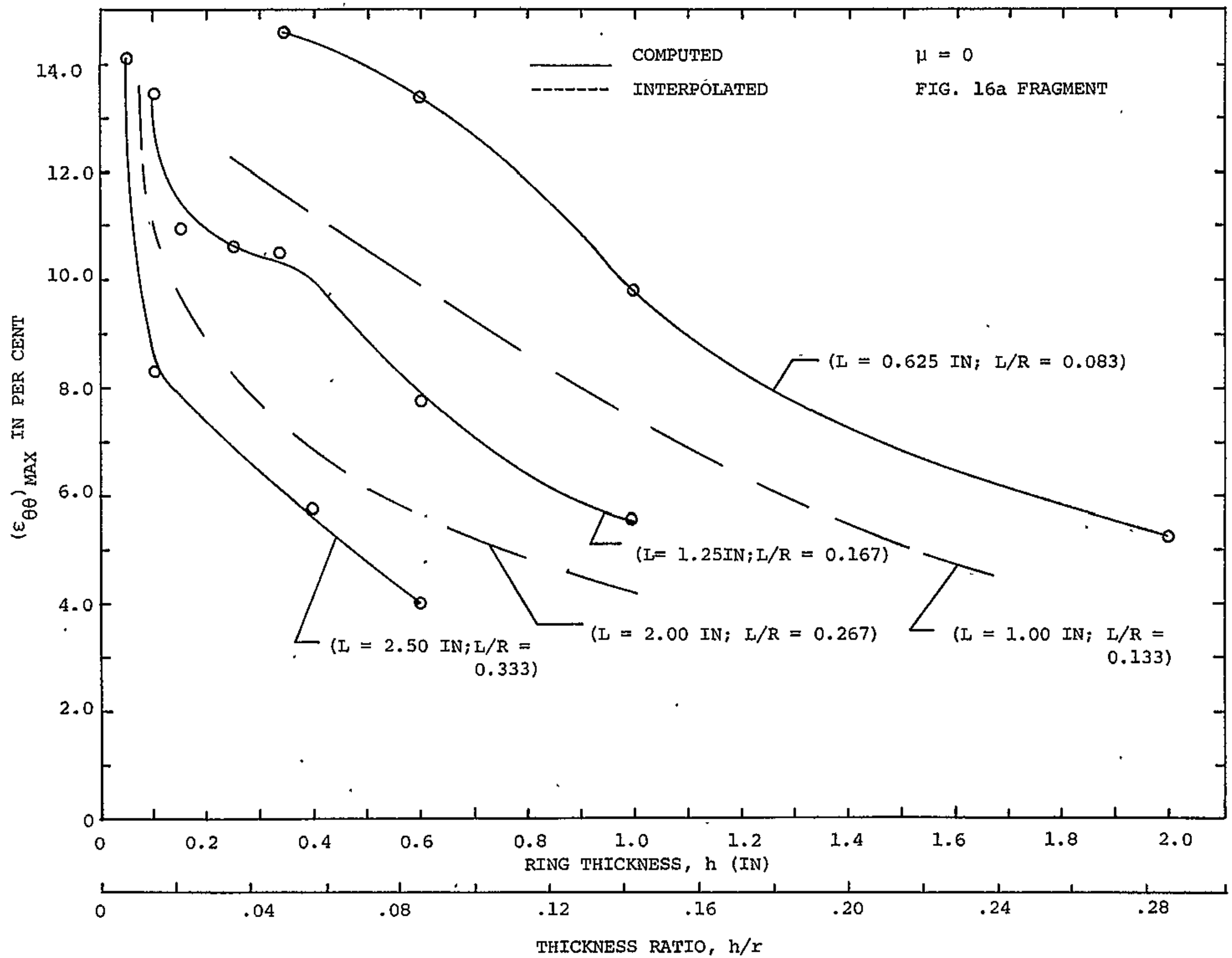

FIG. 19 PREDICTED MAXIMUM CIRCUMFERENTIAL STRAIN FOR SINGLE FRAGMENT ATTACK AS A FUNCTION OF RING THICKNESS FOR FIXED RING AXIAL LENGTHS

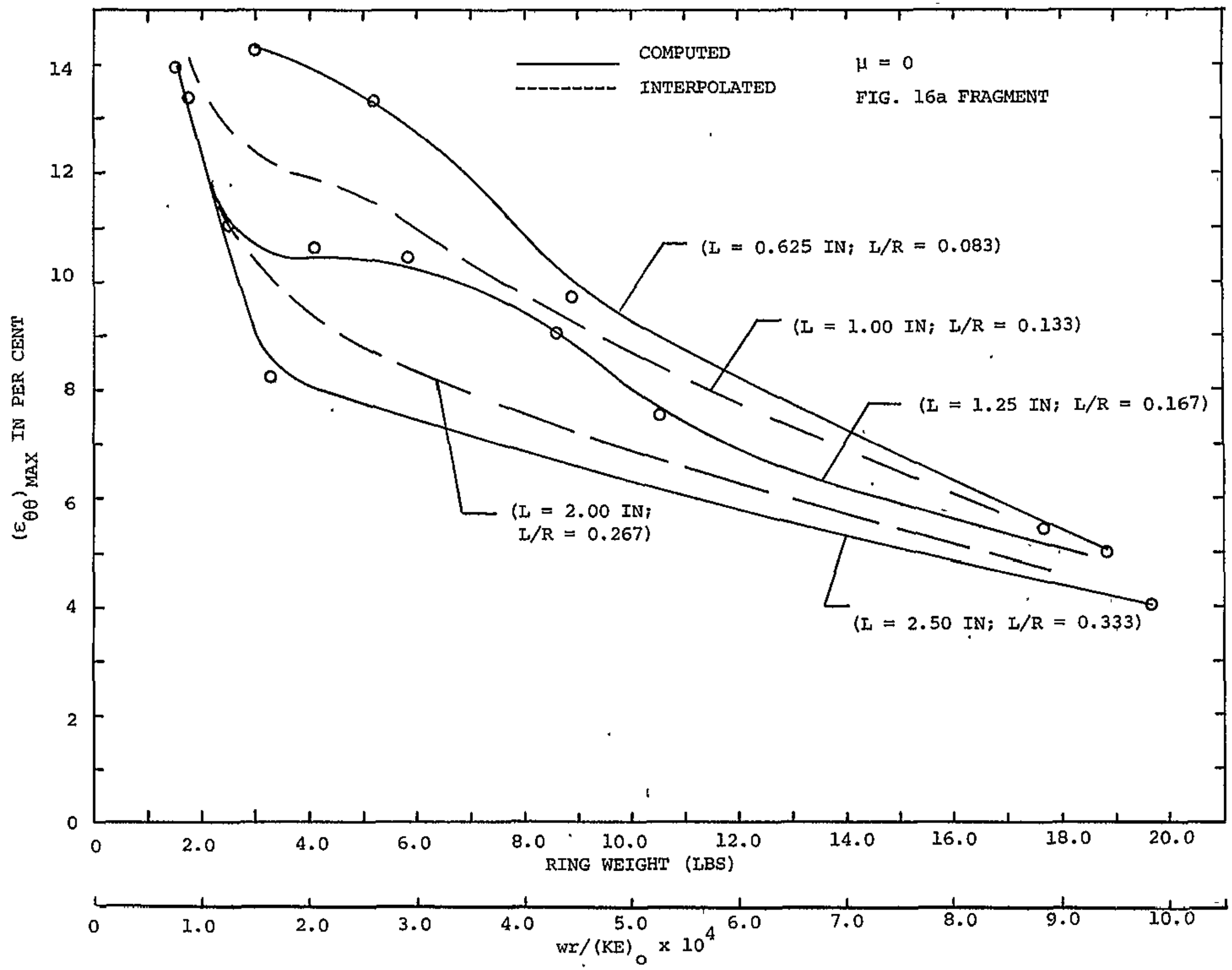

FIG. 20 PREDICTED MAXIMUM CIRCUMFERENTIAL STRAIN FOR SINGLE FRAGMENT ATTACK AS A FUNCTION OF RING WEIGHT FOR FIXED RING AXIAL LENGTHS

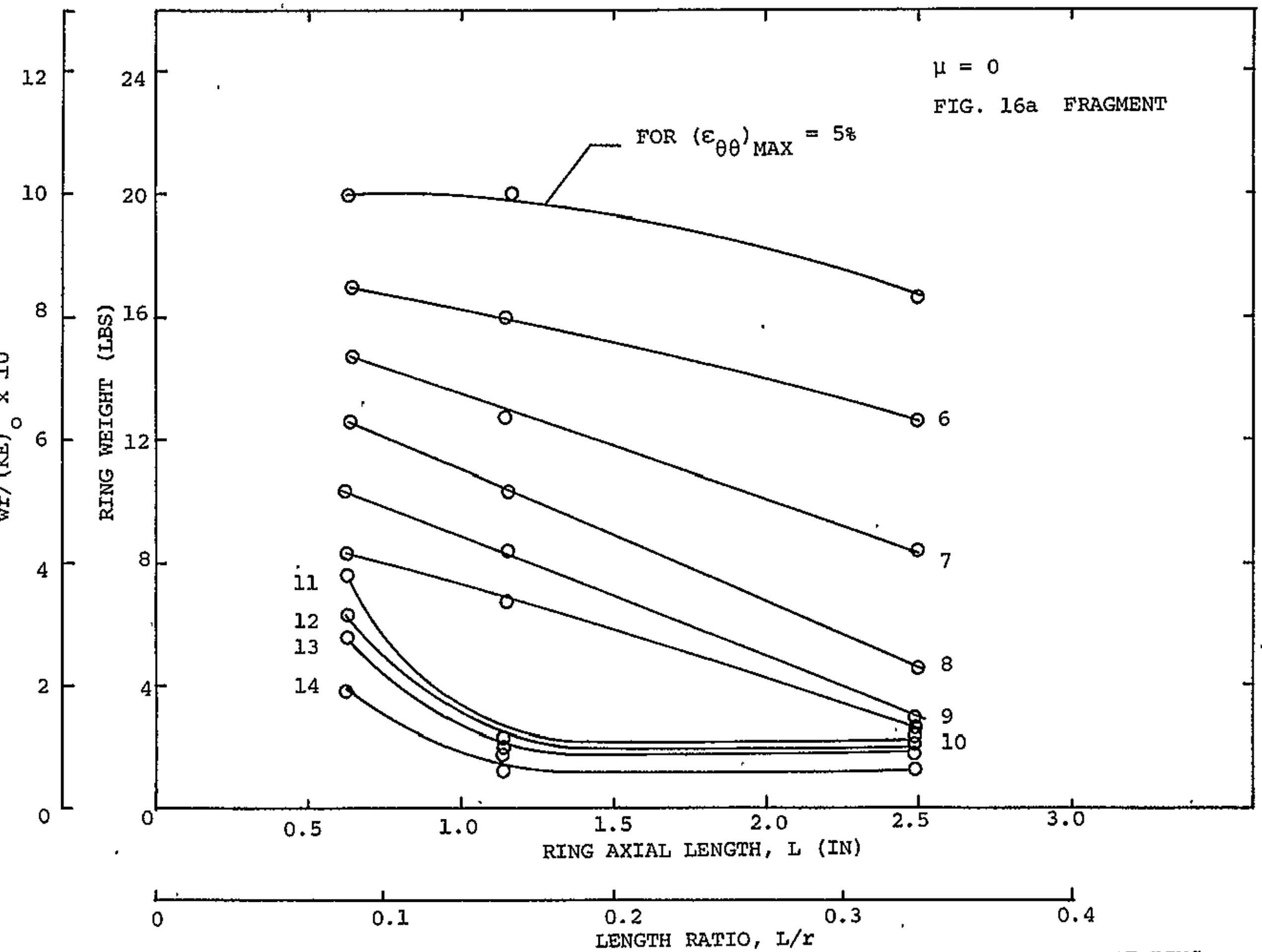

FIG. 21 PREDICTED RING WEIGHT FOR SINGLE FRAGMENT ATTACK AS A FUNCTION OF RING AXIAL LENGTH FOR FIXED VALUES OF MAXIMUM CIRCUMFERENTIAL STRAIN

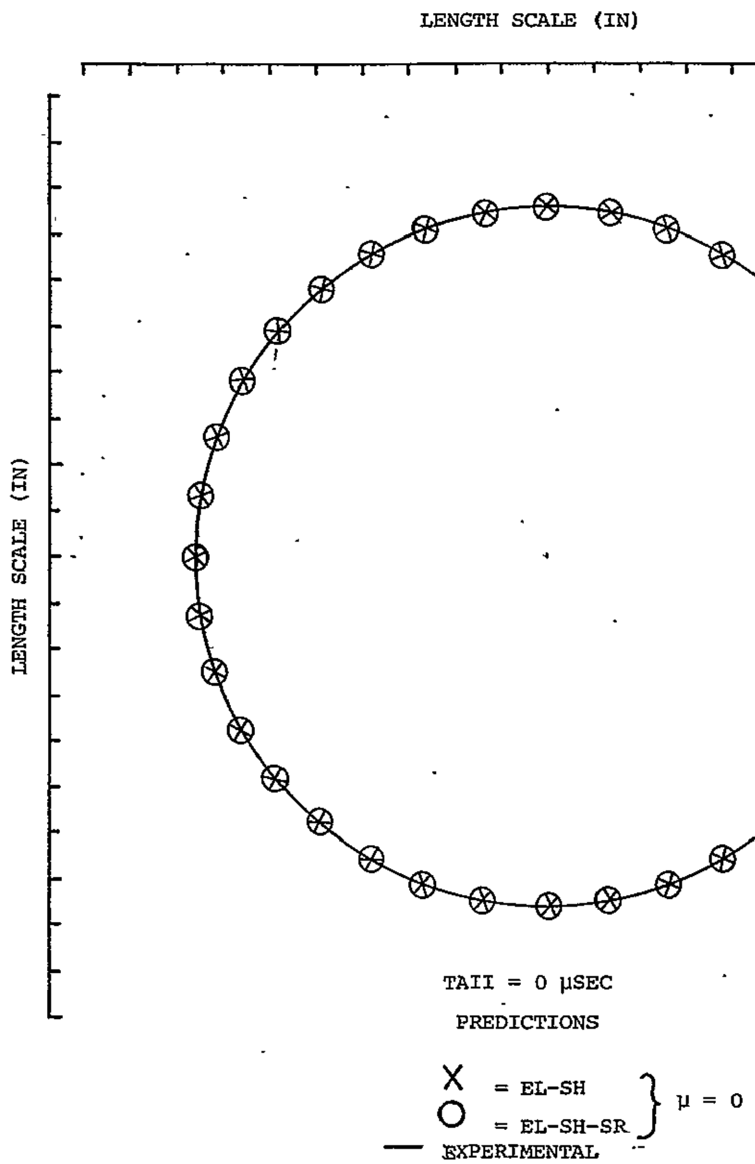

FIG. 22 COMPARISON OF PREDICTED RING PROFILES OBTAINED WITH AND WITHOUT STRAIN RATE EFFECTS WITH NAPTC PHOTOGRAPHIC TEST DATA

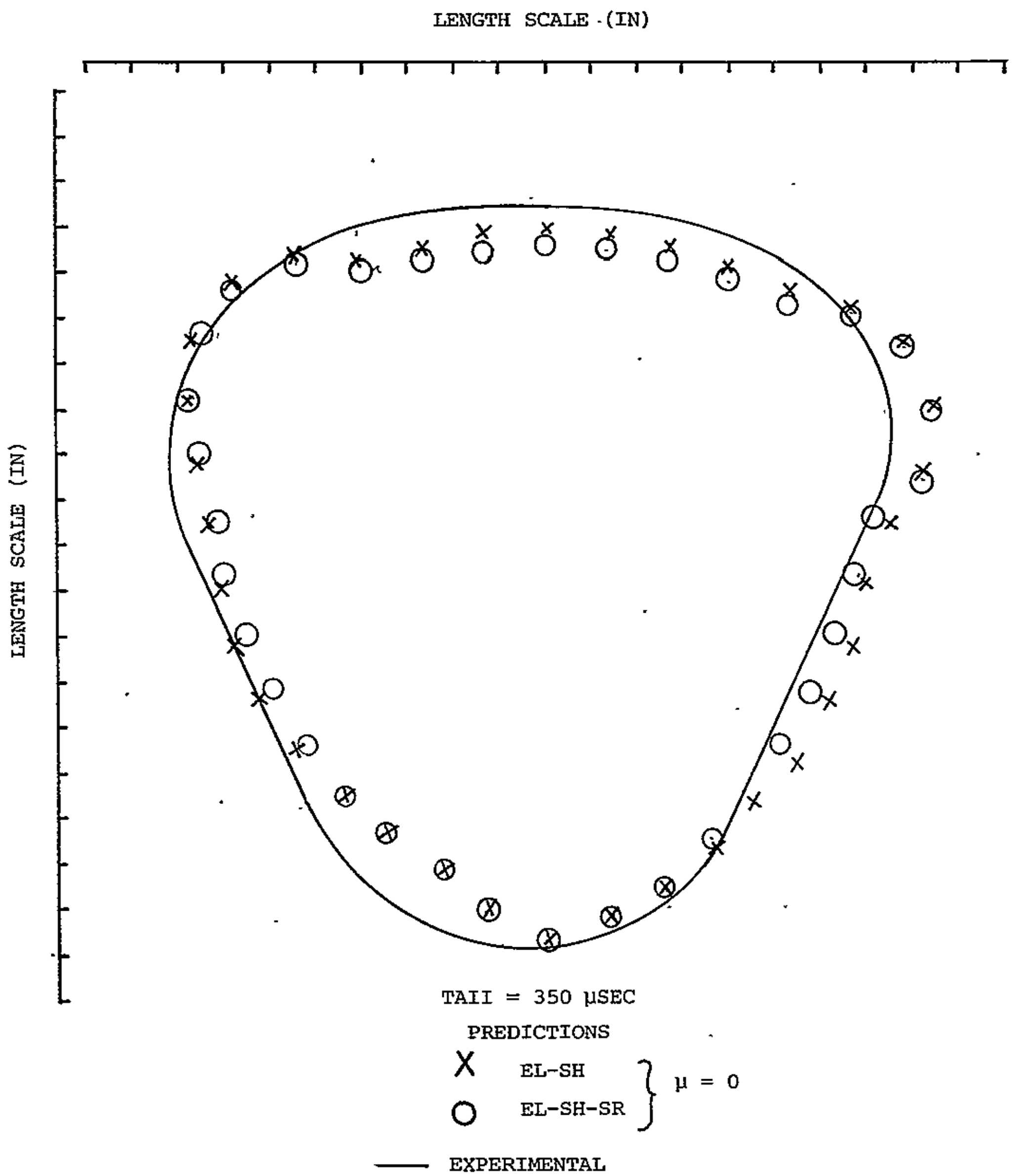

FIG. 22 CONTINUED

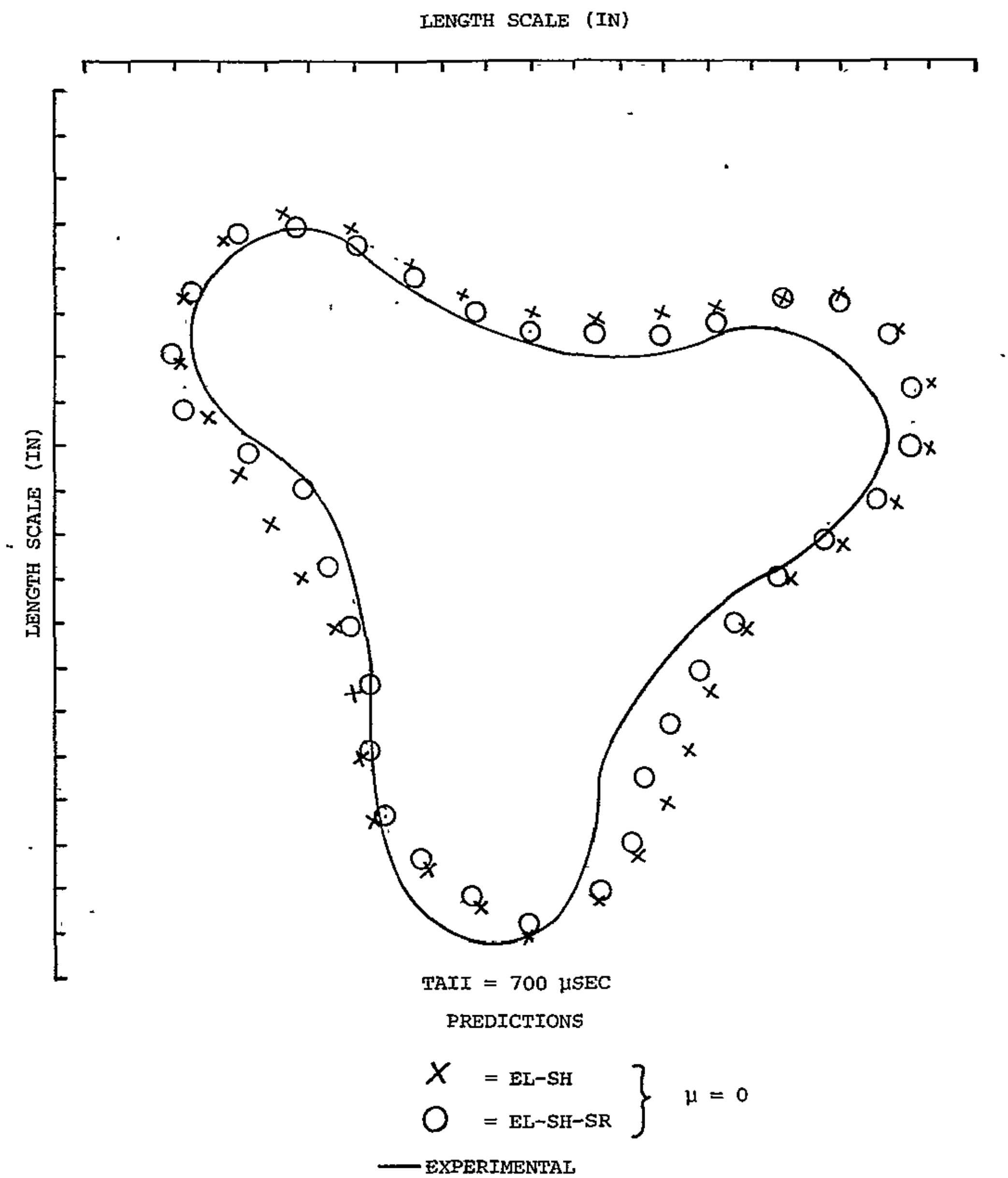

FIG. 22 CONTINUED

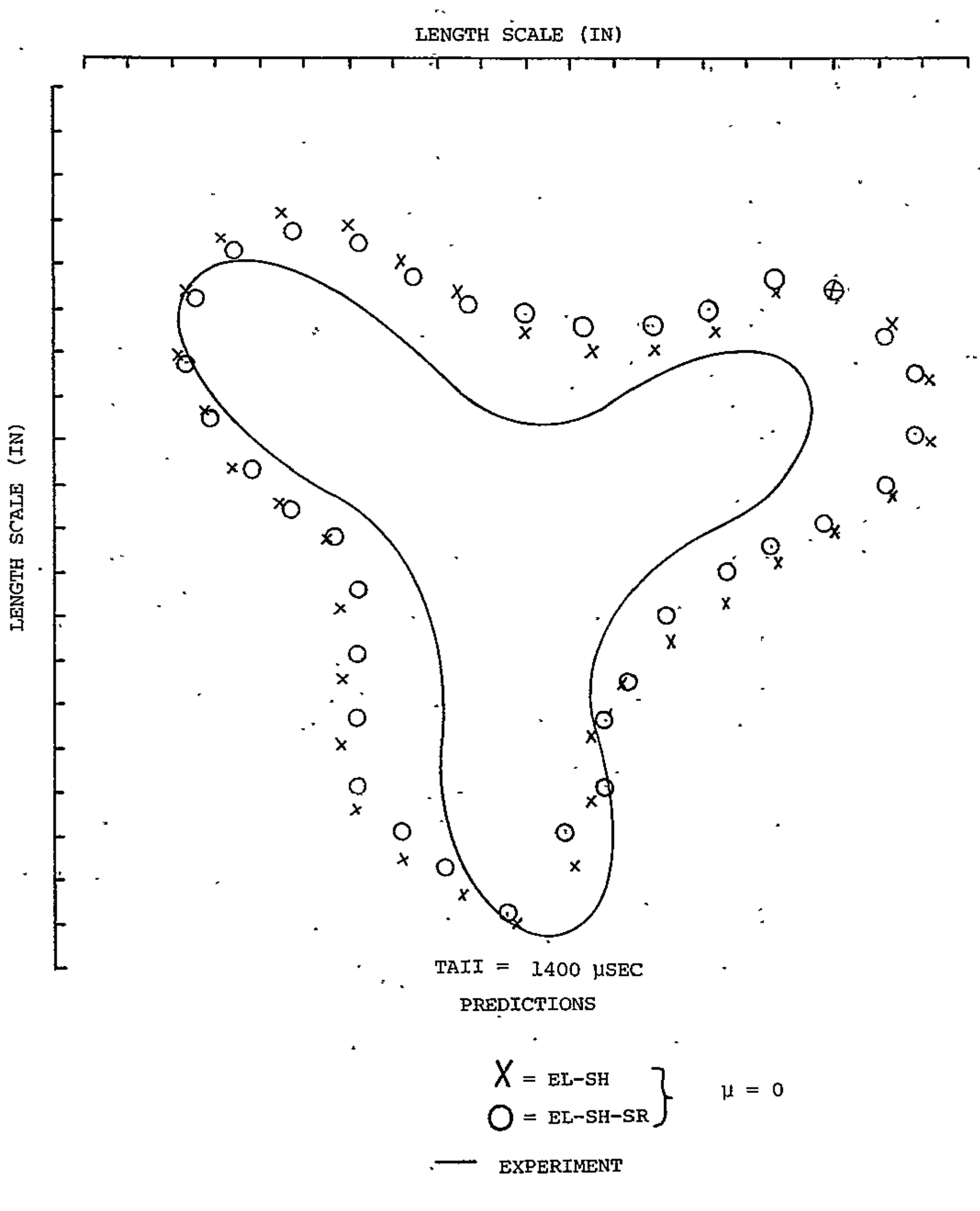

FIG. 22 CONTINUED

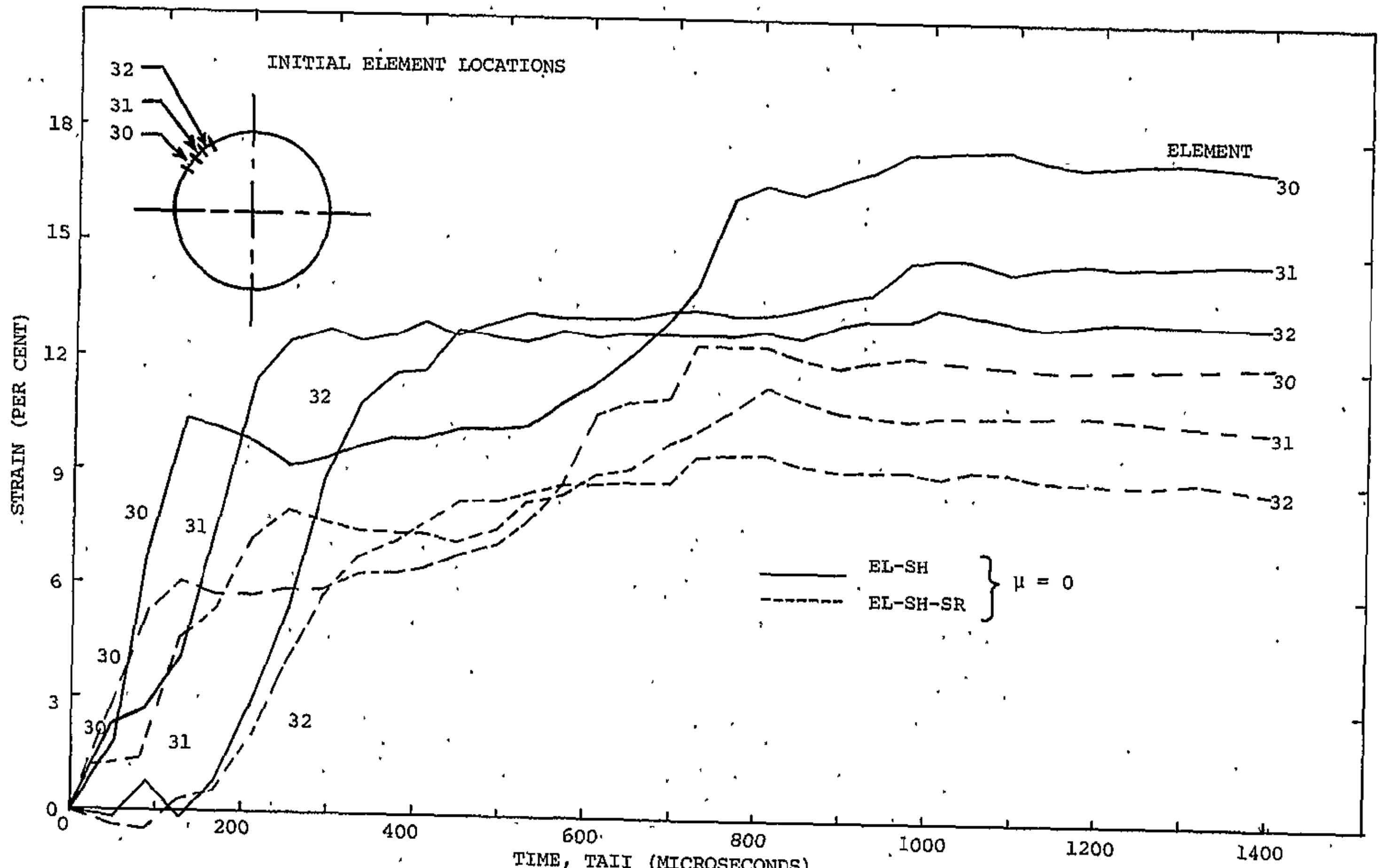

FIG. 23 COMPARISON OF RING OUTER SURFACE STRAINS AT A "LOBE" OF THE RING DEFORMED BY 3-FRAGMENT ATTACK FOR THE EL-SH AND EL-SH-SR CASES AS A FUNCTION OF TIME AFTER INITIAL IMPACT

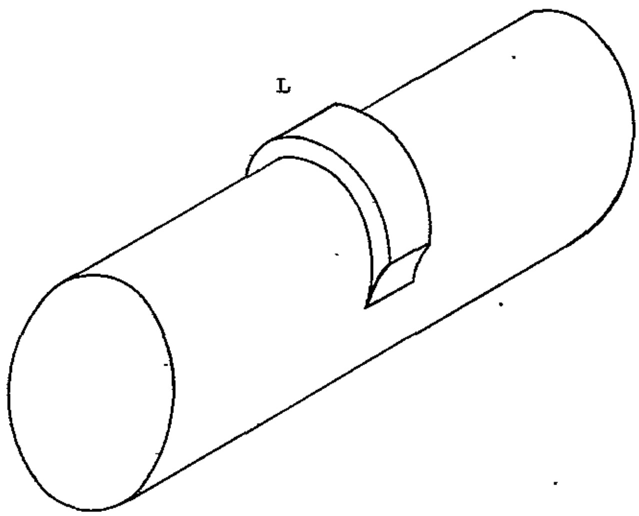

(a) Idealized Engine Casing with an Integral Deflector

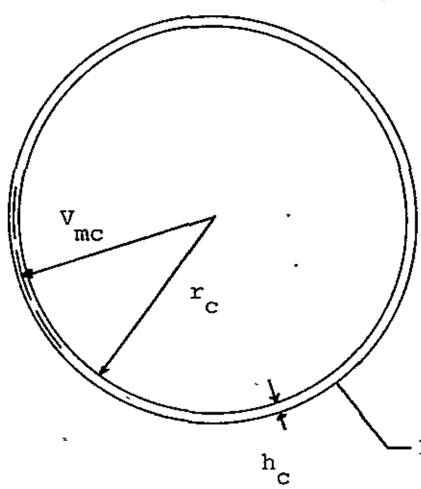

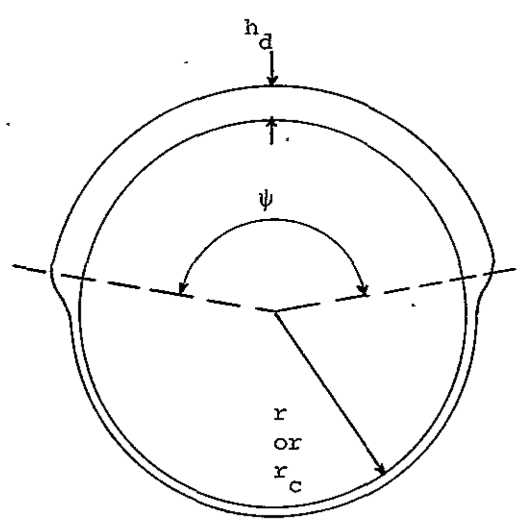

(b) Section Through "Standard" Casing (c) Section Through "Deflector"

FIG. 24 SCHEMATICS AND NOMENCLATURE FOR AN IDEALIZED INTEGRAL-TYPE FRAGMENT DEFLECTOR

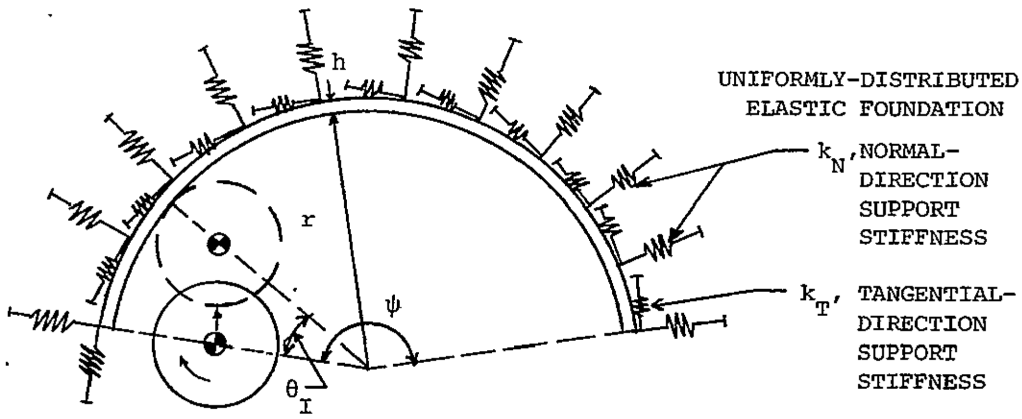

k_N - see Eqs. 4.1a and/or 4.1b

k_T - see Eq. 4.2

(d) Idealized Elastically-Supported Deflector Model Selected for Analysis

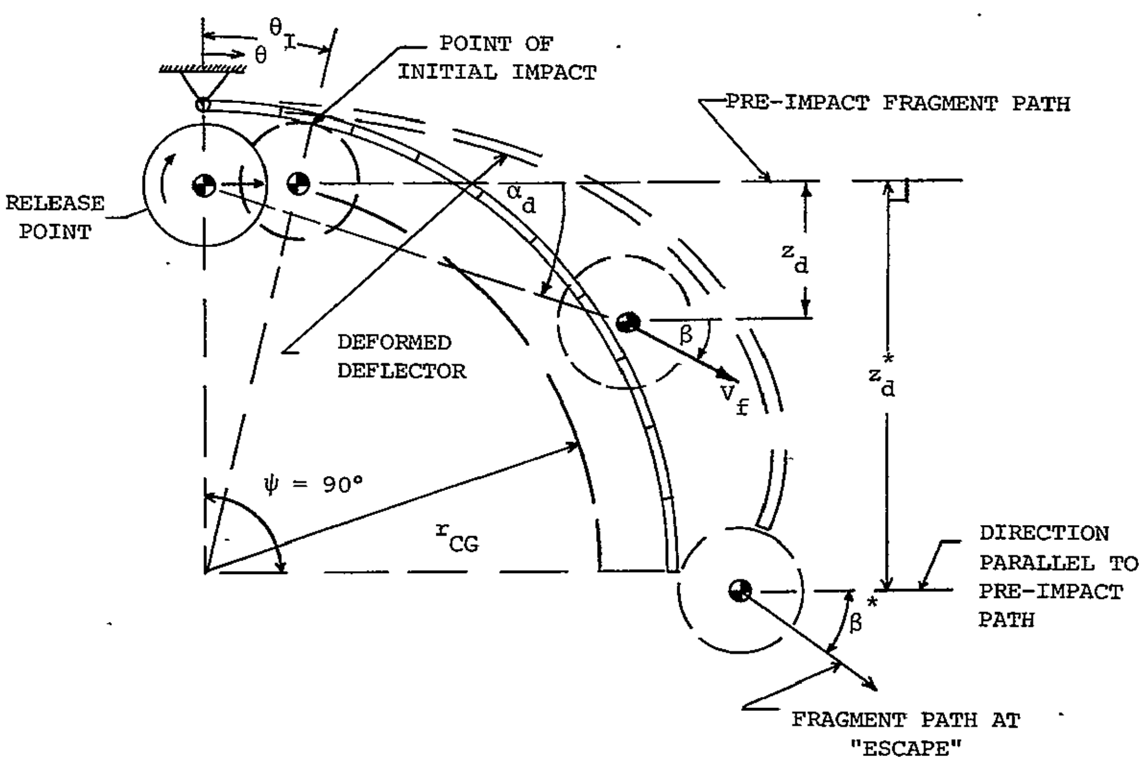

(e) Hinged-Fixed/Free Idealized Deflector Model

FIG. 24 CONCLUDED

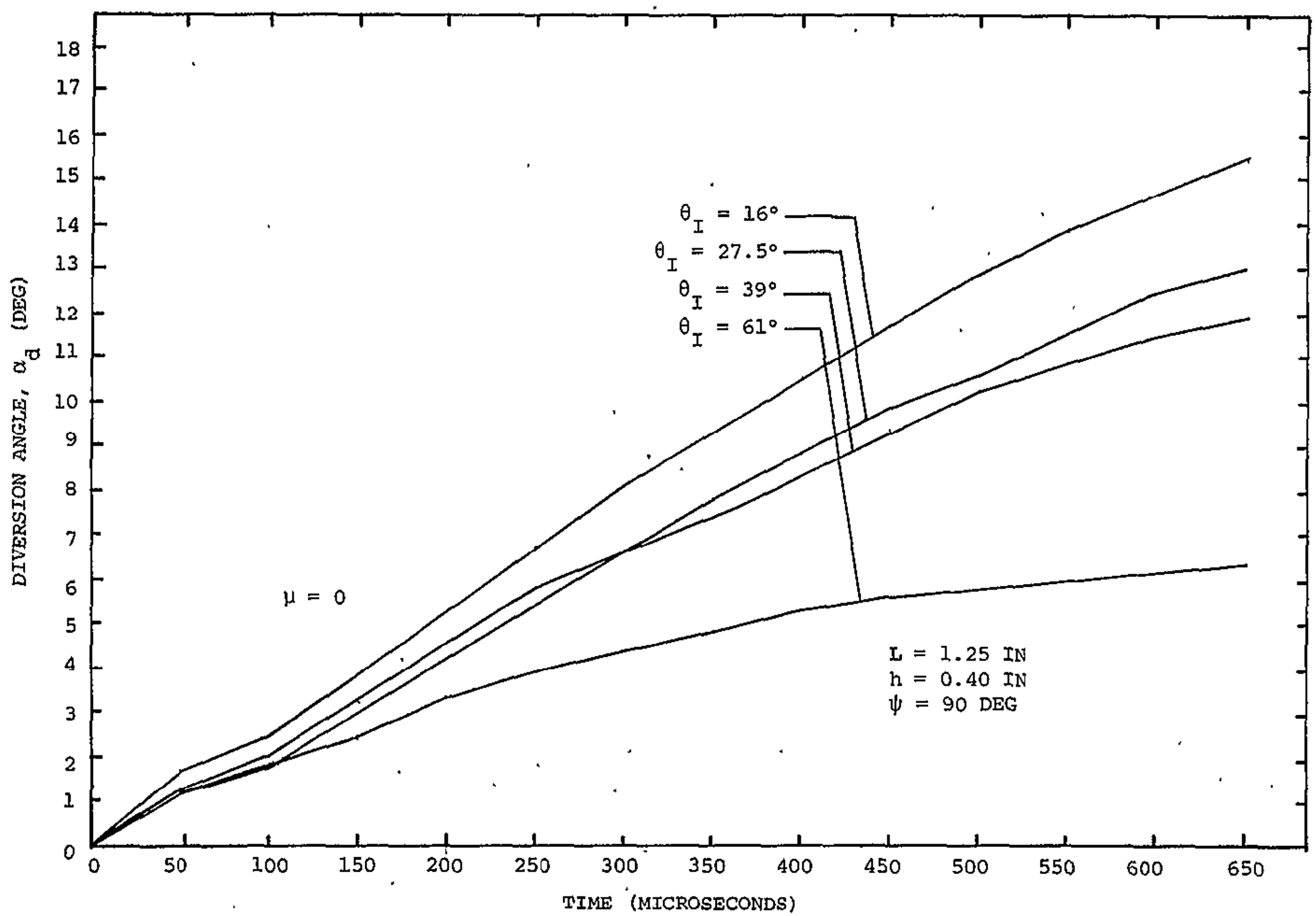

(a) Fragment Path Diversion Angle α_d

FIG. 25 INFLUENCE OF THE INITIAL-IMPACT LOCATION θ_I UPON THE PATH OF THE FRAGMENT WHICH IMPACTS THE IDEALIZED HINGED-FIXED/FREE DEFLECTOR

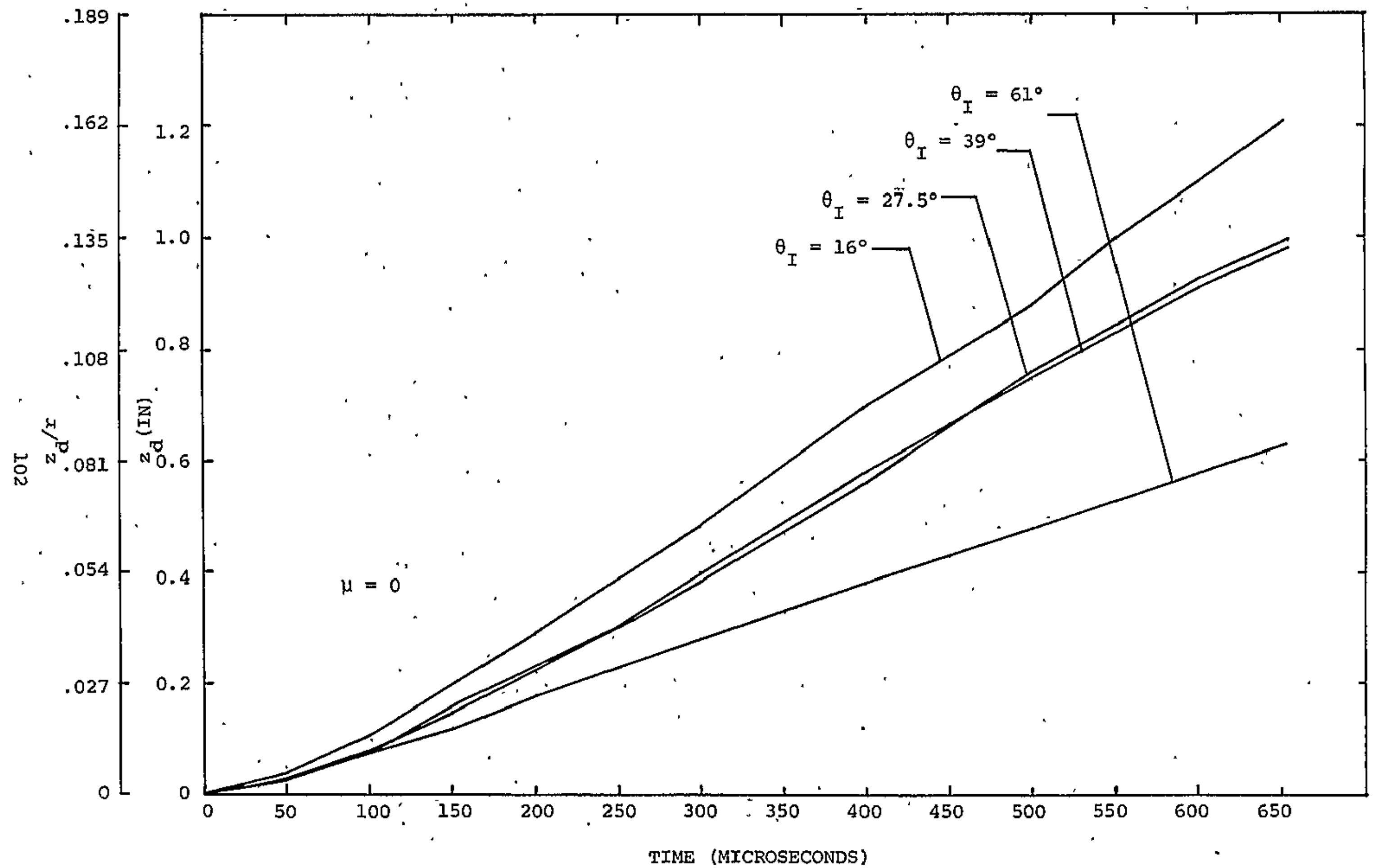

(b) FRAGMENT DIVERSION z_d NORMAL TO ITS PRE-IMPACT PATH

FIG. 25 CONCLUDED

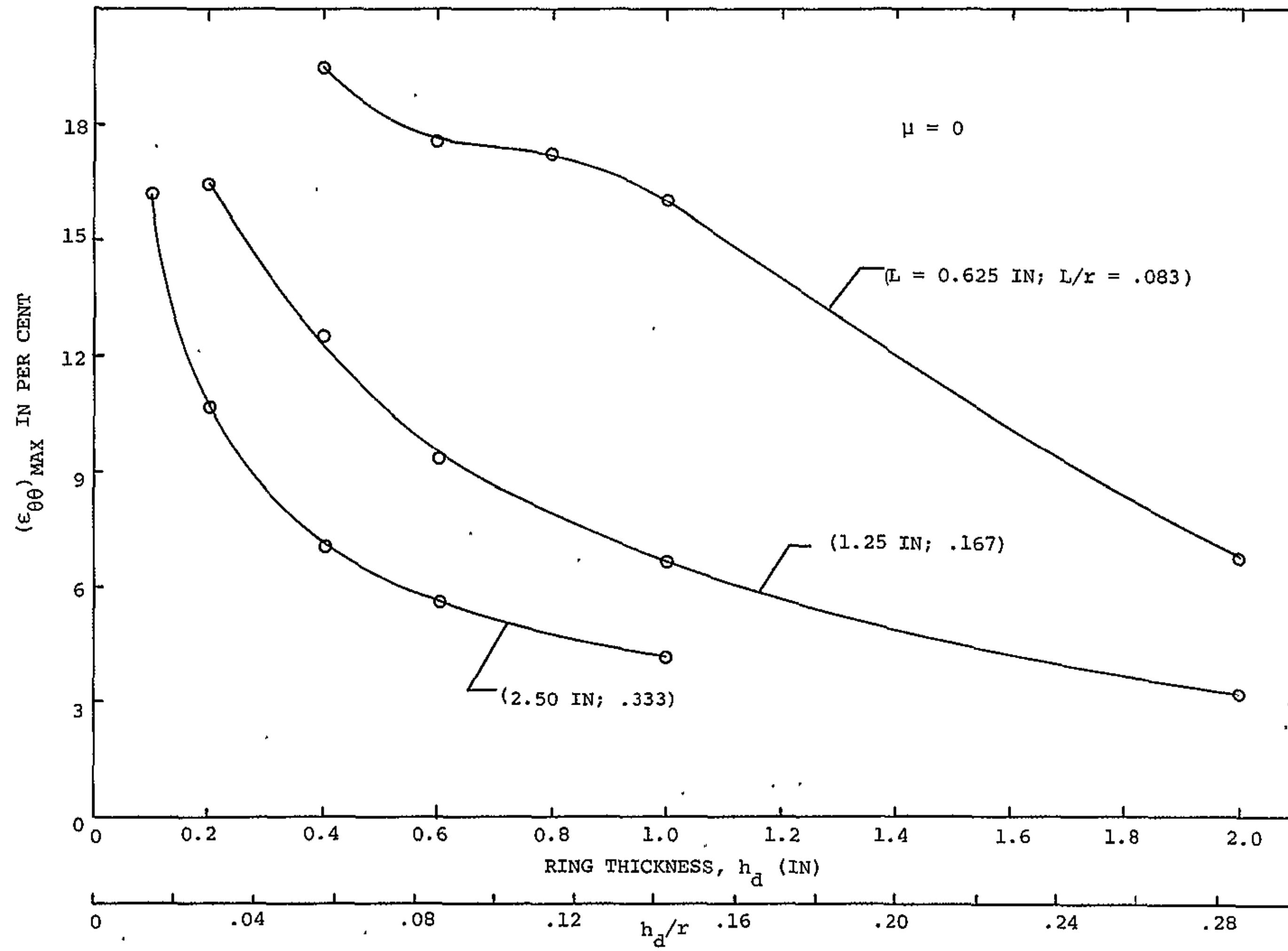

FIG. 26 PREDICTED MAXIMUM CIRCUMFERENTIAL STRAIN AS A FUNCTION OF DEFLECTOR RING THICKNESS (h/r RATIO) FOR VARIOUS AXIAL LENGTHS

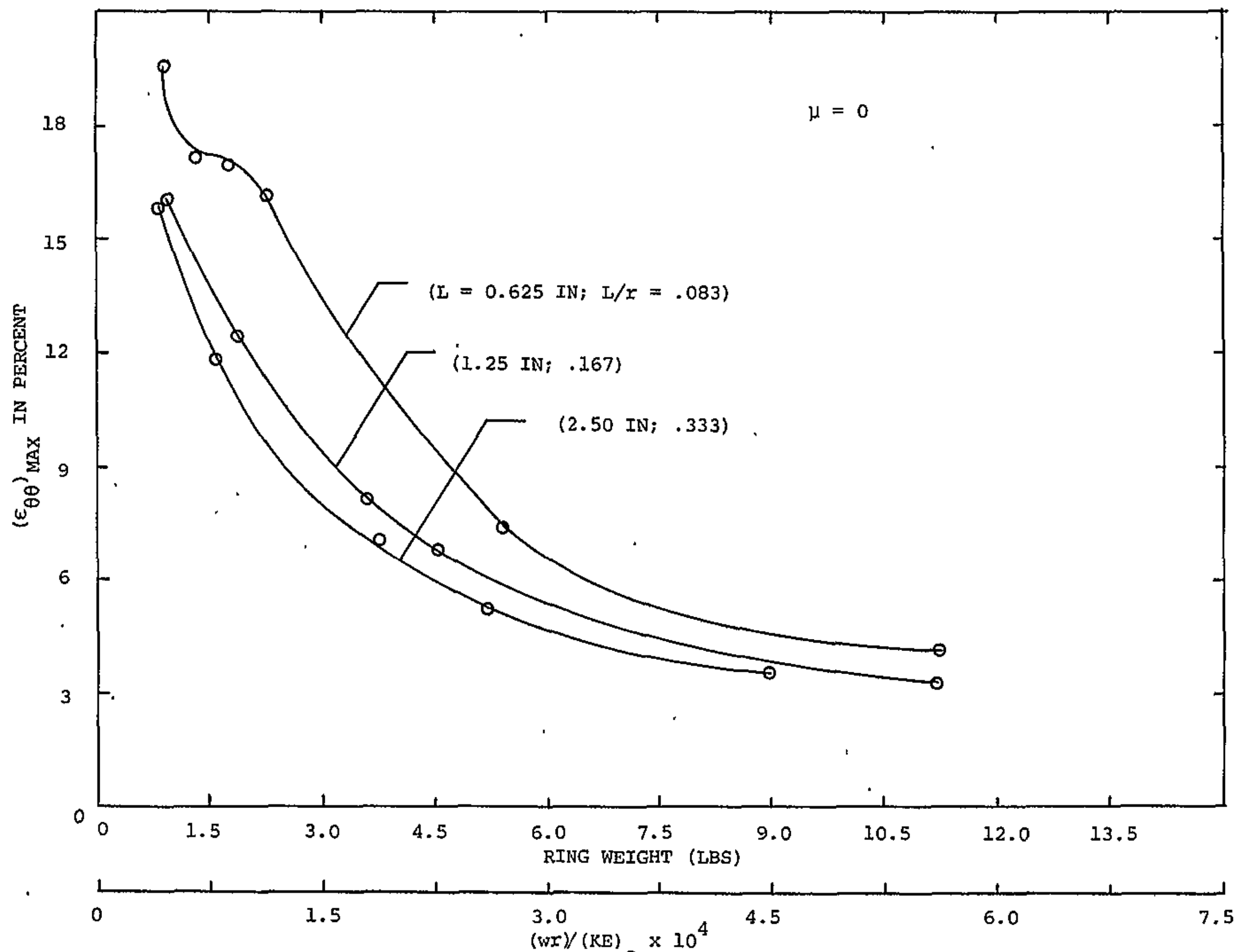

FIG. 27 PREDICTED VARIATION IN MAXIMUM CIRCUMFERENTIAL STRAIN AS A FUNCTION OF DEFLECTOR RING WEIGHT $(wr)/(KE)_o$ RATIO) FOR VARIOUS AXIAL LENGTHS

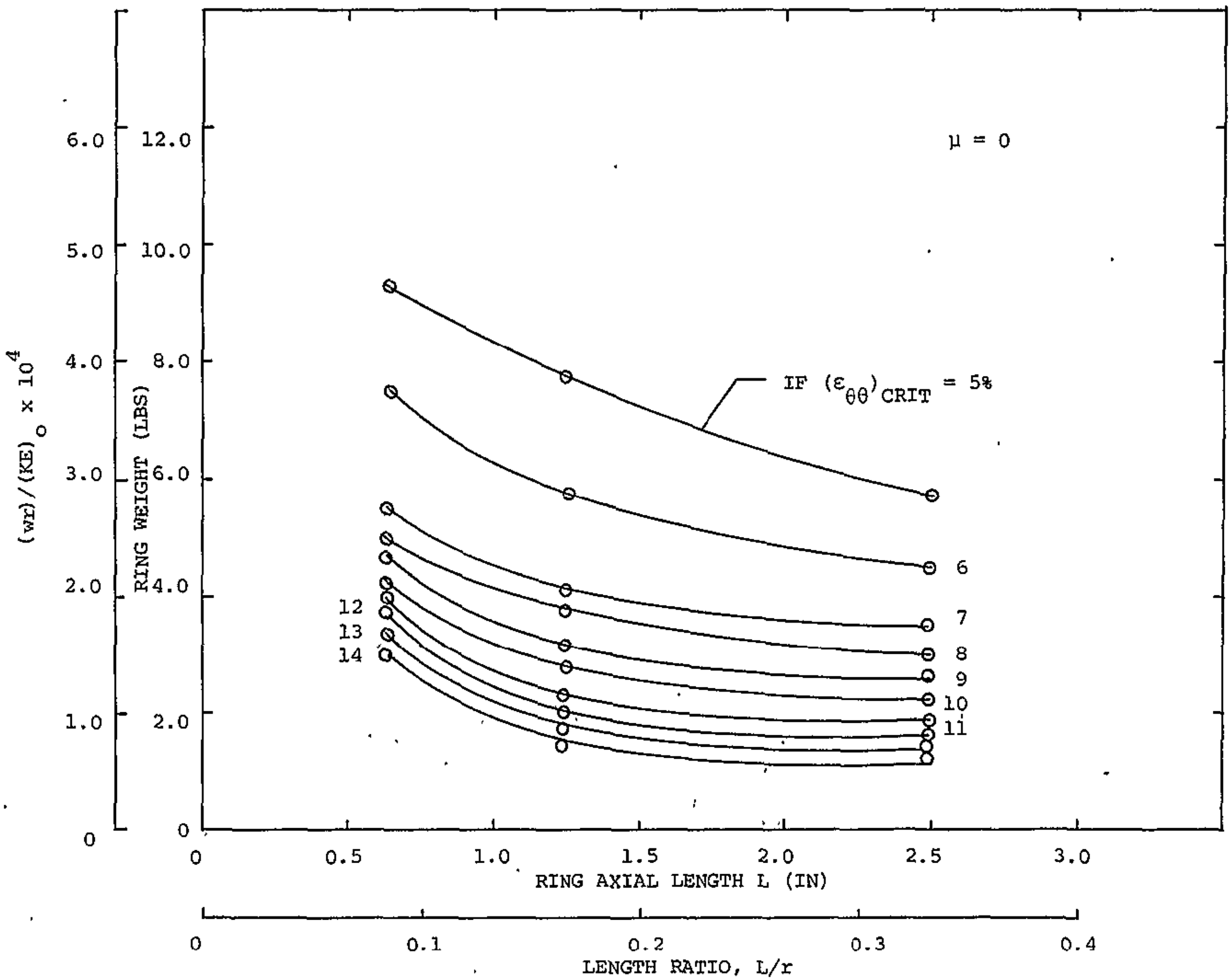

FIG. 28 PREDICTED DEFLECTOR RING WEIGHT FOR SINGLE FRAGMENT ATTACK AS A FUNCTION OF RING AXIAL LENGTH FOR FIXED VALUES OF MAXIMUM CIRCUMFERENTIAL STRAIN

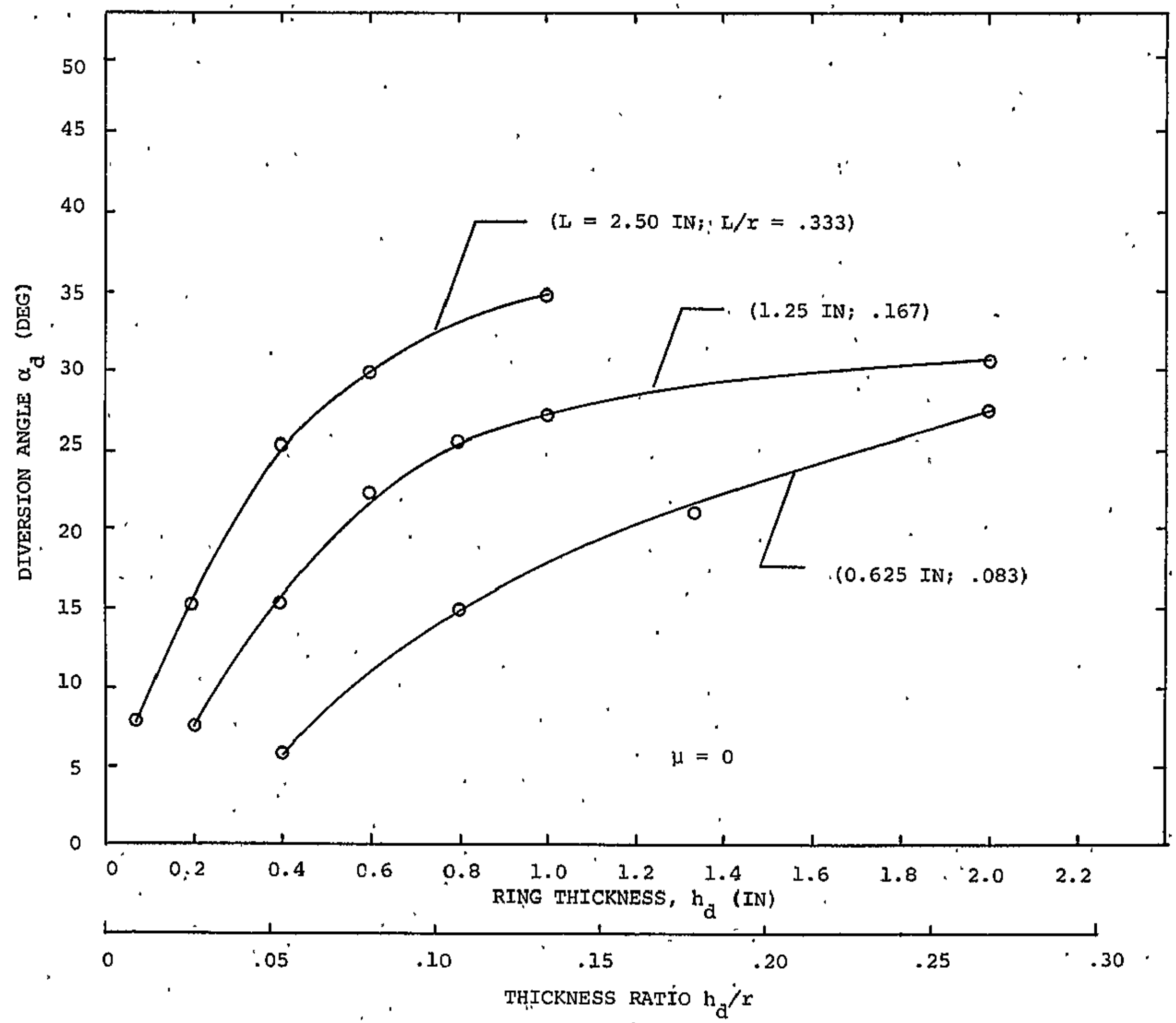

(a) Fragment Path Diversion Angle, α_d

FIG. 29 FRAGMENT PATH DATA AT TAII = 650 MICROSECONDS FOR θ_I = 16 DEGREES AS A FUNCTION OF DEFLECTOR RING THICKNESS FOR FIXED VALUES OF L (IDEALIZED H-F/F DEFLECTOR)

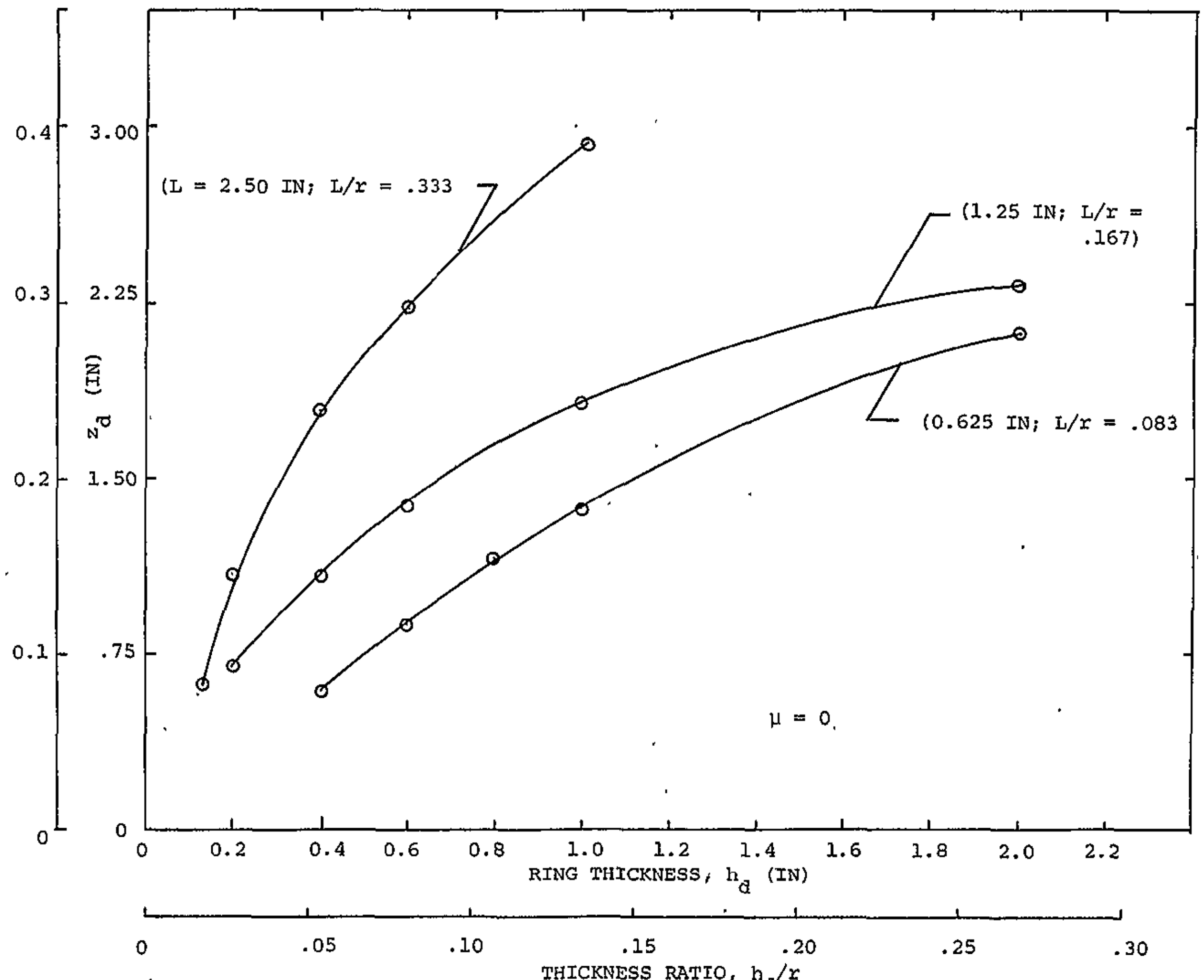

(b) Fragment Diversion z_d Normal to Its Pre-Impact Path

FIG. 29 CONCLUDED

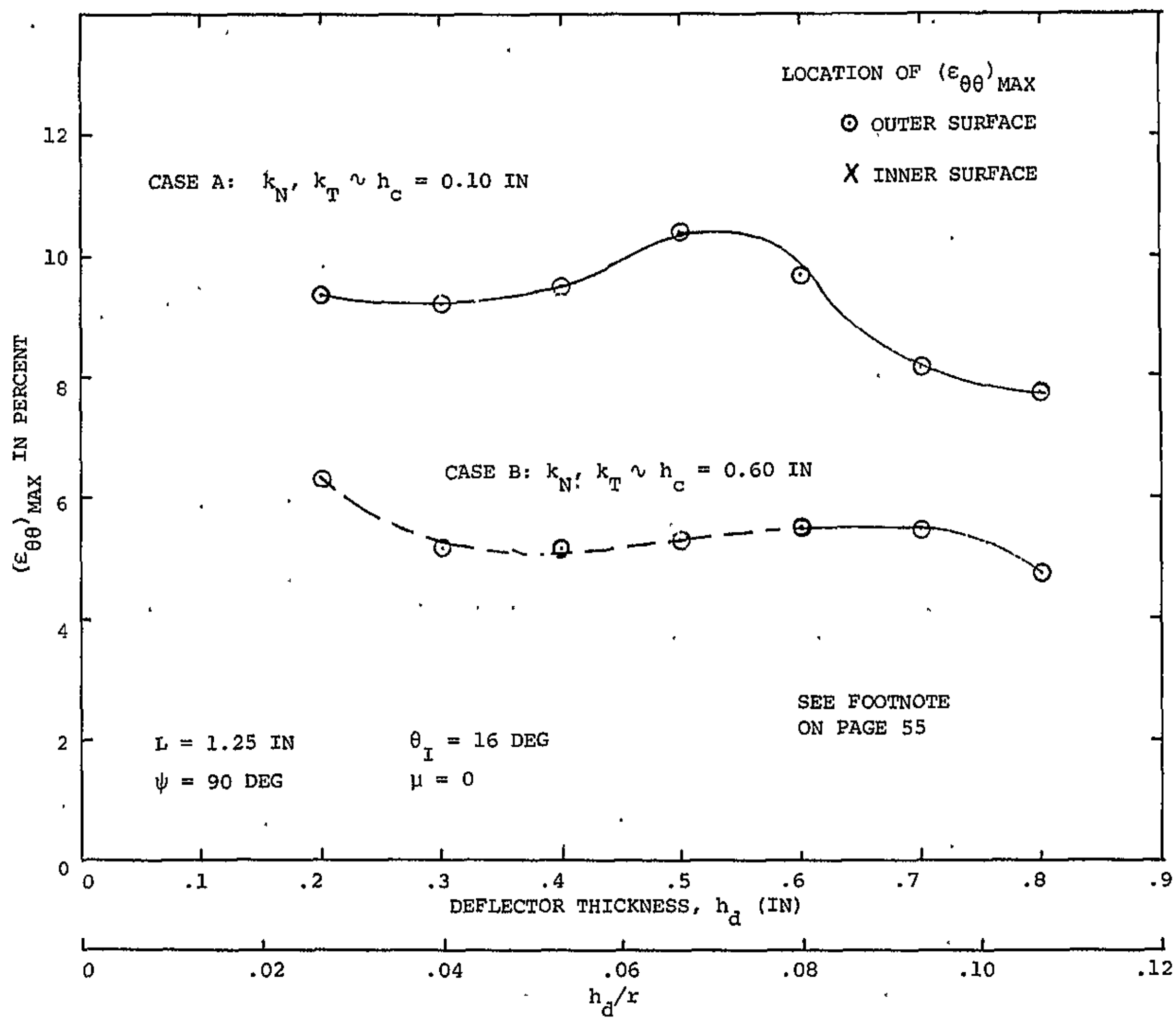

FIG. 30 PREDICTED MAXIMUM CIRCUMFERENTIAL STRAIN OF THE FOUNDATION-SUPPORTED DEFLECTOR AS A FUNCTION OF DEFLECTOR THICKNESS FOR TWO DIFFERENT SETS OF SUPPORT-STRUCTURE RIGIDITIES

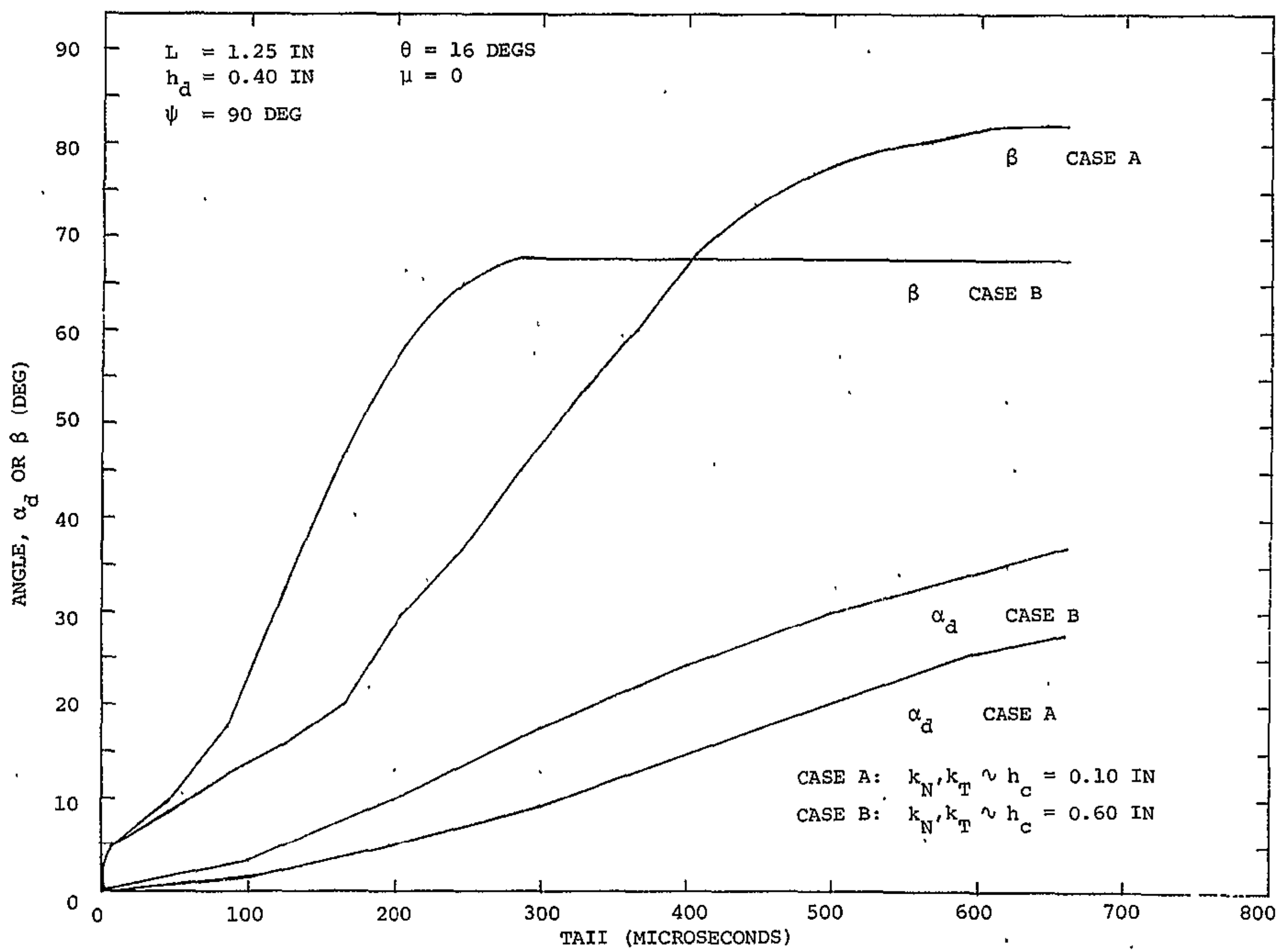

(a) Fragment Path and Diversion Angles α_d and β

FIG. 31 PREDICTED FRAGMENT-PATH DIVERSION AS A FUNCTION OF TIME AFTER INITIAL IMPACT FOR TWO DIFFERENT SETS OF SUPPORT-STRUCTURE RIGIDITIES

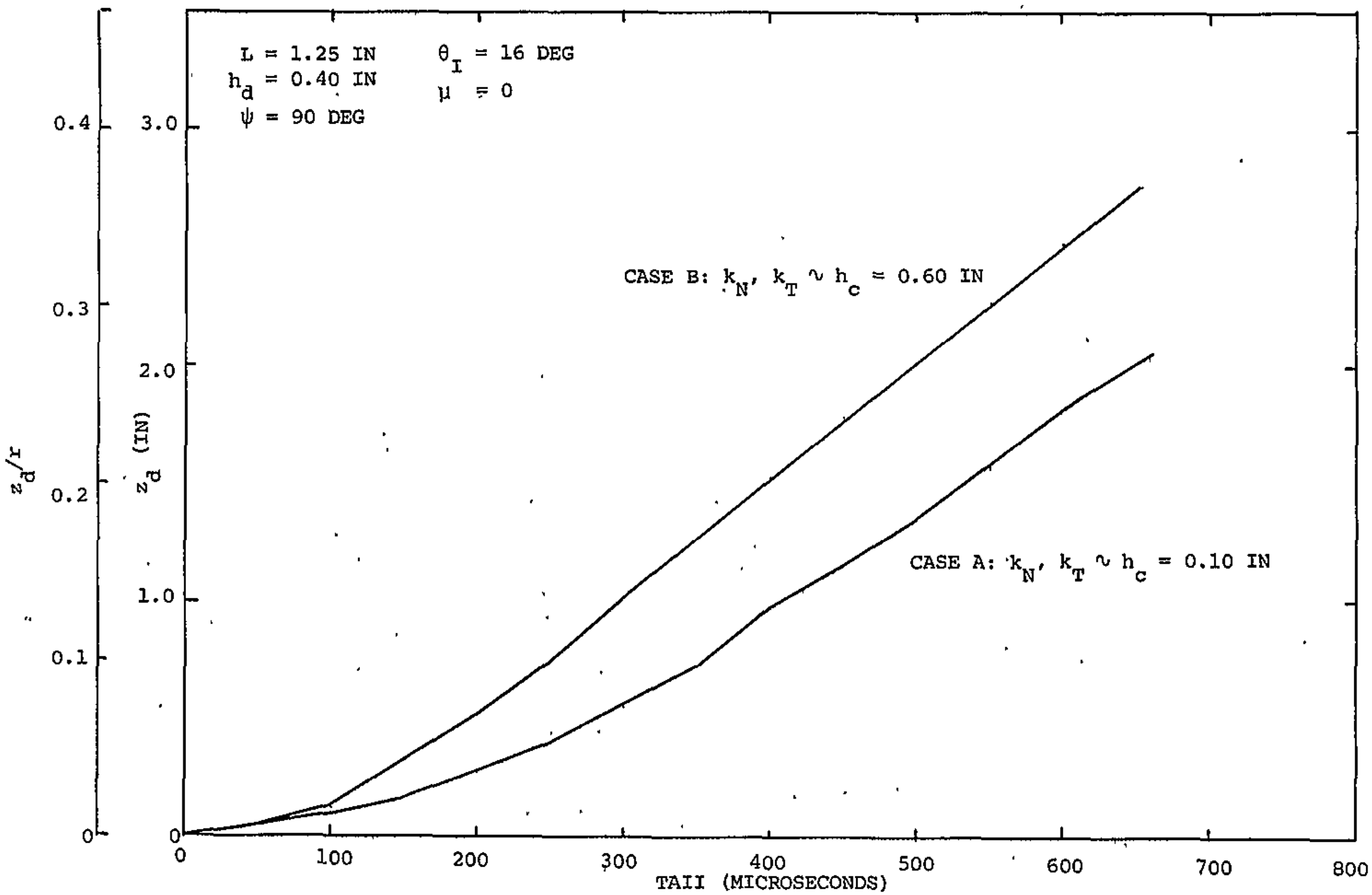

(b) Fragment Diversion z_d Normal to its Pre-Impact Path

FIG. 31 CONCLUDED

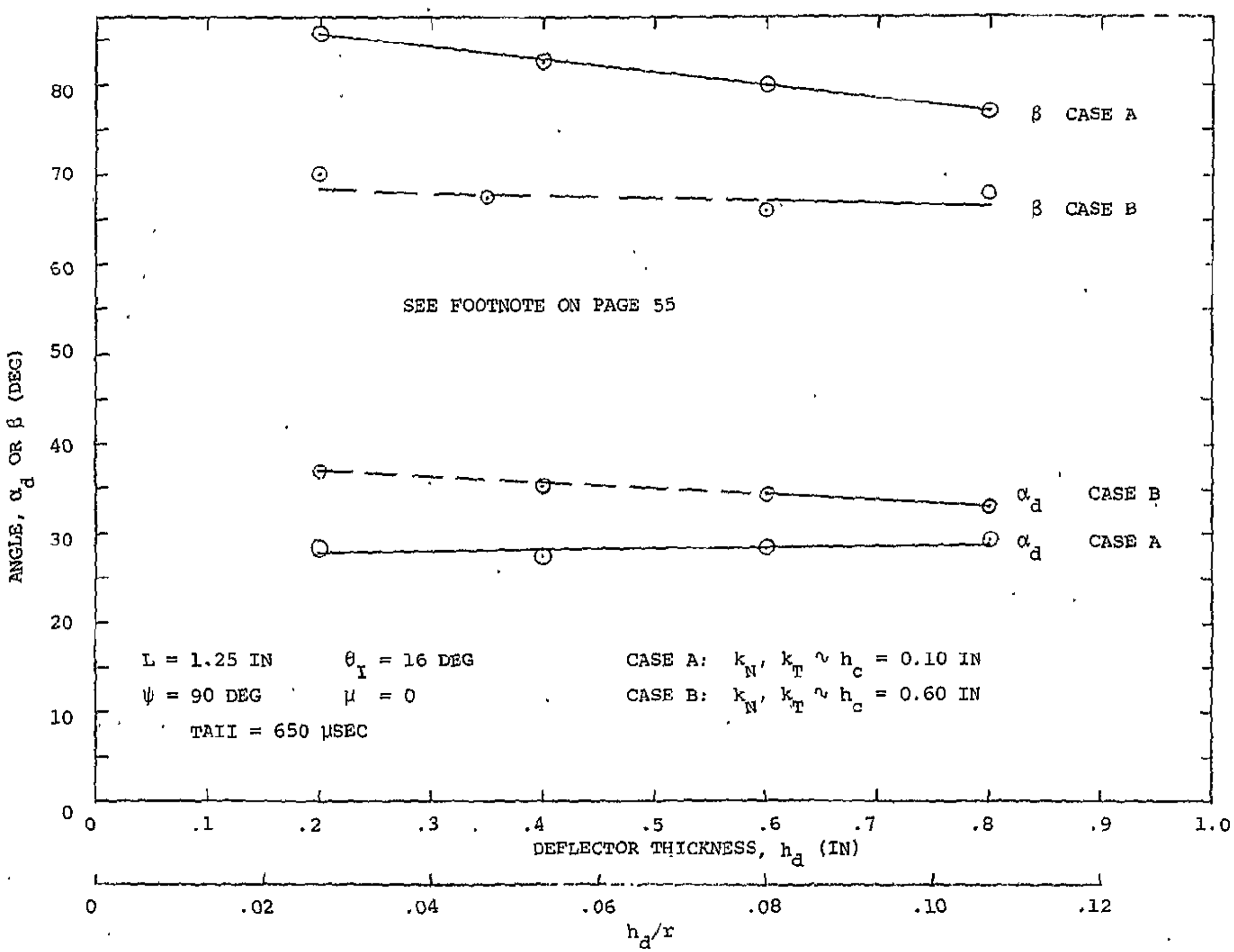

FIG. 32 PREDICTED FRAGMENT PATH DIVERSION DATA AT 650 MICROSECONDS AFTER INITIAL IMPACT AS A FUNCTION OF DEFLECTOR THICKNESS h_d FOR TWO DIFFERENT SETS OF SUPPORT-STRUCTURE RIGIDITIES

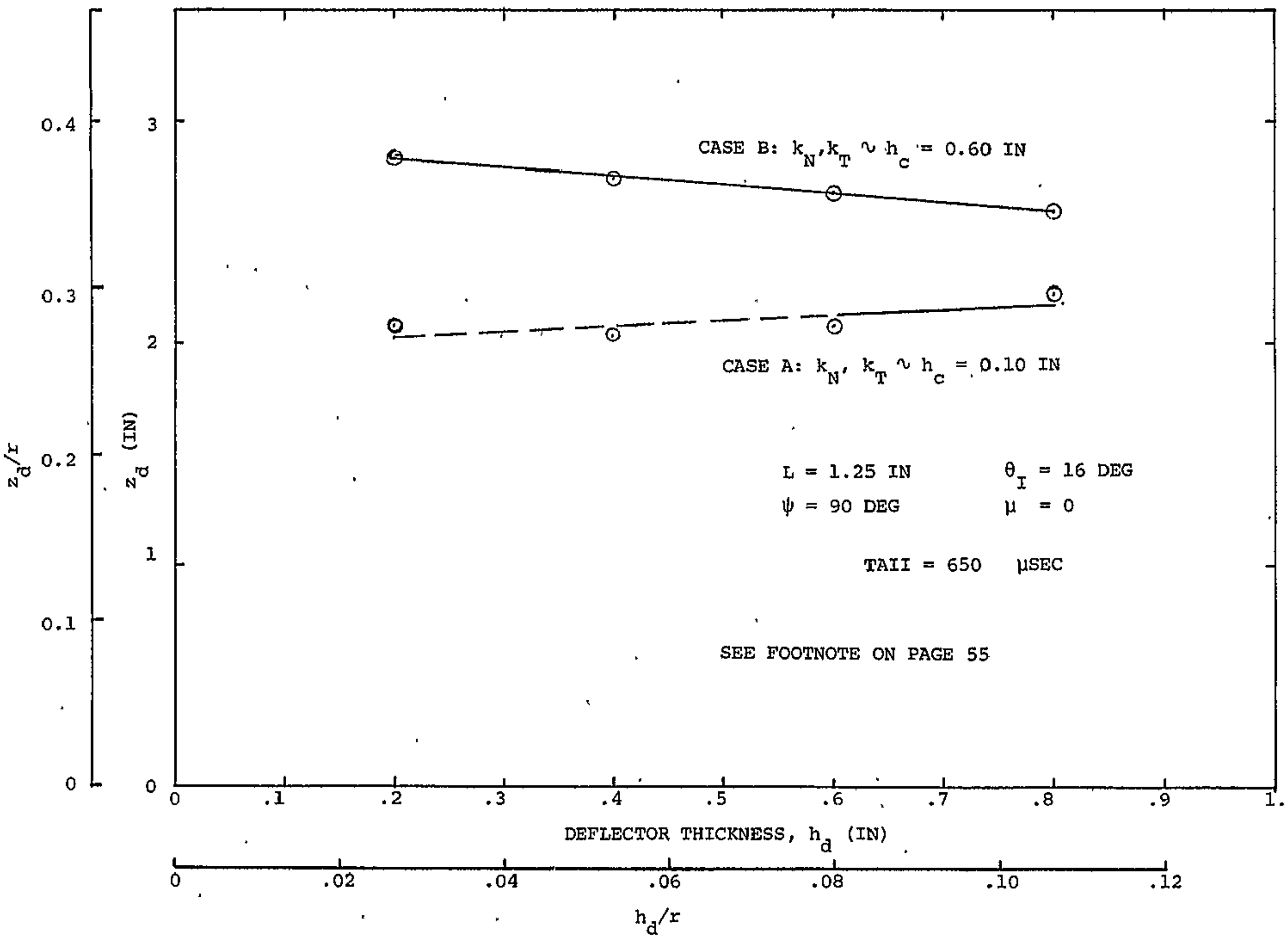

(b) Fragment Diversion z_d Normal to its Pre-Impact Path

FIG. 32 CONCLUDED

APPENDIX A

USER'S GUIDE TO CIVM-JET-4A

A.1 General Description of the Program

A.1.1 Introduction

The CIVM-JET-4A computer program is an addition to the series of computer programs which are intended to be made available to the aircraft industry for possible use in analyzing structural response problems such as containment/deflection rings intended to cope with engine rotor-burst fragments.

The CIVM-JET-4A program written in FORTRAN IV permits one to predict the fragment collision-induced large, two-dimensional, elastic-plastic transient, Kirchoff-type responses of a complete or partial single-layer, variable-thickness ring with various supports, restraints, and/or initially-prescribed displacements.*

The geometric shapes of the structural rings can be simple circular or arbitrarily curved with variable thickness along the circumferential direction. Strain hardening and strain-rate sensitive material behavior are taken into account, as well as the presence of fragment/ring surface friction.

The CIVM-JET-4A program predicts the collision-induced rigid body velocity and position changes of the attacking fragment.

The CIVM-JET-4A program which combines the CIVM scheme with a convenient but modified version of the JET 3C code of Ref.24 embodies the spatial finite element and temporal finite difference analysis features. The relative ease and versatility with which the spatial finite element technique can be applied to a structure with complicated boundary conditions, geometric shape, and material properties makes this method of analysis well suited for use in the present application. The pertinent analytic development and the solution method upon which CIVM-JET-4A is based are presented in Ref. 14. The reader is invited to consult Ref. 14 for a very detailed description of this information. The

---

*See Figs. A.1 through A.4.

CIVM-JET-4A computer program can analyze the collision induced ring responses and rigid-body fragment motions of:

(a) Collisions involving a maximum of six fragments, each possessing different mass, mass moment-of-inertia, velocity-component, radius, and r_{CG} parameters.

(b) Collisions involving the presence of fragment-ring surface friction.

(c) Structural rings, complete or partial, whose geometric shape can be circular or arbitrarily curved, with variable thickness.

(d) A structural ring, with various support conditions, subjected to distributed elastic restraints (Fig. A.3c).

A.1.2 Containment/Deflector Ring Geometry, Supports, Elastic Restraints, and Material Properties

In the present analysis the transient structural responses of the ring are assumed to consist of planar (two-dimensional) deformations. Also the Bernoulli-Euler (Kirchhoff) hypothesis is employed; that is, transverse shear deformation is excluded. In the structural finite element context, such problems are termed "one-dimensional".

The geometric shapes of the ring that can be treated are divided for convenience into the following four groups as shown schematically in Fig. A.1:

(1) Circular partial ring with uniform thickness.

(2) Circular complete ring with uniform thickness.

(3) Arbitrarily curved complete ring with variable thickness.

(4) Arbitrarily curved partial ring with variable thickness.

For each of these configurations, the cross sections of the ring are assumed to be rectangular in shape.

In the spatial finite-element analysis, the ring is represented mathematically by an assemblage of discrete (or finite) elements compatibly joined at the nodal stations. The geometry and nomenclature of an arbitrarily curved ring element is shown in Fig. A.2. For application to arbitrarily-curved, variable-thickness ring structures, the finite elements are described by reading in the global Y and Z coordinates, the local-coordinate slope ϕ, and the thickness of the ring at each node. The displacements within each element are determined from the displacement values at these nodes through the means of appropriate interpolation functions. The reader interested in a detailed derivation of this assumed-displacement method is referred to Ref. 14 for an in-depth discussion.

As for the support conditions of the structure, the CIVM-JET-4A program includes three types of prescribed nodal displacement conditions (see Fig. A.3a):

(1) Symmetry* ($v = \psi = 0$)

(2) Ideally-Clamped* ($v = w = \psi = 0$)

(3) Smoothly-Hinged/Fixed ($v = w = 0$)

and two types of elastic restraints (see Fig. A.3b):

(a) Point elastic restraints (elastic restoring spring) at given locations (3 directions: normal, tangential, and rotational),

(b) Distributed elastically restrained (elastic foundation) over a given number of elements (3 directions; see Fig. A.3c).

In the CIVM-JET-4A program, the mechanical sublayer model is used to describe the material properties of the ring. The input to the program takes the form of a series of stress-strain coordinates that define the straight line segments that the user has chosen to represent the stress-strain diagram of the material used. Various examples of different types of material behavior (elastic-perfectly-plastic (EL-PP), elastic, strain-hardening strain-rate dependent (EL-SH-SR), etc.) input are shown in Fig. A.4.

<u>A.1.3 Fragment Geometry and Initial Conditions</u>

As was shown schematically in Fig. 3, the possible fragment types

---

*Note that here ψ has the meaning specified in Fig. 14.

resulting from turbine engine failure are of various geometric configurations. A wide range of velocity components is also foreseen. The representation chosen for use in the CIVM-JET-4A program is the circular disk model that is shown in Fig. 16. The model-fragment mass, moment of inertia, and velocity components are specified to correspond with those of the actual fragment. The diameter of the idealized circular-disk fragment may be chosen, for example, so that the model covers the actual fragment outline out to a position midway between the fragment center of gravity and the tip of the attached blades for the disk sector shown. The user is free to employ any other plausible value that he chooses.

The specification of the idealized attacking fragment, therefore, is accomplished through the input of the following parameters for each attacking fragment (maximum of six):

(1) Fragment mass
(2) Fragment mass moment of inertia about its center of gravity
(3) Diameter of the idealized fragment
(4) Initial position of fragment in the Y,Z global axes system (center of gravity)
(5) Initial fragment velocity components in the global Y and Z directions
(6) Initial fragment rotational velocity
(7) Coefficient of restitution chosen for the collision behavior of each fragment
(8) Coefficient of ring surface friction chosen for each attacking fragment.

A.1.4 Solution Procedure

The spatial finite-element approach is utilized in conjunction with the Principle of Virtual Work and D'Alembert's Principle to obtain the equations of motion of the structural ring subjected to a collision-induced velocity change at the nodal points. The ring structure studied is permitted to undergo large elastic-plastic transient deformations. In the interest of conciseness and convenience,the reader is invited to consult Ref. 14 for a detailed derivation of this method that results in the following modified form of the equations of motion:

$$[M^*]\{\ddot{q}^*\} + \{P^*\} + [H^*]\{q^*\} = \{F^*\} - [K_s^*]\{q^*\} \tag{A.1}$$

where:

$[M^*]$	=	the mass matrix of the entire structure
$\{q^*\},\{\ddot{q}^*\}$	=	the global generalized displacements and accelerations
$\{P^*\}$	=	$[K^*]\{q^*\}$ and also some plastic behavior contributions
$[K^*]$	=	the usual stiffness matrix of the entire structure
$[H^*]\{q^*\}$	=	generalized loads resulting from large deflections and plastic strains
$\{F^*\}$	=	the prescribed externally-applied generalized loading acting on the structure
$[K_s^*]$	=	the effective stiffness matrix supplied by the presence of the elastic restraints.

The displacement and acceleration vectors in the above equation represent the quantities obtained from the impact-corrected nodal velocities of the structure.

As has been shown in Section 2, the resulting equations of motion are solved through the use of the central difference temporal operator with a time-step value that must be chosen to meet both stability and convergence criteria; this matter is discussed later in conjunction with the input list. In the following paragraph the general solution method used is reviewed briefly.

First, information is provided to define the geometry of the ring including its prescribed displacement conditions and elastic restraints. In addition, the required material property and attacking-fragment parameters are specified. It should be noted that the Gaussian quadrature method is used in the present analysis to evaluate the element-property matrices -- this requires that the stresses and strains be evaluated at a selected number of Gaussian stations over the "spanwise" and depthwise region of each finite element; three spanwise and four depthwise Gaussian stations are used in the CIVM-JET-4A program. The mass and stiffness matrices for the entire structure are assembled from these individual element matrices.

Starting from a set of given initial conditions at time t_o, the collision inspection and correction procedure is begun. If a collision has occurred, the corrected values of the fragment velocities are used to compute the position change of the fragment during the given time interval. The ring responses are evaluated for the impact-induced displacement changes in the following manner. The strain increment developed during the particular time interval is evaluated at each spanwise and depthwise Gaussian station for each element. From a knowledge of the prescribed initial stresses and the strain increments, one can determine the stress increments, the stresses and/or the plastic strains and plastic strain increments through the use of the pertinent elastic-plastic stress-strain relations including the plastic yield condition and the flow rule. Next, the equivalent generalized load vector due to large deformations and plastic strains may be calculated. The resulting system of linear equations is solved for the unknown increments of generalized displacement at each nodal station.

A.2 Description of Programs and Subroutines

A.2.1 Program Contents

The main CIVM-JET-4A program and the name of each subroutine are listed in the following with a brief description of the functions of each:

MAIN Reads the ring geometry, material property data, the structural discretization information, and/or the prescribed displacement conditions and elastic restraints, the fragment geometry parameters and the fragment initial-velocity components. It computes the quantities that are constant throughout the program and initializes most of the variables used in the subroutines. It controls the logical flow of information supplied by the various subroutines and the overall time cycle.

ASSEF This subroutine assembles the generalized nodal load vectors (due to externally applied forces and/or large-deflection elastic-plastic effects) of each individual element into a generalized nodal load vector for the structure as a whole.

ASSEM This subroutine updates the effective stiffness matrix $[K_s^*]$ supplied by the presence of the elastic restraints as the element effective stiffness matrices are generated. The components of the assembled effective stiffness matrix $[K_s^*]$ which is a symmetric matrix are stored in linear-array form; only the lower triangular part of $[K_s^*]$ need be and is stored (row-wise), starting with the first non-zero element in the row and ending with the diagonal term.

DINIT This subroutine initializes all ring response calculation vectors. Advances each of N fragments to its position at time TPRIM. (Time before which no ring impact is possible.)

ELMPP This subroutine evaluates the transformation matrices between the strain at each spanwise checking station (Gaussian) and the generalized nodal displacements for each discrete element.

ENERGY Performs the energy accounting procedure for the ring-fragments system. Calculates the current fragment kinetic energy (for each fragment), ring kinetic energy, ring elastic energy, ring plastic work, and energy stored in the elastic restraints. Use of this subroutine is optional; it may be employed by following the procedure outlined in the input description section. For those cases where there is no need of performing the energy accounting, be sure to replace this subroutine by the dummy subroutine of the same name. (See listing of the CIVM-JET-4A program for both of these subroutines.)

FICOL Finds the corresponding location of an element in the linear-array expression to a location in a two-dimensional array expression of the [K*] matrix.

IDENT The IDENT subroutine is used at the beginning of the run to print out the values of certain input parameters, such as the ring structural discretization, geometry, and material properties; the fragment geometry and initial velocity conditions; and prescribed ring displacement and elastic restraint conditions.

IMPACT This subroutine carries out the search for impact occurrence involving one of N fragments on each element of the ring for all fragments considered. When it is determined that a fragment-ring collision has taken place, IMPACT calculates and applies the appropriate correction factors to the velocities of the fragment and the nodal points of the element impacted.

MINV Performs the matrix inversion; a standard Gauss-Jordan technique is used.

OMULT Computes various linear arrays (in which a two-dimensional array is stored) and vector products. A vector results.

PRINT The PRINT subroutine computes the strain on the inner and outer surface of each element. It also controls the program output and format.

QREM Evaluates the effective stiffness matrix $[K_s^*]$ supplied by the elastic foundation or restoring springs, and then imposes the prescribed displacement conditions accordingly.

STRESS This subroutine evaluates the generalized load vectors, $(\{P^*\} + [H^*]\{q^*\})$ of Eq. A.1 arising from the presence of large deflections and elastic-plastic strains. First the stresses and/or plastic strains are determined at each quadrature station, which involves the use of the strain-displacement relation and the stress-strain relations.

The strain-hardening and strain-sensitivity effects are taken into consideration. Next, the appropriate Gaussian integration scheme is used to form the element generalized nodal load for each element, and finally, an assembled generalized nodal load vector is calculated.

A.2.2 Partial List of Variable Names

A(I,J)	A, an 8x8 matrix, defines the transformation between the element generalized nodal displacements {q} and the parameters {β} in the assumed displacement field of each element. It is destroyed in computation and is replaced by its inverse A^{-1}.
AA(I,M,N)	Equals A^{-1}; it defines the transformation between the element generalized nodal displacements {q} and the parameters {β} in the assumed displacement field of the Ith element.
AINT	Pre-impact approach velocity of the fragment-impacted ring element system normal to the ring element.
AL(I)	Element arc length of the Ith element.
ANG(I)	The slope which is the angle between the tangent vector and the +Y axis at the Ith node.
APD	Work done on the structure by the collision of the fragments during a particular time step.
APDEN	Total work done on the structure by the collision of the fragments.
APN	Fragment induced impulse normal to the impacted ring element surface.
APT	Fragment induced impulse tangential to the impacted ring element surface.
ASFL(I,J,K,L)	Stress and/or plastic strain weighting factor on the Lth sublayer in the Kth depthwise Gaussian point at the Jth spanwise Gaussian station of the Ith element.
AWG(I) AXG(I)	Input vectors with dimension NOGA; contain Gaussian quadrature weights W_i and constants x_i $$\int_0^1 f(x)\,dx = \sum_i f(x_i)\,w_i$$ employed in the spanwise integration of each element.
B	Width of ring.

B1 B2 B3	Fragment-impacted ring element system geometrical constants: (See Eqs. 2.14, 2.15, 2.16) used in subroutine IMPACT.
BE1(J,I,K)	The transformation matrix that relates the strain at the Jth spanwise Gaussian station to the parameter $\{\beta\}$ in the assumed displacement field of each element.
BEP(IR,J,I,K)	Transformation matrix which relates the strain at the Jth spanwise Gaussian station to the generalized nodal displacements of the IRth element -
BETA	Ratio of distance from point of impart to I+1th node; to total straight line element length converted in subroutine IMPACT.
BNG(I)	Orientation angle of the Ith node of the ring measured clockwise from the positive Z axis; used in subroutine IMPACT.
BZER B1 B2	Coefficients in the quadratic representation of the meridional slope ϕ; used in subroutine ASSEM.
C5	Equals 1/P if the material is strain-rate dependent.
C6	Equals 1/(DSxDELTAT)
CELAS	Current ring elastic energy.
CEPS(J,I)	Equals $[D_I)\{q\}$, I = 1, 2, 3 at the spanwise Jth Gaussian station of each element.
CINET	Kinetic energy of the structure at the current time instant.
CINETF(I)	The kinetic energy of the Ith fragment at the current time instant.
CINEV(K)	A work vector used in the calculation of the kinetic energy of the structure.
CL(I) CLP(I)	The fractional distance from the centroid of the element to the Ith and I+1th node, respectively.

CMU, CMW	The Y and Z components of the distance between the centroid of the fragment and the position of the I+1th node.
COIY(I), COIZ(I)	The initial position of nodal point I measured with respect to the Y and Z global coordinate axes.
COPY(I), COPZ(I)	The current position of the Ith node with respect to the global Y and Z coordinate axes.
DALFA(J)	Impact-corrected displacement increment applied to the angular position of fragment J at the current time instant.
DELD(I)	Vector of dimension NI contains the impact-corrected generalized nodal displacement increments during the current time step.
DELTAT	Time step increment size selected by the user and input directly into the program.
DENS	Mass density of the ring material ($lb\text{-}sec^2/in^4$)
DET	Resultant determinant of matrix A
DFCGU(J)	Impact-corrected displacement increment applied to the position of fragment J in the global Y direction.
DFCGW(J)	Impact-corrected displacement increment applied to the position of fragment J in the global Z direction.
DISP(I)	Vector which contains the generalized nodal displacements at the current time instant.
DS	Material constant used in the strain-rate sensitivity formula.
ELAST	Total elastic energy present in the structure during the current time instant.
ELFP(I)	Element generalized nodal load vector due to the presence of large deflections and plastic

strains; it equals {p} + [h]{q} (See Ref. 14)

ELR(I,J) A work matrix of dimension 8x8 for the evaluation of the element effective stiffness matrix supplied by elastic restraints. It equals:

$$\int_0^{l_i} [N]^T [C] [N] d\eta$$

ELRP(I,J) Element effective stiffness matrix supplied by elastic restraints.

EPS(L) Input quantities of abscissa of the uniaxial stress-strain curve for the Lth mechanical sublayer material model (in/in).

EXANG The subtended angle of the ring. For complete rings EXANG = 360 degrees.

FACT1N, FACT2N Impact-induced correction factor applied to the normal-to-impact displacement increment at a given time step; applied to the IBIG and IPLUS nodes of the impacted ring segment, respectively.

FACT1T, FACT2T Impact-induced correction factor applied to the tangential-to-impact displacement increment at a given time step; applied to the IBIG and IPLUS nodes of the impacted ring segment, respectively.

FACTFN Impact-induced correction factor applied to the normal-to-impact displacement increment of the attacking fragment at the current time step; applied to the fragment JBIG.

FACTFT Impact-induced correction factor applied to the tangential-to-impact displacement increment of the attacking fragment at the current time step; applied to the fragment JBIG.

FACTFO Impact-induced correction factor applied to the rotational displacement increment of the attacking fragment at the current time step; applied to the fragment JBIG.

FACTNN Impact-induced correction factor applied to the normal-to-impact displacement increment of node NNBIG at the

	current time instant.
FACTNT	Impact-induced correction factor applied to the tangential-to-impact displacement increment of node NNBIG at the current time instant.
FARE, FCUR	Midplane axial strain and curvature increment, respectively, at the selected spanwise Gaussian station of each element.
FAU(J), FAW(J)	Location of centroid of fragment J at the present time cycle in the global Y,Z plane.
FLVA(I)	Assembled generalized load vector corresponding to large deflections and plastic strain presence; it equals $\{P^*\} + [H^*]\{q^*\}$
GFL(IR,I,J)	Stress and/or plastic strain weighting factor on the Jth depthwise Gaussian point at the Ith spanwise Gaussian station of the IRth element.
GZETA(IR,I,J)	Distance from the centroidal axis of the Jth depthwise Gaussian point at the Ith spanwise Gaussian station of the IRth element.
H(I)	Thickness of the ring at the Ith node.
HHALF(I)	Half the thickness of the ring at the midspan of element I
HNL(I)	Work vector of dimension 8, required for the evaluation of the element generalized nodal load vector due to large deflections and elastic-plastic strains.
HT(I)	Thickness of ring segment I at the point of impact.
IBIG	The subroutine IMPACT, IBIG represents the element number on which impact occurs; element bounded by nodes IBIG and IPLUS=IBIG+1. In the MAIN PROGRAM, IBIG is the element number whose midspan computed tensile strain exhibits the largest value during the run.
ICOL(I)	Vector, of length NI, contains the column number of the first nonzero entry in the Ith row of the structural mass and/or stiffness matrix.

IDET	Work vector used in subroutine FAC
IK	Number of discrete elements into which the whole structure is discretized for analysis.
INUM(I)	Vector of dimension NI contains the corresponding position in the linear array of the first nonzero entry in the Ith row of the structural mass and/or stiffness matrix.
ISIZE	Number of locations necessary for the storage of the structural mass and/or stiffness matrix in the linear array form.
IT	Current time step cycle number. Measured as time cycle after the specified TPRIM value.
JBIG	Number of fragment involved in ring element impact.
KROW(I)	The row number of the Ith irregular row in the structural mass and/or stiffness matrix.
LM(I)	Work vector of length 8 used by subroutine MINV.
M1	Cycle at which regular printout starts.
M2	Printout will occur every M2 cycles.
MM	Time step (cycle) at which run is to stop.
MMI(I)	Work vector of length 8 used by subroutine MINV.
MREAD MWRITE MPUNCH	Number for the data input tape unit, the printed output tape unit, and the punched output tape unit, respectively. These names must be assigned numbers corresponding to the user's computing center requirements.
NBC(I)	The prescribed displacement type number
NCOND	The number of nodes at which displacement conditions are to be specified.
NFL	The number of depthwise Gaussian points through the thickness for the numerical evaluations of stress resultants (axial forces and bending moments) at each spanwise Gaussian station.

NI	Total number of degrees of freedom of structure (unrestrained); it equals the number of nodes times 4. Also, it is the number of rows in the assembled stiffness matrix.
NIRREG	Number of irregular rows in the assembled stiffness matrix.
NNBIG	Node number at which nodal impact occurs.
NODEB(I)	The node at which the prescribed displacements are specified.
NOGA	The number of Gaussian stations to be employed for the spanwise integration of the element properties over each element.
NORP NORU	The number of point elastic restraints (elastic restoring springs) and the number of locally distributed elastic restraints, respectively, which are to be specified over the structure.
NQR	Number which, if greater than zero, indicates that there are elastic restraints specified over the structure.
NREL(I)	The element number at which the Ith point elastic restraint is to be specified.
NRST(I) NREU(I)	The first element and the number of elements, respectively, over which the Ith uniformly distributed elastic foundation is to be specified.
NSFL	Equals the number of mechanical sublayers in the strain hardening material model; also is the number of coordinate pairs defining the piecewise linear stress-strain curve.
P	Material constant used in the strain-rate sensitivity formula.
PAX(I,J)	Projection of the distance between the centroid location of the Jth fragment and the I+1 node along the straight-line-beam-representation axis

PD(I,J)	So-called penetration distance resulting from the impact of the Jth fragment with the Ith element
PDBIG	The largest penetration distance encountered during a given time cycle. Determines the order in which impact-generated corrections are applied in cases involving more than one impact occurrence during a particular time cycle.
PIE	Represents π = 3.14159265
PLAST	Total plastic work done on the structure up to the present time step (mechanical work dissipated by plastic flow)
PM(I) PN(I)	Work vectors of dimension 8, required for the evaluation of the element generalized nodal load vector due to large deflections and elastic-plastic strains used in subroutine STRESS.
PN(I,J)	Perpendicular distance from the axis of the Ith straight-line-beam element representation to the centroid of the fragment J at a point on the axis equal to PAX(I,J) from node I+1, used in subroutine IMPACT.
PND(I,J)	Penetration distance calculated for the impact case involving the Ith node and the Jth fragment.
PNDBIG	The largest penetration distance encountered during a given time cycle for cases involving nodal impact conditions.
REX(I)	The length coordinate along the cnetroidal axis from the node NREL(I) at which the Ith elastic restoring spring is specified.
RH	Thickness at a specified spanwise ring Gaussian station.
RL(I)	Straight line length of ring element I used in the collision inspection and correction procedure.
RMASS(I) RMX(I)	Lumped mass and moment of inertia values, respectively, at ring structure node I

RSIN(I) RCOS(I)	Sine and cosine, respectively, of the angle that element I makes with the global Y axis. Used in transformation from impact to local and local to global coordinate.
SCTP SCXP	The tangential and radial translational restoring spring constants, respectively.
SCRP	The rotational restoring spring constant
SCTU SCTW	Tangential and radial translational elastic foundation stiffness constants, respectively.
SCRU	Rotational elastic stiffness constants.
SIG(L)	Input quantities for the ordinates of the uniaxial static stress-strain curve for the Lth mechanical sublayer material model (lb/in^2).
SINT	Pre-impact relative sliding velocity of the fragment tangential to the impacted ring segment.
SNO(I)	Uniaxial static yield stress of the Ith mechanical sublayer material model.
SNS(I,J,K,L)	Axial stress on the Lth mechanical sublayer at the Kth depthwise Gaussian point at the Jth spanwise Gaussian station of the Ith element.
SNY	Uniaxial yield stress of the mechanical sublayer taking strain rate sensitivity into account.
SOL(I)	Contains the solution vector of a series of matrix equations..
SPDEN	Total energy stored in the elastic restoring springs and/or the elastic foundations at the current time instant.
SPRIN(I)	The assembled effective stiffness matrix supplied by elastic restraints (stored in linear-array form).
TIME	Current time after TPRIM=IT*DELTAT

TWG(I) TXG(I)	Input vectors with dimension NFL; contain Gaussian quadrature weights and constants of $$\int_{-1}^{1} f(x)\,dx = \sum_i f(x_i) W_i$$ used in the numerical integration of stresses and/or plastic strains through the thickness.
UNK(J)	Coefficient of friction between the Jth fragment and the surface of the ring.
VFA	Fragment angular velocity prior to impact.
VFN	Fragment velocity normal to ring surface prior to impact.
VFT	Fragment velocity tangential to ring surface prior to impact.
VNIBIG	Velocity of node IBIG normal to ring surface prior to impact.
VNIPLS	Velocity of node IPLUS normal to ring surface prior to impact.
VTIBIG	Velocity of node IBIG tangential to ring surface prior to impact.
VTIPLS	Velocity of node IPLUS tangential to ring surface prior to impact.
YOUNG	Elastic (Young's) modulus (the slope of the first segment in the piecewise linear representation of the uniaxial stress-strain curve).
Y(I) Z(I)	Initial Y and Z coordinates of node I in the global coordinate system.
YZET ZZET	The Y and Z coordinate, respectively, at a given spanwise quadrature station.

A.3 Input Information and Procedures

The information required to punch a set of data cards for a run of the CIVM-JET-4A program is presented in a step-by-step manner in this section. The variables to be punched on the nth data card are outlined, and in a box to the right is the format to be used for that card; the definition of and some restrictions for each variable are given below. This is done for each card in turn until all are described.

Format

Card 1

B, DENS, EXANG, — 3D15.6

where

- B — The width of the ring (inches)
- DENS — The mass density of the ring material (lb-sec^2/in^4)
- EXANG — The total subtended angle of the ring (degrees) (For a complete ring specify EXANG - 360 degrees)

Card 2

IK, NOGA, NFL, NSFL, MM, M1, M2, NF, — 8I5

where

- IK — The number of discrete elements used to model the whole ring structure. This number cannot exceed 50 (although this limitation may be relaxed by a changing of the appropriate dimension statements of the program).
- NOGA — The number of spanwise Gaussian stations to be used for the spanwise numerical integration over each element in evaluating the element properties {p} and [h]; NOGA = 3 is used in CIVM-JET-4A.
- NFL — The number of depthwise Gaussian points to be used for the numerical integration through the thickness of the element. Used to calculate the stress resultants at each spanwise Gaussian station. NFL = 4 is used in CIVM-JET-4A.
- NSFL — The number of mechanical sublayers in the strain-hardening model of the material. Equals the number

of coordinate pairs defining the polygonal approximation of the stress-strain curve of the material. This number must not exceed 5.

MM — Corresponds to the cycle number at which the run is to stop.

M1 — The cycle number at which the regular printout is to begin. M1 must not equal 0. Cycles are numbered after TPRIM.

M2 — The number of cycles between regular printout (i.e., print every M2 cycles).

NF — The number of fragments considered to be impacting the ring. This number is not to exceed 6.

Card 2a

Y(1), Z(1), ANG(1), H(1) — 4D15.6

Y(1), Z(1) — Initial Y and Z coordinates, respectively, of the the first node (inches)

ANG(1) — The slope (degrees) which is the angle between the tangent vector and the +Y axis at the first node. An angle from the +Y axis to the tangent vector in a counter clockwise direction is defined as a positive ANG(1).

H(1) — The thickness at the first node (inches)

Additional cards 2aa, 2ab, ... are punched in exactly the same format as Card 2a until the total number of 2a cards equals IK+1 for a partial ring and equals IK for a complete (360 degree) ring, where IK is the value appearing on Card 2. Also, the following conditions must be satisfied by ANG(I): (a) $-180° < \text{ANG(I)} \leq 180°$, and (b) $|\text{ANG(I+1)} - \text{ANG(I)}| < 15°$.

Card 3

DELTAT, CRITS, DS, P — 4D15.6

where

DELTAT — The time step Δt, to be employed for the timewise finite-difference operator. This value must meet all stability and convergence criteria.

Format

CRITS Value of the "critical material fracture strain" chosen by the user. Program will indicate the time cycle at which this value is first exceeded.

DS
P The value of the constants D, and p, respectively, used in the strain-rate sensitivity formula

$$\sigma_{y\ell} = \sigma_{o\ell}\left(1 + \left|\frac{\dot{\varepsilon}}{D}\right|^{1/p}\right)$$

where D has units sec^{-1}, $\sigma_{o\ell}$ is the static yield stress of the ℓth mechanical sublayer and $\sigma_{y\ell}$ is the corresponding rate-dependent yield stress. If the material does not exhibit strain-rate sensitive behavior, set DS = 0 and leave P blank.

Generally speaking, the value of $\Delta t \approx .8\ (2/\omega_{max})$ does not produce convergent transient ring response results for the fragment/ring structure impact situation. It is recommended, therefore, that an initial value chosen for this input parameter be tested for convergence by repeating the same calculation only with an appropriately smaller DELTAT value and evaluating the effect upon the ring response. If the change in ring response is negligible, the initial value may be used with confidence that it is a converged result. If large discrepancies exist, however, subsequent calculations must be performed to determine the most economical time step that still maintains convergent behavior.

Card 4

EPS(1), SIG(1), EPS(2), SIG(2) 4D15.6

where

EPS(1)
SIG(1) Make up the first coordinate pair of strain and stress (ε, σ) coordinates which are used to define the piecewise-linear approximation of the uniaxial static stress-strain curve. The stress-strain curve for which these values and those values following are obtained must be upwardly convex with nonnegative slope. (EPS = in/in, SIG = lb/in^2).

Format

EPS(2) } Make up the second coordinate pair of strain
SIG(2) } and stress coordinates.

Additional Cards 4a and 4b are punched in exactly the same format as Card 4 until the number of coordinate pairs equals the value NSFL punched on Card 2. The total number of strain, stress coordinate pairs specified must not exceed 5.

Card 5

FH(I), FCG(I), FCGX(I), FMASS(I), FMOI(I) 5D15.6

Card 6

UNK(I) D15.6

Card 7

UDOT(I), WDOT(I), ADOT(I), TPRIM(I), CR(I) 5D15.6

where

FH(I) The diameter of the circular disk model of fragment (I) (inches).

FCG(I) The initial Z coordinate of the centroid of fragment (I) measured from the global Y axis. The positive direction represents an initial location above the global Y axis (inches).

FCGX(I) The initial Y coordinate of the centroid of fragment (I) measured from the global Z axis. The positive direction represents an initial location to the right of the global Z axis (inches).

FMASS(I) The mass of fragment (I) ($lb\text{-}sec^2/in$).

FMOI(I) The mass moment of inertia of fragment (I) ($lb\text{-}sec^2\text{-}in$)

UNK(I) Coefficient of friction between fragment (I) and the ring surface. For analyses in which the effects of an "infinitely rough" ring surface are to be investigated; the value to be input for this variable is UNK(I) = 10.0. (0.100000 D+02)

UDOT(I) The velocity component of fragment (I) parallel to the global Y axis before initial impact (in/sec).

Positive UDOT(I) represents a fragment traveling to the right.

WDOT(I) The velocity component of fragment (I) parallel to the global Z axis before initial impact. The positive direction denotes a fragment traveling in an upwards (+Z) direction (in/sec.).

ADOT(I) The initial angular velocity of fragment (I) (rad/sec.). Positive sign denotes counter clockwise rotation.

TPRIM(I) A time before which there is no possibility of fragment I impacting anywhere on the ring. The checking process begins at this time instant. It may be used to decrease the number of time cycles considered by the given run. For multiple fragments, all TPRIM values must coincide (sec).

CR(I) Coefficient of restitution between the fragment (I) and the impacted ring surface.

Cards 5, 6, and 7 must be repeated in that order, NF times, where NF is the number of fragments involved in the present analysis.

Card 8

AXG(1), AXG(2), AXG(3) 3F15.10

where

AXG(I) Vector of dimension NOGA contains Gaussian quadrature constants x_i for the numerical integration of

$$\int_0^1 f(x)\,dx = \sum_i f(x_i)\,W_i$$

If NOGA = 3 for example, then the following data appear on this card.

0.1127016654 0.5 0.8872983346

Format

Card 9

AWG(1), AWG(2), AWG(3) 3F15.10

where

AWG(I) Vector of dimension NOGA contains Gaussian quadrature weights W_i for the numerical integration of

$$\int_0^1 f(x)\,dx = \sum_i f(x_i)\,w_i$$

If NOGA = 3, the following data appear on Card 6

0.2777777778 0.4444444444 0.2777777778

Card 10

TXG(1), TXG(2), TXG(3), TXG(4) 4F15.10

Card 11

TWG(1), TWG(2), TWG(3), TWG(4) 4F15.10

where

TXG(I), TWG(I) Vectors of dimension NFL contain Gaussian quadrature constants x_i and weights w_i, respectively, for the numerical integration of:

$$\int_{-1}^{1} f(x)\,dx = \sum_i f(x_i)\,W_i$$

If NFL = 4 for example, then the following data appear on Card 10:

-0.8611363115 -0.3399810435 0.3399810435 0.8611363115

and the data

0.3478548451 0.6521451548 0.6521451548 0.3478548451

appear on Card 11.

Format

Card 12

NBCOND I5

where

NBCOND The total number of prescribed nodal displacement conditions to be specified on the structure. This number must not exceed 4. If NBCOND≠0 punch Cards 12a, ...

Card 12a

NBC(I), NODEB(I) 2I5

where

NBC(I), NODEB(I) The identification number and the node number, respectively, for which the Ith displacement condition is to be imposed.

The appropriate form of the data group NBC(I), NODEB(I) should be repeated NBCOND times. If NBCOND = 0, there are no prescribed displacement conditions to be imposed on the structure; then omit NBC(I) and NODEB(I) on Card 12a.

The prescribed displacement identification number can be equal to 1, 2, or 3, depending on the type of the prescribed displacement condition. Its description follows:

NBC(I)=1 Symmetry displacement condition. Setting the degrees of freedom v and ψ at the node NODEB(I) equal to zero.

NBC(I)=2 Ideally-clamped condition. Setting v, w, and ψ at node NODEB(I) to zero.

NBC(I)=3 Smooth-hinged/fixed condition. Setting v and w at node NODEB(I) to zero.

Card 13

NQR, NORP, NORU 3I5

where

Format

NQR	Indicator which if greater than 0 indicates that the structure is subject to elastic restraints (point and/or distributed).
NORP	The number of point elastic restraints (elastic restoring springs) which are prescribed over the structure. This number must not exceed 4.
NORU	The number of local distributed elastic restraints (elastic foundations) which are to be prescribed over the structure. This number must not exceed 4.

If there are no prescribed elastic foundations on the structure, set NQR = 0 and leave NORP and NORU blank.

Cards 13a and 13b are included only if NQR is greater than zero on Card 13.

If NORP = 0 skip to Card 13b.

Card 13a

SCTP, SCTY, SCRP 3D15.6

Card 13aa

NREL(1), REX(1), NREL(2), REX(2), ... NREL(4), REX(4) 4(I5,D15.6)

where

SCTP	The translational tangential restoring spring constant (lb/in)
SCTY	The translational radial restoring spring constant (lb/in)
SCRP	The torsional restoring spring constant
NREL(I), REX(I)	The element number and the length coordinate, respectively, along the centroidal axis from node NREL(I) of the element at which the Ith point elastic restraint is specified. The positive direction of REX(I) is the clockwise direction from the midpoint of the element.

The data group NREL(I), REX(I) must be repeated NORP times.

If NORU = 0 on Card 13 omit Card 13b and Card 13c. Card 14 then follows immediately.

Card 13b

SCTU, SCRU, NRST(1), NREU(1), ... , NRST(4), NREU(4) 2D15.6,8I5

where

SCTU	Elastic foundation stiffness in translation, tangential to the midsurface of the ring (lb/in^2)
SCRU	Elastic foundation stiffness in torsion (in-lb)/(rad-in)
NRST(I) NREU(I)	The first element and the number of elements respectively, over which the Ith elastic foundation is to be specified (the first elastic foundation is distributed to element NRST(1) through and including element (NRST(1) + NREU(1)-1)

Data group NRST(I) and NREU(I) are repeated NORU times.

Card 13c

SCTW, NRST(1), NREU(1), ... , NRST(4), NREU(4) D15.6,8I5

where

SCTW	Elastic foundation stiffness in translation along the line of the normal to the ring's surface (lb/in^2).

Card 14

ICONT I5

where

ICONT	Indicator which if greater than 0 indicates that this is a continuation run. It should be noted that included in the output of each completed run is a set of continuation cards which contains all of the information that is necessary to continue the same run, if desired, to obtain further time-history information. Each completed continuation run also produces a continuation deck, so the process may be continued indefinitely as long as desired.

Format

If the indicator ICONT is greater than zero, the continuation deck produced from the output of the previous run follows immediately. The continuation deck contains the following information:

Card 14a 4I5

IT, IBIG, ISURF, MCRIT

where

- IT — The number of the time cycle at which the previous run had stopped, and is the beginning time cycle of the present continuation run.
- IBIG — The element number whose midspan computed tensile strain exhibits the largest value during the previous run.
- ISURF — Equals 1 means largest computed tensile strain occurs on the inner surface; equals 2 means on the outer surface.
- MCRIT — A dummy variable which controls the strain checking process to check the location where the strain first exceeds a prescribed value.

Card 14b 4D15.7

TIME, BIG, BTIME

where

- TIME — The absolute time at which the previous run stopped, and is the beginning time of the present continuation run.
- BIG — The largest computed tensile strain during the previous run
- BTIME — The time at which the largest computed tensile strain occurred during the previous run.

Card 14bb 4D15.7

DISP(I)

- DISP(I) — The displacement of the Ith degree of freedom at time cycle IT. Repeat cards until all degree of freedom displacements are specified with 4 different values/card.

Format

Card 14bc

DELD(I) 4D15.7

DELD(I) The displacement increment change of the Ith degree of freedom of the structure at time cycle IT. Repeat cards until all degrees of freedom are included, with 4 different values/card.

Card 14bd

SNS(IR,J,K,L) 4D15.7

SNS(IR,J,K,L) The axial stress on the Lth mechanical sub-layer at the Kth depthwise Gaussian point at the Jth spanwise Gaussian station of the IRth element at time cycle IT. Repeat cards until all values for the entire structure are included, with 4 different values/card.

Card 14be

FCGU(J), FCGW(J), ALFA(J), DFCGU(J), DFCGW(J), DALFA(J) 6D12.6

FCGU(J) The centroidal position of the Jth fragment in the Y direction at time cycle IT (inches).

FCGW(J) The centroidal position of the Jth fragment in the Z direction at time cycle IT (inches).

ALFA(J) The total angular displacement of the Jth fragment at time cycle IT (radians).

DFCGU(J) The displacement increment in the Y global direction of the Jth fragment at the time cycle IT (inches).

DFCGW(J) The displacement increment in the Z global direction of the Jth fragment at time cycle IT (inches).

DALFA(J) The angular displacement increment of the Jth fragment at time cycle IT (rad).

A.3.1 Energy Accounting Option

To exercise the energy accounting option that is included in the CIVM-JET-4A program, the procedure is as follows:

(1) Remove the dummy subroutine ENERGY from the source deck.

(2) Replace this dummy subroutine with the actual ENERGY subroutine that is used to perform the energy-accounting calculation.

(3) No changes or additions to be input described above are needed.

A.3.2 Input for Special Cases of the General Stress-Strain Relations

In the following, the specific input data for three special cases of the general elastic, strain-hardening constitutive relation handled by the computer program are given. Only the relevant data are noted:

1. Purely Elastic Case
   Set NSFL=1 on Card 2, and make EPS(1) and SIG(1) on Card 4 sufficiently high so that no plastic deformation occurs; for example, EPS(1)=1.0, SIG(1)=ES(1), where ES(1) equals the elastic (Young's) modulus.
2. Elastic, Perfectly-Plastic Case
   Set NSFL=1 on Card 2 and make EPS(1)=SIG(1)/ES(1) on Card 4.
3. Elastic, Linear Strain-Hardening Case
   Set NSFL=2 on Card 3 and set EPS(1)=SIG(1)/ES(1). Also EPS(2) and SIG(2) on Card 4 are taken sufficiently high in order to avoid plastic deformation in the second sub-flange. For example, EPS(2)=1.0, and SIG(2)=(1. - EPS(1)) x ES(2) + SIG(1), where ES(2) is the slope of the segment in the plastic range.

A.4 Description of the Output

The printed output begins with a partial re-iteration of the input quantities specified for the ring structural geometry, displacement conditions, and material properties. The fragment-properties output include not only those specified by user input but also the calculated initial kinetic energy of each fragment.

After the initial printout has been completed, the following information is printed at time cycle M1 and at intervals of M2:

```
J = [IT]     TIME = [TIME]
I  V  W  PSI  CHI  COPY  COPZ  L  M  STRAIN(IN)  STRAIN(OUT)
1
2
3
.
.
.
.
.
FRAG NO.=          FCGU =          FCGW =          ALFA =
   [J]           [FCGU(J)]       [FCGW(J)]       [ALFA(J)]
    .                .               .               .
    .                .               .               .
    .                .               .               .
```

IT	Cycle number
TIME=	Elapsed time corresponding to the end of cycle J (sec)
I=	Node number in clockwise order. For a partial ring the total number of nodes is one more than the number of elements. For a complete ring, the number of nodes equals the total number of elements.
V=	The middle plane axial displacement at node I (in)
W=	The middle plane transverse displacement at node I (in)

PSI=	The generalized nodal displacement $\psi = (\partial w/\partial \eta) - v/R$ at node I (rad)
CHI=	The generalized nodal displacement $\chi = (\partial v/\partial \eta) + w/R$ at node I (rad)
COPY=	The current global Y coordinate of nodal point I (in)
COPZ=	The current global Z coordinate of nodal point I (in)
L=	Axial internal force resultant over the cross section at the midspan point of element I (lb)
M=	Internal bending moment of the cross section at the midspan point of element I (in-lb)
STRAIN(IN)=	Strain on the inner surface at the midspan point of element I
STRAIN(OUT)=	Strain on the outer surface at the midspan point of element I
J=	Fragment number
FCGU(J)=	Global Y coordinate of the centroid of fragment J at the current time instant (in)
FCGW(J)=	Global Z coordinate of the centroid of fragment J at the current time instant (in)
ALFA(J)=	Angular rotation of fragment J to the current time instant (rad).

The detection of an impact between a fragment and a ring element during a given time cycle results in the following printout at that cycle:

```
IMPACT IT=[IT]  ELEMENT NO.=[I]   FRAGMENT NO.=[J]
LOCATION ON ELEMENT=[PAX(I,J)]  PENETRATION DIST=[PD(J)]
```

IT=	Time cycle during which impact occurs
I=	Ring element involved in this particular collision
J=	Fragment involved in this particular collision
PAX(I,J)=	Distance from node I+1 of element I to point of impact for this particular collision.

PD(I,J)= "Penetration distance" calculated for this particular collision.

For cases involving impact at a nodal point of the discretized structure, the output is as follows:

IMPACT IT=[IT] NODE NO.=[NNBIG] FRAG NO.=[N] PD=[PND(I,J)]

NNBIG= Node number at which impact occurs

PND(I,J)= "Penetration distance" calculated for this particular collision.

For those analyses in which a check of the energy characteristics of the system is desired, the following information is output for each print time cycle:

CURRENT TIME CYCLE	FRAGMENT	KINETIC ENERGY
[IT]	[J]	[CINETF(J)]

WORK INPUT INTO RING TO TIME STEP [IT] = [RWORK]

RING KINETIC ENERGY AT TIME STEP [IT] = [CINETO]

RING ELASTIC ENERGY TO TIME STEP [IT] = [CELAS]

RING PLASTIC WORK TO TIME STEP [IT] = [PLAST]

ENERGY STORED IN ELASTIC RESTRAINTS = [SPDEN]

CINETF(J)= Kinetic energy of fragment J at the current time instant

CINETO= Ring kinetic energy at current time instant*

RWORK= Total work done on the ring structure to the current time instant

CELAS= Total ring elastic energy to the current time instant.

---

*It should be noted that the rigid body part of the kinetic energy, which is used to accelerate the "rigid body" mass of the structure, can be extracted and identified separately. However, for the present program dealing with rather general structural geometries and with various support/restraint conditions, it would be very unwieldy (but not impossible) to identify these separate kinetic energies; hence, the total kinetic energy is calculated and printed out.

PLAST= Total plastic work done on the ring to the current time instant.*

SPDEN= Energy stored in the elastic restraints (if the presence of elastic restraints is specified).

At each printout cycle, a strain-checking process is carried out. Asterisks are printed to the right of the strain printout only for the cycle when the strain first exceeds the "critical" value. No further strain checking or action is taken by the program, however, and the computational process proceeds until the end of the run as if the material had not "failed".

At the conclusion of each run, a statement "LARGEST COMPUTED STRAIN= ... OCCURS AT THE INNER (or OUTER) SURFACE MIDSPAN OF ELEMENT ... AT TIME (SEC)= ..." is printed out. This statement gives the largest computed strain, and the time and the location at which it occurs during the transient respon se. It should be noted that the strains are computed only at every printout cycle, and also only on the inner and outer surface at the midspan of each element.

A.5 Complete FORTRAN IV Listing of the CIVM-JET-4A Program

The CIVM-JET-4A program consists of the following main program and 14 subroutines:

1. CIVM-JET-4A MAIN PROGRAM
2. ASSEF
3. ASSEM
4. DINIT
5. ELMPP
6. ENERGY

---

*The plastic work done on the ring is estimated by subtracting the sum of the elastic and kinetic energies present in the ring from the total input energy (due to the externally-applied load and the initially-imprted kinetic energy); i.e., RWORK=CINETO+CELAS+PLAST+SPDEN. It should be mentioned that the approximate nature of this numerical calculation will sometimes yield impossible results such as negative values of plastic work or values greater than zero when the ring has not yet reached a plastic condition; thus, the value of plastic work should be considered only approximate, and spurious results as noted above should be ignored. This term may also be considered to contain, in addition, the energy dissipated by friction.

7. ERC
8. FICOL
9. IDENT
10. IMPACT
11. MINV
12. OMULT
13. PRINT
14. QREM
15. STRESS

A complete listing of the CIVM-JET-4A program is given below in the above order. The number of memory locations required on the IBM 370/165 computer at MIT is approximately 350,000 bytes. This includes the locations required for the MIT computer library subroutines.

```
C                *****CIVM JET 4A*****                                  MAIN0010
      IMPLICIT REAL*8(A-H,C-Z)                                           MAIN0020
      DIMENSION AFP(3,3,8), BEPS(3,3)                                    MAIN0030
      DIMENSION RMOI(51),CL(51),CLP(51),CLA(51),CLPA(51)                 MAIN0040
      DIMENSION AA(50,8,8),TXG(6),TWG(6),ES(6),GFL(50,3,6)               MAIN0050
     *,SOL(205),INUM(205),          KROW(8),NDEX(8)                      MAIN0060
       COMMON /BA/ BEP(50,3,3,8),AL(50),AXG(3),AWG(3)                    MAIN0070
      COMMON/ABC/RMX(51),RWORK,CINEY(205)                                MAIN0080
       COMMON /TAPE/ MREAD,MWRITE,MPUNCH                                 MAIN0090
      COMMON/SC/CRITS,BIG,BTIME,MCRIT,IBIG,ISURF                         MAIN0100
       COMMON /VQ/ FLVA(205),DISP(205),DELD(205),SNS(50,3,6,5),          MAIN0110
     *BINP(50,3),BIMP(50,3),TDISP(205),TU(205),TW(205),                  MAIN0120
     *COIY(205),COIZ(205),DELTAT                                         MAIN0130
      COMMON/FG/Y(51),Z(51),ANG(51),H(51),B,EXANG,NS,IK,NOGA,NFL,NSFL,   MAIN0140
     *NI,ICOL(205),NBCOND,NBC(4),NODEB(4)                                MAIN0150
       COMMON /HM/ YOUNG,DS,C5,C6,ASFL(50,3,6,5),GZETA(50,3,6),SNO(5)    MAIN0160
      COMMON/FRAG/FH(6),FCG(6),FMASS(6),FMOI(6),FCGL(6),FCGW(6),ALFA(6),MAIN0170
     *UDOT(6),WDOT(6),ADOT(6),TPRIM(6),CR(6),FCGX(6),UNK(6),NF           MAIN0180
      COMMON /DFRAG/DFCGU(6),DFCGW(6),DALFA(6)                           MAIN0190
      COMMON/ENERG/FK(6),CINETO,CUMW,DELKE,CELAS,ELAS,PLASTC             MAIN0200
      COMMON/LEFT/P,EPS(5),SIG(5),RMASS(51)                              MAIN0210
      COMMON/ELFU/SPRIN(2060),FQREF(205),REX(4),NQR,NORP,NORU,NREL(4),   MAIN0220
     *NRST(4),NREU(4)                                                    MAIN0230
      COMMON /EP/ EPSI(50),EPSO(50)                                      MAIN0225
      SIN(Q)=DSIN(Q)                                                     MAIN0240
      COS(Q)=DCOS(Q)                                                     MAIN0250
      ATAN(Q)=DATAN(Q)                                                   MAIN0260
      ABS(Q)=DABS(Q)                                                     MAIN0270
      SQRT(Q)=DSQRT(Q)                                                   MAIN0280
       MREAD=5                                                           MAIN0290
       MWRITE=6                                                          MAIN0300
      IRRUN= 1                                                           MAIN0305
       MPUNCH=7                                                          MAIN0310
 5555 READ(MREAD,1)B,DENS,EXANG,IK,NOGA,NFL,NSFL,MM,M1,M2,NF             MAIN0320
 1    FORMAT(3D15.6/8I5)                                                 MAIN0330
       PIE=3.14159265                                                    MAIN0340
```

```
      IKP1=IK+1
      NS=IK
      IF(EXANG.NE.360.)NS=IKP1
      READ(MREAC,11) (Y(I),Z(I),ANG(I),H(I),I=1,NS)
 11    FORMAT(4E15.6)
      CO 111 I=1,NS
 111  ANG(I)=ANG(I)*PIE/180.
      IF(EXANG.NE.360.)GO TO 201
      Y(IKP1)=Y(1)
      Z(IKP1)=Z(1)
      H(IKPL)=H(1)
      ANG(IKP1)=ANG(1)
 201  READ(MREAC,2)DELTAT,CRITS,DS,P,(EPS(L),SIG(L),L=1,NSFL)
      DC 202 I=1,NF
      READ(MREAD,601)FH(I),FCG(I),FCGX(I),FMASS(I),FMOI(I)
      READ(MREAD,601)UNK(I)
 202  READ(MREAC,602)UDOT(I),WDOT(I),ACOT(I),TPRIM(I),CR(I)
 601  FCRMAT(6D15.6)
 602  FCRMAT(5D15.6)
 2     FORMAT(4E15.6/(4E15.6))
       READ(MRFAD,3)(AXG(K),K=1,NOGA)
       READ(MREAD,3)(AWG(K),K=1,NOGA)
       READ(MREAD,3)(TXG(K),K=1,NFL)
       RFAC(MREAD,3)(TWG(K),K=1,NFL)
 3     FORMAT(4F15.10)
      NI=NS*4
      READ(MREAC,4)NBCOND
      IF(NBCCNC.EQ.0)GC TO 748
      READ(MRFAD,4)(NBC(I),NODEB(I),I=1,NBCOND)
 4     FCRMAT(9I5)
 748   READ(MREAD,9) NQR,NCRP,NCRU
 9     FORMAT(3I5)
      MX=M1
      MY=M2
      CUMW=0.C
      CELKE=C.C
```

```
      DO 203 I=1,NF                                                     MAIN0710
  203 FK(I)=(FMASS(I)/2.0)*(UDOT(I)**2+WDOT(I)**2)+(FMOI(I)/2.0)*(ADOT(IMAIN0720
     *)**2)                                                             MAIN0730
      CALL IDENT(NQR,DENS)                                              MAIN0740
       DO 70 IR=1,IK                                                    MAIN0750
       DO 70 J=1,NOGA                                                   MAIN0760
       RH=H(IR)*(1.-AXG(J))+H(IR+1)*AXG(J)                              MAIN0770
       DO 70 K=1,NFL                                                    MAIN0780
       GFL(IR,J,K)=RH*TWG(K)*B/2.                                       MAIN0790
   70  GZETA(IR,J,K)=RH*TXG(K)/2.                                       MAIN0800
       ES(1)=SIG(1)/EPS(1)                                              MAIN0810
       IF(NSFL-1)77,77,76                                               MAIN0820
   76  DO 78 L=2,NSFL                                                   MAIN0830
   78  ES(L)=(SIG(L)-SIG(L-1))/(EPS(L)-EPS(L-1))                        MAIN0840
   77  ES(NSFL+1)=0.0                                                   MAIN0850
       DO 79 L=1,NSFL                                                   MAIN0860
   79  SNO(L)=ES(1)*EPS(L)                                              MAIN0870
       YOUNG=ES(1)                                                      MAIN0880
       DO 71 IR=1,IK                                                    MAIN0890
       DO 71 J=1,NOGA                                                   MAIN0900
       DO 71 K=1,NFL                                                    MAIN0910
       DO 71 L=1,NSFL                                                   MAIN0920
   71  ASFL(IR,J,K,L)=GFL(IR,J,K)*(ES(L)-ES(L+1))/ES(1)                 MAIN0930
       DO 15 I=1,8                                                      MAIN0960
   15  ICOL(I)=1                                                        MAIN0970
       IKM1=IK-1                                                        MAIN0980
      IF(EXANG.NE.360.)GO TO 210                                        MAIN0990
       DO 16 I=3,IKM1                                                   MAIN1000
       IK4=I*4                                                          MAIN1010
       IK3=IK4-1                                                        MAIN1020
       IK2=IK4-2                                                        MAIN1030
       IK1=IK4-3                                                        MAIN1040
       JJ=(I-1)*4-3                                                     MAIN1050
       ICOL(IK1)=JJ                                                     MAIN1060
       ICOL(IK2)=JJ                                                     MAIN1070
       ICOL(IK3)=JJ                                                     MAIN1080
```

```
      ICOL(IK4)=JJ
   16 CONTINUE
      ICOL(IK*4)=1
      ICOL(IK*4-1)=1
      ICOL(IK*4-2)=1
      ICOL(IK*4-3)=1
      GO TO 218
  210 DO 211 I=3,IKP1
      IK4=I*4
      IK3=IK4-1
      IK2=IK4-2
      IK1=IK4-3
      JJ=(I-1)*4-3
      ICOL(IK1)=JJ
      ICOL(IK2)=JJ
      ICOL(IK3)=JJ
      ICOL(IK4)=JJ
  211 CONTINUE
  218 INUM(1)=1
      DO 99 I=2,NI
   99 INUM(I)=I-ICOL(I-1)+INUM(I-1)
      DO 990 I=1,NI
  990 INUM(I)=INUM(I)-ICOL(I)
      NIRREG=0
      INDEX=0
      ISET=1
      DO 116 I=1,NI
      L=ICOL(I)
      IF(ICOL(I)-ISET)117,116,119
  119 ISET=ICOL(I)
      GO TO 116
  117 NIRREG=NIRREG+1
      IF(NIRREG-NI/2)711,711,90
  711 KROW(NIRREG)=I
      NDEX(NIRREG)=INDEX
  116 INDEX=INDEX+I-L
```

```
 90    CALL FICCL(NI,NI,L,ICCL)                                          MAIN1450
       ISIZE=L                                                           MAIN1460
       WRITE(MWRITE,17) L                                                MAIN1470
 17    FORMAT(/,'   SIZE OF ASSEMBLED MASS OR STIFFNESS MATRIX =',I5)   MAIN1480
      CALL ELMPP(DELTAT,AA,ISIZE,KROW,NDEX,NIRREG,INUM,DENS,YOUNG)      MAIN1490
 61   DO 981 IR=1,IKP1                                                  MAIN1500
      RMASS(IR)=0.C                                                     MAIN1510
 981  RMX(IR)=0.0                                                       MAIN1520
      DO 980 IR=1,IK                                                    MAIN1530
      CL(IR)=(2.*H(IR+1)+H(IR))/(3.*H(IR+1)+3.*H(IR))                   MAIN1540
      CLP(IR)=1.0-CL(IR)                                                MAIN1550
      CLA(IR)=AL(IR)*CL(IR)                                             MAIN1560
      CLPA(IR)=AL(IR)*CLP(IR)                                           MAIN1570
 980  RMOI(IR)=(H(IR)**2+4.*H(IR)*H(IR+1)+H(IR+1)**2)*AL(IR)**3/        MAIN1580
     *(36.*(H(IR)+H(IR+1)))*B*DENS                                      MAIN1590
      DO 982 I=1,IKM1                                                   MAIN1600
      RMASS(I)=RMASS(I)+(H(I)+H(I+1))*B*DENS*CLPA(I)/2.0                MAIN1610
      RMASS(I+1)=RMASS(I+1)+(H(I)+H(I+1))*B*DENS*CLA(I)/2.0             MAIN1620
      RMX(I)=RMX(I)+RMOI(I)*CLP(I)                                      MAIN1630
 982  RMX(I+1)=RMX(I+1)+RMOI(I)*CL(I)                                   MAIN1640
      IF(EXANG.EQ.360.)GO TO 983                                        MAIN1650
      RMASS(IK)=RMASS(IK)+(H(IK)+H(IK+1))*B*DENS*CLPA(IK)/2.0           MAIN1660
      RMASS(IK+1)=RMASS(IK+1)+(H(IK)+H(IK+1))*B*DENS*CLA(IK)/2.0        MAIN1670
      RMX(IK)=RMX(IK)+RMOI(IK)*CLP(IK)                                  MAIN1680
      RMX(IK+1)=RMX(IK+1)+RMOI(IK)*CL(IK)                               MAIN1690
      GO TO 984                                                         MAIN1700
 983  RMASS(IK)=RMASS(IK)+(H(IK)+H(IK+1))*B*DENS*CLPA(IK)/2.0           MAIN1710
      RMASS(1)=RMASS(1)+(H(IK)+H(IK+1))*B*DENS*CLA(IK)/2.0              MAIN1720
      RMX(IK)=RMX(IK)+RMOI(IK)*CLP(IK)                                  MAIN1730
      RMX(1)=RMX(1)+RMOI(IK)*CL(IK)                                     MAIN1740
 984  CONTINUE                                                          MAIN1750
      DO 5 IR=1,NS                                                      MAIN1760
      SOL(IR*4-3)=RMASS(IR)                                             MAIN1770
      SOL(IR*4-2)=RMASS(IR)                                             MAIN1780
      SOL(IR*4-1)=RMX(IR)                                               MAIN1790
 5    SOL(IR*4)=RMX(IR)                                                 MAIN1800
```

```
      DC 6 I=1,NI
6     SOL(I)=DELTAT**2/SOL(I)
       IF (NQR .EQ. 0) GO TO 22
       DO 23 L=1,ISIZE
 23    SPRIN(L)=0.C
             CALL QREM(AA,AL,AXG,AWG)
 22    IF(DS.EQ.0.C) GO TO 21
       C5=1./P
       C6=1./DS/DELTAT
   21  MCRIT=0
       BIG=10.**(-10)
       IBIG=0
      DC 75 I=1,NS
      CCIY(I)=Y(I)
75    COIZ(I)=Z(I)
      READ(MREAC,82)ICONT
82    FORMAT(I5)
83    FORMAT(4I5)
84    FCRMAT(4E15.7)
385   FCRMAT(6C12.6)
      IF(ICONT-1)80,81,81
80    CALL DINIT(IT,TIME)
      GC TO 992
81    READ(MREAC,83)IT,IBIG,ISURF,MCRIT
      READ(MREAD,84)TIME,BIG,BTIME
      READ(MREAD,84)(DISP(I),I=1,NI)
      READ(MREAD,84)(DELD(I),I=1,NI)
      READ(MREAD,84)((((SNS(IR,J,K,L),L=1,NSFL),K=1,NFL),J=1,NOGA),IR=1
     *,IK)
      READ(MREAC,385)(FCGU(J),FCGW(J),ALFA(J),DFCGU(J),DFCGW(J),
     *CALFA(J),J=1,NF)
992   IT=IT+1
      CALL IMPACT(IT,NIRREG,CENS)
      DC 994 I=1,NI
994   DISP(I)=DISP(I)+DELD(I)
      DO 822 I=1,NF
```

```
      FCGU(I)=FCGU(I)+DFCGU(I)                                          MAIN2170
      FCGW(I)=FCGW(I)+DFCGW(I)                                          MAIN2180
  822 ALFA(I)=ALFA(I)+DALFA(I)                                          MAIN2190
      DO 522 I=1,NI                                                     MAIN2200
      FQREF(I)=0.0                                                      MAIN2210
  522 FLVA(I)=0.0                                                       MAIN2220
      CALL STRESS                                                       MAIN2230
      IF(NQR.EQ.0)GO TO 735                                             MAIN2280
      CALL OMULT(SPRIN,DISP,ICOL,NI,FQREF,KROW,NDEX,NIRREG)             MAIN2290
      DO 736 I=1,NI                                                     MAIN2300
  736 FLVA(I)=FLVA(I)+FQREF(I)                                          MAIN2310
  735 CONTINUE                                                          MAIN2320
      IF(IT-MX)815,816,815                                              MAIN2240
  816 MX=MX+MY                                                          MAIN2250
      CALL ENERGY(IT,KROW,NDEX,NIRREG)                                  MAIN2260
  815 CONTINUE                                                          MAIN2270
  686 IF(NBCOND.EQ.0)GO TO 889                                          MAIN2330
      DO 888 I=1,NBCOND                                                 MAIN2340
      NXY=NODEB(I)                                                      MAIN2350
      IF(NBC(I).EQ.1)GO TO 886                                          MAIN2360
      IF(NBC(I).EQ.2)GO TO 887                                          MAIN2370
      IF(NBC(I).EQ.3)GO TO 885                                          MAIN2380
  886 FLVA(NXY*4-3)=0.0                                                 MAIN2390
      FLVA(NXY*4-1)=0.0                                                 MAIN2400
      GO TO 888                                                         MAIN2410
  887 FLVA(NXY*4-3)=0.0                                                 MAIN2420
      FLVA(NXY*4-2)=0.0                                                 MAIN2430
      FLVA(NXY*4-1)=0.0                                                 MAIN2440
      GO TO 888                                                         MAIN2450
  885 FLVA(NXY*4-3)=0.0                                                 MAIN2460
      FLVA(NXY*4-2)=0.0                                                 MAIN2470
  888 CONTINUE                                                          MAIN2480
  889 NIFE=NI                                                           MAIN2490
      DO 525 I=1,NI                                                     MAIN2492
  525 DELD(I)=DELD(I)-FLVA(I)*SOL(I)                                    MAIN2494
      TIME=IT*DELTAT                                                    MAIN2496
```

```
      DO 60 IR=1,IK
      DO 604 I=1,NOGA
      DO 604 J=1,3
      BEPS (I,J)= 0.0
      DO 604 K=1,8
      INDEX= (IR-1)*4+K
  604 BEPS(I,J)= BEPS(I,J)+ BEP(IR,I,J,K )* DISP(INDEX)
      IP=IR+1
      HDIF=H(IP)-H(IR)
      DO 60 M =1,3
      HHAG=(H(IR)+ AXG(M)* HDIF) /2.0
      FARE= BEPS(M,1)+BEPS(M,2)**2/2.0
      EPI= FARE -HHAG* BEPS(M,3)
      EPO= FARE+ HHAG* BEPS(M,3)
      IF(M-2) 594,595,594
  595 EPSI(IR)=EPI
      EPSO(IR)=EPO
  594 IF (EPI .LE.BIG) GO TO 591
      BIG=EPI
       IBIG=IR
      ISTA=M
       ISURF=1
       BTIME=TIME
  591 IF (EPO .LE . BIG) GO TO 60
      BIG=EPO
      IBIG=IR
      ISTA=M
       ISURF=2
       BTIME=TIME
 60    CONTINUE
      IF(IT-M1)987,988,150
988    M1=M1+M2
      CALL PRINT(IT,TIME)
987   IF(IT-MM)992,965,150
965    IF(IBIG) 62,150,62
 62    IF(ISURF-2) 64,65,65
  580 FORMAT('    AT GAUSSIAN STATION  =',I3)
 64    WRITE(MWRITE,66) BIG,IBIG,BTIME
 66    FORMAT(///,'    LARGEST COMPUTED STRAIN =',D15.6,' OCCURS AT THE
     *INNER SURFACE OF ELEMENT =',I3,' AT TIME (SEC.) =',D15.6)
      WRITE(MWRITE,580) ISTA
       GO TO 150
 65    WRITE(MWRITE,67) BIG,IBIG,BTIME
 67    FORMAT(///,'    LARGEST COMPUTED STRAIN =',D15.6,' OCCURS AT THE
     *OUTER SURFACE OF ELEMENT =',I3,' AT TIME (SEC.) =',D15.6)
      WRITE(MWRITE,580) ISTA
  150 WRITE(MPUNCH,83)IT,IBIG,ISURF,MCRIT
      WRITE(MPUNCH,84)TIME,BIG,BTIME
      WRITE(MPUNCH,84)(DISP(I),I=1,NI)
      WRITE(MPUNCH,84)(DELD(I),I=1,NI)
       WRITE(MPUNCH,84)((((SNS(IR,J,K,L),L=1,NSFL),K=1,NFL),J=1,NOGA),
     *IR=1,IK)
      WRITE(MPUNCH,385)(FCGU(J),FCGW(J),ALFA(J),DFCGU(J),DFCGW(J),
     *DALFA(J),J=1,NF)
 1110 CALL EXIT
      END
```

```
      SUBROUTINE ASSEF(IR,IK,ELFP,FLVA,EXANG)                           ASSF0010
      IMPLICIT REAL*8(A-H,O-Z)                                          ASSF0020
       DIMENSION NN(8),FLVA(1),ELFP(1)                                  ASSF0030
      SIN(Q)=DSIN(Q)                                                    ASSF0040
      COS(Q)=DCOS(Q)                                                    ASSF0050
      ATAN(Q)=DATAN(Q)                                                  ASSF0060
      ABS(Q)=DABS(Q)                                                    ASSF0070
      SQRT(Q)=DSQRT(Q)                                                  ASSF0080
       J1=IR*4                                                          ASSF0090
       NN(1)=J1-3                                                       ASSF0100
       NN(2)=J1-2                                                       ASSF0110
       NN(3)=J1-1                                                       ASSF0120
       NN(4)=J1                                                         ASSF0130
      IF(EXANG.NE.360.)GO TO 121                                        ASSF0140
       IF(IR-IK) 121,122,122                                            ASSF0150
  121  J2=(IR+1)*4                                                      ASSF0160
       NN(5)=J2-3                                                       ASSF0170
       NN(6)=J2-2                                                       ASSF0180
       NN(7)=J2-1                                                       ASSF0190
       NN(8)=J2                                                         ASSF0200
       GO TO 123                                                        ASSF0210
  122  NN(5)=1                                                          ASSF0220
       NN(6)=2                                                          ASSF0230
       NN(7)=3                                                          ASSF0240
       NN(8)=4                                                          ASSF0250
  123  DO 101 I=1,8                                                     ASSF0260
       M=NN(I)                                                          ASSF0270
       FLVA(M)=FLVA(M)+ELFP(I)                                          ASSF0280
  101  CONTINUE                                                         ASSF0290
       RETURN                                                           ASSF0300
      END                                                               ASSF0310
```

```
      SUBROUTINE ASSEM(IR,ELMAS,STIFM)                                  ASSM0010
      IMPLICIT REAL*8(A-H,O-Z)                                          ASSM0020
       DIMENSION ELMAS(8,8),NN(8),STIFM(1)                              ASSM0030
      COMMON/FG/Y(51),Z(51),ANG(51),H(51),B,EXANG,NS,IK,NOGA,NFL,NSFL,  ASSM0040
     *NI,ICOL(205),NBCOND,NBC(4),NODEB(4)                               ASSM0050
      SIN(Q)=DSIN(Q)                                                    ASSM0060
      COS(Q)=DCOS(Q)                                                    ASSM0070
      ATAN(Q)=DATAN(Q)                                                  ASSM0080
      ABS(Q)=DABS(Q)                                                    ASSM0090
      SQRT(Q)=DSQRT(Q)                                                  ASSM0100
       J1=IR*4                                                          ASSM0110
       NN(1)=J1-3                                                       ASSM0120
       NN(2)=J1-2                                                       ASSM0130
       NN(3)=J1-1                                                       ASSM0140
       NN(4)=J1                                                         ASSM0150
      IF(EXANG.NE.360.)GO TO 203                                        ASSM0160
       IF(IR-IK) 203,204,204                                            ASSM0170
  203  J2=(IR+1)*4                                                      ASSM0180
       NN(5)=J2-3                                                       ASSM0190
       NN(6)=J2-2                                                       ASSM0200
       NN(7)=J2-1                                                       ASSM0210
       NN(8)=J2                                                         ASSM0220
       GO TO 202                                                        ASSM0230
  204  NN(5)=1                                                          ASSM0240
       NN(6)=2                                                          ASSM0250
       NN(7)=3                                                          ASSM0260
       NN(8)=4                                                          ASSM0270
  202  DO 402 I=1,8                                                     ASSM0280
       M=NN(I)                                                          ASSM0290
       DO 402 J=1,8                                                     ASSM0300
       N=NN(J)                                                          ASSM0310
       IF(M-N)402,403,403                                               ASSM0320
  403  CALL FICOL(M,N,L,ICOL)                                           ASSM0330
       STIFM(L)=STIFM(L)+ELMAS(I,J)                                     ASSM0340
  402  CONTINUE                                                         ASSM0350
       RETURN                                                           ASSM0360
      END                                                               ASSM0370
```

```
      SUBROUTINE DINIT(IT,TIME)
      IMPLICIT REAL*8(A-H,O-Z)
       COMMON /VQ/ FLVA(205),DISP(205),DELD(205),SNS(50,3,6,5),
     *BINP(50,3),BIMP(50,3),TDISP(205),TU(205),TW(205),
     *COIY(205),COIZ(205),DELTAT
      COMMON/FG/Y(51),Z(51),ANG(51),H(51),B,EXANG,NS,IK,NOGA,NFL,NSFL,
     *NI,ICOL(205),NBCOND,NBC(4),NODEB(4)
       COMMON /HM/ YOUNG,DS,C5,C6,ASFL(50,3,6,5),GZETA(50,3,6),SNO(5)
      COMMON/FRAG/FH(6),FCG(6),FMASS(6),FMOI(6),FCGU(6),FCGW(6),ALFA(6),
     *UDOT(6),WDOT(6),ADOT(6),TPRIM(6),CR(6),FCGX(6),UNK(6),NF
      COMMON /DFRAG/DFCGU(6),DFCGW(6),DALFA(6)
      IT=0
      TIME = 0.
      DO 1 I=1,205
      DELD(I)=0.0
    1 DISP(I)=0.0
      DO 2 IR=1,IK
      DO 2 J=1,NOGA
      DO 2 K=1,NFL
      DO 2 L=1,NSFL
    2 SNS(IR,J,K,L)=0.0
      DO 5 I=1,NF
      DFCGU(I)=UDOT(I)*DELTAT
      DFCGW(I)=WDOT(I)*DELTAT
      DALFA(I)=     ADOT(I)*DELTAT
      FCGU(I)=FCGX(I)+UDOT(I)*TPRIM(I)
      FCGW(I)=FCG(I)+WDOT(I)*TPRIM(I)
    5 ALFA(I)=     ADOT(I)*TPRIM(I)
      RETURN
      END
```

```
      SUBROUTINE ELMPP(DELTAT,AA,ISIZE,KROW,NDEX,NIRREG,INUM,DENS,YOUNG)
      IMPLICIT REAL*8(A-H,O-Z)
      DIMENSION A(8,8),AA(50,8,8),LMI(8),MMI(8)
     *,BE1(3,3,8),KROW(1),NDEX(1),INUM(1),BNG(51)
      COMMON/FG/Y(51),Z(51),ANG(51),H(51),B,EXANG,NS,IK,NOGA,NFL,NSFL,
     *NI,ICOL(205),NBCOND,NBC(4),NODEB(4)
       COMMON /BA/ BEP(50,3,3,8),AL(50),AXG(3),AWG(3)
       COMMON /TAPE/ MREAD,MWRITE,MPUNCH
      SIN(Q)=DSIN(Q)
      COS(Q)=DCOS(Q)
      ATAN(Q)=DATAN(Q)
      ABS(Q)=DABS(Q)
      SQRT(Q)=DSQRT(Q)
50     DO 101 IR=1,IK
       P5=Z(IR+1)-Z(IR)
       P6=Y(IR+1)-Y(IR)
       P7=ANG(IR+1)-ANG(IR)
       APHA=ATAN(P5/P6)
      IF(P6.LT.0.0.AND.P5.LT.0.0)APHA=APHA-3.14159265
       IF(P6.LT.0.0 .AND. P5.GE.0.0) APHA=APHA+3.14159265
       IF(P7 .EQ. 0.0) GO TO 60
       AL(IR)=P7*SQRT(P5**2+P6**2)/SIN(P7/2.)/2.
      IF(P7.GT.4.71238897)AL(IR)=(P7-6.2831853)*SQRT(P5**2+P6**2)
     */SIN(P7/2.-3.14159265)/2.
      IF(P7.LT.(-4.71238897))AL(IR)=(P7+6.2831853)*SQRT(P5**2+P6**2)
     */SIN(P7/2.+3.14159265)/2.
       GO TO 61
60     AL(IR)=SQRT(P5**2+P6**2)
61     BNG(IR+1)=ANG(IR+1)
       BNG(IR)=ANG(IR)
      IF(P7.GT.(4.7124).AND.APHA.LT.0.0) BNG(IR+1)=ANG(IR+1)-6.2831853
      IF(P7.GT.(4.7124).AND.APHA.GT.0.0) BNG(IR)=ANG(IR)+6.2831853
      IF(P7.LT.(-4.7124).AND.APHA.GT.0.0) BNG(IR+1)=ANG(IR+1)+6.2831853
      IF(P7.LT.(-4.7124).AND.APHA.LT.0.0) BNG(IR)=ANG(IR)-6.2831853
       BZER=BNG(IR)-APHA
       B1=(-2.*BNG(IR+1)-4.*BNG(IR)+6.*APHA)/AL(IR)
```

```
      B2=(3.*BNG(IR+1)+3.*BNG(IR)-6.*APHA)/AL(IR)**2
      DO 102 I=1,8
      DO 102 J=1,8
  102 A(I,J)=0.0
      A(1,1)= COS(BNG(IR)-APHA)
      A(1,2)= SIN(BNG(IR)-APHA)
      A(2,1)=-SIN(BNG(IR)-APHA)
      A(2,2)= COS(BNG(IR)-APHA)
      A(3,3)=1.
      A(5,1)=COS(BNG(IR+1)-APHA)
      A(5,2)=SIN(BNG(IR+1)-APHA)
      A(5,3)=P6*SIN(BNG(IR+1))-P5*COS(BNG(IR+1))
      A(6,1)=-SIN(BNG(IR+1)-APHA)
      A(6,2)=COS(BNG(IR+1)-APHA)
      A(6,3)=P6*COS(BNG(IR+1))+P5*SIN(BNG(IR+1))
      A(7,3)=1.
      A(4,4)=1.
      A(5,4)=AL(IR)
      A(5,7)=AL(IR)**2
      A(5,8)=AL(IR)**3
      A(6,5)=AL(IR)**2
      A(6,6)=AL(IR)**3
      P8=B1+2.*B2*AL(IR)
      A(7,4)=AL(IR)*P8
      A(7,5)=2.*AL(IR)
      A(7,6)=3.*AL(IR)**2
      A(7,7)=AL(IR)**2*P8
      A(7,8)=AL(IR)**3*P8
     A(8,4)=1.0
     A(8,5)=-AL(IR)**2*P8
      A(8,7)=2.*AL(IR)
      A(8,6)=-AL(IR)**3*P8
      A(8,8)=3.*AL(IR)**2
      CALL MINV(A,8,DET,LMI,MMI)
      DO 52 I=1,8
      DO 52 J=1,8
```

```
52    AA(IR,I,J)=A(I,J)                                          ELMP0730
      DO 103 J=1,NOGA                                            ELMP0740
      ZET=AL(IR)*AXG(J)                                          ELMP0750
      PHIP=B1+2.*B2*ZET                                          ELMP0760
      PHI=BZER+B1*ZET+B2*ZET**2                                  ELMP0770
      WET=AL(IR)*AWG(J)                                          ELMP0780
      YZET=0.0                                                   ELMP0790
      ZZET=0.0                                                   ELMP0800
      DO 104 JJ=1,NOGA                                           ELMP0810
      P2=BZER+B1*ZET*AXG(JJ)+B2*(ZET*AXG(JJ))**2+APHA            ELMP0820
      YZET=YZET+COS(P2)*ZET*AWG(JJ)                              ELMP0830
104   ZZET=ZZET+SIN(P2)*ZET*AWG(JJ)                              ELMP0840
      P3=YZET*SIN(PHI+APHA)-ZZET*COS(PHI+APHA)                   ELMP0850
      P4=YZET*COS(PHI+APHA)+ZZET*SIN(PHI+APHA)                   ELMP0860
      DO 201 M=1,3                                               ELMP0870
      DO 201 N=1,8                                               ELMP0880
201   BE1(J,M,N)=0.0                                             ELMP0890
      BE1(J,1,4)=1.                                              ELMP0900
      BE1(J,1,5)=-ZET**2*PHIP                                    ELMP0910
      BE1(J,1,6)=-ZET**3*PHIP                                    ELMP0920
      BE1(J,1,7)=2.*ZET                                          ELMP0930
      BE1(J,1,8)=3.*ZET**2                                       ELMP0940
      BE1(J,2,3)=1.                                              ELMP0950
      BE1(J,2,4)=ZET*PHIP                                        ELMP0960
      BE1(J,2,5)=2.*ZET                                          ELMP0970
      BE1(J,2,6)=3.*ZET**2                                       ELMP0980
      BE1(J,2,7)=ZET**2*PHIP                                     ELMP0990
      BE1(J,2,8)=ZET**3*PHIP                                     ELMP1000
      BE1(J,3,4)=-PHIP-ZET*2.*B2                                 ELMP1010
      BE1(J,3,5)=-2.                                             ELMP1020
     BE1(J,3,6)=-6.*ZET                                          ELMP1030
      BE1(J,3,7)=-2.*ZET*PHIP-ZET**2*2.*B2                       ELMP1040
      BE1(J,3,8)=-3.*ZET**2*PHIP-ZET**3*2.*B2                    ELMP1050
      DO 202 M=1,3                                               ELMP1060
      DO 202 N=1,8                                               ELMP1070
      BEP(IR,J,M,N)=0.0                                          ELMP1080
```

```
      DO 202 K=1,8
202   BEP(IR,J,M,N)=BEP(IR,J,M,N)+BE1(J,M,K)*A(K,N)
103   CONTINUE
101   CONTINUE
      RETURN
      END
```

```
      SUBROUTINE ENERGY(IT,KROW,NCEX,NIRREG,NOPE)
C     THIS SUBROUTINE IS THE DUMMY ROUTINE THAT MUST BE REPLACED BY THE
C     CALCULATION ROUTINE IN THOSE CASES IN WHICH AN ENERGY ACCOUNTING
C     IS DESIRED
      RETURN
      END
```

```
      SUBROUTINE ENERGY(IT,KROW,NDEX,NIRREG,NOPE)
C     THIS IS THE ENERGY CALCULATION SUBROUTINE
      IMPLICIT REAL*8(A-H,O-Z)
      DIMENSION AMKE(205)
      DIMENSION CINETF(6)
       COMMON /BA/ BEP(50,3,3,8),AL(50),AXG(3),AWG(3)
       COMMON /TAPE/ MREAD,MWRITE,MPUNCH
      COMMON/SC/CRITS,BIG,BTIME,NCRIT,IBIG,ISURF
       COMMON /VQ/ FLVA(205),DISP(205),DELD(205),SNS(50,3,6,5),
     *BINP(50,3),BIMP(50,3),TDISP(205),TU(205),TW(205),
     *COIY(205),COIZ(205),DELTAT
      COMMON/FG/Y(51),Z(51),ANG(51),H(51),B,EXANG,NS,IK,NOGA,NFL,NSFL,
     *NI,ICOL(205),NBCOND,NBC(4),NODEB(4)
       COMMON /HM/ YOUNG,DS,C5,C6,ASFL(50,3,6,5),GZETA(50,3,6),SNO(5)
      COMMON/FRAG/FH(6),FCG(6),FMASS(6),FMOI(6),FCGU(6),FCGW(6),ALFA(6),
     *UDOT(6),WDOT(6),ADOT(6),TPRIM(6),CR(6),FCGX(6),UNK(6),NF
      COMMON /DFRAG/DFCGU(6),DFCGW(6),DALFA(6)
      COMMON/ENERG/FK(6),CINETO,CUMW,DELKE,CELAS,ELAS,PLASTC
      COMMON/ABC/RMX(51),RWORK,CINEY(205)
      COMMON/LEFT/P,EPS(5),SIG(5),RMASS(51)
      COMMON/ELFU/SPRIN(2060),FQREF(205),REX(4),NQR,NORP,NORU,NREL(4),
     *NRST(4),NREU(4)
      SIN(Q)=DSIN(Q)
      COS(Q)=DCOS(Q)
      ATAN(Q)=DATAN(Q)
      ABS(Q)=DABS(Q)
      SQRT(Q)=DSQRT(Q)
      NOPE=1
      WRITE(MWRITE,7)
    7 FORMAT('      CURRENT TIME CYCLE',10X,' FRAGMENT',10X,'KINETIC
     *ENERGY',/)
      IMX=IK+1
      IF(EXANG.NE.360.)GO TO 1
      DO 2 I=1,IK
      AMKE(I*4-3)=RMASS(I)
      AMKE(I*4-2)=RMASS(I)
```

```
            AMKE(I*4-1)=RMX(I)                                                  ENER0370
    2       AMKE(I*4)=RMX(I)                                                    ENER0380
            AMKE(IMX*4-3)=RMASS(1)                                              ENER0390
            AMKE(IMX*4-2)=RMASS(1)                                              ENER0400
            AMKE(IMX*4-1)=RMX(1)                                                ENER0410
            AMKE(IMX*4)=RMX(1)                                                  ENER0420
            GO TO 3                                                             ENER0430
    1       DO 4 I=1,IMX                                                        ENER0440
            AMKE(I*4-3)=RMASS(I)                                                ENER0450
            AMKE(I*4-2)=RMASS(I)                                                ENER0460
            AMKE(I*4-1)=RMX(I)                                                  ENER0470
    4       AMKE(I*4)=RMX(I)                                                    ENER0480
      3     RWORK=0.0                                                           ENER0490
            DO 5 I=1,NF                                                         ENER0500
            FUV=DFCGU(I)/DELTAT                                                 ENER0510
            FWV=DFCGW(I)/DELTAT                                                 ENER0520
            FAV=DALFA(I)/DELTAT                                                 ENER0530
            CINETF(I)=FMASS(I)/2.0*(FUV**2+FWV**2)+FMOI(I)/2.0*(FAV**2)         ENER0540
            RWORK=RWORK+(FK(I)-CINETF(I))                                       ENER0550
            WRITE(MWRITE,6)IT,I,CINETF(I)                                       ENER0560
    6       FORMAT(10X,I5,15X,I5,9X,D15.6)                                      ENER0570
    5       CONTINUE                                                            ENER0580
            WRITE(MWRITE,8)IT,RWORK                                             ENER0590
    8       FORMAT(/,'     WORK INPUT INTO RING TO TIME STEP',I5,'=',D15.6)    ENER0600
            DO 9 K=1,NI                                                         ENER0610
    9       CINEY(K)=         AMKE(K)*DELD(K)                                   ENER0620
            CINETO=0.0                                                          ENER0630
            DO 10 K=1,NI                                                        ENER0640
   10       CINETO=CINETO+DELD(K)*CINEY(K)                                      ENER0650
            CINETO=CINETO/2.0/DELTAT**2                                         ENER0660
            WRITE(MWRITE,11)IT,CINETO                                           ENER0670
   11       FORMAT('     RING KINETIC ENERGY AT TIME STEP',I5,' = ',D15.6)     ENER0680
            IF(EXANG.NE.360.)GO TO 13                                           ENER0690
            DO 12 K=1,4                                                         ENER0700
            DISP(IK*4+K)=DISP(K)                                                ENER0710
   12       DELD(IK*4+K)=DELD(K)                                                ENER0720
```

```
   13 ELAST=C.0                                                         ENER0730
      DO 15 IR=1,IK                                                     ENER0740
      DO 16 J=1,NOGA                                                    ENER0750
      SUM=0.0                                                           ENER0760
      DO 17 K=1,NFL                                                     ENER0770
      DO 17 L=1,NSFL                                                    ENER0780
 17   SUM=SUM+SNS(IR,J,K,L)**2*ASFL(IR,J,K,L)                           ENER0790
 16   ELAST=ELAST+SUM*AWG(J)+AL(IR)                                     ENER0800
 15   CONTINUE                                                          ENER0810
      SPDEN=0.0                                                         ENER0820
      IF(NQR.EQ.0)GC TO 18                                              ENER0830
      DO 19 I=1,NI                                                      ENER0840
 19   FQREF(I)=0.0                                                      ENER0850
      CALL OMULT(SPRIN,DISP,ICOL,NI,FQREF,KROW,NDEX,NIRREG)             ENER0860
      DO 20 I=1,NI                                                      ENER0870
 20   SPDEN=SPDEN+DISP(I)*FQREF(I)                                      ENER0880
      SPDEN=SPDEN/2.0                                                   ENER0890
 18   CELAS=ELAST/YOUNG/2.0                                             ENER0900
      WRITE(MWRITE,21)IT,CELAS                                          ENER0910
 21   FORMAT('      RING ELASTIC ENERGY TO TIME STEP',I5,' = ',D15.6)   ENER0920
      PLAST=RWORK-CINETO-CELAS-SPDEN                                    ENER0930
      WRITE(MWRITE,22)IT,PLAST                                          ENER0940
 22   FORMAT('      RING PLASTIC WORK TO TIME STEP',I5,' = ',D15.6)     ENER0950
      WRITE(MWRITE,23)SPDEN                                             ENER0960
 23   FORMAT('      ENERGY STORED IN ELASTIC RESTRAINTS =',D15.6)       ENER0970
      RETURN                                                            ENER0980
      END                                                               ENER0990
```

```
      SUBROUTINE ERC(II,STIFM,NI,ICOL)
      IMPLICIT REAL*8(A-H,O-Z)
C      FOR ELIMINATING ROWS AND COLUMNS IN STIFM
       DIMENSION STIFM(1),ICOL(1)
      IC=ICOL(II)
      DO 101 J=IC,II
      CALL FICOL(II,J,L,ICOL)
101   STIFM(L)=0.
      DO 102 I=II,NI
      IC1=ICOL(I)
      IF(II-IC1)102,103,103
103   CALL FICOL(I,II,L,ICOL)
      STIFM(L)=0.
102   CONTINUE
      CALL FICOL(II,II,L,ICOL)
      STIFM(L)=1.
      RETURN
      END
```

```
      SUBROUTINE FICOL(I,J,L,ICOL)
      IMPLICIT REAL*8(A-H,O-Z)
C     USING FORMULA L=J+SUM(K-ICOL(K)),K=1,I TC RELATE I,J,TC L
       DIMENSION ICOL(1)
      IF(J-ICCL(I))200,300,300
  300 ISUM=0
      DO 305 K=1,I
      ISUM=K-ICOL(K)+ISUM
  305 CONTINUE
      L=J+ISUM
      RETURN
  200  WRITE(6,4)I,J
    4 FORMAT(31H ELEMENT IS NOT IN BAND REGION,3H I=,I5,3H J=,I5)
      RETURN
      END
```

```
      SUBROUTINE IDENT(NQR,DENS)
      IMPLICIT REAL*8(A-H,O-Z)
       COMMON /TAPE/ MREAD,MWRITE,MPUNCH
       COMMON /HM/ YOUNG,DS,C5,C6,ASFL(50,3,6,5),GZETA(50,3,6),SNO(5)
      COMMON/SC/CRITS,BIG,BTIME,MCRIT,IBIG,ISURF
       COMMON /VQ/ FLVA(205),DISP(205),DELD(205),SNS(50,3,6,5),
     *BINP(50,3),BIMP(50,3),TDISP(205),TU(205),TW(205),
     *COIY(205),COIZ(205),DELTAT
      COMMON/FG/Y(51),Z(51),ANG(51),H(51),B,EXANG,NS,IK,NOGA,NFL,NSFL,
     *NI,ICOL(205),NBCOND,NBC(4),NODEB(4)
      COMMON/FRAG/FH(6),FCG(6),FMASS(6),FMOI(6),FCGU(6),FCGW(6),ALFA(6),
     *UDOT(6),WDOT(6),ADOT(6),TPRIM(6),CR(6),FCGX(6),UNK(6),NF
      COMMON/ENERG/FK(6),CINETO,CUMW,DELKE,CELAS,ELAS,PLASTC
      COMMON/LEFT/P,EPS(5),SIG(5),RMASS(51)
      SIN(Q)=DSIN(Q)
      COS(Q)=DCOS(Q)
      ATAN(Q)=DATAN(Q)
      ABS(Q)=DABS(Q)
      SQRT(Q)=DSQRT(Q)
      IF(EXANG.EQ.360.)GO TO 81
      WRITE(MWRITE,2)EXANG
      GO TO 80
81    WRITE(MWRITE,1)EXANG
1     FORMAT('     COMPLETE RING **JET** CONTAINMENT ANALYSIS',//,
     *10X,'RING PROPERTIES',/,12X,'SUBTENDED ANGLE OF RING',25X,'=',D15.
     *6,/)
2     FORMAT('     PARTIAL RING **JET** DEFLECTION ANALYSIS',//,10X,'RIN
     *G PROPERTIES',/,12X,'SUBTENDED ANGLE OF RING',25X,'=',D15.6,/)
80    WRITE(MWRITE,3)B,DENS,IK,NOGA,NFL,NSFL
3     FORMAT(12X,'WIDTH OF RING(IN)',30X,'=',D15.6,/,12X,'DENSITY OF RIN
     *G',33X,'=',D15.6,/,12X,'NUMBER OF ELEMENTS',30X,'=',I5,/,12X,'NUMB
     *ER OF SPANWISE GAUSSIAN PTS.',16X,'=',I5,/,12X,'NUMBER OF DEPTHWIS
     *E GAUSSIAN PTS.',15X,'=',I5,/,12X,'NUMBER OF MECHANICAL SUBLAYERS'
     *,18X,'=',I5,/)
      WRITE(MWRITE,4)(L,EPS(L),L,SIG(L),L=1,NSFL)
4     FORMAT(15X,'STRAIN (',I1,') =',D15.6,'STRESS (',I1,') =',D15.6,/)
```

```
      WRITE(MWRITE,5)                                                   IDNT0370
    5 FORMAT(12X,'NODE NO.',10X,'Y COORD',10X,'Z COORD',10X,'SLOPE',10X,IDNT0380
     *'RING THICKNESS AT NODE I',/)                                     IDNT0390
      WRITE(MWRITE,6)(I,Y(I),Z(I),ANG(I),H(I),I=1,NS)                   IDNT0400
    6 FORMAT(12X,I5,4D15.6,//)                                          IDNT0410
      WRITE(MWRITE,7)                                                   IDNT0420
    7 FORMAT(10X,'FRAGMENT PROPERTIES',/)                               IDNT0430
      WRITE(MWRITE,8)                                                   IDNT0440
    8 FORMAT(12X,'FRAG.NO.',5X,'WIDTH OF FRAG.',5X,'MASS OF FRAG.',5X,'MIDNT0450
     *OMENT OF INERTIA OF FRAG.',/)                                     IDNT0460
      WRITE(MWRITE,9)(I,FH(I),FMASS(I),FMOI(I),I=1,NF)                  IDNT0470
    9 FORMAT(15X,I5,3D15.6,//)                                          IDNT0480
      WRITE(MWRITE,10)                                                  IDNT0490
      WRITE(MWRITE,11)                                                  IDNT0500
      WRITE(MWRITE,12)(I,UDOT(I),WDOT(I),ADOT(I),CR(I),FK(I),UNK(I),    IDNT0510
     *I=1,NF)                                                           IDNT0520
   10 FORMAT(10X,'COLLISION PARAMETERS',/)                              IDNT0530
   11 FORMAT(12X,'FRAG.NO.',3X,'VEL IN Y DIR.',3X,'VEL IN Z DIR.',3X,'ANIDNT0540
     *G. VEL.',3X,'COEFF.OF RESTIT.',3X,'INITIAL KINETIC ENERGY',3X,    IDNT0550
     *'COEFF. OF FRICT',/)                                              IDNT0560
   12 FORMAT(15X,I5,6D15.6,//)                                          IDNT0570
      IF(NBCOND .EQ. 0) GO TO 28                                        IDNT0580
      DO 14 I=1,NBCOND                                                  IDNT0590
      IF(NBC(I) .EQ. 1) WRITE(MWRITE,15) NODEB(I)                       IDNT0600
      IF(NBC(I) .EQ. 2) WRITE(MWRITE,16) NODEB(I)                       IDNT0610
      IF(NBC(I) .EQ. 3) WRITE(MWRITE,17) NODEB(I)                       IDNT0620
   14 CONTINUE                                                          IDNT0630
   15 FORMAT('   SYMMETRY DISPLACEMENT CONDITION AT NODE =',I5)         IDNT0640
   16 FORMAT('    CLAMPED DISPLACEMENT CONDITION AT NODE =',I5)         IDNT0650
   17 FORMAT('    HINGED  DISPLACEMENT CONDITION AT NODE =',I5)         IDNT0660
      GO TO 18                                                          IDNT0670
   28 WRITE(MWRITE,13)                                                  IDNT0680
   13 FORMAT(/,'    THERE IS NO PRESCRIBED DISPLACEMENT CONDITION')     IDNT0690
   18 IF(NQR .EQ. 0) GO TO 19                                           IDNT0700
      WRITE(MWRITE,20)                                                  IDNT0710
   20 FORMAT(/,'    CONSTRAINTS (ELASTIC FOUNDATION/SPRING) AS DESCRIBEDIDNT0720
```

```
     * BY INPUT ')                                                      IDNT0730
      GO TO 23                                                          IDNT0740
   19 WRITE(MWRITE,21)                                                  IDNT0750
   21 FORMAT(/,'     THERE ARE NO ELASTIC SPRING CONSTANTS')            IDNT0760
   23 RETURN                                                            IDNT0770
      END                                                               IDNT0780
```

```
      SUBROUTINE IMPACT(IT,NIRREG,DENS)
      IMPLICIT REAL*8(A-H,O-Z)
      DIMENSION CELU(6),CELW(6)
      DIMENSION BNG(51),PND(51,6)
      DIMENSION FACT3(6),ABC(51)
      DIMENSION TFCGU(6),TFCGW(6),TALFA(6),FAU(6),FAW(6),RL(51),RSIN(51)
     *,RCOS(51),DELU(6),DELW(6),PAX(51,6),HT(51),PN(51,6),PD(51,6)
      DIMENSION TAP(51)
       COMMON /BA/ BEP(50,3,3,8),AL(50),AXG(3),AWG(3)
       COMMON /TAPE/ MREAD,MWRITE,MPUNCH
       COMMON /VQ/ FLVA(205),DISP(205),DELD(205),SNS(50,3,6,5),
     *BINP(50,3),BIMP(50,3),TDISP(205),TU(205),TW(205),
     *COIY(205),COIZ(205),DELTAT
      COMMON/FG/Y(51),Z(51),ANG(51),H(51),B,EXANG,NS,IK,NOGA,NFL,NSFL,
     *NI,ICOL(205),NBCOND,NBC(4),NODEB(4)
       COMMON /HM/ YOUNG,DS,C5,C6,ASFL(50,3,6,5),GZETA(50,3,6),SNO(5)
      COMMON/FRAG/FH(6),FCG(6),FMASS(6),FMOI(6),FCGU(6),FCGW(6),ALFA(6),
     *UDOT(6),WDOT(6),ADOT(6),TPRIM(6),CR(6),FCGX(6),UNK(6),NF
      COMMON /DFRAG/DFCGU(6),DFCGW(6),DALFA(6)
      COMMON/ENERG/FK(6),CINETO,CUMW,DELKE,CELAS,ELAS,PLASTC
      COMMON/LEFT/P,EPS(5),SIG(5),RMASS(51)
      ICHECK=0
      DO 88 I=1,NS
      IF(ANG(I))89,87,87
   87 BNG(I)=6.28318530-ANG(I)
      GO TO 88
   89 BNG(I)=DABS(ANG(I))
   88 CONTINUE
      DO 2 I=1,NS
      DO 2 J=1,NF
      PAX(I,J)=0.0
      PN(I,J)=0.0
      PND(I,J)=0.0
    2 PD(I,J)=0.0
      IF(EXANG.NE.360.)GO TO 92
      IM=IK+1
```

```
      DISP(IM*4-3)=DISP(1)
      DISP(IM*4-2)=DISP(2)
      DISP(IM*4-1)=DISP(3)
      DISP(IM*4)=DISP(4)
      DELD(IM*4-3)=DELD(1)
      DELD(IM*4-2)=DELD(2)
      DELD(IM*4-1)=DELD(3)
      DELD(IM*4)=DELD(4)
      COIY(IM)=COIY(1)
      COIZ(IM)=COIZ(1)
   92 DO 11 I=1,NS
      TDISP(I*4-3)=DISP(I*4-3)+DELD(I*4-3)
      TDISP(I*4-2)=DISP(I*4-2)+DELD(I*4-2)
      TU(I)=COIY(I)+TDISP(I*4-3)*DCOS(BNG(I))+TDISP(I*4-2)*DSIN(BNG(I))
   11 TW(I)=COIZ(I)-TDISP(I*4-3)*DSIN(BNG(I))+TDISP(I*4-2)*DCOS(BNG(I))
      IF(EXANG.NE.360.)GO TO 12
      TDISP((NS+1)*4-3)=TDISP(1)
      TDISP((NS+1)*4-2)=TDISP(2)
      TU(NS+1)=TU(1)
      TW(NS+1)=TW(1)
   12 DO 13 I=1,NF
      TFCGU(I)=FCGU(I)+DFCGU(I)
      TFCGW(I)=FCGW(I)+DFCGW(I)
      TALFA(I)=ALFA(I)+DALFA(I)
      FAU(I)=TFCGU(I)
   13 FAW(I)=TFCGW(I)
      DO 15 I=1,IK
      IR=I+1
      RL(I)=DSQRT((TU(IR-1)-TU(IR))**2+(TW(IR-1)-TW(IR))**2)
      RSIN(I)=(TW(IR)-TW(IR-1))/RL(I)
      RCOS(I)=(TU(IR)-TU(IR-1))/RL(I)
      DO 14 J=1,NF
      DELU(J)=TU(IR)-FAU(J)
      DELW(J)=TW(IR)-FAW(J)
      DIST=DSQRT(DELU(J)**2+DELW(J)**2)
      TIPC=(H(IR)+FH(J))/2.0
```

```
      PND(I,J)=TIPC-DIST
      PAX(I,J)=RCOS(I)*DELU(J)+RSIN(I)*DELW(J)
      IF(PAX(I,J))14,16,16
16    IF(RL(I)-PAX(I,J))14,17,17
17    HT(I)=H(IR-1)+(H(IR)-H(IR-1))*PAX(I,J)/RL(I)
      TIPD=HT(I)/2.0+FH(J)/2.0
      PN(I,J)=RCOS(I)*DELW(J)-RSIN(I)*DELU(J)
      IF(PN(I,J).GT.TIPD)GO TO 14
      PD(I,J)=TIPD-PN(I,J)
14    CONTINUE
15    CONTINUE
      PNDBIG=0.0
      PDBIG=0.0
30    DO 23 I=1,IK
      DO 23 J=1,NF
82    IF(PD(I,J).LE.PDBIG.OR.PD(I,J).EQ.PDBIG) GO TO 19
      PDBIG=PD(I,J)
      IBIG=I
      JBIG=J
19    IF(PND(I,J).LE.PNDBIG.OR.PND(I,J).EQ.PNDBIG)GO TO 23
      PNDBIG=PND(I,J)
      INBIG=I
      NNBIG=I+1
      JNBIG=J
23    CONTINUE
      IF(PDBIG.EQ.0.0.AND.PNDBIG.EQ.0.0)GO TO 31
      IF(PNDBIG.GT.PDBIG.OR.PNDBIG.EQ.PDBIG)GO TO 77
      IPLUS=IBIG+1
      POP=RCOS(IBIG)
      TOP=RSIN(IBIG)
      POM=DCOS(BNG(IBIG))
      POX=DCOS(BNG(IPLUS))
      TOM=DSIN(BNG(IBIG))
      TOX=DSIN(BNG(IPLUS))
      BAT=H(IBIG)-H(IPLUS)
      CAT=2.0*RL(IBIG)
```

```
      TAP(IBIG)=DATAN2(BAT,CAT)                                         IMPT1090
      BETA=PAX(IBIG,JBIG)/RL(IBIG)                                      IMPT1100
      GAMA=1.0-BETA                                                     IMPT1110
      VFN=DFCGW(JBIG)*POP-DFCGU(JBIG)*TOP                               IMPT1120
      VFT=DFCGW(JBIG)*TOP+DFCGU(JBIG)*POP                               IMPT1130
      VFN=VFN/DELTAT                                                    IMPT1140
      VFT=VFT/DELTAT                                                    IMPT1150
      VFA=DALFA(JBIG)/DELTAT                                            IMPT1160
      VNIBIG=DELD(IBIG*4-2)*(POP*POM-TOP*TOM)-DELD(IBIG*4-3)*(TOP*POM+  IMPT1170
     *POP*TOM)                                                          IMPT1180
      VTIBIG=DELD(IBIG*4-2)*(TOP*POM+POP*TOM)+DELD(IBIG*4-3)*(POP*POM-  IMPT1190
     *TOP*TOM)                                                          IMPT1200
      VNIPLS=DELD(IPLUS*4-2)*(POP*POX-TOP*TOX)-DELD(IPLUS*4-3)*(TOP*POX+IMPT1210
     *POP*TOX)                                                          IMPT1220
      VTIPLS=DELD(IPLUS*4-2)*(TOP*POX+POP*TOX)+DELD(IPLUS*4-3)*(POP*POX-IMPT1230
     *TOP*TOX)                                                          IMPT1240
      VNIBIG=VNIBIG/DELTAT                                              IMPT1250
      VTIBIG=VTIBIG/DELTAT                                              IMPT1260
      VNIPLS=VNIPLS/DELTAT                                              IMPT1270
      VTIPLS=VTIPLS/DELTAT                                              IMPT1280
      AINT=VFN-(BETA*VNIBIG+GAMA*VNIPLS)                                IMPT1290
      SINT=(VFT-VFA*FH(JBIG)/2.0)-((BETA*VTIBIG+GAMA*VTIPLS)+(HT(IBIG)/ IMPT1300
     *2.0*(VNIPLS-VNIBIG)/RL(IBIG)))                                    IMPT1310
      B1=1.0/FMASS(JBIG)+(FH(JBIG)/2.0)**2/FMOI(JBIG)+BETA**2/RMASS(IBIGIMPT1320
     *)+GAMA**2/RMASS(IPLUS)+(HT(IBIG)/2.0/RL(IBIG))**2*(1.0/RMASS(IBIG)IMPT1330
     *+1.0/RMASS(IPLUS))                                                IMPT1340
      B2=1.0/FMASS(JBIG)+BETA**2/RMASS(IBIG)+GAMA**2/RMASS(IPLUS)       IMPT1350
      B3=(HT(IBIG)/2.0/RL(IBIG))*(GAMA/RMASS(IPLUS)-BETA/RMASS(IBIG))   IMPT1360
      DELTP=PD(IBIG,JBIG)/AINT                                          IMPT1370
      IF(UNK(JBIG).EQ.0.0)GO TO 702                                     IMPT1380
      IF(UNK(JBIG).EQ.10.0)GO TO 703                                    IMPT1390
      BAT1=B2*SINT-B3*AINT                                              IMPT1400
      BAT2=B1*AINT-B3*SINT                                              IMPT1410
      ANX=DATAN2(BAT1,BAT2)                                             IMPT1420
      TANX=BAT1/BAT2                                                    IMPT1430
      AXY=1.0                                                           IMPT1440
```

```
      BNX=DATAN2(UNK(JBIG),AXY)
      CNX=DATAN2(B3,B1)
      IF(B3.LE.0.0)              GO TO 705
      IF(UNK(JBIG).GT.TANX)GO TO 707
      PN1=AINT/(B2+UNK(JBIG)*B3)
      APN=(1.0+CR(JBIG))*PN1
      APT=UNK(JBIG)*APN
      GO TO 760
  707 IF(CNX.LE.BNX)GO TO 708
      PN2=SINT/(UNK(JBIG)*B1+B3)
      PN4=(AINT-2.0*UNK(JBIG)*B3*PN2)/(B2-UNK(JBIG)*B3)
      APN=(1.0+CR(JBIG))*PN4
      APT=UNK(JBIG)*(2.0*PN2-(1.0+CR(JBIG))*PN4)
      GO TO 760
  708 PN3=(B1*AINT-B3*SINT)/(B1*B2-B3**2)
      APN=(1.0+CR(JBIG))*PN3
      APT=(SINT-(B3*(1.0+CR(JBIG))*PN3))/B1
      GO TO 760
  705 IF(UNK(JBIG).LE.TANX)GO TO 706
      PN3=(B1*AINT-B3*SINT)/(B1*B2-B3**2)
      APN=(1.0+CR(JBIG))*PN3
      APT=(SINT-B3*APN)/B1
      GO TO 760
  706 PN1=AINT/(B2+UNK(JBIG)*B3)
      APN=(1.0+CR(JBIG))*PN1
      APT=UNK(JBIG)*APN
      GO TO 760
  702 APN=(1.0+CR(JBIG))*AINT/B2
      APT=0.0
      GO TO 760
  703 ETP1=SINT/B1
      ETP2=AINT/B3
      IF(ETP1.LE.ETP2.OR.ETP2.LE.0.0)GO TO 704
      APN=0.0
      APT=ETP1
      GO TO 760
```

```
704   PN3=(B1*AINT-B3*SINT)/(B1*B2-B3**2)
      APN=(1.0+CR(JBIG))*PN3
      APT=(SINT-(B3*(1.0+CR(JBIG))*PN3))/B1
760   CONTINUE
      FACT1N=(BETA*RL(IBIG)*APN-(HT(IBIG)/2.0*APT))/(RMASS(IBIG)*RL(IBIG
     *))
      FACT1T=(BETA*APT)/RMASS(IBIG)
      FACT2N=(GAMA*RL(IBIG)*APN+(HT(IBIG)/2.0*APT))/(RMASS(IPLUS)*RL(IBI
     *G))
      FACT2T=(GAMA*APT)/RMASS(IPLUS)
      FACTFN=-1.0*APN/FMASS(JBIG)
      FACTFT=-1.0*APT/FMASS(JBIG)
      FACTFO=APT*FH(JBIG)/FMOI(JBIG)/2.0
      DFCGU(JBIG)=DFCGU(JBIG)-DELTP*(FACTFN*TOP-FACTFT*POP)
      DFCGW(JBIG)=DFCGW(JBIG)-DELTP*(-1.0*FACTFN*POP-FACTFT*TOP)
513   DALFA(JBIG)=DALFA(JBIG)+DELTP*FACTFO
      DELD(IBIG*4-3)=DELD(IBIG*4-3)+DELTP*(-1.0*FACT1N*(TOM*POP+POM*TOP)
     *+FACT1T*(POM*POP-TOM*TOP))
      DELD(IBIG*4-2)=DELD(IBIG*4-2)+DELTP*(FACT1N*(POM*POP-TOM*TOP)
     *+FACT1T*(TOM*POP+POM*TOP))
      DELD(IBIG*4-3)=DELD(IBIG*4-3)*DCOS(TAP(IBIG))-DELD(IBIG*4-2)*DSIN(
     *TAP(IBIG))
      DELD(IBIG*4-2)=DELD(IBIG*4-3)*DSIN(TAP(IBIG))+DELD(IBIG*4-2)*
     *DCOS(TAP(IBIG))
      DELD(IPLUS*4-3)=DELD(IPLUS*4-3)+DELTP*(-1.0*FACT2N*(TOX*POP+POX*
     *TOP)+FACT2T*(POX*POP-TOX*TOP))
      DELD(IPLUS*4-2)=DELD(IPLUS*4-2)+DELTP*(FACT2N*(POX*POP-TOX*TOP)
     *+FACT2T*(TOX*POP+POX*TOP))
      DELD(IPLUS*4-3)=DELD(IPLUS*4-3)*DCOS(TAP(IBIG))-DELD(IPLUS*4-2)
     **DSIN(TAP(IBIG))
      DELD(IPLUS*4-2)=DELD(IPLUS*4-3)*DSIN(TAP(IBIG))+DELD(IPLUS*4-2)*
     *DCOS(TAP(IBIG))
263   WRITE(MWRITE,25)IT,IBIG,JBIG,PAX(IBIG,JBIG),PD(IBIG,JBIG)
25    FORMAT(10X,'IMPACT IT=',I5,3X,'ELEMENT NO. =',I5,3X,'FRAGMENT NO.
     *=',I5,/,10X,'LOCATION ON ELEMENT =',D15.6,3X,'PENETRATION DIST =',
     *D15.6,/)
```

```
50     PDBIG=0.0                                                          IMPT2170
       PD(IBIG,JBIG)=0.0                                                  IMPT2180
       GO TO 30                                                           IMPT2190
77     CMU=TU(NNBIG)-TFCGU(JNBIG)                                         IMPT2200
       CMW=TW(NNBIG)-TFCGW(JNBIG)                                         IMPT2210
       SDIST=DSQRT(CMU**2+CMW**2)                                         IMPT2220
       SINA=CMW/SDIST                                                     IMPT2230
       COSA=CMU/SDIST                                                     IMPT2240
       AND=DCOS(BNG(NNBIG))*COSA                                          IMPT2250
       ANC=DSIN(BNG(NNBIG))*SINA                                          IMPT2260
       ANB=DSIN(BNG(NNBIG))*COSA                                          IMPT2270
       ANA=DCOS(BNG(NNBIG))*SINA                                          IMPT2280
       VY1=(DELD(NNBIG*4-2)*RSIN(INBIG)+DELD(NNBIG*4-3)*RCOS(INBIG))/     IMPT2290
      *DELTAT                                                             IMPT2300
       VZ1=(DELD(NNBIG*4-2)*RCOS(INBIG)-DELD(NNBIG*4-3)*RSIN(INBIG))/     IMPT2310
      *DELTAT                                                             IMPT2320
       VRT=VZ1*COSA-VY1*SINA                                              IMPT2330
       VRN=VZ1*SINA+VY1*COSA                                              IMPT2340
       VFT=(DFCGU(JNBIG)*SINA+DFCGW(JNBIG)*COSA)/DELTAT                   IMPT2350
       VFN=(DFCGU(JNBIG)*COSA-DFCGW(JNBIG)*SINA)/DELTAT                   IMPT2360
       VFA=DALFA(JNBIG)/DELTAT                                            IMPT2370
       SINT=(VFT-VFA*FH(JNBIG)/2.0)-VRT                                   IMPT2380
       AINT=VFN-VRN                                                       IMPT2390
       B1=1.0/FMASS(JNBIG)+(FH(JNBIG)/2.0)**2/FMOI(JNBIG)+1.0/RMASS(NNBIGIMPT2400
      *)                                                                  IMPT2410
       B2=1.0/FMASS(JNBIG)+1.0/RMASS(NNBIG)                               IMPT2420
       TANN=(B2*SINT)/(B1*AINT)                                           IMPT2430
       IF(UNK(JNBIG).EQ.0.0)GO TO 735                                     IMPT2440
       IF(UNK(JNBIG).EQ.10.0)GO TO 736                                    IMPT2450
       IF(UNK(JNBIG).GT.TANN)GO TO 737                                    IMPT2460
       PN1=AINT/B2                                                        IMPT2470
       APN=(1.0+CR(JNBIG))*PN1                                            IMPT2480
       APT=UNK(JNBIG)*APN                                                 IMPT2490
       GO TO 740                                                          IMPT2500
737    PN3=(B1*AINT)/(B1*B2)                                              IMPT2510
       APN=(1.0+CR(JNBIG))*PN3                                            IMPT2520
```

```
      APT=SINT/B1
      GO TO 740
  735 APN=(1.0+CR(JNBIG))*AINT/B2
      APT=0.0
      GO TO 740
  736 PN3=B1*AINT/B1/B2
      APN=(1.0+CR(JNBIG))*PN3
      APT=SINT/B1
  740 CONTINUE
      FACTNN=APN/RMASS(NNBIG)
      FACTNT=APT/RMASS(NNBIG)
      FACTFN=APN/FMASS(JNBIG)
      FACTFT=APT/FMASS(JNBIG)
      FACTFO=APT*FH(JNBIG)/2.0/FMOI(JNBIG)
      DELTP=PND(INBIG,JNBIG)/AINT
      DFCGU(JNBIG)=DFCGU(JNBIG)+DELTP*(-1.0*FACTFN*COSA+FACTFT*SINA)
      DFCGW(JNBIG)=DFCGW(JNBIG)+DELTP*(-1.0*FACTFN*SINA-FACTFT*COSA)
      DALFA(JNBIG)=DALFA(JNBIG)+DELTP*FACTFO
      DELD(NNBIG*4-3)=DELD(NNBIG*4-3)+DELTP*(FACTNN*(AND-ANC)+FACTNT*
     *(ANB+ANA))
      DELD(NNBIG*4-2)=DELD(NNBIG*4-2)+DELTP*(FACTNN*(ANB+ANA)-FACTNT*
     *(AND-ANC))
  463 WRITE(MWRITE,201)IT,NNBIG,JNBIG,PND(INBIG,JNBIG)
  201 FORMAT(/,'     IMPACT IT = ',I5,'  NODE NO. =',I5,'   FRAG NO = '
     *,I5,'     PD =',D15.6)
      PNDBIG=0.0
      PND(INBIG,JNBIG)=0.0
      GO TO 30
   31 RETURN
      END
```

```
      SUBROUTINE MINV(A,N,DET,L,M)                                      MINV0010
      IMPLICIT REAL*8(A-H,O-Z)                                          MINV0020
C                                                                       MINV0030
C        SEARCH FOR LARGEST ELEMENT                                     MINV0040
C                                                                       MINV0050
      DIMENSION A(1),L(1),M(1)                                          MINV0060
      DET=1.0                                                           MINV0070
      NK=-N                                                             MINV0080
      DO 80 K=1,N                                                       MINV0090
      NK=NK+N                                                           MINV0100
      L(K)=K                                                            MINV0110
      M(K)=K                                                            MINV0120
      KK=NK+K                                                           MINV0130
      BIGA=A(KK)                                                        MINV0140
      DO 20 J=K,N                                                       MINV0150
      IZ=N*(J-1)                                                        MINV0160
      DO 20 I=K,N                                                       MINV0170
      IJ=IZ+I                                                           MINV0180
   10 IF(DABS(BIGA)-DABS(A(IJ)))15,20,20                                MINV0190
   15 BIGA=A(IJ)                                                        MINV0200
      L(K)=I                                                            MINV0210
      M(K)=J                                                            MINV0220
   20 CONTINUE                                                          MINV0230
C                                                                       MINV0240
C        INTERCHANGE ROWS                                               MINV0250
C                                                                       MINV0260
      J=L(K)                                                            MINV0270
      IF(J-K) 35,35,25                                                  MINV0280
   25 KI=K-N                                                            MINV0290
      DO 30 I=1,N                                                       MINV0300
      KI=KI+N                                                           MINV0310
      HOLD=-A(KI)                                                       MINV0320
      JI=KI-K+J                                                         MINV0330
      A(KI)=A(JI)                                                       MINV0340
   30 A(JI) =HOLD                                                       MINV0350
C        INTERCHANGE COLUMNS                                            MINV0360
```

```
C                                                                       MINV0370
   35 I=M(K)                                                            MINV0380
      IF(I-K) 45,45,38                                                  MINV0390
   38 JP=N*(I-1)                                                        MINV0400
      DO 40 J=1,N                                                       MINV0410
      JK=NK+J                                                           MINV0420
      JI=JP+J                                                           MINV0430
      HOLD=-A(JK)                                                       MINV0440
      A(JK)=A(JI)                                                       MINV0450
   40 A(JI) =HCLD                                                       MINV0460
C                                                                       MINV0470
C        DIVIDE COLUMN BY MINUS PIVOT (VALUE OF PIVOT ELEMENT IS        MINV0480
C        CCNTAINED IN BIGA)                                             MINV0490
C                                                                       MINV0500
   45 IF(BIGA) 48,46,48                                                 MINV0510
   46 DET=0.0                                                           MINV0520
      RETURN                                                            MINV0530
   48 DO 55 I=1,N                                                       MINV0540
      IF(I-K) 50,55,50                                                  MINV0550
   50 IK=NK+I                                                           MINV0560
      A(IK)=A(IK)/(-BIGA)                                               MINV0570
   55 CONTINUE                                                          MINV0580
C                                                                       MINV0590
C        REDUCE MATRIX                                                  MINV0600
C                                                                       MINV0610
      DO 65 I=1,N                                                       MINV0620
      IK=NK+I                                                           MINV0630
      HOLD=A(IK)                                                        MINV0640
      IJ=I-N                                                            MINV0650
      DO 65 J=1,N                                                       MINV0660
      IJ=IJ+N                                                           MINV0670
      IF(I-K) 60,65,60                                                  MINV0680
   60 IF(J-K) 62,65,62                                                  MINV0690
   62 KJ=IJ-I+K                                                         MINV0700
      A(IJ)=HOLD*A(KJ)+A(IJ)                                            MINV0710
   65 CCNTINUE                                                          MINV0720
```

```
C
C        DIVIDE ROW BY PIVOT
C
      KJ=K-N
      DO 75 J=1,N
      KJ=KJ+N
      IF(J-K) 70,75,70
   70 A(KJ)=A(KJ)/BIGA
   75 CONTINUE
C
C        PRODUCT OF PIVOTS
C
      DET=DET*BIGA
C
C        REPLACE PIVOT BY RECIPROCAL
C
      A(KK)=1.0/BIGA
   80 CONTINUE
C
C        FINAL ROW AND COLUMN INTERCHANGE
C
      K=N
  100 K=(K-1)
      IF(K) 150,150,105
  105 I=L(K)
      IF(I-K) 120,120,108
  108 JQ=N*(K-1)
      JR=N*(I-1)
      DO 110 J=1,N
      JK=JQ+J
      HOLD=A(JK)
      JI=JR+J
      A(JK)=-A(JI)
  110 A(JI) =HOLD
  120 J=M(K)
      IF(J-K) 100,100,125
```

```
  125 KI=K-N                                                          MINV1090
      DO 130 I=1,N                                                    MINV1100
      KI=KI+N                                                         MINV1110
      HOLD=A(KI)                                                      MINV1120
      JI=KI-K+J                                                       MINV1130
      A(KI)=-A(JI)                                                    MINV1140
  130 A(JI) =HOLD                                                     MINV1150
      GO TO 100                                                       MINV1160
  150 RETURN                                                          MINV1170
      END                                                             MINV1180
```

```
      SUBROUTINE OMULT(SQVCT,RWVCT,NCOL,NROWS,ACC,KROW,NDEX,NIRREG)     OMLT0010
     IMPLICIT REAL*8(A-H,O-Z)                                           OMLT0020
C     TO FIND ACC OF (SQVCT)*(RWVCT)=(ACC)                              OMLT0030
      DIMENSION SQVCT(1),RWVCT(1),NCOL(1),ACC(1),KROW(1),NDEX(1)        OMLT0040
      INDEX=0                                                           OMLT0050
      NROWM=NROWS-1                                                     OMLT0060
      IF (NIRREG .GT. 0) GO TO 200                                      OMLT0070
C     HIGH SPEED PRODUCT FOR REGULAR MATRICES                           OMLT0080
      DO 100 NN=1,NROWM                                                 OMLT0090
      SUM=0.0                                                           OMLT0100
      IP1=NN+1                                                          OMLT0110
      KST=NCOL(NN)                                                      OMLT0120
      INDEX=INDEX+NN-KST                                                OMLT0130
      DO 101 KPL=KST,NN                                                 OMLT0140
      IJ=INDEX+KPL                                                      OMLT0150
  101 SUM=SUM+SQVCT(IJ)*RWVCT(KPL)                                      OMLT0160
C     NOW FOR THE COLUMN ELEMENTS                                       OMLT0170
      JNDEX=IJ                                                          OMLT0180
      DO 102 KPL=IP1,NROWS                                              OMLT0190
      IF(NN.LT.NCOL(KPL))GO TO 100                                      OMLT0200
      JNDEX=JNDEX+KPL-NCOL(KPL)                                         OMLT0210
  102 SUM=SUM+SQVCT(JNDEX)*RWVCT(KPL)                                   OMLT0220
  100 ACC(NN)=ACC(NN)+SUM                                               OMLT0230
C     NOW FOR THE LAST ROW                                              OMLT0240
  104 KADD=NCOL(NROWS)                                                  OMLT0250
      SUM=0.0                                                           OMLT0260
      INDEX=INDEX+NROWS-KADD                                            OMLT0270
      DO 103 KPL=KADD,NROWS                                             OMLT0280
      IJ=INDEX+KPL                                                      OMLT0290
  103 SUM=SUM+SQVCT(IJ)*RWVCT(KPL)                                      OMLT0300
      ACC(NROWS)=ACC(NROWS)+SUM                                         OMLT0310
      RETURN                                                            OMLT0320
C     MEDIUM SPEED PRODUCT FOR NIRREG .LE. NROWS/2                      OMLT0330
  200 IF (NIRREG .GT. NROWS/2) GO TO 201                                OMLT0340
      DO 105 NN=1,NROWM                                                 OMLT0350
      IP1=NN+1                                                          OMLT0360
```

```
      KST=NCOL(NN)                                                      OMLT0370
      INDEX=INDEX+NN-KST                                                OMLT0380
      SUM=0.0                                                           OMLT0390
      DO 106 KPL=KST,NN                                                 OMLT0400
      IJ=INDEX+KPL                                                      OMLT0410
  106 SUM=SUM+SQVCT(IJ)*RWVCT(KPL)                                      OMLT0420
      NCK=0                                                             OMLT0430
      JNDEX=IJ                                                          OMLT0440
  107 DO 108 KPL=IP1,NROWS                                              OMLT0450
      IF(NN .LT. NCOL(KPL)) GO TO 109                                   OMLT0460
      JNDEX=JNDEX+KPL-NCOL(KPL)                                         OMLT0470
  108 SUM=SUM+SQVCT(JNDEX)*RWVCT(KPL)                                   OMLT0480
      GO TO 105                                                         OMLT0490
  109 NCK=NCK+1                                                         OMLT0500
      IF (NCK .GT.NIRREG) GO TO 105                                     OMLT0510
      IF (KPL .GE. KROW(NCK)) GO TO 109                                 OMLT0520
      IP1=KROW(NCK)                                                     OMLT0530
      JNDEX=NDEX(NCK)+NN                                                OMLT0540
      GO TO 107                                                         OMLT0550
  105 ACC(NN)=ACC(NN)+SUM                                               OMLT0560
      GO TO 104                                                         OMLT0570
  201 DO 503 NN=1,NROWM                                                 OMLT0580
      IP1=NN+1                                                          OMLT0590
      K=NCOL(NN)                                                        OMLT0600
      INDEX=INDEX+NN-K                                                  OMLT0610
      SUM=0.0                                                           OMLT0620
      DO 502 KRX=K,NN                                                   OMLT0630
      IJ=INDEX+KRX                                                      OMLT0640
  502 SUM=SUM+SQVCT(IJ)*RWVCT(KRX)                                      OMLT0650
      JNDEX=IJ                                                          OMLT0660
      DO 504 KRX=IP1,NROWS                                              OMLT0670
      K=NCOL(KRX)                                                       OMLT0680
      JNDEX=JNDEX+KRX-K                                                 OMLT0690
      IF (NN .LT. K) GC TO 504                                          OMLT0700
      SUM=SUM+SQVCT(JNDEX)*RWVCT(KRX)                                   OMLT0710
  504 CONTINUE                                                          OMLT0720
```

```
  503   ACC(NN)=ACC(NN)+SUM
        GO TO 104
        END
```

```
      SUBROUTINE PRINT(IT,TIME,HHALF)                                   PRIN0010
      IMPLICIT REAL*8(A-H,O-Z)                                          PRIN0020
      DIMENSION HHALF(50)                                               PRIN0030
      DIMENSION COPY(51),COPZ(51),FAILI(51),FAILO(51)                   PRIN0040
       COMMON /VQ/ FLVA(205),DISP(205),DELD(205),SNS(50,3,6,5),         PRIN0050
     *BINP(50,3),BIMP(50,3),TDISP(205),TU(205),TW(205),                 PRIN0060
     *COIY(205),COIZ(205),DELTAT                                        PRIN0070
      COMMON/FG/Y(51),Z(51),ANG(51),H(51),B,EXANG,NS,IK,NOGA,NFL,NSFL,  PRIN0080
     *NI,ICOL(205),NBCOND,NBC(4),NODEB(4)                               PRIN0090
       COMMON /HM/ YCUNG,DS,C5,C6,ASFL(50,3,6,5),GZETA(50,3,6),SNO(5)   PRIN0100
       COMMON /BA/ BEP(50,3,3,8),AL(50),AXG(3),AWG(3)                   PRIN0110
      COMMON/SC/CRITS,BIG,BTIME,MCRIT,IBIG,ISURF                        PRIN0120
      COMMON/FRAG/FH(6),FCG(6),FMASS(6),FMOI(6),FCGU(6),FCGW(6),ALFA(6),PRIN0130
     *UDOT(6),WDOT(6),ADOT(6),TPRIM(6),CR(6),FCGX(6),UNK(6),NF          PRIN0140
      COMMON /DFRAG/DFCGU(6),DFCGW(6),DALFA(6)                          PRIN0142
       COMMON /TAPE/ MREAD,MWRITE,MPUNCH                                PRIN0150
      COMMON /EP/ EPSI(50),EPSO(50)                                     PRIN0155
       DATA ASTER/'*'/,BLANK/' '/                                       PRIN0160
      SIN(Q)=DSIN(Q)                                                    PRIN0170
      COS(Q)=DCOS(Q)                                                    PRIN0180
      ATAN(Q)=DATAN(Q)                                                  PRIN0190
      ABS(Q)=DABS(Q)                                                    PRIN0200
      SQRT(Q)=DSQRT(Q)                                                  PRIN0210
      DO 11 I=1,NS                                                      PRIN0220
       COPY(I)=Y(I)+DISP(I*4-3)*COS(ANG(I))-DISP(I*4-2)*SIN(ANG(I))     PRIN0230
   11  COPZ(I)=Z(I)+DISP(I*4-3)*SIN(ANG(I))+DISP(I*4-2)*COS(ANG(I))     PRIN0240
      WRITE(MWRITE,1)IT,TIME                                            PRIN0250
 1    FORMAT(///,'    J=',I5,'    TIME=',D12.5)                         PRIN0260
       WRITE(MWRITE,2)                                                  PRIN0500
  2    FORMAT(/,'   I ',5X,'V',11X,'W',9X,'PSI',9X,'CHI',10X,'COPY',    PRIN0510
     *8X,'COPZ',9X,'L',11X,'M',7X,'STRAIN(IN)',4X,'STRAIN(OUT)')        PRIN0520
       IF(MCRIT .GT. 0) GO TO 50                                        PRIN0530
       DO 51 I=1,IK                                                     PRIN0540
       FAILI(I)=BLANK                                                   PRIN0550
       FAILO(I)=BLANK                                                   PRIN0560
       IF(EPSI(I) .LT. CRITS) GO TO 52                                  PRIN0570
```

```
      FAILI(I)=ASTER                                                    PRIN0580
      IF(MCRIT .GT. 0) GO TO 52                                         PRIN0590
      MCRIT=1                                                           PRIN0600
 52   IF(EPSO(I) .LT. CRITS) GO TO 51                                   PRIN0610
      FAILO(I)=ASTER                                                    PRIN0620
      IF(MCRIT .GT. 0) GO TO 51                                         PRIN0630
      MCRIT=1                                                           PRIN0640
 51   CONTINUE                                                          PRIN0650
      IF(MCRIT .LE. 0) GO TO 50                                         PRIN0660
      DO 53 I=1,IK                                                      PRIN0670
 53   WRITE(MWRITE,54) I,DISP(I*4-3),DISP(I*4-2),DISP(I*4-1),DISP(I*4),PRIN0680
     *COPY(I),COPZ(I),BINP(I,2),BIMP(I,2),EPSI(I),FAILI(I),             PRIN0690
     *EPSO(I),FAILO(I)                                                  PRIN0700
     IF(EXANG.EQ.360.)GO TO 932                                         PRIN0710
     IKP1=IK+1                                                          PRIN0720
     WRITE(MWRITE,22)IKP1,DISP(IKP1*4-3),DISP(IKP1*4-2),DISP(IKP1*4-1),PRIN0730
     *DISP(IK*4),COPY(IKP1),COPZ(IKP1)                                  PRIN0740
 932 WRITE(MWRITE,55)ASTER                                              PRIN0750
 54   FORMAT(I5,9D12.4,A2,D12.4,A2)                                     PRIN0760
      WRITE(MWRITE,55) ASTER                                            PRIN0770
 55   FORMAT(//,5X,A2,'   STRAIN EXCEEDS THE CRITICAL VALUE')           PRIN0780
     GO TO 189                                                          PRIN0790
 50   DO 21 I=1,IK                                                      PRIN0800
 21   WRITE(MWRITE,22)I,DISP(I*4-3),DISP(I*4-2),DISP(I*4-1),DISP(I*4), PRIN0810
     *COPY(I),COPZ(I),BINP(I,2),BIMP(I,2),EPSI(I),EPSO(I)               PRIN0820
     IF(EXANG.EQ.360.)GO TO 189                                         PRIN0830
 22   FORMAT(I5,9D12.4,2X,D12.4)                                        PRIN0840
     IKP1=IK+1                                                          PRIN0850
     WRITE(MWRITE,22) IKP1,DISP(IKP1*4-3),DISP(IKP1*4-2),DISP(IKP1*4-1)PRIN0860
     *,DISP(IKP1*4),COPY(IKP1),COPZ(IKP1)                               PRIN0870
 189 WRITE(MWRITE,35)                                                   PRIN0880
   35 FORMAT(10X,'FRAG NO.=',5X,'FCGU =',9X,'FCGW =',9X,'ALFA =',9X,    PRIN0890
     *'FRUV =',9X,'FRWV =',9X,'FRAV =',/)                               PRIN0892
     DO 36 I=1,NF                                                       PRIN0900
     FRUV= DFCGU(I)/DELTAT                                              PRIN0902
     FRWV= DFCGW(I)/DELTAT                                              PRIN0904
```

```
      FRAV= DALFA(I)/DELTAT                                             PRIN0906
   36 WRITE(MWRITE,37) I,FCGU(I),FCGW(I),ALFA(I),FRUV,FRWV,FRAV         PRIN0910
   37 FORMAT(10X,I5,3X,6D15.6,/)                                        PRIN0920
      RETURN                                                            PRIN0930
      END                                                               PRIN0940
```

```
      SUBROUTINE QREM(AA,AL,AXG,AWG)                                    QREM0010
      IMPLICIT REAL*8(A-H,O-Z)                                          QREM0020
C     TO FIND EFFECTIVE STIFFNESS MATRIX DUE TO ELASTIC RESTRAINTS      QREM0030
      DIMENSION AA(50,8,8),AL(1),AXG(1),AWG(1),BNG(51)                  QREM0040
     *,ELR(8,8),ELRR(8,8),ELRP(8,8)                                     QREM0050
      COMMON/FG/Y(51),Z(51),ANG(51),H(51),B,EXANG,NS,IK,NOGA,NFL,NSFL,  QREM0060
     *NI,ICOL(205),NBCOND,NBC(4),NODEB(4)                               QREM0070
      COMMON/ELFU/SPRIN(2060),FQREF(205),REX(4),NCR,NORP,NCRU,NREL(4),  QREM0080
     *NRST(4),NREU(4)                                                   QREM0090
      COMMON /TAPE/ MREAD,MWRITE,MPUNCH                                 QREM0100
      SIN(Q)=DSIN(Q)                                                    QREM0110
      COS(Q)=DCOS(Q)                                                    QREM0120
      ATAN(Q)=DATAN(Q)                                                  QREM0130
      ABS(Q)=DABS(Q)                                                    QREM0140
      SQRT(Q)=DSQRT(Q)                                                  QREM0150
      IF (NCRP .EQ. 0) GO TO 1                                          QREM0160
      READ(MREAD,2)SCTP,SCTY,SCRP,(NREL(I),REX(I),I=1,NORP)             QREM0170
    2 FORMAT(3D15.6/(4(I5,D15.6)))                                      QREM0180
      WRITE(MWRITE,777)SCTP,SCTY,SCRP                                   QREM0190
      DO 10 IQ=1,NORP                                                   QREM0200
      SL=REX(IQ)                                                        QREM0210
      NE=NREL(IQ)                                                       QREM0220
      P5=Z(NE+1)-Z(NE)                                                  QREM0230
      P6=Y(NE+1)-Y(NE)                                                  QREM0240
      P7=ANG(NE+1)-ANG(NE)                                              QREM0250
      APHA=ATAN(P5/P6)                                                  QREM0260
      IF(P6.LT.0.0 .AND. P5.LT.0.0) APHA=APHA-3.14159265                QREM0270
      IF(P6.LT.0.0 .AND. P5.GE.0.0) APHA=APHA+3.14159265                QREM0280
      BNG(NE+1)=ANG(NE+1)                                               QREM0290
      BNG(NE)=ANG(NE)                                                   QREM0300
      IF(P7.GT.(4.7124).AND.APHA.LT.0.0) BNG(NE+1)=ANG(NE+1)-6.2831853  QREM0310
      IF(P7.GT.(4.7124).AND.APHA.GT.0.0) BNG(NE)=ANG(NE)+6.2831853      QREM0320
      IF(P7.LT.(-4.7124).AND.APHA.GT.0.0) BNG(NE+1)=ANG(NE+1)+6.2831853 QREM0330
      IF(P7.LT.(-4.7124).AND.APHA.LT.0.0) BNG(NE)=ANG(NE)-6.2831853     QREM0340
      BZER=BNG(NE)-APHA                                                 QREM0350
      B1=(-2.*BNG(NE+1)-4.*BNG(NE)+6.*APHA)/AL(NE)                      QREM0360
```

```
      B2=(3.*BNG(NE+1)+3.*BNG(NE)-6.*APHA)/AL(NE)**2                    QREM0370
      PHI=BZER+B1*SL+B2*SL**2                                           QREM0380
      PHIP=B1+2.*B2*SL                                                  QREM0390
      YZET=0.0                                                          QREM0400
      ZZET=0.0                                                          QREM0410
      DO 104 JJ=1,NOGA                                                  QREM0420
      P2=BZER+B1*SL*AXG(JJ)+B2*(SL*AXG(JJ))**2+APHA                     QREM0430
      YZET=YZET+COS(P2)*SL*AWG(JJ)                                      QREM0440
  104 ZZET=ZZET+SIN(P2)*SL*AWG(JJ)                                      QREM0450
      P3=YZET*SIN(PHI+APHA)-ZZET*COS(PHI+APHA)                          QREM0460
      P4=YZET*COS(PHI+APHA)+ZZET*SIN(PHI+APHA)                          QREM0470
      ELR(1,1)=SCTP*COS(PHI)**2+SCTY*SIN(PHI)**2                        QREM0480
      ELR(2,1)= (SCTP-SCTY)*COS(PHI)*SIN(PHI)                           QREM0490
      ELR(3,1)=P3*COS(PHI)*SCTP-P4*SIN(PHI)*SCTY                        QREM0500
      ELR(4,1)=SL*COS(PHI)*SCTP                                         QREM0510
      ELR(5,1)=-SL**2*SIN(PHI)*SCTY                                     QREM0520
      ELR(6,1)=-SL**3*SIN(PHI)*SCTY                                     QREM0530
      ELR(7,1)=SL**2*COS(PHI)*SCTP                                      QREM0540
      ELR(8,1)=SL**3*COS(PHI)*SCTP                                      QREM0550
      ELR(2,2)=SCTP*SIN(PHI)**2+SCTY*COS(PHI)**2                        QREM0560
      ELR(3,2)=P3*SIN(PHI)*SCTP+P4*COS(PHI)*SCTY                        QREM0570
      ELR(4,2)=SL*SIN(PHI)*SCTP                                         QREM0580
      ELR(5,2)=SL**2*COS(PHI)*SCTY                                      QREM0590
      ELR(6,2)=SL**3*COS(PHI)*SCTY                                      QREM0600
      ELR(7,2)=SL**2*SIN(PHI)*SCTP                                      QREM0610
      ELR(8,2)=SL**3*SIN(PHI)*SCTP                                      QREM0620
      ELR(3,3)=P3**2*SCTP+P4**2*SCTY+SCRP                               QREM0630
      ELR(4,3)=P3*SL*SCTP+SL*PHIP*SCRP                                  QREM0640
      ELR(5,3)=P4*SL**2*SCTY+2.*SL*SCRP                                 QREM0650
      ELR(6,3)=P4*SL**3*SCTY+3.*SL**2*SCRP                              QREM0660
      ELR(7,3)=(P3*SCTP+PHIP*SCRP)*SL**2                                QREM0670
      ELR(8,3)=(P3*SCTP+PHIP*SCRP)*SL**3                                QREM0680
      ELR(4,4)=(SCTP+PHIP**2*SCRP)*SL**2                                QREM0690
      ELR(5,4)=2.*SL**2*PHIP*SCRP                                       QREM0700
      ELR(6,4)=3.*SL**3*PHIP*SCRP                                       QREM0710
      ELR(7,4)=(SCTP+PHIP**2*SCRP)*SL**3                                QREM0720
```

```
      ELR(8,4)=(SCTP+PHIP**2*SCRP)*SL**4
     ELR(5,5)=SL**4*SCTY+4.*SL**2*SCRP
      ELR(6,5)=SL**5*SCTY+6.*SL**3*SCRP
      ELR(7,5)=2.*SL**3*PHIP*SCRP
      ELR(8,5)=2.*SL**4*PHIP*SCRP
     ELR(6,6)=SL**6*SCTY+9.*SL**4*SCRP
      ELR(7,6)=3.*SL**4*PHIP*SCRP
      ELR(8,6)=3.*SL**5*PHIP*SCRP
      ELR(7,7)=(SCTP+PHIP**2*SCRP)*SL**4
      ELR(8,7)=(SCTP+PHIP**2*SCRP)*SL**5
      ELR(8,8)=(SCTP+PHIP**2*SCRP)*SL**6
      DO 12 I=1,7
      IP1=I+1
      DO 12 J=IP1,8
 12   ELR(I,J)=ELR(J,I)
      DO 13 I=1,8
      DO 13 J=1,8
      ELRR(I,J)=0.0
      DO 13 K=1,8
 13   ELRR(I,J)=ELRR(I,J)+ELR(I,K)*AA(NE,K,J)
      DO 14 I=1,8
      DO 14 J=1,8
      ELRP(I,J)=0.0
      DO 14 K=1,8
 14   ELRP(I,J)=ELRP(I,J)+AA(NE,K,I)*ELRR(K,J)
      CALL ASSEM(NE,ELRP,SPRIN)
 10   CONTINUE
 1    IF(NORU .EQ.0) GO TO 4
      READ(MREAD,3) SCTU,SCRU,(NRST(I),NREU(I),I=1,NORU)
 3    FORMAT(2E15.6,8I5)
     READ(MREAD,83)SCTW,(NRST(I),NREU(I),I=1,NORU)
 83  FORMAT(D15.6,8I5)
     WRITE(MWRITE,777)SCTU,SCTW,SCRU
 777 FORMAT(/,10X,'THE VALUE OF THE TANGENTIAL SPRING CONSTANT IS =',D1
    *5.6,/,10X,'THE VALUE OF THE RADIAL SPRING CONSTANT IS =',D15.6,/,
    *10X,'THE VALUE OF THE TORSIONAL SPRING CONSTANT IS =',D15.6,/)
```

```
      DO 15 IQ=1,NORU
      NSTAT=NRST(IQ)
      NEND=NREU(IQ)
      DO 16 IR=1,NEND
      NE=(NSTAT-1)+IR
      IF(NE .GT. IK) NE=NE-IK
      P5=Z(NE+1)-Z(NE)
      P6=Y(NE+1)-Y(NE)
      P7=ANG(NE+1)-ANG(NE)
      APHA=ATAN(P5/P6)
      IF(P6.LT.0.0 .AND. P5.LT.0.0) APHA=APHA-3.14159265
      IF(P6.LT.0.0 .AND. P5.GE.0.0) APHA=APHA+3.14159265
      BNG(NE+1)=ANG(NE+1)
      BNG(NE)=ANG(NE)
     IF(P7.GT.(4.7124).AND.APHA.LT.0.0) BNG(NE+1)=ANG(NE+1)-6.2831853
     IF(P7.GT.(4.7124).AND.APHA.GT.0.0) BNG(NE)=ANG(NE)+6.2831853
     IF(P7.LT.(-4.7124).AND.APHA.GT.0.0) BNG(NE+1)=ANG(NE+1)+6.2831853
     IF(P7.LT.(-4.7124).AND.APHA.LT.0.0) BNG(NE)=ANG(NE)-6.2831853
      BZER=BNG(NE)-APHA
      B1=(-2.*BNG(NE+1)-4.*BNG(NE)+6.*APHA)/AL(NE)
      B2=(3.*BNG(NE+1)+3.*BNG(NE)-6.*APHA)/AL(NE)**2
      DO 102 I=1,8
      DO 102 J=1,8
  102  ELR(I,J)=0.0
      DO 103 J=1,NOGA
      ZET=AL(NE)*AXG(J)
      PHIP=B1+2.*B2*ZET
      PHI=BZER+B1*ZET+B2*ZET**2
      WET=AL(NE)*AWG(J)
      YZET=0.0
      ZZET=0.0
      DO 105 JJ=1,NOGA
      P2=BZER+B1*ZET*AXG(JJ)+B2*(ZET*AXG(JJ))**2+APHA
      YZET=YZET+COS(P2)*ZET*AWG(JJ)
  105 ZZET=ZZET+SIN(P2)*ZET*AWG(JJ)
      P3=YZET*SIN(PHI+APHA)-ZZET*COS(PHI+APHA)
```

```
      P4=YZET*COS(PHI+APHA)+ZZET*SIN(PHI+APHA)
      ELR(1,1)=ELR(1,1)+(SCTU*COS(PHI)**2+SCTW*SIN(PHI)**2)*WET
      ELR(2,1)=ELR(2,1)+((SCTU-SCTW)*SIN(PHI)*COS(PHI))*WET
      ELR(3,1)=ELR(3,1)+(P3*SCTU*COS(PHI)-P4*SCTW*SIN(PHI))*WET
      ELR(5,1)=ELR(5,1)-(ZET**2*SCTW*SIN(PHI))*WET
      ELR(6,1)=ELR(6,1)-(ZET**3*SCTW*SIN(PHI))*WET
      ELR(2,2)=ELR(2,2)+(SCTU*SIN(PHI)**2+SCTW*COS(PHI)**2)*WET
      ELR(3,2)=ELR(3,2)+(P3*SCTU*SIN(PHI)+P4*SCTW*COS(PHI))*WET
      ELR(5,2)=ELR(5,2)+(ZET**2*SCTW*COS(PHI))*WET
      ELR(6,2)=ELR(6,2)+(ZET**3*SCTW*COS(PHI))*WET
      ELR(3,3)=ELR(3,3)+(P3**2*SCTU+P4**2*SCTW+SCRU)*WET
      ELR(5,3)=ELR(5,3)+(P4*SCTW*ZET**2+2.0*SCRU*ZET)*WET
      ELR(6,3)=ELR(6,3)+(P4*SCTW*ZET**3+3.0*SCRU*ZET**2)*WET
      ELR(5,5)=ELR(5,5)+(ZET**4*SCTW+4.0*ZET**2*SCRU)*WET
      ELR(6,5)=ELR(6,5)+(ZET**5*SCTW+6.0*ZET**3*SCRU)*WET
      ELR(6,6)=ELR(6,6)+(ZET**6*SCTW+9.0*ZET**4*SCRU)*WET
      ELR(4,1)=ELR(4,1)+ZET*COS(PHI)*SCTU*WET
      ELR(7,1)=ELR(7,1)+ZET**2*COS(PHI)*SCTU*WET
      ELR(8,1)=ELR(8,1)+ZET**3*COS(PHI)*SCTU*WET
      ELR(4,2)=ELR(4,2)+ZET*SIN(PHI)*SCTU*WET
      ELR(7,2)=ELR(7,2)+ZET**2*SIN(PHI)*SCTU*WET
      ELR(8,2)=ELR(8,2)+ZET**3*SIN(PHI)*SCTU*WET
      ELR(4,3)=ELR(4,3)+(P3*SCTU+PHIP*SCRU)*ZET*WET
      ELR(7,3)=ELR(7,3)+(P3*SCTU+PHIP*SCRU)*ZET**2*WET
      ELR(8,3)=ELR(8,3)+(P3*SCTU+PHIP*SCRU)*ZET**3*WET
      ELR(4,4)=ELR(4,4)+(SCTU+PHIP**2*SCRU)*ZET**2*WET
      ELR(5,4)=ELR(5,4)+2.*ZET**2*PHIP*SCRU*WET
      ELR(6,4)=ELR(6,4)+3.*ZET**3*PHIP*SCRU*WET
      ELR(7,4)=ELR(7,4)+(SCTU+PHIP**2*SCRU)*ZET**3*WET
      ELR(8,4)=ELR(8,4)+(SCTU+PHIP**2*SCRU)*ZET**4*WET
      ELR(7,5)=ELR(7,5)+2.*ZET**3*PHIP*SCRU*WET
      ELR(8,5)=ELR(8,5)+2.*ZET**4*PHIP*SCRU*WET
      ELR(7,6)=ELR(7,6)+3.*ZET**4*PHIP*SCRU*WET
      ELR(8,6)=ELR(8,6)+3.*ZET**5*PHIP*SCRU*WET
      ELR(7,7)=ELR(7,7)+(SCTU+PHIP**2*SCRU)*ZET**4*WET
      ELR(8,7)=ELR(8,7)+(SCTU+PHIP**2*SCRU)*ZET**5*WET
```

```
      ELR(8,8)=ELR(8,8)+(SCTU+PHIP**2*SCRU)*ZET**6*WET                  QREM1810
  103 CONTINUE                                                          QREM1820
      DO 5 I=1,7                                                        QREM1830
      IP1=I+1                                                           QREM1840
      DO 5 J=IP1,8                                                      QREM1850
    5 ELR(I,J)=ELR(J,I)                                                 QREM1860
      DO 6 I=1,8                                                        QREM1870
      DO 6 J=1,8                                                        QREM1880
      ELRR(I,J)=0.0                                                     QREM1890
      DO 6 K=1,8                                                        QREM1900
    6 ELRR(I,J)=ELRR(I,J)+ELR(I,K)*AA(NE,K,J)                           QREM1910
      DO 7 I=1,8                                                        QREM1920
      DO 7 J=1,8                                                        QREM1930
      ELRP(I,J)=0.0                                                     QREM1940
      DO 7 K=1,8                                                        QREM1950
    7 ELRP(I,J)=ELRP(I,J)+AA(NE,K,I)*ELRR(K,J)                          QREM1960
   16 CALL ASSEM(NE,ELRP,SPRIN)                                         QREM1970
   15 CONTINUE                                                          QREM1980
    4 IF(NBCOND .EQ. 0) RETURN                                          QREM1990
      DO 91 I=1,NBCOND                                                  QREM2000
      JT4=NODER(I)*4                                                    QREM2010
      JT4M3=JT4-3                                                       QREM2020
      JT4M2=JT4-2                                                       QREM2030
      JT4M1=JT4-1                                                       QREM2040
      CALL ERC(JT4M3,SPRIN,NI,ICOL)                                     QREM2050
      IF(NBC(I).EQ.1 .OR. NBC(I).EQ.2) CALL ERC(JT4M1,SPRIN,NI,ICOL)    QREM2060
      IF(NBC(I).EQ.2 .OR. NBC(I).EQ.3) CALL ERC(JT4M2,SPRIN,NI,ICOL)    QREM2070
   91 CONTINUE                                                          QREM2080
      RETURN                                                            QREM2090
      END                                                               QREM2100
```

```
      SUBROUTINE STRESS
      IMPLICIT REAL*8(A-H,O-Z)
C     TO EVALUATE GENERALIZED NODAL LOAD VECTOR DUE TO LARGE DEFLECTION
C     AND ELASTIC-PLASTIC STRAIN
      DIMENSION ELFP(8),BEPS(3),CEPS(3,3),BINPW(3),BIMPW(3),HWB(3,3),
     *PN(8),PM(8),HNL(8)
      COMMON/FG/Y(51),Z(51),ANG(51),H(51),B,EXANG,NS,IK,NOGA,NFL,NSFL,
     *NI,ICOL(205),NBCOND,NBC(4),NODEB(4)
      COMMON /VQ/ FLVA(205),DISP(205),DELD(205),SNS(50,3,6,5),
     *BINP(50,3),BIMP(50,3),TDISP(205),TU(205),TW(205),
     *COIY(205),COIZ(205),DELTAT
      COMMON /HM/ YOUNG,DS,C5,C6,ASFL(50,3,6,5),GZETA(50,3,6),SNC(5)
      COMMON /BA/ BEP(50,3,3,8),AL(50),AXG(3),AWG(3)
      SIN(Q)=DSIN(Q)
      COS(Q)=DCOS(Q)
      ATAN(Q)=DATAN(Q)
      ABS(Q)=DABS(Q)
      SQRT(Q)=DSQRT(Q)
      DO 502 IR=1,IK
      DO 503 J=1,NOGA
      BINP(IR,J)=0.
      BIMP(IR,J)=0.
  202 DO 402 I=1,3
      BEPS(I)=0.
      DO 402 K=1,8
      INDEX=(IR-1)*4+K
  402 BEPS(I)=BEPS(I)+BEP(IR,J,I,K)*DELD(INDEX)
      CEPS(J,2)=0.0
      DO 403 K=1,8
      INDEX=(IR-1)*4+K
  403 CEPS(J,2)=CEPS(J,2)+BEP(IR,J,2,K)*DISP(INDEX)
  205 FARE=BEPS(1)+CEPS(J,2)*BEPS(2)-BEPS(2)**2/2.
      FCUR=BEPS(3)
      DO 151 K=1,NFL
      BFNP=0.
      BEPX=FARE+GZETA(IR,J,K)*FCUR
```

```
      IF(DS.GT. 0.0) RFACTR=1.+(C6*ABS(BEPX))**C5                       STRS0370
      DO 35 L=1,NSFL                                                    STRS0380
      SNS(IR,J,K,L)=SNS(IR,J,K,L)+YOUNG*BEPX                            STRS0390
      IF(DS.EQ. 0.0) GO TO 255                                          STRS0400
      IF(SNS(IR,J,K,L)-SNO(L))30,301,91                                 STRS0410
 91   SNY=SNO(L)*RFACTR                                                 STRS0420
      IF(SNS(IR,J,K,L)-SNY)301,301,20                                   STRS0430
 20   SNS(IR,J,K,L)=SNY                                                 STRS0440
      GO TO 301                                                         STRS0450
 30   IF(SNS(IR,J,K,L)+SNO(L))92,301,301                                STRS0460
 92   SNY=SNO(L)*RFACTR                                                 STRS0470
      IF(SNS(IR,J,K,L)+SNY)40,301,301                                   STRS0480
 40   SNS(IR,J,K,L)=-SNY                                                STRS0490
      GO TO 301                                                         STRS0500
 255  IF(SNS(IR,J,K,L)-SNO(L)) 18,301,17                                STRS0510
 17   SNS(IR,J,K,L)=SNO(L)                                              STRS0520
      GO TO 301                                                         STRS0530
 18   IF(SNS(IR,J,K,L)+SNO(L)) 19, 301,301                              STRS0540
 19   SNS(IR,J,K,L)=-SNO(L)                                             STRS0550
 301  BFNP=BFNP+SNS(IR,J,K,L)*ASFL(IR,J,K,L)                            STRS0560
 35   CONTINUE                                                          STRS0570
      BINP(IR,J)=BINP(IR,J)+BFNP                                        STRS0580
      BIMP(IR,J)=BIMP(IR,J)+BFNP*GZETA(IR,J,K)                          STRS0590
 151  CONTINUE                                                          STRS0600
 503  CONTINUE                                                          STRS0610
 107  DO 101 J=1,NOGA                                                   STRS0620
      HWB(J,2)=CEPS(J,2)*AWG(J)*BINP(IR,J)*AL(IR)                       STRS0630
      BINPW(J)=BINP(IR,J)*AWG(J)*AL(IR)                                 STRS0640
      BIMPW(J)=BIMP(IR,J)*AWG(J)*AL(IR)                                 STRS0650
 101   CONTINUE                                                         STRS0660
      DO 102 I=1,8                                                      STRS0670
      PN(I)=0.                                                          STRS0680
      PM(I)=0.                                                          STRS0690
      HNL(I)=0.0                                                        STRS0700
      DO 102 J=1,NOGA                                                   STRS0710
      PN(I)=PN(I)+BEP(IR,J,1,I)*BINPW(J)                                STRS0720
```

```
      PM(I)=PM(I)+BEP(IR,J,3,I)*BIMPW(J)                                STRS0730
  102 HNL(I)=HNL(I)+BEP(IR,J,2,I)*HWB(J,2)                              STRS0740
  200 DO 105 I=1,8                                                      STRS0750
  105 ELFP(I)=PN(I)+PM(I)+HNL(I)                                        STRS0760
  502 CALL ASSEF(IR,IK,ELFP,FLVA,EXANG)                                 STRS0770
      RETURN                                                            STRS0780
      END                                                               STRS0790
```

A.6 Illustrative Examples

A.6.1 Free Circular Uniform-Thickness Containment Ring Subjected to Single-Fragment Attack

In this example a free, initially-circular ring: 7.70-in midsurface radius, 0.40-in thick, and 1.25-in long is subjected to attack by a circular-disk fragment with radius r_f = 3.37 in, mass 4.60 x 10^{-3} (lb-sec^2)/in, mass moment of inertia 2.61 x 10^{-2} lb-sec^2-in, initial translational velocity 6,400 in/sec, rotational velocity 20,000 rpm (2100 rad/sec), and r_{CG} = 3.63 in. (see Fig. A.5).

The stress-strain curve is approximated by straight-line segments having the following stress-strain coordinates: (σ,ε) = (0 psi, 0 in/in); (80,950 psi, .00279 in/in); (105,300 psi, .0225 in/in); and (121,000 psi, .200 in/in). Strain-rate effects are neglected. The mass density of the material is taken to be 0.732 x 10^{-3} (lb-sec^2)/in^4.

The number of equal-length finite elements to be used to describe the complete ring is 40.

Let the CIVM-JET-4A program calculate the transient response of the ring. The time increment $\Delta t \doteq 1$ μsec is chosen, which has been shown (by numerical experimentation) to be suitable to provide a converged solution for this case. By consideration of the ring and fragment geometry and the velocity components of the fragment, a calculation has determined that there is no possibility of initial impact before approximately 303 μsec after fragment release which is assumed to occur at the condition (instant) shown in Fig. A.5. To expedite the calculation and to eliminate the possibility of accumulation of error in the calculation of fragment position (while not significant in this example, a major consideration in calculation involving obliquely-oriented translational velocity vectors), the fragment is advanced to its position at 300 μsec after release through the use of the TPRIM value specified in the input data.

Six hundred and fifty computational cycles (650 μsec) of structural response and the associated impact interactions are to be computed. These computational cycles, it should be noted, start at TPRIM = 300 μsec. Printout is desired at 5 cycles after TPRIM and every 40 cycles thereafter. An energy accountin calculation for the system is desired.

A.6.1.1 Input Data

The values to be punched on the data cards are as follows:

			Format
Card 1			3D15.6
	B	= 0.125000 D+01	
	DENS	= 0.732000 D-03	
	EXANG	= 0.360000 D+03 (complete ring = 360 deg)	
Card 2			8I5
	IK	= 40	
	NOGA	= 3	
	NFL	= 4	
	NSFL	= 3	
	MM	= 650	
	M1	= 5	
	M2	= 40	
	NF	= 1	
Card 2a			4D15.6
	Y(1)	= 0.000000 D+00	
	Z(1)	= 0.770000 D+01	
	ANG(1)	= 0.000000 D+00	
	H(1)	= 0.400000 D+00	

.
.
.

Additional 2a cards are provided in the same format until all 40 nodal points are described.

.
.
.

Y(40)	= 0.120454 D+01
Z(40)	= 0.760520 D+01
ANG(40)	= 0.900000 D+01
H(40)	= 0.400000 D+00

			Format
Card 3			4D15.6
	DELTAT	= 0.100000 D-05	
	CRITS	= 0.200000 D+00	
	DS	= 0.000000 D+00 (strain-rate effects are neglected)	
Card 4			4D15.6
	EPS(1)	= 0.279000 D-02	
	SIG(1)	= 0.809500 D+05	
	EPS(2)	= 0.225000 D-01	
	SIG(2)	= 0.105300 D+06	
Card 4a			4D15.6
	EPS(3)	= 0.200000 D+00	
	SIG(3)	= 0.121000 D+06	
Card 5			5D15.6
	FH(1)	= 0.674000 D+01	
	FCG(1)	= 0.363000 D+01	
	FCGX(1)	= 0.000000 D+00	
	FMASS(1)	= 0.460000 D-02	
	FMOI(1)	= 0.261000 D-01	
Card 6			D15.6
	UNK(1)	= 0.000000 D+00	
Card 7			5D15.6
	UDOT(1)	= 0.640000 D+04	
	WDOT(1)	= 0.000000 D+00	
	ADOT(1)	= - 0.210000 D+04	
	TPRIM(1)	= 0.300000 D-03 (300 μsec after	
	CR(1)	= 0.100000 D+01 release)	
Card 8			3F15.10
	AXG(1)	= 0.1127016654	
	AXG(2)	= 0.5	
	AXG(3)	= 0.8872983346	

			Format
Card 9			3F15.10
AWG(1)	= 0.2777777778		
AWG(2)	= 0.4444444444		
AWG(3)	= 0.2777777778		
Card 10			4F15.10
TXG(1)	= -0.8611363115		
TXG(2)	= -0.3399810435		
TXG(3)	= 0.3399810435		
TXG(4)	= 0.8611363115		
Card 11			4F15.10
TWG(1)	= 0.3478548451		
TWG(2)	= 0.6521451548		
TWG(3)	= 0.6521451548		
TWG(4)	= 0.3478548451		
Card 12			I5
NBCOND	= 0	(no prescribed displacement conditions)	
Card 13			3I5
NQR	= 0	(no prescribed elastic restraints)	
Card 14			I5
ICONT	= 0	(no initial conditions)	

The total input deck for this example should appear as follows:

```
 0.125000D 01    0.732000D-03    0.360000D 03
 40     3     4    3  650      5    40     1
 0.000000D000    0.770000D 01    0.000000D 00    0.400000D 00
 0.120455D 01   00.760520D 01   -0.900000D 01   00.400000D 00
00.237943D 01   00.732314D 01   -0.180000D 02   00.400000D 00
00.349573D 01   00.686075D 01   -0.270000D 02   00.400000D000
00.452595D 01   00.622943D 01   -0.360000D 02   00.400000D 00
00.544472D 01   00.544472D 01   -0.450000D 02   00.400000D 00
00.622943D 01   00.452595D 01   -0.540000D 02   00.400000D 00
00.686075D 01   00.349573D 01   -0.630000D 02   00.400000D 00
00.732314D 01   00.237943D 01   -0.720000D 02   00.400000D 00
00.760520D 01   00.120454D 01   -0.810000D 02   00.400000D 00
00.770000D 01   -0.125449D-05   -0.900000D 02   00.400000D 00
00.760520D 01   -0.120455D 01   -0.990000D 02   00.400000D 00
00.732314D 01   -0.237943D 01   -0.108000D 03   00.400000D 00
00.686075D 01   -0.349573D 01   -0.117000D 03   00.400000D 00
00.622943D 01   -0.452595D 01   -0.126000D 03   00.400000D 00
00.544472D 01   -0.544472D 01   -0.135000D 03   00.400000D 00
00.452594D 01   -0.622943D 01   -0.144000D 03   00.400000D 00
00.349572D 01   -0.686075D 01   -0.153000D 03   00.400000D 00
00.237943D 01   -0.732314D 01   -0.162000D 03   00.400000D 00
00.120454D 01   -0.760520D 01   -0.171000D 03   00.400000D 00
-0.250898D-05   -0.770000D 01   00.180000D 03   00.400000D 00
-0.120455D 01   -0.760520D 01   00.171000D 03   00.400000D 00
-0.237943D 01   -0.732313D 01   00.162000D 03   00.400000D 00
-0.349573D 01   -0.686075D 01   00.153000D 03   00.400000D 00
-0.452595D 01   -0.622943D 01   00.144000D 03   00.400000D 00
-0.544472D 01   -0.544472D 01   00.135000D 03   00.400000D 00
-0.622943D 01   -0.452594D 01   00.126000D 03   00.400000D 00
-0.686075D 01   -0.349572D 01   00.117000D 03   00.400000D 00
-0.732314D 01   -0.237943D 01   00.108000D 03   00.400000D 00
-0.760520D 01   -0.120454D 01   00.990000D 02   00.400000D 00
-0.770000D 01   00.376347D-05   00.900000D 02   00.400000D 00
-0.760520D 01   00.120455D 01   00.810000D 02   00.400000D 00
-0.732313D 01   00.237943D 01   00.720000D 02   00.400000D 00
-0.686075D 01   00.349573D 01   00.630000D 02   00.400000D 00
```

```
-0.622943D 01  00.452595D 01  00.540000D 02  00.400000D 00
-0.544472D 01  00.544473D 01  00.450000D 02  00.400000D 00
-0.452594D 01  00.622943D 01  00.360000D 02  00.400000D 00
-0.349572D 01  00.686075D 01  00.270000D 02  00.400000D 00
-0.237943D 01  00.732314D 01  00.180000D 02  00.400000D 00
-0.120454D 01  00.760520D 01  00.900000D 01  00.400000D 00
 00.100000D-05  00.200000D 00  00.000000D 00
 00.279000D-02  00.809500D 05  00.225000D-01  00.105300D 06
 00.200000D 00  00.121000D 06
 00.674000D 01  00.363000D 01  00.000000D 00  00.460000D-02  00.261000D-01
 00.000000D 00
 00.640000D 04  00.000000D 00  -0.210000D 04  00.300000D-03  00.100000D 01
  0.1127016654   0.5            0.8872983346
  0.2777777778   0.4444444444   0.2777777778
 -0.8611363115  -0.3399810435   0.3399810435   0.8611363115
  0.3478548451   0.6521451548   0.6521451548   0.3478548451
   0
   0
   0
```

A.6.1.2 Solution Output Data

The following output for example 1 was obtained through the use of a CIVM-JET-4A analysis. In the interest of conciseness, only the output obtained at time cycles 5, 45, 325, 405, 605, and 645 after TPRIM is presented to enable a user to check the proper adaptation of CIVM-JET-4A to his computing facility.

The ring material and geometric properties, and prescribed displacements or restraints, the initial nodal coordinates, and the fragment geometric and initial velocity and energy properties are output to provide an input-data-consistency check.

The initial impact is detected at 3 cycles after TPRIM at a position along the length of element 4. During the subsequent computational cycles, impact positions are detected indicating that the fragment is traveling in a clockwise direction along the surface of the ring.

The maximum circumferential strain response of the ring reaches 9.84 per cent at 382 μsec after TPRIM at the outer surface midspan of element 7.+

The energy "breakdown" at a given time cycle is presented immediately before the structural response data for that time cycle.

+In the present example, the strain responses were computed only at the midspan station of each ring finite element.

COMPLETE RING **JET** CONTAINMENT ANALYSIS

```
RING PROPERTIES
  SUBTENDED ANGLE OF RING                         =  0.360000D+03

  WIDTH OF RING(IN)                               =  0.125000D+01
  DENSITY OF RING                                 =  0.732000D-03
  NUMBER OF ELEMENTS                              =  40
  NUMBER OF SPANWISE GAUSSIAN PTS.                =  3
  NUMBER OF DEPTHWISE GAUSSIAN PTS.               =  4
  NUMBER OF MECHANICAL SUBLAYERS                  =  3

     STRAIN (1) =  0.279000D-02 STRESS (1) =  0.809500D+05

     STRAIN (2) =  0.225000D-01 STRESS (2) =  0.105300D+06

     STRAIN (3) =  0.200000D+00 STRESS (3) =  0.121000D+06
```

NODE NO.	Y COORD	Z COORD	SLOPE	RING THICKNESS AT NODE I
1	0.0	0.770000D+01	0.0	0.400000D+00
2	0.120455D+01	0.760520D+01	-0.157080D+00	0.400000D+00
3	0.237943D+01	0.732314D+01	-0.314159D+00	0.400000D+00
4	0.349573D+01	0.686075D+01	-0.471239D+00	0.400000D+00
5	0.452595D+01	0.622943D+01	-0.628319D+00	0.400000D+00
6	0.544472D+01	0.544472D+01	-0.785398D+00	0.400000D+00
7	0.622943D+01	0.452595D+01	-0.942478D+00	0.400000D+00
8	0.686075D+01	0.349573D+01	-0.109956D+01	0.400000D+00
9	0.732314D+01	0.237943D+01	-0.125664D+01	0.400000D+00
10	0.760520D+01	0.120454D+01	-0.141372D+01	0.400000D+00
11	0.770000D+01	0.0	-0.157080D+01	0.400000D+00
12	0.760520D+01	-0.120455D+01	-0.172788D+01	0.400000D+00
13	0.732314D+01	-0.237943D+01	-0.188496D+01	0.400000D+00

14	0.686075D+01	-0.349573D+01	-0.204204D+01	0.400000D+00
15	0.622943D+01	-0.452595D+01	-0.219912D+01	0.400000D+00
16	0.544472D+01	-0.544472D+01	-0.235619D+01	0.400000D+00
17	0.452595D+01	-0.622943D+01	-0.251327D+01	0.400000D+00
18	0.349573D+01	-0.686075D+01	-0.267035D+01	0.400000D+00
19	0.237943D+01	-0.732314D+01	-0.282743D+01	0.400000D+00
20	0.120454D+01	-0.760520D+01	-0.298451D+01	0.400000D+00
21	0.0	-0.770000D+01	0.314159D+01	0.400000D+00
22	-0.120455D+01	-0.760520D+01	0.298451D+01	0.400000D+00
23	-0.237943D+01	-0.732314D+01	0.282743D+01	0.400000D+00
24	-0.349573D+01	-0.686075D+01	0.267035D+01	0.400000D+00
25	-0.452595D+01	-0.622943D+01	0.251327D+01	0.400000D+00
26	-0.544472D+01	-0.544472D+01	0.235619D+01	0.400000D+00
27	-0.622943D+01	-0.452595D+01	0.219912D+01	0.400000D+00
28	-0.686075D+01	-0.349573D+01	0.204204D+01	0.400000D+00
29	-0.732314D+01	-0.237943D+01	0.188496D+01	0.400000D+00
30	-0.760520D+01	-0.120454D+01	0.172788D+01	0.400000D+00
31	-0.770000D+01	0.0	0.157080D+01	0.400000D+00
32	-0.760520D+01	0.120455D+01	0.141372D+01	0.400000D+00
33	-0.732314D+01	0.237943D+01	0.125664D+01	0.400000D+00

34	-0.686075D+01	0.349573D+01	0.109956D+01	0.400000D+00
35	-0.622943D+01	0.452595D+01	0.942478D+00	0.400000D+00
36	-0.544472D+01	0.544472D+01	0.785398D+00	0.400000D+00
37	-0.452595D+01	0.622943D+01	0.628319D+00	0.400000D+00
38	-0.349573D+01	0.686075D+01	0.471239D+00	0.400000D+00
39	-0.237943D+01	0.732314D+01	0.314159D+00	0.400000D+00
40	-0.120454D+01	0.760520D+01	0.157080D+00	0.400000D+00

FRAGMENT PROPERTIES

FRAG.NO.	WIDTH OF FRAG.	MASS OF FRAG.	MOMENT OF INERTIA OF FRAG.	FCGY	FCGZ
1	0.674000D+01	0.460000D-02	0.261000D-01	0.0	0.363000D+01

COLLISION PARAMETERS

FRAG.NO.	VEL IN Y DIR.	VEL IN Z DIR.	ANG. VEL.	COEFF.OF RESTIT.	INITIAL KINETIC ENERGY	COEFF. OF FRICT
1	0.640000D+04	0.0	-0.210000D+04	0.100000D+01	C.151758D+06	0.C

THERE IS NO PRESCRIBED DISPLACEMENT CONDITION

THERE ARE NO ELASTIC SPRING CONSTANTS

SIZE OF ASSEMBLED MASS OR STIFFNESS MATRIX = 1632

```
IMPACT IT=    3   ELEMENT NO. =     4 - FRAGMENT NO. -     1
LOCATION ON ELEMENT =   0.847368D+00   PENETRATION DIST =   0.204819D-02

CURRENT TIME CYCLE            FRAGMENT           KINETIC ENERGY

        5                        1                 0.143584D+06

WORK INPUT INTO RING TO TIME STEP       5 =   0.817419D+04
RING KINETIC ENERGY AT TIME STEP        5 =   0.459540D+04
RING ELASTIC ENERGY TO TIME STEP        5 =   0.792677D+02
RING PLASTIC WORK TO TIME STEP          5 =   0.349952D+04
ENERGY STORED IN ELASTIC RESTRAINTS       =    0.0

J=    5    TIME= 0.500000D-05
```

I	V	W	PSI	CHI	COPY	COPZ	L	M	STRAIN(IN)	STRAIN(OUT)
1	0.0	0.0	0.0	0.0	0.0	0.7700D+01	0.8680D+01	0.4773D-01	0.5490D-06	0.6477D-06
2	0.6566D-06	-0.1281D-06	-0.2891D-06	0.8296D-06	0.1205D+01	0.7605D+01	0.1196D+04	-0.3169D+02	0.1152D-03	0.4965D-04
3	0.8690D-04	0.3636D-04	0.1999D-03	0.9481D-04	0.2380D+01	0.7323D+01	0.3397D+05	0.3728D+02	0.2303D-02	0.2380D-02
4	0.9169D-03	0.1261D-01	0.7922D-04	0.5543D-04	0.3502D+01	0.6872D+01	0.2261D+04	0.5342D+02	0.1006D-03	0.2111D-03
5	-0.3943D-03	0.5408D-02	-0.2514D-03	0.3432D-04	0.4529D+01	0.6234D+01	0.1407D+05	-0.1658D+02	0.9872D-03	0.9530D-03
6	-0.3780D-04	0.1823D-04	-0.9959D-04	0.3765D-04	0.5445D+01	0.5445D+01	0.5331D+03	-0.1578D+02	0.5307D-04	0.2043D-04
7	-0.2774D-06	-0.5440D-07	0.1230D-06	0.3500D-06	0.6229D+01	0.4526D+01	0.3669D+01	0.2030D-01	0.2319D-06	0.2739D-06
8	0.0	0.0	0.0	0.0	0.6861D+01	0.3496D+01	0.0	0.0	0.0	0.0
9	0.0	0.0	0.0	0.0	0.7323D+01	0.2379D+01	0.0	0.0	0.0	0.0
10	0.0	0.0	0.0	0.0	0.7605D+01	0.1205D+01	0.0	0.0	0.0	0.0
11	0.0	0.0	0.0	0.0	0.7700D+01	0.0	0.0	0.0	0.0	0.0
12	0.0	0.0	0.0	0.0	0.7605D+01	-0.1205D+01	0.0	0.0	0.0	0.0
13	0.0	0.0	0.0	0.0	0.7323D+01	-0.2379D+01	0.0	0.0	0.0	0.0
14	0.0	0.0	0.0	0.0	0.6861D+01	-0.3496D+01	0.0	0.0	0.0	0.0
15	0.0	0.0	0.0	0.0	0.6229D+01	-0.4526D+01	0.0	0.0	0.0	0.0
16	0.0	0.0	0.0	0.0	0.5445D+01	-0.5445D+01	0.0	0.0	0.0	0.0
17	0.0	0.0	0.0	0.0	0.4526D+01	-0.6229D+01	0.0	0.0	0.0	0.0
18	0.0	0.0	0.0	0.0	0.3496D+01	-0.6861D+01	0.0	0.0	0.0	0.0
19	0.0	0.0	0.0	0.0	0.2379D+01	-0.7323D+01	0.0	0.0	0.0	0.0
20	0.0	0.0	0.0	0.0	0.1205D+01	-0.7605D+01	0.0	0.0	0.0	0.0
21	0.0	0.0	0.0	0.0	0.0	-0.7700D+01	0.0	0.0	0.0	0.0
22	0.0	0.0	0.0	0.0	-0.1205D+01	-0.7605D+01	0.0	0.0	0.0	0.0
23	0.0	0.0	0.0	0.0	-0.2379D+01	-0.7323D+01	0.0	0.0	0.0	0.0
24	0.0	0.0	0.0	0.0	-0.3496D+01	-0.6861D+01	0.0	0.0	0.0	0.0
25	0.0	0.0	0.0	0.0	-0.4526D+01	-0.6229D+01	0.0	0.0	0.0	0.0
26	0.0	0.0	0.0	0.0	-0.5445D+01	-0.5445D+01	0.0	0.0	0.0	0.0
27	0.0	0.0	0.0	0.0	-0.6229D+01	-0.4526D+01	0.0	0.0	0.0	0.0
28	0.0	0.0	0.0	0.0	-0.6861D+01	-0.3496D+01	0.0	0.0	0.0	0.0
29	0.0	0.0	0.0	0.0	-0.7323D+01	-0.2379D+01	0.0	0.0	0.0	0.0
30	0.0	0.0	0.0	0.0	-0.7605D+01	-0.1205D+01	0.0	0.0	0.0	0.0
31	0.0	0.0	0.0	0.0	-0.7700D+01	0.0	0.0	0.0	0.0	0.0
32	0.0	0.0	0.0	0.0	-0.7605D+01	0.1205D+01	0.0	0.0	0.0	0.0
33	0.0	0.0	0.0	0.0	-0.7323D+01	0.2379D+01	0.0	0.0	0.0	0.0
34	0.0	0.0	0.0	0.0	-0.6861D+01	0.3496D+01	0.0	0.0	0.0	0.0
35	0.0	0.0	0.0	0.0	-0.6229D+01	0.4526D+01	0.0	0.0	0.0	0.0
36	0.0	0.0	0.0	0.0	-0.5445D+01	0.5445D+01	0.0	0.0	0.0	0.0
37	0.0	0.0	0.0	0.0	-0.4526D+01	0.6229D+01	0.0	0.0	0.0	0.0
38	0.0	0.0	0.0	0.0	-0.3496D+01	0.6861D+01	0.0	0.0	0.0	0.0
39	0.0	0.0	0.0	0.0	-0.2379D+01	0.7323D+01	0.0	0.0	0.0	0.0
40	0.0	0.0	0.0	0.0	-0.1205D+01	0.7605D+01	0.0	0.0	0.0	0.0

FRAG NO.=	FCGU =	FCGW =	ALFA =	FRUV =	FRWV =	FRAV =
1	0.195109D+01	0.362851D+01	-0.640500D+00	0.609588D+04	-0.496285D+03	-0.210000D+04

IMPACT IT= 31 ELEMENT NO. = 4 FRAGMENT NO. = 1
LOCATION CN ELEMENT = 0.543087D+00 PENETRATION DIST = 0.512610D-03

CURRENT TIME CYCLE	FRAGMENT	KINETIC ENERGY
45	1	0.141390D+06

WORK INPUT INTO RING TO TIME STEP 45 = 0.103684D+05
RING KINETIC ENERGY AT TIME STEP 45 = 0.448911D+04
RING ELASTIC ENERGY TO TIME STEP 45 = 0.446245D+03
RING PLASTIC WORK TO TIME STEP 45 = 0.543302D+04
ENERGY STORED IN ELASTIC RESTRAINTS = 0.0

J= 45 TIME= C.45000D-04

210

I	V	W	PSI	CHI	COPY	COPZ	L	M	STRAIN(IN)	STRAIN(OUT)
1	0.5980D-02	-0.2681D-02	-0.3268D-02	0.8004D-03	0.5980D-02	0.7697D+01	0.1855D+05	-0.1980D+03	0.1484D-02	0.1074D-02
2	0.8153D-02	-0.5926D-02	-0.2020D-02	0.1420D-02	0.1212D+01	0.7598D+01	0.2405D+05	-0.3093D+04	0.1661D-01	-0.5547D-02
3	0.1545D-01	0.2034D-01	C.6496D-01	0.1337D-01	0.2400D+01	0.7338D+01	0.2664D+05	0.2119D+04	-0.1384D-02	0.1078D-01
4	0.4421D-02	0.1518D+00	0.2698D-01	0.2131D-01	0.3569D+01	0.6994D+01	0.3266D+05	0.2629D+04	-0.8154D-02	0.2518D-01
5	-0.6288D-C2	0.9021D-01	-0.7420D-01	0.2188D-02	0.4574D+01	0.6306D+01	0.3030D+05	-0.2046D+04	0.1150D-01	-0.2102D-02
6	-0.1042D-01	0.9928D-02	-0.3308D-01	0.4406D-02	0.5444D+01	0.5459D+01	0.1686D+05	-0.3174D+04	0.8238D-02	-0.3355D-02
7	-0.7130D-02	-0.5564D-02	0.1993D-02	0.1227D-02	0.6221D+01	0.4528D+01	0.1821D+05	-0.1580D+03	0.1418D-02	G.1092D-02
8	-0.5045D-02	-0.1946D-02	0.2986D-02	0.1109D-02	0.6857D+01	0.3499D+01	0.1714D+05	0.3566D+03	0.8127D-03	C.1550D-02
9	-0.3521D-02	-0.8434D-03	0.7657D-03	0.8045D-03	0.7321D+01	0.2383D+01	0.1418D+05	0.3927D+02	0.9368D-03	0.1018D-02
10	-C.2270D-02	-0.4603D-03	0.5243D-03	0.9882D-03	0.7604D+01	0.1207D+01	0.1304D+05	0.4703D+02	0.8502D-03	0.9475D-03
11	-0.1134D-02	-0.1794D-03	C.2299D-03	0.8143D-03	0.7700D+01	0.1134D-0?	0.8518D+04	0.2482D+02	0.5615D-03	G.6128D-03
12	-0.4026D-03	-0.5321D-04	0.7406D-04	0.3809D-03	0.7605D+01	-0.1204D+01	0.3522D+04	0.8979D+01	0.2335D-03	0.2521D-03
13	-0.1C23D-03	-0.1194D-04	0.1766D-04	0.1136D-03	0.7323D+01	-0.2379D+01	0.9779D+03	0.2304D+01	0.6502D-04	0.6979D-04
14	-0.1927D-04	-0.2061D-05	0.3185D-05	0.2365D-04	0.6861D+01	-0.3496D+01	0.1945D+03	0.4359D+00	0.1295D-04	0.1385D-04
15	-0.2780D-05	-0.2794D-06	0.4459D-06	0.3651D-05	0.6229D+01	-0.4526D+01	0.2909D+02	0.6303D-01	0.1940D-05	0.2070D-05
16	-0.3162D-06	-0.3034D-07	0.4963D-07	0.4356D-06	0.5445D+01	-0.5445D+01	0.3393D+01	0.7181D-02	0.2265D-06	0.2413D-06
17	-0.2902D-07	-0.2689D-08	0.4481D-08	0.4140D-07	0.4526D+01	-0.6229D+01	0.3171D+00	0.6594D-03	0.2118D-07	0.2254D-07
18	-0.2189D-08	-0.1973D-09	0.3338D-09	0.3207D-08	0.3496D+01	-0.6861D+01	0.2424D-01	0.4975D-04	0.1620D-08	0.1722D-08
19	-0.1376D-C9	-0.1214D-10	0.2078D-10	0.2059D-09	0.2379D+01	-0.7323D+01	0.1541D-02	0.3129D-05	0.1030D-09	0.1094D-09
20	-C.7305D-11	-0.6333D-12	0.1095D-11	0.1111D-10	0.1205D+01	-0.7605D+01	0.8246D-04	0.1661D-06	0.5512D-11	0.5856D-11
21	-0.3305D-12	-0.2825D-13	0.4921D-13	0.5094D-12	0.3305D-12	-0.7700D+01	0.3756D-05	0.7516D-08	0.2511D-12	0.2667D-12
22	-0.1285D-13	-0.1085D-14	C.1904D-14	0.2002D-13	-0.1205D+01	-0.7605D+01	0.1468D-06	0.2923D-09	0.9820D-14	0.1042D-13
23	-0.4324D-15	-0.3616D-16	0.6377D-16	0.6799D-15	-0.2379D+01	-0.7323D+01	0.4971D-08	0.9849D-11	0.3324D-15	0.3528D-15
24	-0.1195D-16	-0.1107D-17	0.1756D-17	0.2118D-16	-0.3496D+01	-0.6861D+01	0.4614D-09	0.9105D-12	0.3086D-16	0.3274D-16
25	0.2707D-16	-0.2299D-17	-0.3977D-17	0.4391D-16	-0.4526D+01	-0.6229D+01	0.1066D-07	0.2112D-10	0.7131D-15	0.7568D-15
26	C.9288D-15	-0.7771D-16	-0.1370D-15	0.1460D-14	-0.5445D+01	-0.5445D+01	0.3127D-06	0.6223D-09	0.2091D-13	0.2220D-13
27	0.2738D-13	-0.2314D-14	-0.4C54D-14	0.4263D-13	-0.6229D+01	-0.4526D+01	0.7924D-05	0.1586D-07	0.5298D-12	0.5626D-12
28	0.6976D-12	-0.5967D-13	-0.1039D-12	0.1074D-11	-0.6861D+01	-0.3496D+01	0.1722D-03	0.3468D-06	0.1151D-10	0.1223D-10
29	0.1526D-10	-0.1325D-11	-0.2287D-11	0.2318D-10	-0.7323D+01	-0.2379D+01	0.3179D-02	0.6459D-05	0.2125D-09	0.2258D-09
30	0.2842D-09	-0.2511D-10	-0.4293D-10	0.4246D-09	-0.7605D+01	-0.1205D+01	0.4938D-01	0.1014D-03	0.3299D-08	0.3509D-08
31	0.4462D-08	-0.4030D-09	-0.6807D-09	0.6527D-08	-0.7700D+01	0.4462D-08	0.6365D+00	0.1325D-02	0.4250D-07	0.4524D-07
32	G.5833D-07	-0.5417D-08	-C.9012D-08	0.8303D-07	-0.7605D+01	0.1205D+01	0.6697D+01	0.1419D-01	0.4470D-06	0.4763D-06
33	0.6253D-06	-0.6020D-07	-0.9824D-07	0.8587D-06	-0.7323D+01	0.2379D+01	0.5631D+02	0.1223D+00	0.3755D-05	0.4008D-05
34	0.5395D-05	-0.5446D-06	-0.8669D-06	0.7054D-05	-0.6861D+01	0.3496D+01	0.3678D+03	0.8271D+00	0.2450D-04	0.2621D-04
35	0.3659D-04	-0.3940D-05	-0.6065D-05	0.4462D-04	-0.6229D+01	0.4526D+01	0.1797D+04	0.4260D+01	0.1195D-03	0.1283D-03
36	C.1893D-03	-0.2231D-04	-0.3283D-04	0.2078D-03	-0.5445D+01	0.5445D+01	0.6218D+04	0.1603D+02	0.4121D-03	0.4452D-03
37	G.7198D-03	-0.9670D-04	-0.1335D-03	0.6654D-03	-0.4525D+01	0.6230D+01	0.1404D+05	0.4202D+02	0.9244D-03	0.1011D-02
38	0.1928D-02	-0.3143D-03	-0.3973D-03	0.1303D-02	-0.3494D+01	0.6861D+01	0.1836D+05	0.7151D+02	0.1192D-02	0.1340D-02
39	0.3538D-02	-0.7625D-03	-0.8446D-03	0.1224D-02	-0.2376D+01	0.7324D+01	0.1333D+05	0.6153D+02	0.8554D-03	0.9827D-03
40	0.4760D-02	-0.1345D-02	-0.1223D-02	0.3610D-03	-0.1200D+01	0.7605D+01	0.1260D+05	0.3291D+03	0.5283D-03	0.1209D-02

FRAG NO.=	FCGU =	FCGW =	ALFA =	FRUV =	FRWV =	FRAV =
1	0.219355D+01	0.360662D+01	-0.724500D+00	0.600435D+04	-0.632312D+03	-0.210000D+04

CURRENT TIME CYCLE	FRAGMENT	KINETIC ENERGY
325	1	0.905814D+05

```
WORK INPUT INTO RING TO TIME STEP      325 =   0.611771D+05
RING KINETIC ENERGY AT TIME STEP       325 =   0.343892D+05
RING ELASTIC ENERGY TO TIME STEP       325 =   0.154364D+04
RING PLASTIC WORK TO TIME STEP         325 =   0.252443D+05
ENERGY STORED IN ELASTIC RESTRAINTS        =    0.0
```

J= 325 TIME= 0.32500D-03

I	V	W	PSI	CHI	COPY	COPZ	L	M	STRAIN(IN)	STRAIN(OUT)
1	0.3391D+00	-0.2732D+00	0.2022D-01	0.3488D-02	0.3391D+00	0.7427D+01	0.7429D+04	-0.3657D+04	0.2213D-01	-0.1161D-01
2	0.3754D+00	-0.1324D+00	0.1224D+00	-0.1254D-02	0.1555D+01	0.7416D+01	0.3733D+04	-0.2787D+04	0.2762D-01	-0.1040D-01
3	0.3682D+00	0.1406D+00	0.2375D+00	-0.1347D-01	0.2773D+01	0.7343D+01	0.1063D+05	-0.3560D+04	0.2112D-01	0.9609D-03
4	0.2729D+00	0.5657D+00	0.2970D+00	-0.1409D-01	0.3996D+01	0.7241D+01	0.9618D+04	-0.4249D+04	0.1686D-01	0.5463D-01
5	0.1572D+00	0.9121D+00	0.1823D+00	0.2685D-01	0.5189D+01	0.6875D+01	0.1482D+05	-0.3278D+04	0.9252D-02	0.7379D-01
6	0.3847D-01	0.1086D+01	-0.1379D-01	0.6121D-01	0.6240D+01	0.6186D+01	0.2234D+05	-0.8236D+03	-0.5221D-02	0.8671D-01
7	-0.7970D-01	0.9166D+00	-0.2926D+00	0.2689D-01	0.6924D+01	0.5129D+01	0.2079D+05	0.4162D+04	0.4963D-03	0.7564D-01
8	-0.2356D+00	0.3956D+00	-0.5212D+00	-0.8085D-01	0.7106D+01	0.3885D+01	0.1068D+05	0.2785D+04	0.5925D-01	-0.2504D-01
9	-0.3348D+00	-0.1752D+00	-0.2683D+00	-0.4013D-02	0.7053D+01	0.2644D+01	0.1472D+05	-0.4597D+04	0.7184D-01	-0.3631D-01
10	-0.2781D+00	-0.3330D+00	0.5985D-01	0.3941D-02	0.7233D+01	0.1427D+01	0.4778D+04	-0.3235D+04	0.4141D-02	-0.3153D-02
11	-0.2312D+00	-0.2801D+00	0.8173D-01	-0.2076D-02	0.7420D+01	0.2312D+00	0.4549D+04	0.7605D+03	-0.7186D-03	0.1656D-02
12	-0.1952D+00	-0.2175D+00	0.7450D-01	-0.1684D-02	0.7421D+01	-0.9778D+00	0.1062D+05	0.2772D+04	-0.2572D-02	0.4590D-02
13	-0.1665D+00	-0.1677D+00	0.5281D-01	-0.2500D-03	0.7215D+01	-0.2169D+01	0.8515D+04	0.2739D+04	-0.2415D-02	0.3804D-02
14	-0.1427D+00	-0.1407D+00	0.3399D-01	-0.1169D-03	0.6800D+01	-0.3305D+01	0.7082D+04	0.1600D+04	-0.1166D-02	0.2143D-02
15	-0.1217D+00	-0.1269D+00	0.2397D-01	0.3214D-03	0.6198D+01	-0.4353D+01	0.1036D+05	-0.1411D+03	0.8602D-03	0.5685D-03
16	-0.1021D+00	-0.1157D+00	0.2485D-01	0.5904D-03	0.5435D+01	-0.5291D+01	0.1072D+05	-0.3538D+02	0.7759D-03	0.7027D-03
17	-0.8455D-01	-0.9985D-01	0.2507D-01	0.4197D-03	0.4536D+01	-0.6099D+01	0.1021D+05	0.7991D+03	-0.1228D-03	0.1530D-02
18	-0.6957D-01	-0.8413D-01	0.2006D-01	0.7460D-03	0.3520D+01	-0.6754D+01	0.1186D+05	0.8376D+03	-0.4867D-04	0.1683D-02
19	-0.5645D-01	-0.7304D-01	0.1481D-01	0.7095D-03	0.2411D+01	-0.7236D+01	0.1279D+05	0.8618D+03	-0.9432D-05	0.1773D-02
20	-0.4462D-01	-0.6673D-01	0.9430D-02	0.5782D-03	0.1238D+01	-0.7532D+01	0.1326D+05	-0.1312D+03	0.1050D-02	0.7787D-03
21	-0.3358D-01	-0.6088D-01	0.1026D-01	0.8060D-03	0.3358D-01	-0.7639D+01	0.9289D+04	0.6864D+03	-0.6947D-04	0.1350D-02
22	-0.2374D-01	-0.5523D-01	0.5959D-02	0.5919D-03	-0.1172D+01	-0.7554D+01	0.2283D+04	0.3558D+03	-0.2105D-03	0.5253D-03
23	-0.1503D-01	-0.5272D-01	0.3723D-02	0.2921D-04	-0.2349D+01	-0.7278D+01	0.5756D+03	0.2954D+03	-0.2658D-03	0.3451D-03
24	-0.6879D-02	-0.5086D-01	0.1875D-02	-0.9130D-05	-0.3467D+01	-0.6819D+01	0.2360D+04	0.3746D+03	-0.2246D-03	0.5500D-03
25	0.1198D-02	-0.5040D-01	-0.4628D-03	0.8283D-04	-0.4497D+01	-0.6188D+01	0.1139D+04	0.2776D+03	-0.2085D-03	0.3656D-03
26	0.9290D-02	-0.5131D-01	-0.2203D-02	0.1782D-03	-0.5415D+01	-0.5402D+01	0.1325D+04	0.3379D+03	-0.2581D-03	0.4407D-03
27	0.1766D-01	-0.5302D-01	-0.4330D-02	0.4127D-03	-0.6197D+01	-0.4480D+01	0.5784D+04	0.5953D+03	-0.2168D-03	0.1014D-02
28	0.2674D-01	-0.5732D-01	-0.8056D-02	0.3516D-03	-0.6822D+01	-0.3446D+01	0.8243D+04	0.4564D+02	0.5210D-03	0.6154D-03
29	0.3670D-01	-0.6237D-01	-0.8328D-02	0.2000D-03	-0.7275D+01	-0.2325D+01	0.5679D+04	0.4722D+03	-0.9678D-04	0.8796D-03
30	0.4722D-01	-0.6713D-01	-0.1128D-01	0.2616D-03	-0.7546D+01	-0.1147D+01	0.4955D+04	0.1031D+04	-0.7240D-03	0.1407D-02
31	0.5870D-01	-0.7594D-01	-0.1773D-01	0.3600D-03	-0.7624D+01	0.5870D-01	0.6815D+04	0.7544D+03	-0.3102D-03	0.1250D-02
32	0.7206D-01	-0.9076D-01	-0.2246D-01	0.2137D-03	-0.7504D+01	0.1262D+01	0.7492D+04	-0.4686D+03	0.1001D-02	0.3197D-04
33	0.8783D-01	-0.1045D+00	-0.1953D-01	0.4328D-03	-0.7197D+01	0.2431D+01	0.8009D+04	-0.1257D+03	0.6820D-03	0.4221D-03
34	0.1053D+00	-0.1112D+00	-0.1874D-01	0.5686D-03	-0.6714D+01	0.3539D+01	0.8854D+04	0.1878D+04	-0.1331D-02	0.2552D-02
35	0.1240D+00	-0.1222D+00	-0.3050D-01	0.3418D-03	-0.6058D+01	0.4554D+01	0.1131D+05	0.2693D+04	-0.2225D-02	0.4064D-02
36	0.1451D+00	-0.1484D+00	-0.4953D-01	-0.1098D-03	-0.5237D+01	0.5442D+01	0.8390D+04	0.2408D+04	-0.2047D-02	0.3375D-02
37	0.1706D+00	-0.1940D+00	-0.6596D-01	-0.1627D-02	-0.4274D+01	0.6173D+01	0.4885D+04	0.4572D+03	-0.3132D-03	0.1211D-02
38	0.2030D+00	-0.2485D+00	-0.7057D-01	-0.2070D-02	-0.3202D+01	0.6731D+01	0.5526D+04	-0.1908D+04	0.2346D-02	-0.1574D-02
39	0.2437D+00	-0.2931D+00	-0.5871D-01	-0.1418D-02	-0.2057D+01	0.7120D+01	0.3863D+04	-0.3009D+04	0.4541D-02	-0.3495D-02
40	0.2907D+00	-0.3100D+00	-0.3440D-01	0.3252D-03	-0.8689D+00	0.7345D+01	0.1318D+04	-0.3961D+04	0.1009D-01	-0.7976D-02

FRAG NO.=	FCGU =	FCGW =	ALFA =	FRUV =	FRWV =	FRAV =
1	0.350351D+01	0.320048D+01	-0.131250D+01	0.335680D+04	-0.175873D+04	-0.210000D+04

```
IMPACT IT=  327   ELEMENT NO. =     8   FRAGMENT NO. =    1
LOCATION ON ELEMENT =   0.374743D+00   PENETRATION DIST =   0.136819D-03

IMPACT IT=  331   ELEMENT NO. =     8   FRAGMENT NO. =    1



LOCATION ON ELEMENT =   0.319467D+00   PENETRATION DIST =   0.782766D-04

IMPACT IT=  333   ELEMENT NO. =     8   FRAGMENT NO. =    1
LOCATION ON ELEMENT =   0.293027D+00   PENETRATION DIST =   0.787990D-04

IMPACT IT=  336   ELEMENT NO. =     8   FRAGMENT NO. =    1
LOCATION ON ELEMENT =   0.254672D+00   PENETRATION DIST =   0.113511D-03

IMPACT IT=  340   ELEMENT NO. =     8   FRAGMENT NO. =    1
LOCATION ON ELEMENT =   0.206143D+00   PENETRATION DIST =   0.162760D-05

IMPACT IT=  341   ELEMENT NO. =     8   FRAGMENT NO. =    1
LOCATION ON ELEMENT =   0.193966D+00   PENETRATION DIST =   0.158350D-03

IMPACT IT=  348   ELEMENT NO. =     8   FRAGMENT NO. =    1
LOCATION ON ELEMENT =   0.115253D+00   PENETRATION DIST =   0.800680D-04

IMPACT IT=  350   ELEMENT NO. =     8   FRAGMENT NO. =    1
LOCATION ON ELEMENT =   0.940288D-01   PENETRATION DIST =   0.730994D-04

IMPACT IT=  353   ELEMENT NO. =     8   FRAGMENT NO. =    1
LOCATION ON ELEMENT =   0.634190D-01   PENETRATION DIST =   0.122451D-04

IMPACT IT=  354   ELEMENT NO. =     8   FRAGMENT NO. =    1
LOCATION ON ELEMENT =   0.533236D-01   PENETRATION DIST =   0.666637D-04

IMPACT IT=  358   ELEMENT NO. =     8   FRAGMENT NO. =    1
LOCATION ON ELEMENT =   0.149461D-01   PENETRATION DIST =   0.599060D-04

IMPACT IT =   358  NODE NO. =     9   FRAG NO =     1     PD =   0.286192D-04
```

CURRENT TIME CYCLE   FRAGMENT   KINETIC ENERGY

405   1   0.849322D+05

WORK INPUT INTO RING TO TIME STEP   405 =   0.668263D+05
RING KINETIC ENERGY AT TIME STEP   405 =   0.353492D+05
RING ELASTIC ENERGY TO TIME STEP   405 =   0.181917D+04
RING PLASTIC WORK TO TIME STEP.   405 =   0.296579D+05
ENERGY STORED IN ELASTIC RESTRAINTS   =   0.0

J= 405   TIME= 0.405000D-03

I	V	W	PSI	CHI	COPY	COPZ	L	M	STRAIN(IN)	STRAIN(OUT)
1	0.4884D+00	-0.3624D+00	0.2832D-01	0.3549D-02	0.4884D+00	0.7338D+01	0.6533D+04	-0.3760D+04	0.2218D-01	-0.1178D-01
2	0.5354D+00	-0.1876D+00	0.1312D+00	-0.2401D-02	0.1704D+01	0.7336D+01	0.8508D+04	-0.3685D+04	0.2940D-01	-0.1184D-01
3	0.5310D+00	0.1257D+00	0.2561D+00	-0.1841D-01	0.2923D+01	0.7279D+01	0.6037D+04	-0.3560D+04	0.2402D-01	-0.1542D-02
4	0.4242D+00	0.6065D+00	0.3319D+00	-0.2408D-01	0.4149D+01	0.7209D+01	0.9308D+04	-0.4301D+04	0.1761D-01	0.5364D-01
5	0.2842D+00	0.1021D+01	0.2224D+00	0.1893D-01	0.5356D+01	0.6888D+01	0.1322D+05	-0.4278D+04	0.2011D-01	0.6701D-01
6	0.1340D+00	0.1283D+01	0.7952D-01	0.5910D-01	0.6447D+01	0.6257D+01	0.1348D+05	-0.1869D+03	0.7789D-04	0.8214D-01
7	-0.1448D-01	0.1264D+01	-0.1697D+00	0.5394D-01	0.7244D+01	0.5281D+01	0.1110D+05	0.4236D+04	-0.1422D-01	0.9802D-01
8	-0.1959D+00	0.8585D+00	-0.5094D+00	-0.6823D-01	0.7537D+01	0.4060D+01	0.2176D+05	0.3880D+04	0.3004D-01	0.3750D-01
9	-0.4132D+00	0.1413D+00	-0.5342D+00	-0.1060D+00	0.7330D+01	0.2816D+01	0.7443D+04	0.5012D+03	0.8142D-01	-0.3880D-01
10	-0.4528D+00	-0.3920D+00	-0.1709D+00	0.1365D-01	0.7147D+01	0.1590D+01	0.2089D+05	-0.4149D+04	0.6204D-01	-0.2936D-01
11	-0.3662D+00	-0.4595D+00	0.1064D+00	-0.3320D-02	0.7240D+01	0.3662D+00	0.1504D+05	-0.1130D+04	0.1959D-02	0.4243D-03
12	-0.3059D+00	-0.3784D+00	0.1110D+00	-0.4656D-02	0.7279D+01	-0.8433D+00	0.1381D+05	0.1125D+04	-0.6530D-03	0.3116D-02
13	-0.2586D+00	-0.2926D+00	0.9956D-01	-0.3403D-02	0.7125D+01	-0.2043D+01	0.1305D+05	0.3377D+04	-0.3613D-02	0.6655D-02
14	-0.2206D+00	-0.2288D+00	0.6849D-01	-0.1031D-02	0.6757D+01	-0.3195D+01	0.7826D+04	0.3154D+04	-0.3068D-02	0.4584D-02
15	-0.1887D+00	-0.1930D+00	0.4533D-01	-0.5239D-03	0.6184D+01	-0.4260D+01	0.7648D+04	0.1992D+04	-0.1533D-02	0.2587D-02
16	-0.1602D+00	-0.1741D+00	0.3286D-01	0.2402D-03	0.5435D+01	-0.5208D+01	0.1179D+05	0.5151D+03	0.2802D-03	0.1345D-02
17	-0.1336D+00	-0.1601D+00	0.2964D-01	0.3706D-03	0.4540D+01	-0.6021D+01	0.9041D+04	-0.1151D+02	0.6351D-03	0.6113D-03
18	-0.1095D+00	-0.1428D+00	0.2971D-01	-0.1043D-03	0.3529D+01	-0.6684D+01	0.4105D+04	0.1399D+03	0.1383D-03	0.4277D-03
19	-0.8892D-01	-0.1221D+00	0.2883D-01	-0.2250D-03	0.2426D+01	-0.7180D+01	0.3917D+04	0.1441D+04	-0.1220D-02	0.1760D-02
20	-0.7120D-01	-0.1054D+00	0.1982D-01	0.1092D-03	0.1258D+01	-0.7490D+01	0.4178D+04	0.1184D+04	-0.9358D-03	0.1512D-02
21	-0.5523D-01	-0.9647D-01	0.1241D-01	0.1766D-03	0.5523D-01	-0.7604D+01	-0.5561D+03	0.4382D+03	-0.4914D-03	0.4147D-03
22	-0.4059D-01	-0.9068D-01	0.9657D-02	0.5278D-05	-0.1150D+01	-0.7522D+01	-0.3419D+04	0.4601D+03	-0.7114D-03	0.2400D-03
23	-0.2695D-01	-0.8607D-01	0.6764D-02	-0.4066D-04	-0.2327D+01	-0.7250D+01	0.5950D+02	0.1385D+03	-0.1392D-03	0.1474D-03
24	-0.1394D-01	-0.8067D-01	0.5905D-02	-0.3557D-03	-0.3447D+01	-0.6795D+01	-0.1001D+04	0.1149D+04	-0.1257D-02	0.1119D-02
25	-0.1719D-02	-0.7939D-01	-0.1264D-02	-0.6550D-03	-0.4478D+01	-0.6166D+01	-0.7292D+04	0.2790D+03	-0.7911D-03	-0.2142D-03
26	0.1032D-01	-0.8194D-01	-0.3009D-02	-0.4379D-03	-0.5394D+01	-0.5379D+01	-0.6582D+04	0.3693D+03	-0.8355D-03	-0.7185D-04
27	0.2293D-01	-0.8462D-01	-0.5333D-02	0.5021D-05	-0.6174D+01	-0.4458D+01	0.1820D+04	0.2219D+03	-0.1039D-03	0.3549D-03
28	0.3654D-01	-0.8675D-01	-0.6724D-02	0.2804D-03	-0.6800D+01	-0.3424D+01	0.5561D+04	0.1235D+04	-0.8934D-03	0.1660D-02
29	0.5085D-01	-0.9175D-01	-0.1445D-01	0.2419D-03	-0.7252D+01	-0.2303D+01	0.4320D+04	0.1525D+04	-0.1279D-02	0.1874D-02
30	0.6646D-01	-0.1066D+00	-0.2400D-01	0.1588D-03	-0.7510D+01	-0.1122D+01	0.4745D+04	-0.2732D+03	0.6096D-03	0.4460D-04
31	0.8472D-01	-0.1236D+00	-0.2230D-01	0.2565D-03	-0.7576D+01	0.8472D-01	0.5185D+04	-0.2914D+03	0.6587D-03	0.5608D-04
32	0.1053D+00	-0.1346D+00	-0.2047D-01	0.1251D-03	-0.7456D+01	0.1287D+01	0.5730D+04	0.5456D+03	-0.1691D-03	0.9590D-03
33	0.1272D+00	-0.1422D+00	-0.2389D-01	0.2454D-03	-0.7149D+01	0.2456D+01	0.5540D+04	0.2139D+04	-0.1830D-02	0.2594D-02
34	0.1504D+00	-0.1562D+00	-0.3728D-01	-0.3337D-03	-0.6653D+01	0.3559D+01	0.5248D+04	0.3095D+04	-0.3202D-02	0.4114D-02
35	0.1763D+00	-0.1880D+00	-0.5941D-01	-0.1552D-02	-0.5974D+01	0.4558D+01	0.4135D+04	0.2619D+04	-0.2850D-02	0.3671D-02
36	0.2073D+00	-0.2431D+00	-0.7915D-01	-0.2570D-02	-0.5126D+01	0.5419D+01	0.1337D+04	0.1212D+04	-0.1296D-02	0.1651D-02
37	0.2467D+00	-0.3097D+00	-0.8809D-01	-0.3512D-02	-0.4144D+01	0.6124D+01	0.4247D+04	-0.7539D+03	0.8951D-03	-0.8570D-04
38	0.2964D+00	-0.3731D+00	-0.8513D-01	-0.3042D-02	-0.3062D+01	0.6663D+01	0.7473D+04	-0.2375D+04	0.3051D-02	-0.1961D-02
39	0.3558D+00	-0.4171D+00	-0.6998D-01	-0.1461D-02	-0.1912D+01	0.7036D+01	0.8392D+04	-0.3544D+04	0.6196D-02	-0.4246D-02
40	0.4220D+00	-0.4247D+00	-0.3841D-01	0.1516D-02	-0.7213D+00	0.7252D+01	0.1078D+05	-0.3743D+04	0.1397D-01	-0.8066D-02

FRAG NO.=	FCGU =	FCGW =	ALFA =	FRUV =	FRWV =	FRAV =
1	0.375680D+01	0.306097D+01	-0.148050D+01	0.298958D+04	-0.172264D+04	-0.210000D+04

IMPACT IT= 409   ELEMENT NO. =   9   FRAGMENT NO. =   1
LOCATION ON ELEMENT =   0.890602D+00   PENETRATION DIST =   0.116420D-03

CURRENT TIME CYCLE	FRAGMENT	KINETIC ENERGY
605	1	0.701341D+05

WORK INPUT INTO RING TO TIME STEP 605 = 0.816244D+05
RING KINETIC ENERGY AT TIME STEP 605 = 0.409119D+05
RING ELASTIC ENERGY TO TIME STEP 605 = 0.207633D+04
RING PLASTIC WORK TO TIME STEP 605 = 0.386361D+05
ENERGY STORED IN ELASTIC RESTRAINTS = 0.0

J= 605 TIME= 0.60500D-03

I	V	W	PSI	CHI	COPY	COPZ	L	M	STRAIN(IN)	STRAIN(OUT)
1	0.8978D+00	-0.6013D+00	0.3405D-01	0.3027D-02	0.8978D+00	0.7099D+01	0.5228D+04	-0.4267D+04	0.2416D-01	-0.1398D-01
2	0.9745D+00	-0.3440D+00	0.1496D+00	-0.5000D-02	0.2113D+01	0.7113D+01	0.4651D+04	-0.3752D+04	0.3033D-01	-0.1337D-01
3	0.9811D+00	0.6749D-01	0.2820D+00	-0.2581D-01	0.3333D+01	0.7084D+01	0.5373D+04	-0.3580D+04	0.2551D-01	-0.5632D-02
4	0.8606D+00	0.6552D+00	0.3747D+00	-0.4184D-01	0.4560D+01	0.7054D+01	0.8619D+04	-0.4581D+04	0.2295D-01	0.4524D-01
5	0.6772D+00	0.1209D+01	0.3067D+00	-0.2563D-02	0.5785D+01	0.6810D+01	0.6575D+04	-0.4186D+04	0.2422D-01	0.5859D-01
6	0.4521D+00	0.1651D+01	0.2013D+00	0.3866D-01	0.6932D+01	0.6293D+01	0.6184D+04	-0.1533D+04	0.5952D-02	0.7391D-01
7	0.2198D+00	0.1851D+01	-0.5548D-02	0.6716D-01	0.7856D+01	0.5436D+01	0.6976D+04	0.7838D+03	-0.9921D-02	0.9327D-01
8	-0.2772D-01	0.1692D+01	-0.3181D+00	0.7302D-02	0.8358D+01	0.4284D+01	0.8789D+04	-0.3029D+01	-0.1716D-02	0.8220D-01
9	-0.3087D+00	0.1162D+01	-0.5712D+00	-0.1249D+00	0.8333D+01	0.3032D+01	0.8992D+04	0.4962D+04	0.1781D-01	0.6303D-01
10	-0.6155D+00	0.3414D+00	-0.7066D+00	-0.2206D+00	0.7846D+01	0.1866D+01	0.7369D+04	0.3378D+04	0.6996D-01	-0.2755D-01
11	-0.7828D+00	-0.4753D+00	-0.4120D+00	-0.6692D-01	0.7725D+01	0.7828D+00	0.6266D+04	-0.4346D+04	0.9154D-01	-0.5206D-01
12	-0.6840D+00	-0.8384D+00	0.2384D-01	0.1702D-01	0.6884D+01	-0.3978D+00	0.1322D+04	-0.5105D+04	0.3030D-01	-0.2474D-01
13	-0.5619D+00	-0.7710D+00	0.1900D+00	-0.1796D-01	0.6764D+01	-0.1607D+01	0.3171D+04	-0.1804D+04	0.5591D-03	0.1045D-02
14	-0.4744D+00	-0.6185D+00	0.1885D+00	-0.1736D-01	0.6525D+01	-0.2792D+01	0.4529D+03	0.2221D+04	-0.5045D-02	0.6301D-02
15	-0.4060D+00	-0.4773D+00	0.1541D+00	-0.9663D-02	0.6082D+01	-0.3917D+01	0.2478D+04	0.3047D+04	-0.6387D-02	0.8834D-02
16	-0.3480D+00	-0.3796D+00	0.1080D+00	-0.5230D-02	0.5422D+01	-0.4930D+01	0.9940D+03	0.3861D+04	-0.6042D-02	0.6248D-02
17	-0.2977D+00	-0.3242D+00	0.7085D-01	-0.2326D-02	0.4576D+01	-0.5792D+01	0.1312D+04	0.2742D+04	-0.2745D-02	0.2926D-02
18	-0.2515D+00	-0.2935D+00	0.5368D-01	-0.1131D-02	0.3587D+01	-0.6485D+01	0.2300D+04	0.1075D+04	-0.9526D-03	0.1270D-02
19	-0.2085D+00	-0.2697D+00	0.4695D-01	-0.8680D-03	0.2494D+01	-0.7002D+01	0.2229D+04	0.7507D+03	-0.6226D-03	0.9299D-03
20	-0.1691D+00	-0.2453D+00	0.4226D-01	-0.9873D-03	0.1333D+01	-0.7336D+01	0.2506D+04	0.1291D+04	-0.1162D-02	0.1507D-02
21	-0.1331D+00	-0.2228D+00	0.3419D-01	-0.3785D-03	0.1331D+00	-0.7477D+01	0.4399D+04	0.4563D+03	-0.1686D-03	0.7751D-03
22	-0.1001D+00	-0.2013D+00	0.3133D-01	-0.1411D-03	-0.1074D+01	-0.7422D+01	0.4750D+04	0.9114D+03	-0.6150D-03	0.1270D-02
23	-0.7029D-01	-0.1799D+00	0.2563D-01	-0.5190D-04	-0.2257D+01	-0.7174D+01	0.5704D+04	0.1621D+04	-0.1283D-02	0.2069D-02
24	-0.4324D-01	-0.1634D+00	0.1548D-01	0.2941D-03	-0.3383D+01	-0.6735D+01	0.5565D+04	0.2327D+04	-0.2022D-02	0.2789D-02
25	-0.1769D-01	-0.1584D+00	0.9167D-03	0.5374D-03	-0.4419D+01	-0.6112D+01	0.4269D+04	0.1660D+04	-0.1422D-02	0.2010D-02
26	0.8032D-02	-0.1652D+00	-0.9483D-02	0.4602D-03	-0.5334D+01	-0.5322D+01	0.4931D+04	0.9151D+03	-0.6062D-03	0.1286D-02
27	0.3525D-01	-0.1773D+00	-0.1522D-01	0.2889D-03	-0.6107D+01	-0.4393D+01	0.7385D+04	0.9620D+02	0.4096D-03	0.6085D-03
28	0.6444D-01	-0.1876D+00	-0.1582D-01	0.5056D-03	-0.6723D+01	-0.3353D+01	0.8094D+04	0.5651D+03	-0.2631D-04	0.1142D-02
29	0.9510D-01	-0.1967D+00	-0.1935D-01	0.2492D-03	-0.7165D+01	-0.2228D+01	0.6777D+04	0.4740D+03	-0.2294D-04	0.9572D-03
30	0.1269D+00	-0.2042D+00	-0.2231D-01	-0.5208D-04	-0.7423D+01	-0.1047D+01	0.5237D+04	0.1280D+04	-0.9625D-03	0.1685D-02
31	0.1595D+00	-0.2128D+00	-0.3032D-01	-0.2639D-03	-0.7487D+01	0.1595D+00	0.4488D+04	0.2628D+04	-0.2407D-02	0.3026D-02
32	0.1936D+00	-0.2311D+00	-0.4675D-01	-0.9012D-03	-0.7347D+01	0.1360D+01	0.4432D+04	0.3442D+04	-0.4501D-02	0.5290D-02
33	0.2309D+00	-0.2707D+00	-0.7638D-01	-0.2403D-02	-0.6994D+01	0.2515D+01	0.3247D+04	0.3084D+04	-0.4358D-02	0.4777D-02
34	0.2739D+00	-0.3410D+00	-0.1040D+00	-0.5171D-02	-0.6433D+01	0.3585D+01	0.2562D+04	0.2127D+04	-0.3236D-02	0.3685D-02
35	0.3267D+00	-0.4327D+00	-0.1250D+00	-0.7606D-02	-0.5687D+01	0.4536D+01	0.1617D+04	0.1302D+04	-0.1661D-02	0.2136D-02
36	0.3924D+00	-0.5355D+00	-0.1365D+00	-0.9340D-02	-0.4789D+01	0.5344D+01	0.7912D+03	-0.6626D+03	0.6043D-03	-0.3241D-03
37	0.4733D+00	-0.6324D+00	-0.1337D+00	-0.8897D-02	-0.3771D+01	0.5996D+01	0.1470D+04	-0.2072D+04	0.2067D-02	-0.1640D-02
38	0.5690D+00	-0.7064D+00	-0.1225D+00	-0.7227D-02	-0.2668D+01	0.6490D+01	0.3534D+04	-0.3284D+04	0.4445D-02	-0.3800D-02
39	0.6763D+00	-0.7438D+00	-0.9751D-01	-0.4501D-02	-0.1506D+01	0.6825D+01	0.2302D+04	-0.3888D+04	0.8551D-02	-0.7134D-02
40	0.7897D+00	-0.7212D+00	-0.5005D-01	0.6150D-03	-0.3117D+00	0.7016D+01	0.2800D+04	-0.4373D+04	0.1635D-01	-0.1142D-01

FRAG NO.=	FCGU =	FCGW =	ALFA =	FRUV =	FRWV =	FRAV =
1	0.423686D+01	0.274900D+01	-0.190050D+01	0.190929D+04	-0.135121D+04	-0.210000D+04

645 1 0.692067D+05

WORK INPUT INTO RING TO TIME STEP 645 = 0.825518D+05
RING KINETIC ENERGY AT TIME STEP 645 = 0.402544D+05
RING ELASTIC ENERGY TO TIME STEP 645 = 0.213615D+04
RING PLASTIC WORK TO TIME STEP 645 = 0.401613D+05
ENERGY STORED IN ELASTIC RESTRAINTS = 0.0

J= 645 TIME= 0.64500D-03

I	V	W	PSI	CHI	COPY	COPZ	L	M	STRAIN(IN)	STRAIN(OUT)
1	0.9851D+00	-0.6477D+00	0.3594D-01	0.2648D-02	0.9851D+00	0.7052D+01	0.1038D+04	-0.3846D+04	0.2344D-01	-0.1384D-01
2	0.1067D+01	-0.3748D+00	0.1489D+00	-0.5384D-02	0.2200D+01	0.7068D+01	-0.1240D+04	-0.3740D+04	0.2999D-01	-0.1394D-01
3	0.1077D+01	0.5057D-01	0.2819D+00	-0.2588D-01	0.3420D+01	0.7038D+01	0.9810D+02	-0.4219D+04	0.2587D-01	-0.6712D-02
4	0.9564D+00	0.6569D+00	0.3790D+00	-0.4401D-01	0.4646D+01	0.7012D+01	0.1156D+04	-0.4219D+04	0.2332D-01	0.4017D-01
5	0.7628D+00	0.1241D+01	0.3273D+00	-0.1074D-01	0.5872D+01	0.6785D+01	-0.9015D+03	-0.2567D+04	0.2216D-01	0.5901D-01
6	0.5218D+00	0.1718D+01	0.2144D+00	0.3563D-01	0.7028D+01	0.6290D+01	0.1144D+04	-0.1547D+04	0.5620D-02	0.7355D-01
7	0.2755D+00	0.1938D+01	0.7633D-02	0.6668D-01	0.7960D+01	0.5442D+01	0.5111D+04	-0.2024D+04	-0.6298D-02	0.8910D-01
8	0.2098D-01	0.1818D+01	-0.2815D+00	0.1834D-01	0.8490D+01	0.4302D+01	0.2207D+04	0.8076D+03	-0.3007D-02	0.8258D-01
9	-0.2714D+00	0.1338D+01	-0.5397D+00	-0.1062D+00	0.8512D+01	0.3051D+01	0.2913D+04	0.4856D+04	0.7170D-02	0.6753D-01
10	-0.6023D+00	0.5371D+00	-0.7208D+00	-0.2329D+00	0.8042D+01	0.1883D+01	0.7278D+04	0.4127D+04	0.5827D-01	-0.9575D-02
11	-0.8302D+00	-0.3454D+00	-0.5159D+00	-0.1117D+00	0.7355D+01	0.8302D+00	0.5328D+04	-0.1562D+03	0.8715D-01	-0.4779D-01
12	-0.7764D+00	-0.8670D+00	-0.1068D+00	0.1378D-01	0.6870D+01	-0.3021D+00	0.8075D+04	-0.5018D+04	0.6138D-01	-0.3937D-01
13	-0.6306D+00	-0.6770D+00	0.1986D+00	-0.1908D-01	0.6684D+01	-0.1509D+01	0.7410D+04	-0.2799D+04	0.2270D-02	-0.1701D-03
14	-0.5296D+00	-0.7182D+00	0.2060D+00	-0.2055D-01	0.6461D+01	-0.2698D+01	0.3649D+03	0.9194D+03	-0.3706D-02	0.4949D-02
15	-0.4521D+00	-0.5573D+00	0.1797D+00	-0.1416D-01	0.6044D+01	-0.3833D+01	-0.5100D+03	0.3724D+04	-0.7757D-02	0.9533D-02
16	-0.3878D+00	-0.4380D+00	0.1274D+00	-0.8227D-02	0.5409D+01	-0.4861D+01	-0.5313D+03	0.4079D+04	-0.7124D-02	0.7000D-02
17	-0.3320D+00	-0.3675D+00	0.8463D-01	-0.3750D-02	0.4579D+01	-0.5737D+01	-0.1831D+04	0.3103D+04	-0.3462D-02	0.3138D-02
18	-0.2810D+00	-0.3273D+00	0.6466D-01	-0.2150D-02	0.3598D+01	-0.6441D+01	-0.1701D+04	0.1905D+04	-0.2087D-02	0.1853D-02
19	-0.2344D+00	-0.2967D+00	0.5273D-01	-0.1636D-02	0.2511D+01	-0.6969D+01	-0.2130D+04	0.1983D+04	-0.2198D-02	0.1904D-02
20	-0.1911D+00	-0.2747D+00	0.4033D-01	-0.1216D-02	0.1350D+01	-0.7304D+01	-0.2903D+04	0.7495D+03	-0.9751D-03	0.5748D-03
21	-0.1506D+00	-0.2562D+00	0.3565D-01	-0.8897D-03	0.1506D+00	-0.7444D+01	-0.3143D+04	-0.1700D+03	-0.4089D-04	-0.3924D-03
22	-0.1131D+00	-0.2333D+00	0.3671D-01	-0.6277D-03	-0.1056D+01	-0.7393D+01	-0.2235D+04	0.4629D+03	-0.6327D-03	0.3246D-03
23	-0.7967D-01	-0.2044D+00	0.3381D-01	-0.8355D-03	-0.2240D+01	-0.7153D+01	-0.1583D+04	0.2376D+04	-0.2566D-02	0.2348D-02
24	-0.5020D-01	-0.1817D+00	0.1895D-01	-0.5473D-03	-0.3369D+01	-0.6722D+01	-0.4218D+04	0.3050D+04	-0.3724D-02	0.2987D-02
25	-0.2279D-01	-0.1770D+00	-0.1363D-02	-0.2891D-03	-0.4403D+01	-0.6100D+01	-0.4248D+04	0.1952D+04	-0.2311D-02	0.1725D-02
26	0.5460D-02	-0.1890D+00	-0.1359D-01	-0.1771D-03	-0.5315D+01	-0.5307D+01	-0.1458D+04	0.2786D+03	-0.3885D-03	0.1876D-03
27	0.3616D-01	-0.2043D+00	-0.1534D-01	-0.5867D-04	-0.6085D+01	-0.4377D+01	0.2948D+03	-0.4352D+03	0.4703D-03	-0.4297D-03
28	0.6895D-01	-0.2123D+00	-0.1262D-01	0.1386D-03	-0.6703D+01	-0.3338D+01	0.1819D+04	0.2960D+03	-0.1807D-03	0.4315D-03
29	0.1026D+00	-0.2145D+00	-0.1447D-01	0.2378D-05	-0.7151D+01	-0.2216D+01	0.3699D+04	0.1713D+04	-0.1516D-02	0.2026D-02
30	0.1366D+00	-0.2191D+00	-0.2518D-01	-0.1483D-03	-0.7410D+01	-0.1035D+01	0.4106D+04	0.1806D+04	-0.1584D-02	0.2150D-02
31	0.1716D+00	-0.2322D+00	-0.3648D-01	-0.3963D-03	-0.7468D+01	0.1716D+00	0.2523D+04	0.2902D+04	-0.2925D-02	0.3397D-02
32	0.2089D+00	-0.2568D+00	-0.5562D-01	-0.1193D-02	-0.7319D+01	0.1371D+01	0.4177D+04	0.3566D+04	-0.4759D-02	0.5653D-02
33	0.2502D+00	-0.3066D+00	-0.8712D-01	-0.3208D-02	-0.6954D+01	0.2523D+01	0.6279D+04	0.3069D+04	-0.4232D-02	0.5195D-02
34	0.2986D+00	-0.3865D+00	-0.1157D+00	-0.6198D-02	-0.6381D+01	0.3586D+01	0.9183D+04	0.2189D+04	-0.2843D-02	0.4205D-02
35	0.3581D+00	-0.4891D+00	-0.1370D+00	-0.8786D-02	-0.5623D+01	0.4528D+01	0.7620D+04	0.6635D+03	-0.5877D-03	0.1890D-02
36	0.4322D+00	-0.5983D+00	-0.1445D+00	-0.9850D-02	-0.4716D+01	0.5327D+01	0.5938D+04	-0.4820D+03	0.7723D-03	0.2174D-03
37	0.5222D+00	-0.6987D+00	-0.1428D+00	-0.9608D-02	-0.3693D+01	0.5971D+01	0.5823D+04	-0.2324D+04	0.2628D-02	-0.1601D-02
38	0.6276D+00	-0.7746D+00	-0.1301D+00	-0.7735D-02	-0.2585D+01	0.6455D+01	0.5867D+04	-0.3282D+04	0.4910D-02	-0.3773D-02
39	0.7449D+00	-0.8100D+00	-0.1038D+00	-0.4961D-02	-0.1421D+01	0.6783D+01	0.6047D+04	-0.3977D+04	0.9704D-02	-0.7356D-02
40	0.8684D+00	-0.7817D+00	-0.5216D-01	0.9698D-03	-0.2246D+00	0.6969D+01	0.4002D+04	-0.4440D+04	0.1716D-01	-0.1194D-01

FRAG NO.=	FCGU =	FCGW =	ALFA =	FRUV =	FRWV =	FRAV =
1	0.431114D+01	0.269620D+01	-0.198450D+01	0.183377D+04	-0.130583D+04	-0.210000D+04

IMPACT IT = 646 NODE NO. = 11 FRAG NO = 1 PD = 0.212552D-04

LARGEST COMPUTED STRAIN = 0.984228D-01 OCCURS AT THE OUTER SURFACE MIDSPAN OF ELEMENT = 7 AT TIME (SEC.) = 0.382000D-03

NO CARDS PUNCHED DURING THIS RUN FOR CONTINUATION.

A.6.2 Elastic Foundation-Supported Variable-Thickness Partial Ring (Deflector) Subjected to Single-Fragment Attack

The geometry of the structure, as shown in Fig. A.6, is a 90-deg partial ring of constant midsurface radius 8.733 in. and width 1.5 in. The thickness of the ring varies linearly from 0.3 in. at the ideally hinged-fixed end to 0.1 in. at the free end. A portion of the ring consisting of a sector of 27 degrees from the free end is supported by a uniform elastic foundation. This foundation consists of arbitrarily chosen normal k_N and tangential k_T stiffnesses equal to 1500 psi and 3000 psi, respectively.

The ring material is considered to be elastic, perfectly-plastic (EL-PP) with an elastic modulus of 29×10^6 psi and a yield stress of 80,950 psi. For purposes of illustration, the strain-rate constants of the ring material are chosen to be those of mild steel: D = 40.4 and P = 5. The mass density of the material is 0.732×10^{-3} $(\text{lb-sec}^2)/\text{in}^4$. The "critical strain" is assumed to be 20 per cent.

Ten equal-length finite elements are to be used to model the partial ring.

The attacking fragment is identical to that considered in Subsection A.6.1. The presence of fragment-ring surface friction is considered by the use of a value of 0.5 (arbitrarily) for the coefficient of friction $\tilde{\mu}$.

The CIVM-JET-4A program will be used to calculate the structural response of the ring and the motion of the fragment, using a time step of 1 microsecond. It has been calculated from the geometry of the ring structure and the fragment geometric and initial velocity properties that no impact will occur before 593 μsec after fragment release (which is assumed to occur at the condition (instant) shown in Fig. A.6). To expedite the calculation, the fragment is advanced to its position at 575 μsec after release by the use of the appropriate input value for TPRIM. Printout of structural response and fragment position data is desired starting at 5 cycles after TPRIM at intervals of 40 cycles thereafter until 600 computational cycles have been completed.

The energy accounting option will not be used for this example.

A.6.2.1 Input Data

The values to be punched on the data cards are as follows:

			Format
Card 1			3D15.6
	B	= 0.150000 D+01	
	DENS	= 0.732000 D-03	
	EXANG	= 0.900000 D+02	
Card 2			8I5
	IK	= 10	
	NOGA	= 3	
	NFL	= 4	
	NSFL	= 1	
	MM	= 600	
	M1	= 5	
	M2	= 40	
	NF	= 1	
Card 2a			4D15.6
	Y(1)	= 0.000000 D+00	
	Z(1)	= 0.873300 D+01	
	ANG(1)	= 0.000000 D+00	
	H(1)	= 0.300000 D+00	

.
.
.

Additional cards in same format until all 11 nodal points are described.

.
.
.

Y(11)	= 0.873300 D+01
Z(11)	= 0.000000 D+00
ANG(11)	= 0.900000 D+02
H(11)	= 0.100000 D+00

		Format
Card 3		4D15.6
DELTAT	= 0.100000 D-05	
CRITS	= 0.200000 D+00	
DS	= 0.404000 D+02	
P	= 0.500000 D+01	
Card 4		4D15.6
EPS(1)	= 0.279138 D-02	
SIG(1)	= 0.809500 D+05	
Card 5		5D15.6
FH(I)	= 0.674000 D+01	
FCG(I)	= 0.363000 D+01	
FCGX(I)	= 0.000000 D+00	
FMASS(I)	= 0.460000 D-02	
FMOI(I)	= 0.261000 D-01	
Card 6		D15.6
UNK(I)	= 0.500000 D+00	
Card 7		5D15.6
UDOT(I)	= 0.640000 D+04	
WDOT(I)	= 0.000000 D+00	
ADOT(I)	= - 0.210000 D+04	
TPRIM(I)	= 0.575000 D-03	
CR(I)	= 0.100000 D+01	
Card 8		3F15.10
AXG(1)	= 0.1127016654	
AXG(2)	= 0.5	
AXG(3)	= 0.8872983346	
Card 9		3F15.10
AWG(1)	= 0.2777777778	
AWG(2)	= 0.4444444444	
AWG(3)	= 0.2777777778	

Format

4F15.10

= -0.8611363115

= -0.3399810435

= 0.3399810435

= 0.8611363115

4F15.10

= 0.3478548451

= 0.6521451548

= 0.6521451548

= 0.3478548451

I5

= 1 (one prescribed displacement condition)

2I5

(Hinged-fixed support located at node 1)

1

3I5

= 1 (one elastic restraint)

= 0 (no point elastic springs)

= 1 (one uniform elastic foundation)

2D15.6,8I5

= 0.300000 D+04 (tangential stiffness)

= 0.000000 D+00

= 8 (Uniform elastic foundation over

= 3 elements 8, 9, 10)

D15.6,8I5

= 0.150000 D+04 (radial stiffness)

= 8

= 3

I5

= 0

1 input deck for this example should appear as follows:

```
00.150000D001  00.732000D-03  00.900000D 02
 10    3    4     1  600     5    40     1
00.000000D 00  00.873300D 01  00.000000D 00  00.300000D 00
00.136614D 01  00.862548D 01  -0.900000D 01  00.280000D 00
00.269864D 01  00.830558D 01  -0.180000D 02  00.260000D 00
00.396470D 01  00.778116D 01  -0.270000D 02  00.240000D 00
00.513313D 01  00.706514D 01  -0.360000D 02  00.220000D 00
00.617516D 01  00.617516D 01  -0.450000D 02  00.200000D 00
00.706514D 01  00.513313D 01  -0.540000D 02  00.180000D 00
00.778116D 01  00.396470D 01  -0.630000D 02  00.160000D 00
00.830558D 01  00.269864D 01  -0.720000D 02  00.140000D 00
00.862548D 01  00.136614D 01  -0.810000D 02  00.120000D 00
00.873300D 01  00.000000D 00  -0.900000D 02  00.100000D 00
00.100000D-05  00.200000D 00  00.404000D 02  00.500000D 01
00.279138D-02  00.809500D 05
00.674000D 01  00.363000D 01  00.000000D 00  00.460000D-02  00.261000D-01
00.500000D 00
00.640000D 04  00.000000D 00  -0.210000D 04  00.575000D-03  00.100000D 01
 0.1127016654   0.5            0.8872983346
 0.2777777778   0.4444444444   0.2777777778
-0.8611363115  -0.3399810435   0.3399810435   0.8611363115
 0.3478548451   0.6521451548   0.6521451548   0.3478548451
  1
  3    1
  1    0    1
00.300000D 04  00.000000D 00     8    3
00.150000D 04     8    3
  0
```

A.6.2.2 Solution Output Data

The following is the output obtained as a result of the CIVM-JET-4A analysis of this partial ring example.

The ring geometric and material properties, prescribed displacement conditions, and applied elastic restraint constants are output as well as the fragment geometric, initial velocity, and energy parameters, in order to provide a means of conducting an input-data check.

The initial impact is observed to have occurred at 18 μsec after TPRIM along the length of element 6, approximately 55 degrees from the support ($\theta_I \doteq 55$ deg).

The strain exceeds the specified "critical" strain magnitude for the first time at cycle 245 in the location denoted by the asterisk (*).

The maximum strain of 8.44 percent occurs on the inner surface at the midspan of Element 5 at 600 μsec after TPRIM. In this example, the strain responses were computed only at the midspan station of each finite element.

PARTIAL RING **JET** DEFLECTION ANALYSIS

RING PROPERTIES

SUBTENDED ANGLE OF RING	=	0.900000D+02
WIDTH OF RING(IN)	=	0.150000D+01
DENSITY OF RING	=	0.732000D-03
NUMBER OF ELEMENTS	=	10
NUMBER OF SPANWISE GAUSSIAN PTS.	=	3
NUMBER OF DEPTHWISE GAUSSIAN PTS.	=	4
NUMBER OF MECHANICAL SUBLAYERS	=	1

STRAIN (1) = 0.279138D-02STRESS (1) = 0.809500D+05

NODE NO.	Y COORD	Z COORD	SLOPE	RING THICKNESS AT NODE I
1	0.0	0.873300D+01	0.0	0.300000D+00
2	0.136614D+01	0.862548D+01	-0.157080D+00	0.280000D+00
3	0.269864D+01	0.830558D+01	-0.314159D+00	0.260000D+00
4	0.396470D+01	0.778116D+01	-0.471239D+00	0.240000D+00
5	0.513313D+01	0.706514D+01	-0.628319D+00	0.220000D+00
6	0.617516D+01	0.617516D+01	-0.785398D+00	0.200000D+00
7	0.706514D+01	0.513313D+01	-0.942478D+00	0.180000D+00
8	0.778116D+01	0.396470D+01	-0.109956D+01	0.160000D+00
9	0.830558D+01	0.269864D+01	-0.125664D+01	0.140000D+00
10	0.862548D+01	0.136614D+01	-0.141372D+01	0.120000D+00
11	0.873300D+01	0.0	-0.157080D+01	0.100000D+00

FRAGMENT PROPERTIES

FRAG.NO.	WIDTH OF FRAG.	MASS OF FRAG.	MOMENT OF INERTIA OF FRAG.	FCGY	FCGZ
1	0.674000D+01	0.460000D-02	0.261000D-01	0.0	0.363000D+01

COLLISION PARAMETERS

FRAG.NO.	VEL IN Y DIR.	VEL IN Z DIR.	ANG. VEL.	COEFF.OF RESTIT.	INITIAL KINETIC ENERGY	COEFF. OF FRICT
1	0.640000D+04	0.0	-0.210000D+04	0.100000D+01	0.151758D+06	0.500000D+00

HINCED DISPLACEMFNT CONDITION AT NODE = 1

CONSTRAINTS (ELASTIC FOUNDATION/SPRING) AS DESCRIBED BELOW

SIZE CF ASSEMBLED MASS OR STIFFNESS MATRIX = 270

THE VALUF OF THE TANGENTIAL SPRING CCNSTANT IS = 0.300000D+04
THE VALUF OF THE RADIAL SPRING CONSTANT IS = 0.150000D+04
THE VALUE OF THE TORSIONAL SPRING CCNSTANT IS = 0.0

CURRENT TIMF CYCLE	FRAGMENT	KINETIC ENERGY
5	1	0.151758D+06

WORK INPUT INTO RING TO TIME STEP 5 = 0.291038D-10
RING KINETIC ENERGY AT TIME STEP 5 = 0.0
RING ELASTIC ENERGY TO TIME STEP 5 = 0.7C9540D-06
RING PLASTIC WORK TO TIME STEP 5 = -0.709510D-06
ENERGY STORED IN ELASTIC RESTRAINTS = 0.0

J= 5 TIMF= 0.50000D-C5

I	V	W	PSI	CHI	COPY	COPZ	L	M	STRAIN(IN)	STRAIN(OUT)
1	0.C	0.C	C.0	0.C	0.0	0.8733D+01	0.0	0.0	0.0	0.0
2	C.C	0.0	0.0	0.0	0.1366D+01	0.8625D+01	0.0	0.0	0.0	0.0
3	C.C	0.C	0.0	0.C	0.2699D+01	0.8306D+01	0.0	0.0	0.0	0.0
4	C.C	0.0	0.0	0.C	0.3965D+01	0.7781D+01	0.0	0.0	0.0	0.0
5	C.C	0.0	0.0	0.C	0.5133D+01	0.7065D+01	0.0	0.0	0.0	0.0
6	C.0	0.0	C.0	0.C	0.6175D+01	0.6175D+01	0.0	0.0	0.0	0.0
7	0.0	0.0	0.0	0.C	0.7065D+01	0.5133D+01	0.0	0.0	0.0	0.0
8	C.C	0.0	C.0	0.0	0.7781D+01	0.3965D+01	0.0	0.0	0.0	0.0
9	0.0	0.0	C.0	0.C	0.8306D+01	0.2699D+01	0.0	0.0	0.0	0.0
1C	0.C	0.0	0.0	0.0	0.8625D+01	0.1366D+01	0.0	0.0	0.0	0.0
11	C.C	0.C	C.0	0.0	0.8733D+01	0.0				

FRAG NO.=	FCGU =	FCGW =	ALFA =	FRUV =	FRWV =	FRAV =
1	C.371200D+01	0.363000D+01	-0.121800D+01	0.640000D+04	0.0	-0.210000D+04

IMPACT IT= 18 ELEMENT NO. = 6 FRAGMENT NO. = 1
LOCATION ON ELEMENT = C.980672D+00 PENETRATION DIST = 0.158228D-03

IMPACT IT= 19 ELEMENT NO. = 6 FRAGMENT NO. = 1
LOCATION ON ELEMENT = 0.975897D+0C PENETRATION DIST = 0.442547D-02

IMPACT IT= 19 ELEMENT NO. = 5 FRAGMENT NO. = 1
LOCATION ON ELEMENT = 0.153914D+00 PENETRATION DIST = 0.142683D-02

CURRENT TIME CYCLE	FRAGMENT	KINETIC ENERGY
45	1	0.112231D+06

WORK INPUT INTO RING TO TIME STEP 45 = 0.395280D+05
RING KINETIC ENERGY AT TIME STEP 45 = 0.199736D+05
RING ELASTIC ENERGY TO TIME STEP 45 = 0.125094D+04

RING PLASTIC WORK TO TIME STEP 45 = 0.183031D+05
ENERGY STORED IN ELASTIC RESTRAINTS = 0.334094D+00

J= 45 TIME= 0.450000D-04

I	V	W	PSI	CHI	COPY	COPZ	L	M	STRAIN(IN)	STRAIN(OUT)
1	0.0	0.0	-0.1563D-03	0.1161D-02	0.0	0.8733D+01	0.2671D+05	0.1320D+02	0.2096D-02	0.2139D-02
2	0.2896D-02	-0.3396D-03	-0.3568D-03	0.2910D-02	0.1369D+01	0.8625D+01	0.5616D+05	0.4965D+02	0.4688D-02	0.4875D-02
3	0.5572D-02	-0.1424D-02	-0.1310D-02	0.6580D-02	0.2707D+01	0.8301D+01	0.5248D+05	-0.2248D+03	0.6368D-02	0.6084D-02
4	0.1926D-01	-0.3169D-02	0.1664D-03	0.9127D-02	0.3980D+01	0.7770D+01	0.6011D+05	-0.5657D+03	0.1162D-01	0.7292D-02
5	0.3555D-01	0.1533D-01	0.2556D-01	0.2651D-01	0.5171D+01	0.7057D+01	0.7162D+05	0.3367D+02	0.6186D-01	0.6375D-01
6	0.4217D-01	0.2986D+00	0.1273D-01	0.3172D-01	0.6416D+01	0.6356D+01	0.4774D+05	0.5281D+03	0.6892D-02	0.1349D-01
7	0.1435D-01	0.1447D+00	-0.3644D-01	0.1810D-01	0.7191D+01	0.5207D+01	0.2899D+05	-0.2093D+03	0.5091D-02	0.2497D-02
8	0.3463D-02	0.6438D-02	-0.1649D-01	0.8409D-02	0.7788D+01	0.3965D+01	0.2926D+05	-0.1393D+03	0.5338D-02	0.3630D-02
9	0.9034D-02	0.1836D-02	-0.8249D-03	-0.4111D-03	0.8310D+01	0.2691D+01	-0.3956D+04	-0.9338D-01	-0.6988D-03	-0.7003D-03
10	0.7091D-02	0.8310D-03	-0.7209D-03	-0.4355D-02	0.8627D+01	0.1359D+01	-0.5851D+04	-0.5972D+00	-0.1216D-02	-0.1230D-02
11	0.4111D-02	0.3083D-03	-0.4125D-03	-0.3390D-02	0.8733D+01	-0.4111D-02				

FRAG NO.=	FCGU =	FCGW =	ALFA =	FRUV =	FRWV =	FRAV =
1	0.393900D+01	0.361683D+01	-0.129621D+01	0.532730D+04	-0.487381D+03	-0.188582D+04

CURRENT TIME CYCLE	FRAGMENT	KINETIC ENERGY
85	1	0.112231D+06

WORK INPUT INTO RING TO TIME STEP 85 = 0.395280D+05
RING KINETIC ENERGY AT TIME STEP 85 = 0.111410D+05
RING ELASTIC ENERGY TO TIME STEP 85 = 0.123268D+04
RING PLASTIC WORK TO TIME STEP 85 = 0.271424D+05
ENERGY STORED IN ELASTIC RESTRAINTS = 0.118876D+02

J= 85 TIME= 0.850000D-04

I	V	W	PSI	CHI	COPY	COPZ	L	M	STRAIN(IN)	STRAIN(OUT)
1	0.0	0.0	-0.3096D-01	0.1520D-01	0.0	0.8733D+01	0.7235D+05	-0.9176D+03	0.1604D-01	0.1103D-01
2	0.2123D-01	-0.2553D-01	-0.7313D-02	0.1354D-01	0.1383D+01	0.8597D+01	0.6957D+05	-0.5192D+02	0.1062D-01	0.1108D-01
3	0.4203D-01	-0.3328D-01	-0.9787D-02	0.1401D-01	0.2728D+01	0.8261D+01	0.6668D+05	-0.2086D+03	0.1326D-01	0.9799D-02
4	0.6556D-01	-0.3534D-01	0.8968D-02	0.1777D-01	0.4007D+01	0.7720D+01	0.6167D+05	-0.8026D+03	0.3054D-01	0.4541D-02
5	0.9605D-01	0.7297D-01	0.1631D+00	0.5369D-01	0.5254D+01	0.7068D+01	0.3943D+05	0.6446D+03	0.6427D-01	0.7481D-01
6	0.3476D-01	0.5765D+00	0.8829D-01	0.8266D-01	0.6607D+01	0.6558D+01	0.3568D+05	0.1341D+04	-0.8074D-03	0.3372D-01
7	-0.2949D-01	0.3386D+00	-0.1647D+00	0.2259D-01	0.7322D+01	0.5356D+01	0.3558D+05	-0.2850D+03	0.1742D-01	0.8571D-02
8	-0.6531D-01	0.3065D-01	-0.9568D-01	0.2847D-01	0.7779D+01	0.4037D+01	0.2688D+05	-0.1664D+03	0.1624D-01	0.5639D-02
9	-0.4567D-01	-0.9894D-02	0.8397D-03	0.1332D-01	0.8282D+01	0.2739D+01	0.1379D+05	-0.1735D+02	0.5047D-02	0.4846D-02
10	-0.3535D-01	-0.5205D-02	0.2693D-02	0.6873D-02	0.8615D+01	0.1400D+01	0.6684D+03	0.2576D+01	0.1103D-03	0.1691D-03
11	-0.3135D-01	-0.1919D-02	0.1582D-02	0.7770D-02	0.8731D+01	0.3135D-01				

FRAG NO.=	FCGU =	FCGW =	ALFA =	FRUV =	FRWV =	FRAV =
1	0.415209D+01	0.359734D+01	-0.137164D+01	0.532730D+04	-0.487381D+03	-0.188582D+04

IMPACT IT= 119 ELEMENT NO. = 7 FRAGMENT NO. = 1
LOCATION ON ELEMENT = 0.351180D+00 PENETRATION DIST = 0.140538D-02

IMPACT IT= 121 ELEMENT NO. = 7 FRAGMENT NO. = 1
LOCATION ON ELEMENT = 0.350183D+00 PENETRATION DIST = 0.108074D-02

CURRENT TIME CYCLE	FRAGMENT	KINETIC ENERGY
125	1	0.968516D+C5

WORK INPUT INTO RING TO TIME STEP	125 =	0.549069D+05
RING KINETIC ENERGY AT TIME STEP	125 =	0.138231D+05
RING ELASTIC ENERGY TO TIME STEP	125 =	0.598090D+03
RING PLASTIC WORK TO TIME STEP	125 =	0.403146D+05
ENERGY STORED IN ELASTIC RESTRAINTS	=	0.171117D+03

J= 125 TIME= 0.12500D-03

I	V	W	PSI	CHI	COPY	COPZ	L	M	STRAIN(IN)	STRAIN(OUT)
1	C.C	0.0	-0.9005D-01	0.9662D-02	0.0	0.8733D+01	0.3218D+05	-0.1404D+04	0.1941D-01	0.6843D-02
2	0.2306D-01	-0.8668D-01	-0.3056D-C1	0.1283D-01	0.1375D+C1	0.8536D+01	0.2432D+05	-0.7894D+03	0.1155D-01	0.7963D-02
3	C.5320D-01	-0.1076D+00	-0.1249D-01	0.1226D-01	0.2716D+01	0.8187D+01	0.1528D+05	-0.1344D+04	0.1580D-01	0.4135D-02
4	0.8530D-C1	-0.8661D-01	0.5134D-01	0.1626D-01	0.4001D+01	0.7665D+01	0.1206D+05	-0.7530D+03	0.3439D-01	-0.9406D-03
5	C.9730D-01	0.1479D+00	0.2614D+00	0.2640D-01	0.5299D+01	0.7128D+01	0.1126D+05	0.1259D+04	0.5873D-01	0.7557D-C1
6	-0.4685D-C2	0.7093D+00	0.1456D+00	0.7116D-01	0.6673D+01	0.6680D+01	0.4280D+05	0.1380D+04	-0.6503D-02	0.4581D-01
7	-C.8890D-01	0.5061D+00	-0.2344D+0C	0.4396D-02	0.7422D+01	0.5503D+01	0.4825D+05	-0.4305D+02	0.1979D-01	0.1171D-C1
8	-0.1639D+00	0.9909D-01	-0.1715D+00	0.1413D-01	0.7795D+01	0.4156D+01	-0.4904D+05	-0.2574D+02	0.2755D-02	-0.1672D-01
9	-0.1699D+00	-0.4042D-C1	0.5653D-02	0.7108D-02	0.8215D+01	0.2848D+01	-0.1709D+05	-0.1158D+03	0.3898D-03	-0.1419D-02
10	-0.1626D+00	-0.2684D-01	0.2438D-01	0.4994D-02	0.8574D+01	0.1523D+01	-0.3895D+04	0.3067D+02	-0.1164D-02	-C.4644D-03
11	-C.1577D+C0	-C.1187D-01	0.1520D-01	0.9381D-02	0.8721D+01	C.1577D+00				

FRAG NO.=	FCGU =	FCGW =	ALFA =	FRUV =	FRWV =	FRAV =
1	0.436263D+01	0.357836D+01	-0.144638D+01	0.491058D+04	-0.402738D+03	-0.177287D+04

CURRENT TIME CYCLE	FRAGMENT	KINETIC ENERGY
165	1	0.968516D+05

WORK INPUT INTO RING TO TIME STEP	165 =	0.549069D+05
RING KINETIC ENERGY AT TIME STEP	165 =	0.121063D+05
RING ELASTIC ENERGY TO TIME STEP	165 =	0.492656D+03
RING PLASTIC WORK TO TIME STEP	165 =	0.418349D+05
ENERGY STORED IN ELASTIC RESTRAINTS	=	0.473040D+03

J= 165 TIME= C.16500D-C3

I	V	W	PSI	CHI	COPY	COPZ	L	M	STRAIN(IN)	STRAIN(OUT)
1	0.0	0.0	-0.1364D+00	0.3406D-02	0.0	0.8733D+01	0.8710D+04	-0.1740D+04	0.1810D-01	C.4433D-C2
2	C.1999D-01	-0.1535D+00	-0.7177D-01	0.8408D-02	0.1362D+01	0.8471D+01	-0.8230D+04	-0.3373D+04	0.1366D-01	0.3025D-03
3	0.5863D-01	-0.2C13D+00	-0.3937D-02	0.6283D-02	0.2692D+01	0.8096D+01	-0.1767D+05	-0.3024D+04	0.1862D-01	-0.5238D-02
4	C.9490D-01	-0.1228D+00	0.1271D+00	0.5122D-02	0.3994D+C1	0.7629D+01	-0.3782D+04	0.1299D+03	0.3043D-01	-0.3001D-03
5	C.8613D-C1	0.1997D+00	0.3095D+00	0.1175D-01	0.5320D+01	0.7176D+01	-0.6810D+02	0.1191D+04	0.5700D-01	0.7640D-01
6	-0.4695D-01	0.8031D+00	C.1766D+00	0.6729D-01	0.6710D+01	0.6776D+01	-0.5772D+04	-0.8417D+02	-0.7977D-02	0.3988D-C1
7	-C.1406D+00	0.6886D+00	-0.1712D+00	0.2448D-01	0.7540D+01	0.5652D+01	0.2893D+05	0.1238D+04	0.9994D-02	0.1775D-01
8	-0.2317D+00	0.3327D+C0	-0.2357D+00	0.8638D-02	0.7972D+01	C.4322D+01	0.1118D+05	-0.1342D+03	0.1235D-01	-C.1091D-01
9	-0.2853D+00	-C.5212D-01	-0.2623D-01	0.2601D-01	0.8168D+01	0.2954D+01	0.9621D+04	-0.4953D+03	0.8231D-02	0.1637D-03
10	-0.2652D+C0	-0.4743D-01	0.5826D-01	0.7962D-02	0.8537D+01	0.1621D+01	0.6415D+04	0.6999D+02	0.5429D-03	0.2139D-02
11	-0.2558D+C0	-0.2146D-01	C.3786D-01	0.1076D-01	0.8712D+01	0.2558D+00				

FRAG NO.=	FCGU =	FCGW =	ALFA =	FRUV =	FRWV =	FRAV =
1	C.455905D+01	0.356225D+01	-0.151730D+01	0.491058D+04	-0.402738D+03	-0.177287D+04

CURRENT TIME CYCLE	FRAGMENT	KINETIC ENERGY
205	1	0.836077D+05

```
WORK INPUT INTO RING TO TIME STEP    205 =   0.681508D+05
RING KINETIC ENERGY AT TIME STEP     205 =   0.140220D+05
RING ELASTIC ENERGY TO TIME STEP     205 =   0.626543D+03
RING PLASTIC WORK TO TIME STEP       205 =   0.525326D+05
ENERGY STORED IN ELASTIC RESTRAINTS      =     0.969686D+03
```

J= 205 TIME= 0.20500D-03

I	V	W	PSI	CHI	COPY	COPZ	L	M	STRAIN(IN)	STRAIN(OUT)
1	0.0	0.0	-0.1811D+00	-0.3064D-02	0.0	0.8733D+01	0.2822D+05	-0.1823D+04	0.1978D-01	0.5843D-02
2	0.1864D-01	-0.2121D+00	-0.1152D+00	0.5565D-02	0.1351D+01	0.8413D+01	0.1346D+05	-0.4017D+04	0.2111D-01	-0.3338D-02
3	0.7075D-01	-0.2920D+00	0.9004D-02	0.1273D-01	0.2676D+01	0.8006D+01	0.1137D+05	-0.2745D+04	0.2604D-01	-0.5840D-02
4	0.1167D+00	-0.1479D+00	0.1841D+00	-0.4957D-03	0.4001D+01	0.7596D+01	0.2857D+05	0.9440D+03	0.3154D-01	0.5057D-02
5	0.9679D-01	0.2356D+00	0.3412D+00	0.3085D-02	0.5350D+01	0.7199D+01	0.2922D+05	0.9253D+03	0.6075D-01	0.7098D-01
6	-0.6546D-01	0.6891D+00	0.2154D+00	0.6057D-01	0.6758D+01	0.6850D+01	0.3222D+05	-0.4170D+03	0.4002D-02	0.4241D-01
7	-0.1652D+00	0.8449D+00	-0.6365D-01	0.3780D-01	0.7652D+01	0.5763D+01	0.9184D+04	0.8404D+03	0.4988D-02	0.3354D-01
8	-0.2676D+00	0.5813D+00	-0.2949D+00	-0.1452D-02	0.8178D+01	0.4467D+01	0.1149D+05	0.5491D+03	0.8206D-02	-0.6671D-02
9	-0.3934D+00	0.3403D-01	-0.1637D+00	0.1220D-01	0.8216D+01	0.3083D+01	0.1778D+05	-0.3998D+03	0.1130D-01	-0.1141D-01
10	-0.3831D+00	-0.7309D-01	0.7582D-01	0.2475D-02	0.8493D+01	0.1733D+01	0.1186D+05	0.3916D+02	0.2033D-02	0.2926D-02
11	-0.3743D+00	-0.3337D-01	0.6457D-01	0.1034D-02	0.8700D+01	0.3743D+00				

FRAG NO.=	FCGU =	FCGW =	ALFA =	FRUV =	FRWV =	FRAV =
1	0.474786D+01	0.354922D+01	-0.158603D+01	0.453419D+04	-0.250379D+03	-0.166501D+04

```
IMPACT IT=  222   ELEMENT NO. =   8   FRAGMENT NO. =   1
LOCATION ON ELEMENT =  0.385076D+00   PENETRATION DIST =  0.579554D-03
```

CURRENT TIME CYCLE	FRAGMENT	KINETIC ENERGY
245	1	0.808256D+05

```
WORK INPUT INTO RING TO TIME STEP    245 =   0.709329D+05
RING KINETIC ENERGY AT TIME STEP     245 =   0.126213D+05
RING ELASTIC ENERGY TO TIME STEP     245 =   0.621927D+03
RING PLASTIC WORK TO TIME STEP       245 =   0.559764D+05
ENERGY STORED IN ELASTIC RESTRAINTS      =     0.171332D+04
```

J= 245 TIME= 0.24500D-03

I	V	W	PSI	CHI	COPY	COPZ	L	M	STRAIN(IN)	STRAIN(OUT)
1	0.0	0.0	-0.2264D+00	-0.1215D-01	0.0	0.8733D+01	0.3217D+05	-0.1815D+04	0.2167D-01	0.5712D-02
2	0.1446D-01	-0.2704D+00	-0.1510D+00	0.2999D-02	0.1338D+01	0.8356D+01	0.2659D+05	-0.3385D+04	0.3069D-01	-0.3675D-02
3	0.8258D-01	-0.3694D+00	0.2366D-01	0.2099D-01	0.2663D+01	0.7929D+01	0.2595D+05	-0.2202D+04	0.3131D-01	-0.4383D-02
4	0.1372D+00	-0.1748D+00	0.2195D+00	-0.2944D-02	0.4008D+01	0.7563D+01	0.3414D+05	0.1308D+04	0.3114D-01	0.6935D-02
5	0.1072D+00	0.2561D+00	0.3628D+00	-0.1901D-02	0.5370D+01	0.7209D+01	0.2290D+05	0.7727D+03	0.6054D-01	0.7781D-01
6	-0.6584D-01	0.9263D+00	0.2434D+00	0.5214D-01	0.6784D+01	0.6877D+01	0.2156D+05	-0.1258D+04	0.7549D-02	0.3733D-01
7	-0.1780D+00	0.9804D+00	0.2690D-01	0.4070D-01	0.7754D+01	0.5853D+01	0.1453D+05	0.1118D+04	0.1919D-02	0.4148D-01
8	-0.2977D+00	0.8421D+00	-0.2928D+00	0.5280D-02	0.8396D+01	0.4612D+01	0.6830D+04	0.1219D+04	0.6602D-03	0.2603D-02
9	-0.4796D+00	0.2312D+00	-0.3150D+00	-0.3276D-01	0.8377D+01	0.3226D+01	-0.1053D+05	-0.5748D+03	0.1437D-01	-0.2048D-01
10	-0.5084D+00	-0.9068D-01	0.5233D-01	0.1825D-01	0.8456D+01	0.1854D+01	0.3186D+04	-0.1575D+03	0.2462D-02	-0.1130D-02
11	-0.4921D+00	-0.4768D-01	0.9602D-01	0.1758D-01	0.8685D+01	0.4921D+00				

FRAG NO.=	FCGU =	FCGW =	ALFA =	FRUV =	FRWV =	FRAV =
1	0.492727D+01	0.354020D+01	-0.165204D+01	0.445246D+04	-0.209090D+03	-0.164069D+04

CURRENT TIME CYCLE FRAGMENT KINETIC ENERGY

405 1 0.435650D+05

WORK INPUT INTO RING TO TIME STEP 405 = 0.108194D+06
RING KINETIC ENERGY AT TIME STEP 405 = 0.102610D+05
RING ELASTIC ENERGY TO TIME STEP 405 = 0.108282D+04
RING PLASTIC WORK TO TIME STEP 405 = 0.910306D+05
ENERGY STORED IN ELASTIC RESTRAINTS = 0.581914D+04

J= 405 TIME= 0.40500D-03

I	V	W	PSI	CHI	COPY	COPZ	L	M	STRAIN(IN)	STRAIN(OUT)
1	0.0	0.0	-0.3468D+00	-0.4222D-01	0.0	0.8733D+01	0.7992D+05	-0.6355D+03	0.3348D-01	0.9379D-02
2	0.4703D-03	-0.4189D+00	-0.2330D+00	-0.3310D-03	0.1301D+01	0.8212D+01	0.7621D+05	0.6531D+02	0.5337D-01	-0.1443D-02
3	0.1072D+00	-0.5490D+00	0.4607D-01	0.2929D-01	0.2631D+01	0.7750D+01	0.6263D+05	-0.3173D+03	0.3983D-01	0.3065D-02
4	0.1935D+00	-0.3149D+00	0.2478D+00	-0.2387D-02	0.3994D+01	0.7413D+01	0.5051D+05	-0.3642D+03	0.4113D-01	0.1583D-01
5	0.1676D+00	0.1994D+00	0.3969D+00	-0.3574D-02	0.5386D+01	0.7128D+01	0.3442D+05	-0.1563D+03	0.7705D-01	0.7895D-01
6	-0.1349D-01	0.9434D+00	0.3783D+00	0.2809D-01	0.6833D+01	0.6852D+01	0.3231D+05	-0.1439D+03	0.4923D-01	0.6934D-01
7	-0.1883D+00	0.1392D+01	0.2311D+00	0.3709D-01	0.8081D+01	0.6104D+01	0.1809D+05	0.7254D+02	0.2196D-01	0.5271D-01
8	-0.3679D+00	0.1498D+01	-0.1838D-01	0.6667D-01	0.8949D+01	0.4972D+01	0.7410D+04	-0.1052D+03	0.1480D-01	0.5664D-01
9	-0.5615D+00	0.1150D+01	-0.4013D+00	-0.3763D-01	0.9226D+01	0.3588D+01	0.5517D+04	0.8737D+03	-0.1291D-01	-0.1010D-01
10	-0.8764D+00	0.2963D+00	-0.4381D+00	-0.7295D-01	0.8781D+01	0.2278D+01	0.4172D+04	-0.3780D+03	0.2006D-01	-0.1608D-01
11	-0.5100D+00	-0.1180D+00	0.1367D-01	0.1728D-01	0.8615D+01	0.9100D+00				

FRAG NO.=	FCGU =	FCGW =	ALFA =	FRUV =	FRWV =	FRAV =
1	0.556975D+01	0.354521D+01	-0.187238D+01	0.332673D+04	-0.199876D+03	-0.117505D+04

IMPACT IT= 433 ELEMENT NO. = 5 FRAGMENT NO. = 1
LOCATION ON ELEMENT = 0.544378D+00 PENETRATION DIST = 0.255157D-03

CURRENT TIME CYCLE FRAGMENT KINETIC ENERGY

445 1 0.425371D+05

WORK INPUT INTO RING TO TIME STEP 445 = 0.109221D+06
RING KINETIC ENERGY AT TIME STEP 445 = 0.826122D+04
RING ELASTIC ENERGY TO TIME STEP 445 = 0.292276D+03
RING PLASTIC WORK TO TIME STEP 445 = 0.930481D+05
ENERGY STORED IN ELASTIC RESTRAINTS = 0.761980D+04

J= 445 TIME= 0.44500D-03

I	V	W	PSI	CHI	COPY	COPZ	L	M	STRAIN(IN)	STRAIN(OUT)
1	0.0	0.0	-0.3583D+00	-0.4808D-01	0.0	0.8733D+01	0.2963D+05	-0.6169D+03	0.3571D-01	0.6878D-02
2	-0.8809D-04	-0.4193D+00	-0.2220D+00	0.1768D-02	0.1300D+01	0.8211D+01	0.2554D+05	0.9484D+03	0.4962D-01	0.1688D-02
3	0.1063D+00	-0.5540D+00	0.2200D-01	0.2875D-01	0.2629D+01	0.7746D+01	0.1987D+05	-0.8707D+03	0.4069D-01	-0.1122D-02
4	0.1968D+00	-0.3438D+00	0.2516D+00	-0.3264D-02	0.3984D+01	0.7386D+01	0.1787D+05	-0.4405D+03	0.4014D-01	0.1233D-01
5	0.1621D+00	0.1950D+00	0.4154D+00	-0.1280D-01	0.5379D+01	0.7128D+01	0.1318D+05	-0.4482D+03	0.7564D-01	0.7571D-01
6	-0.2883D-01	0.9523D+00	0.4091D+00	0.1410D-01	0.6828D+01	0.6869D+01	0.1919D+05	-0.6817D+03	0.4970D-01	0.6570D-01
7	-0.2340D+00	0.1459D+01	0.2914D+00	0.1871D-01	0.8108D+01	0.6180D+01	0.1311D+05	0.5537D+03	0.1899D-01	0.5433D-01
8	-0.4418D+00	0.1627D+01	0.4867D-02	0.6614D-01	0.9030D+01	0.5097D+01	0.9076D+04	-0.4103D+03	0.1693D-01	0.5502D-01
9	-0.6462D+00	0.1330D+01	-0.3439D+00	-0.1579D-01	0.9371D+01	0.3724D+01	0.5465D+04	0.9626D+03	-0.1937D-01	-0.4944D-02
10	-0.9710D+00	0.5070D+00	-0.5017D+00	-0.1048D+00	0.8974D+01	0.2404D+01	0.5556D+04	0.1626D+02	0.1586D-01	-0.1129D-01
11	-0.1067D+01	-0.1149D+00	-0.1631D+00	0.1032D-01	0.8618D+01	0.1067D+01				

FRAG NO.=	FCGU =	FCGW =	ALFA =	FRUV =	FRWV =	FRAV =
1	0.570233D+01	0.353656D+01	-0.191916D+01	0.328903D+04	-0.249769D+03	-0.115844D+04

IMPACT IT= 458 ELEMENT NO. = 6 FRAGMENT NO. = 1
LOCATION ON ELEMENT = 0.858016D+00 PENETRATION DIST = 0.358018D-03

CURRENT TIME CYCLE   FRAGMENT   KINETIC ENERGY

485   1   0.408357D+05

WORK INPUT INTO RING TO TIME STEP 485 = 0.110923D+06
RING KINETIC ENERGY AT TIME STEP 485 = 0.665037D+04
RING ELASTIC ENERGY TO TIME STEP 485 = 0.202132D+03
RING PLASTIC WORK TO TIME STEP 485 = 0.945684D+05
ENERGY STORED IN ELASTIC RESTRAINTS = 0.950198D+04

J= 485   TIME= 0.48500D-03

I	V	W	PSI	CHI	COPY	COPZ	L	M	STRAIN(IN)	STRAIN(OUT)
1	0.0	0.0	-0.3450D+00	-0.4580D-01	0.0	0.8733D+01	-0.3878D+04	0.6319D+03	0.3101D-01	0.6270D-02
2	-0.2524D-02	-0.4144D+00	-0.2282D+00	-0.1770D-02	0.1299D+01	0.8217D+01	-0.2996D+04	0.7836D+03	0.4750D-01	-0.1054D-02
3	0.9981D-01	-0.5588D+00	0.1899D-01	0.2738D-01	0.2621D+01	0.7743D+01	-0.1279D+05	-0.8464D+03	0.3763D-01	-0.4072D-02
4	0.1882D+00	-0.3544D+00	0.2475D+00	-0.6281D-02	0.3971D+01	0.7380D+01	-0.9263D+04	-0.9461D+03	0.3874D-01	0.8299D-02
5	0.1534D+00	0.1787D+00	0.4278D+00	-0.2057D-01	0.5362D+01	0.7120D+01	-0.5389D+04	-0.5878D+03	0.7404D-01	0.7325D-01
6	-0.6319D-01	0.9711D+00	0.4264D+00	0.5028D-02	0.6817D+01	0.6907D+01	-0.5185D+02	-0.1023D+04	0.4983D-01	0.6155D-01
7	-0.2940D+00	0.1516D+01	0.3395D+00	0.1607D-02	0.8119D+01	0.6262D+01	0.2189D+03	0.5208D+03	0.1734D-01	0.5256D-01
8	-0.5214D+00	0.1708D+01	0.5428D-01	0.6309D-01	0.9067D+01	0.5205D+01	0.6229D+04	-0.3281D+03	0.1598D-01	0.5509D-01
9	-0.7355D+00	0.1479D+01	-0.3036D+00	-0.3834D-02	0.9485D+01	0.3855D+01	0.2578D+04	0.9265D+03	-0.2105D-01	-0.1669D-02
10	-0.1056D+01	0.7080D+00	-0.5120D+00	-0.1097D+00	0.9160D+01	0.2520D+01	0.2186D+04	0.6036D+03	0.7551D-02	-0.4065D-02
11	-0.1230D+01	-0.8902D-01	-0.3682D+00	-0.4565D-01	0.8644D+01	0.1230D+01				

FRAG NO.=	FCGU =	FCGW =	ALFA =	FRUV =	FRWV =	FRAV =
1	0.583190D+01	0.352513D+01	-0.196485D+01	0.321771D+04	-0.301249D+03	-0.113507D+04

IMPACT IT= 515   ELEMENT NO. = 10   FRAGMENT NO. = 1
LOCATION ON ELEMENT = 0.753888D+00   PENETRATION DIST = 0.145281D-02

CURRENT TIME CYCLE   FRAGMENT   KINETIC ENERGY

525   1   0.380970D+05

WORK INPUT INTO RING TO TIME STEP 525 = 0.113661D+06
RING KINETIC ENERGY AT TIME STEP 525 = 0.528119D+04
RING ELASTIC ENERGY TO TIME STEP 525 = 0.327557D+03
RING PLASTIC WORK TO TIME STEP 525 = 0.969999D+05
ENERGY STORED IN ELASTIC RESTRAINTS = 0.110528D+05

J= 525   TIME= 0.52500D-03

I	V	W	PSI	CHI	COPY	COPZ	L	M	STRAIN(IN)	STRAIN(OUT)
1	0.0	0.0	-0.3360D+00	-0.4352D-01	0.0	0.8733D+01	-0.1668D+05	0.1961D+04	0.2770D-01	0.7487D-02
2	-0.4213D-02	-0.4135D+00	-0.2405D+00	-0.7460D-02	0.1297D+01	0.8218D+01	-0.2182D+05	-0.2416D+03	0.4784D-01	-0.4596D-02
3	0.9503D-01	-0.5691D+00	0.2639D-01	0.2607D-01	0.2613D+01	0.7735D+01	-0.1410D+05	0.2353D+01	0.3564D-01	-0.2319D-02
4	0.1837D+00	-0.3586D+00	0.2346D+00	-0.1670D-02	0.3966D+01	0.7378D+01	0.1280D+04	-0.1860D+04	0.4222D-01	0.6867D-02
5	0.1548D+00	0.1666D+00	0.4440D+00	-0.2521D-01	0.5356D+01	0.7109D+01	-0.1185D+04	-0.1259D+04	0.7660D-01	0.7161D-01
6	-0.9021D-01	0.1004D+01	0.4695D+00	-0.1433D-01	0.6822D+01	0.6949D+01	0.1060D+05	-0.3896D+01	0.4723D-01	0.6672D-01
7	-0.3416D+00	0.1573D+01	0.3262D+00	0.8227D-02	0.8137D+01	0.6334D+01	0.4746D+04	-0.1646D+03	0.2123D-01	0.4990D-01
8	-0.5800D+00	0.1781D+01	0.9358D-01	0.6137D-01	0.9105D+01	0.5290D+01	0.2737D+05	-0.5777D+03	0.2075D-01	0.5680D-01
9	-0.7997D+00	0.1594D+01	-0.2364D+00	0.1536D-01	0.9575D+01	0.3952D+01	0.2479D+05	0.2664D+03	-0.1585D-01	0.7897D-02
10	-0.1102D+01	0.8961D+00	-0.4900D+00	-0.9398D-01	0.9338D+01	0.2595D+01	0.7691D+04	0.5151D+03	0.2719D-02	0.8178D-02
11	-0.1343D+01	-0.1156D-01	-0.5590D+00	-0.1305D+00	0.8721D+01	0.1343D+01				

FRAG NO.=	FCGU =	FCGW =	ALFA =	FRUV =	FRWV =	FRAV =
1	0.595955D+01	0.351445D+01	-0.200979D+01	0.312229D+04	-0.176959D+03	-0.109345D+04

CURRENT TIME CYCLE	FRAGMENT	KINETIC ENERGY
565	1	0.380970D+05

WORK INPUT INTO RING TO TIME STEP 565 = 0.113661D+06
RING KINETIC ENERGY AT TIME STEP 565 = 0.381220D+04
RING ELASTIC ENERGY TO TIME STEP 565 = 0.330169D+03
RING PLASTIC WORK TO TIME STEP 565 = 0.974103D+05
ENERGY STORED IN ELASTIC RESTRAINTS = 0.121089D+05

J= 565 TIME= 0.565000D-03

I	V	W	PSI	CHI	COPY	COPZ	L	M	STRAIN(IN)	STRAIN(OUT)
1	0.0	0.0	-0.3559D+00	-0.4718D-01	0.0	0.8733D+01	0.2169D+05	0.4100D+03	0.3328D-01	0.7984D-02
2	-0.2142D-02	-0.4253D+00	-0.2363D+00	-0.1832D-02	0.1297D+01	0.8206D+01	0.3085D+05	0.3904D+03	0.5113D-01	0.1085D-02
3	0.1052D+00	-0.5734D+00	0.1846D-01	0.2960D-01	0.2622D+01	0.7728D+01	0.3021D+05	-0.8122D+03	0.4151D-01	-0.4249D-04
4	0.2006D+00	-0.3669D+00	0.2466D+00	-0.1993D-02	0.3977D+01	0.7363D+01	0.6676D+04	-0.1450D+04	0.4264D-01	0.7543D-02
5	0.1687D+00	0.1734D+00	0.4545D+00	-0.2857D-01	0.5372D+01	0.7106D+01	-0.1198D+04	-0.1749D+04	0.7928D-01	0.6939D-01
6	-0.9664D-01	0.1041D+01	0.5120D+00	-0.3845D-01	0.6843D+01	0.6979D+01	-0.3270D+04	0.9729D+03	0.4182D-01	0.6878D-01
7	-0.3634D+00	0.1618D+01	0.3152D+00	0.1053D-01	0.8160D+01	0.6378D+01	-0.1375D+05	-0.2444D+03	0.1924D-01	0.4696D-01
8	-0.6108D+00	0.1820D+01	0.9012D-01	0.5980D-01	0.9126D+01	0.5335D+01	-0.5978D+04	-0.7650D+03	0.2151D-01	0.4893D-01
9	-0.8376D+00	0.1654D+01	-0.1613D+00	0.2544D-01	0.9620D+01	0.4006D+01	0.1352D+04	0.3055D+03	-0.2032D-01	0.4080D-02
10	-0.1117D+01	0.1092D+01	-0.4209D+00	-0.6459D-01	0.9529D+01	0.2640D+01	-0.1210D+03	0.7832D+03	-0.7250D-02	0.1434D-01
11	-0.1359D+01	0.1786D+00	-0.6897D+00	-0.2119D+00	0.8912D+01	0.1399D+01				

FRAG NO.=	FCGU =	FCGW =	ALFA =	FRUV =	FRWV =	FRAV =
1	0.608445D+01	0.350737D+01	-0.205353D+01	0.312229D+04	-0.176959D+03	-0.109345D+04

IMPACT IT= 580 ELEMENT NO. = 7 FRAGMENT NO. = 1
LOCATION ON ELEMENT = 0.668612D+00 PENETRATION DIST = 0.133133D-02

LARGEST COMPUTED STRAIN = 0.844211D-01 OCCURS AT THE INNER SURFACE MIDSPAN OF ELEMENT = 5 AT TIME (SEC.) = 0.600000D-03

NO CARDS PUNCHED DURING THIS RUN FOR CONTINUATION.

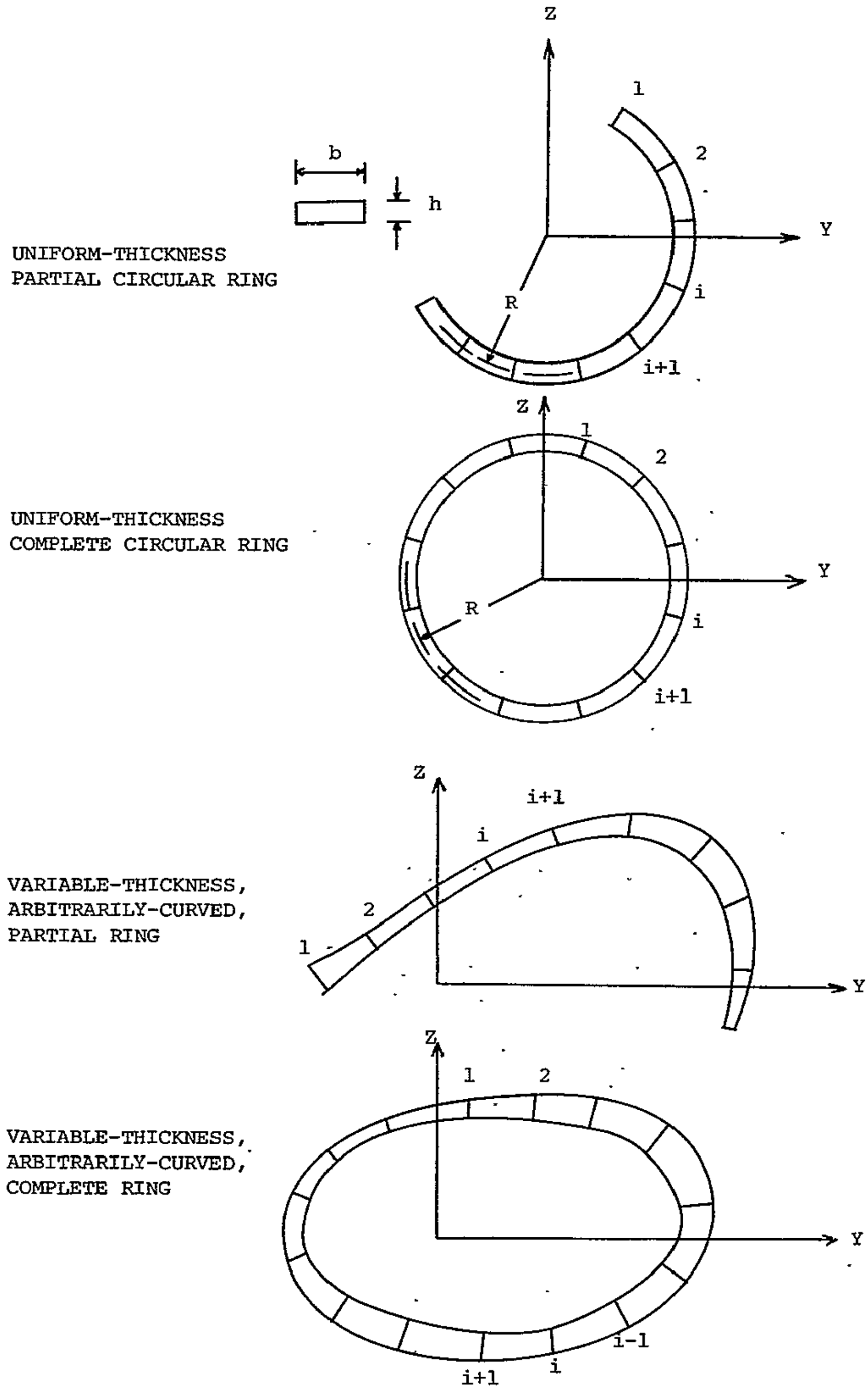

FIG. A.1 GEOMETRICAL SHAPES OF STRUCTURAL RINGS ANALYZED BY THE CIVM-JET-4A PROGRAM

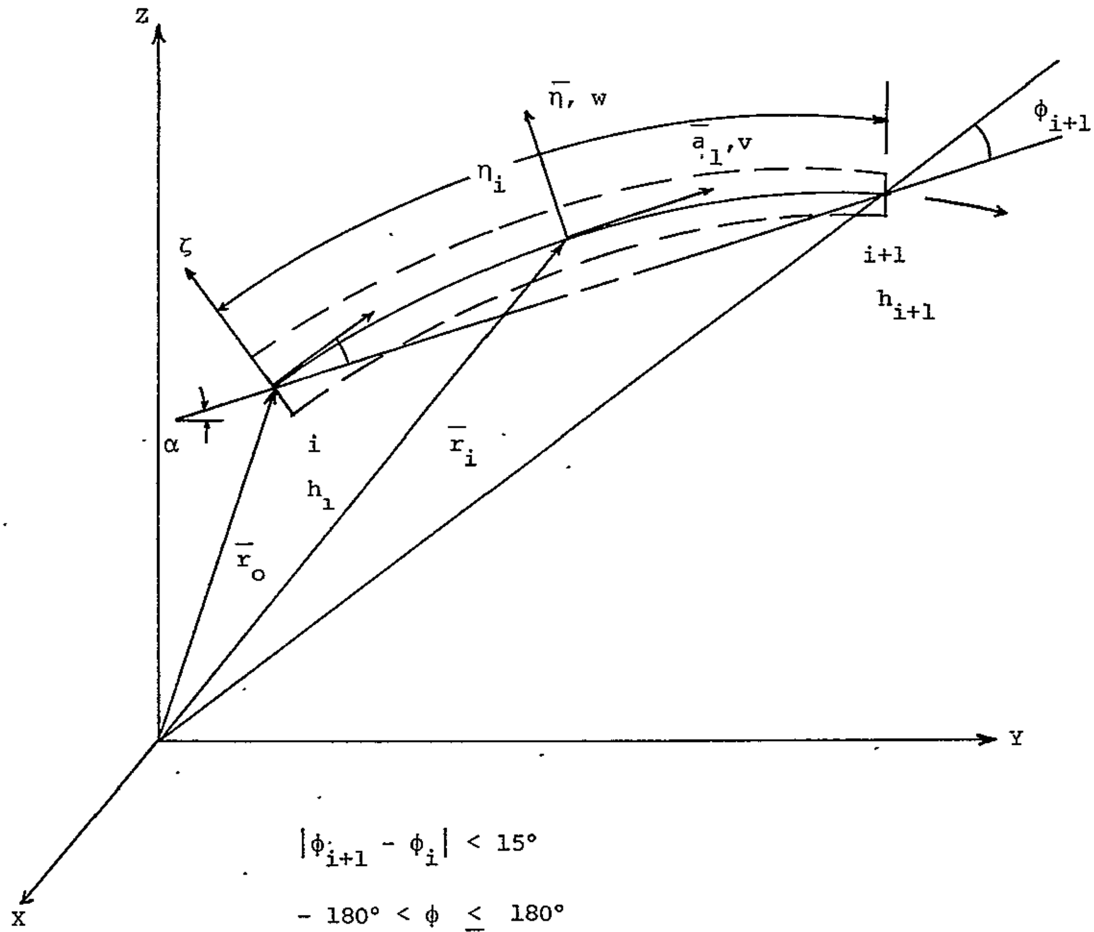

$$|\phi_{i+1} - \phi_i| < 15°$$

$$-180° < \phi \leq 180°$$

$$\phi = b_o + b_1\eta + b_2\eta^2$$

$$h = h_i \left(1 - \frac{\eta}{\eta_i}\right) + h_{i+1} \frac{\eta}{\eta_i}$$

FIG. A.2 NOMENCLATURE FOR GEOMETRY, COORDINATES, AND DISPLACEMENTS OF ARBITRARILY-CURVED VARIABLE-THICKNESS RING ELEMENTS

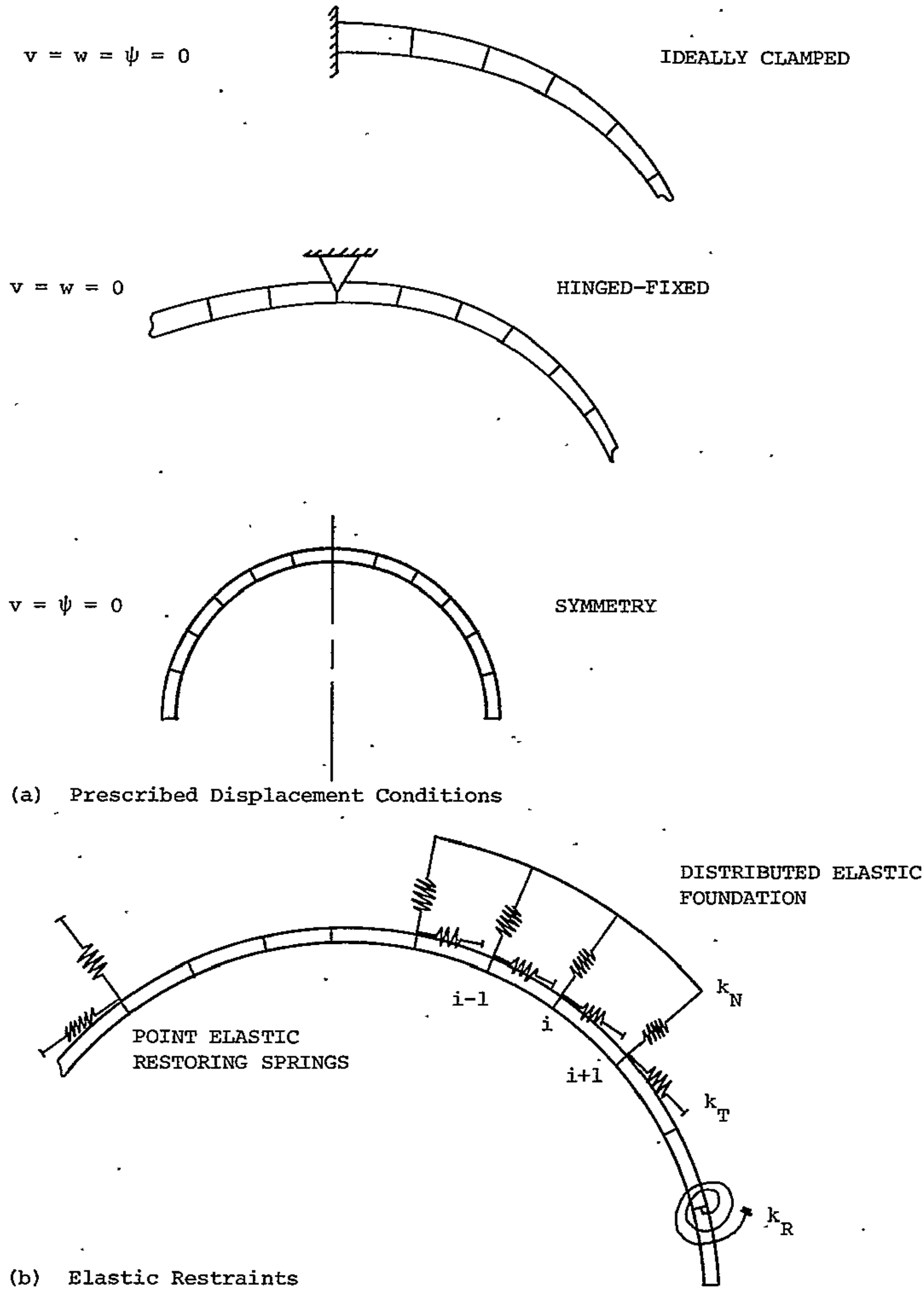

(a) Prescribed Displacement Conditions

(b) Elastic Restraints

FIG. A.3 SCHEMATICS FOR THE SUPPORT CONDITIONS OF THE STRUCTURE

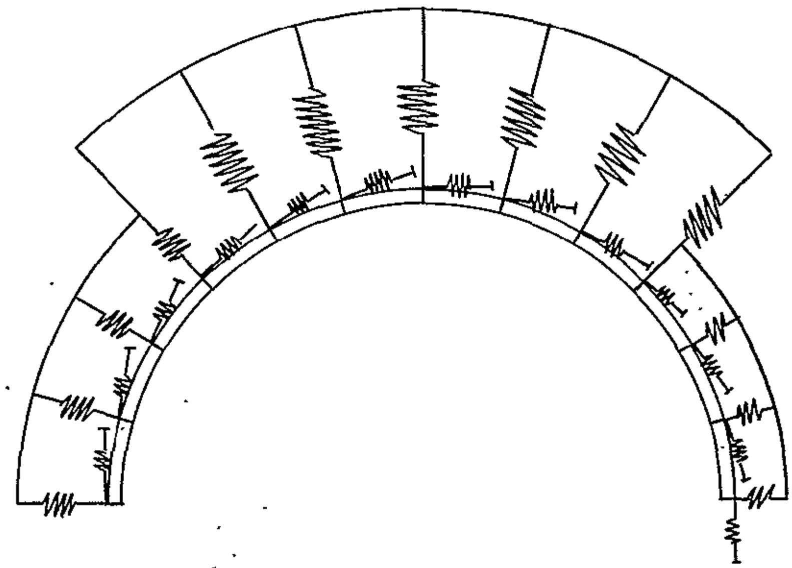

(c) Distributed Elastic Foundation Provisions

FIG. A.3 CONCLUDED

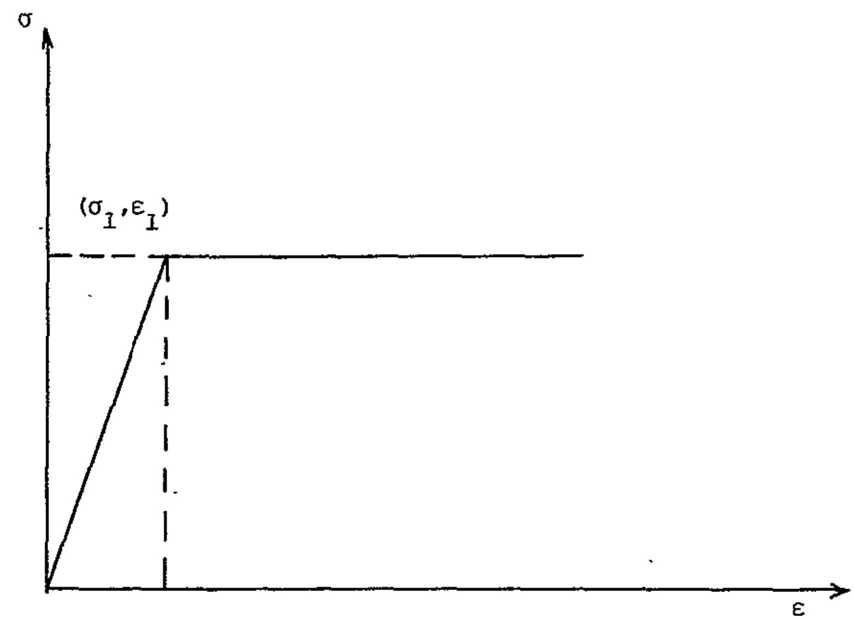

(a) Elastic, Perfectly Plastic (EL-PP)

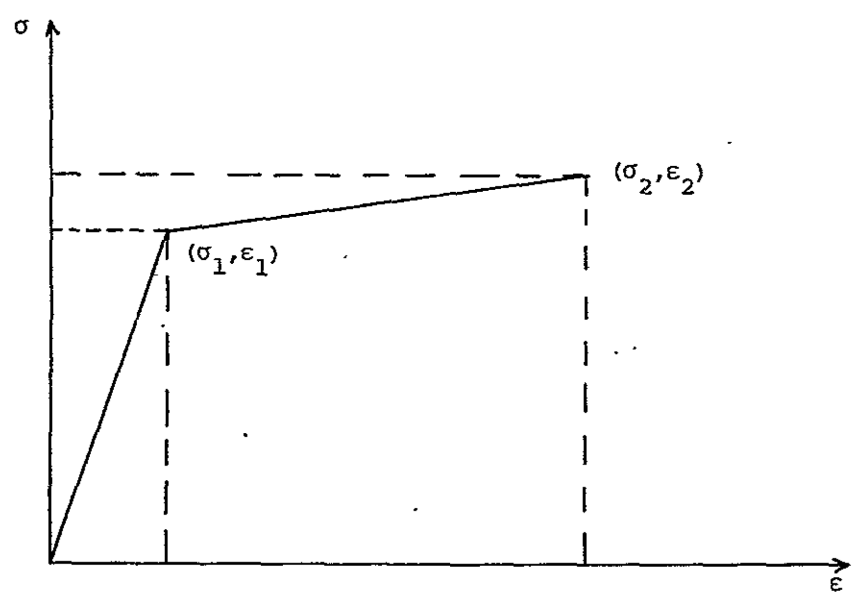

(b) Elastic, Strain-Hardening (EL-SH)

FIG. A.4 SCHEMATIC OF POSSIBLE PIECEWISE LINEAR REPRESENTATION OF UNIAXIAL STATIC STRESS-STRAIN MATERIAL BEHAVIOR

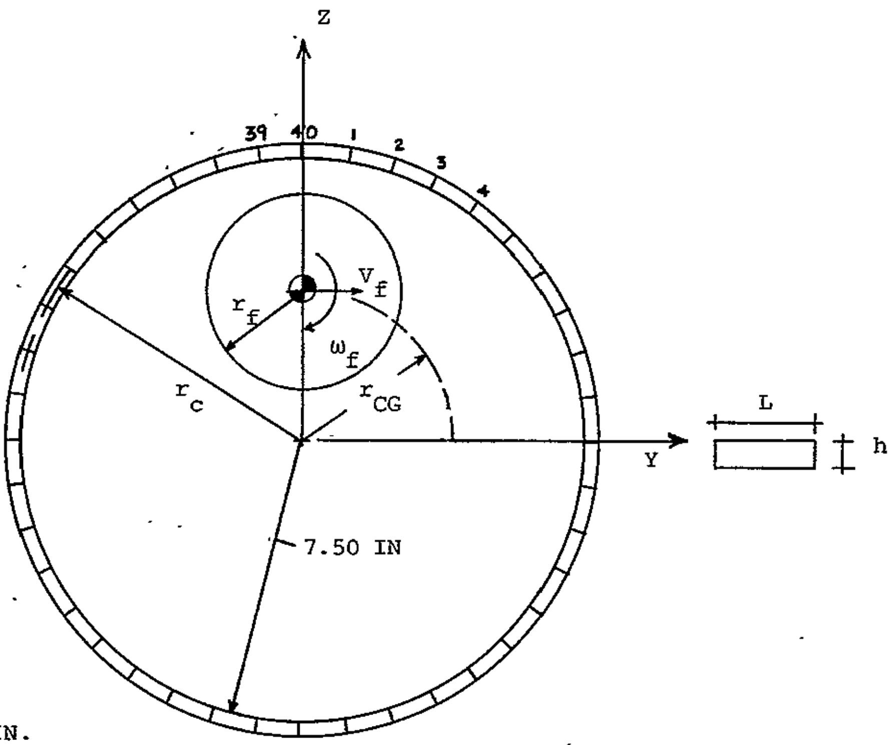

RING
4130 CAST STEEL
r_c = 7.70 IN.
L = 1.25 IN.
h = 0.40 IN.
ρ = 0.283 LB/CU.IN.
40 FINITE ELEMENTS USED

FRAGMENT
r_f = 3.37 IN.
m_f = 4.6 x 10^{-3} LB-SEC^2/IN.
I_f = 2.61 x 10^{-2} LB-SEC^2-IN.
V_f = 6400 IN/SEC.
ω_f = -2100 RAD/SEC.
r_{CG} = 3.63 IN.

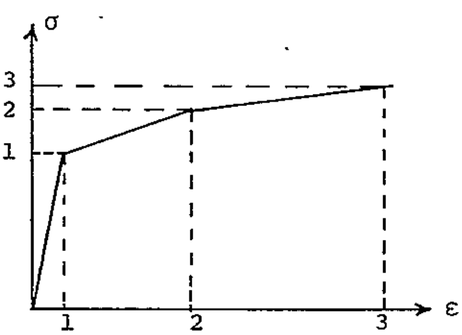

STRESS-STRAIN REPRESENTATION

σ_1 = 80,950 PSI	ε_1 = 2.79 x 10^{-3}
σ_2 = 105,300 PSI	ε_2 = 2.25 x 10^{-2}
σ_3 = 121,000 PSI	ε_3 = 2.00 x 10^{-1}

FIG. A.5 EXAMPLE PROBLEM: UNIFORM THICKNESS CONTAINMENT RING

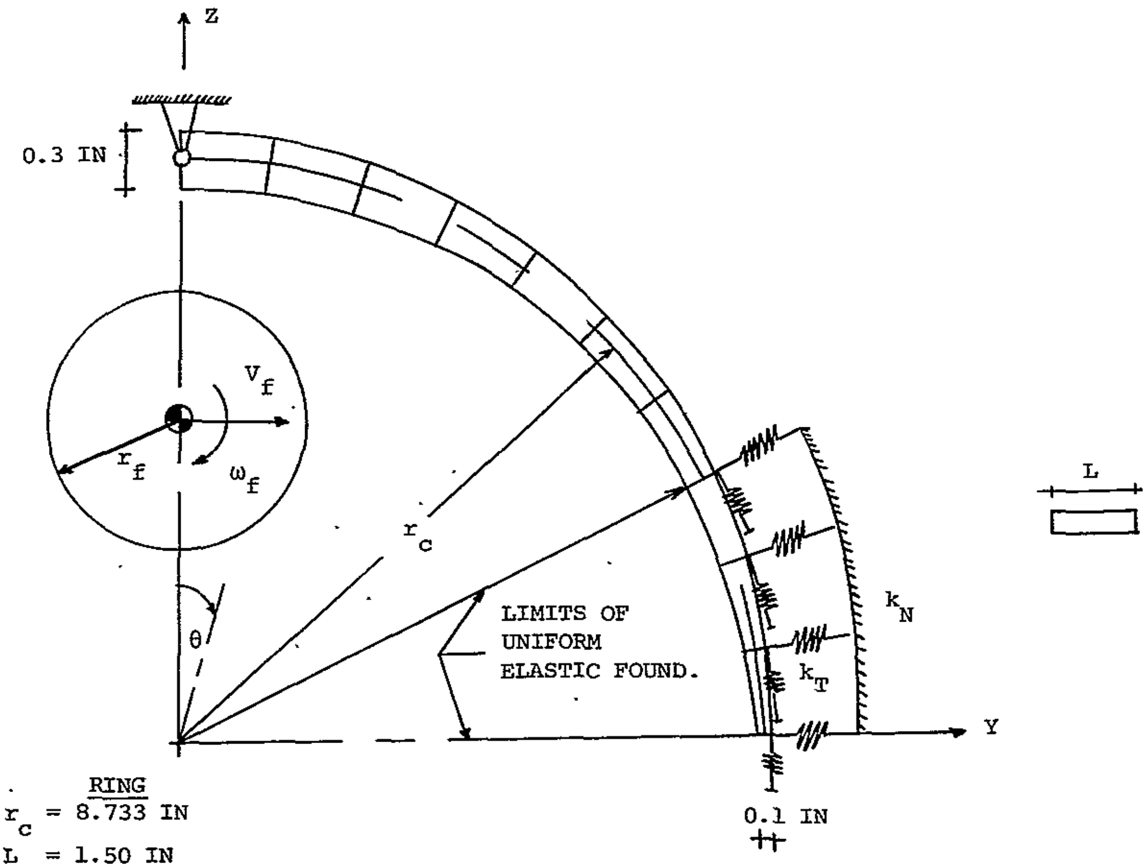

RING

r_c = 8.733 IN
L = 1.50 IN
ρ = 0.283 LB/CU.IN.
10 FINITE ELEMENTS
LINEARLY-VARYING THICKNESS

FRAGMENT

r_f = 3.37 IN
m_f = 4.6×10^{-3} LB-SEC^2/IN
I_f = 2.61×10^{-2} LB-SEC^2-IN
V_f = 6400 IN/SEC
ω_f = − 2100 RAD/SEC
(counterclockwise is +)
r_{CG} = 3.63 IN

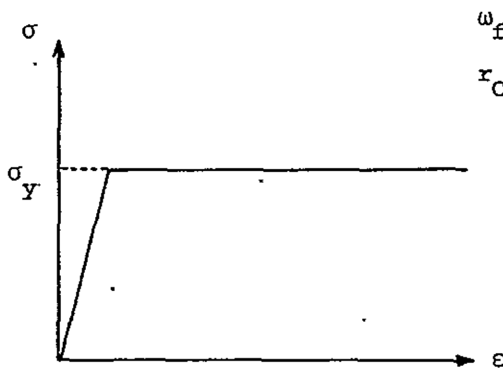

σ_y = 80,950 PSI
E = 29×10^6 PSI

FIG. A.6 EXAMPLE PROBLEM: VARIABLE-THICKNESS 90-DEG PARTIAL RING (DEFLECTOR) WITH UNIFORM ELASTIC FOUNDATION APPLIED TO A PORTION OF THE RING

APPENDIX B

SUMMARY OF THE CAPABILITIES OF THE COMPUTER CODES JET 1, JET 2, AND JET 3 FOR PREDICTING TWO-DIMENSIONAL TRANSIENT RESPONSES OF RING STRUCTURES

This appendix is intended to provide for the reader a convenient tabular summary of the principal features and capabilities of the two-dimensional transient large-deflection elastic-plastic structural response ring codes JET 1 (Ref. 15), JET 2 (Ref. 16), and JET 3A-3D (Ref. 24) developed under NASA NGR 22-009-339. The present code CIVM-JET-4A has been developed by combining the CIVM procedure with a modified version of the JET 3C two-dimensional structural response code.

The JET 1 code of Ref. 15 pertains to single-layer complete, uniform-thickness, initially-circular rings of either temperature-independent or temperature dependent material properties. These rings may be subjected to prescribed: (a) initial velocities, (b) transient mechanical loading, and/or (c) steady nonuniform temperatures. The finite-difference method employed in this code had been shown previously (Ref. 12) to provide reliable predictions for the case of temperature-independent material properties.

The JET 2 code was written in order to extend this finite-difference analysis capability to treat multilayer rings — cases anticipated to be of future concern. In the interests of efficiency and the minimization of computer storage requirements, temperature-dependent material properties and thermal loading features were omitted from JET 2; if these omitted features should turn out to be needed urgently (but this, thus far, has not been the case), they could be added later.

Since the JET 1 and JET 2 codes pertained to initially-circular, complete rings of uniform thickness whereas there was interest also in variable-thickness, arbitrarily curved, partial as well as complete rings, the JET 3 series of codes was developed. To accommodate these latter features as well as a variety of types of (1) boundary conditions, (2) elastic-foundation supports, and (3) point elastic supports, the more versatile finite-element analysis procedure was developed and employed. For efficiency and user convenience, four versions of the JET 3 program were developed; each version accommodates both complete rings and partial rings. JET 3A and JET 3B pertain to uniform-thickness, initially-circular rings, and employ, respectively, the central-difference and the Houbolt finite-difference time operator; for certain cases, the latter finite-difference time operator may permit more economic converged transient response predictions than the former. The codes JET 3C and JET 3D are corresponding codes which accommodate variable-thickness, arbitrarily-curved rings.

In all of these codes (JET 1 through JET 3D), the stimulii: (1) initial velocity or impulse conditions and/or (2) transient mechanical loading must be <u>prescribed</u> by the user or analyst. The externally-applied forces experienced by a complete or a partial ring from fragment impact are <u>not</u> provided within these codes. The user must supply his own estimate of the distribution and time histories of these forces. However, in the CIVM-JET-4A code, fragment/ring interaction and response effects are handled internally automatically, for the idealized single-fragment and n-fragment cases provided and discussed in Appendix A.

In convenient tabular form, the principal features and capabilities of the codes JET 1, JET2, and JET 3A-3D are given in ths following:

Feature	JET 1 (Ref.15)	JET 2 (Ref.16)	JET 3A (Ref.24)	JET 3B (Ref.24)	JET 3C (Ref.24)	JET 3D (Ref.24)
Type of Spatial Analysis Formulation						
Finite Difference	x	x	–	–	–	–
Finite Element	–	–	x	x	x	x
Type of Finite-Difference Time Operator						
Central Difference	x	x	x	–	x	–
Houbolt (Backward Difference)	–	–	–	x	–	x
Ring Geometry						
Complete Ring	x	x	x	x	x	x
Partial Ring	–	–	x	x	x	x
Initial Configuration						
Circular	x	x	x	x	x	x
Arb. Curved	–	–	–	–	x	x
Constant Thickness	x	x	x	x	x	x
Variable Thickness	–	–	–	–	x	x
Single Layer	x	x	x	x	x	x
Multilayer Hard-Bonded (1 to 3 layers)	–	x	–	–	–	–
Boundary Conditions						
Ideally Clamped	–	–	x	x	x	x
Hinged Fixed	–	–	x	x	x	x
Symmetry	–	–	x	x	x	x
Free	–	–	x	x	x	x
Other Support Conditions						
Distributed Elastic Foundation	–	–	x	x	x	x
Point Elastic Springs	–	–	x	x	x	x

Feature	JET 1	JET 2	JET 3A	JET 3B	JET 3C	JET 3D
Material						
Single Material	x	-	x	x	x	x
Different for Each Layer	-	x	-	-	-	-
Homogeneous	x	x	x	x	x	x
Initially Isotropic	x	x	x	x	x	x
Temperature Independent	x	x	x	x	x	x
Temperature Dependent	x	-	-	-	-	-
EL	x	x	x	x	x	x
EL-PP	x	x	x	x	x	x
EL-LSH	x	x	x	x	x	x
EL-SH	x	x	x	x	x	x
EL-SH-SR	x	x	x	x	x	x
Stimulii						
Initial Velocity						
Arbitrary	x	x	x	x	x	x
Half-Sine over each of Selected Regions	x	x	x	x	x	x
Mechanical Loading						
Arbitrary Spatial Distribution with Arb. Time History	-	x	x	x	x	x
Half-Sine over each of Selected Regions	x	x	x	x	x	x
Triangular Time History	x	x	x	x	x	x
Arbitrary Time History	-	x	x	x	x	x
Thermal Loads (Temp. Distribution)						
Distribution Thru Thickness	x	-	-	-	-	-
Time-Independent Prescribed Circum-ferential Distribution	x	-	-	-	-	-

Feature	JET 1	JET 2	JET 3A	JET 3B	JET 3C	JET 3D
Deformations: Kirchhoff Type Only						
Small	x	x	x	x	x	x
Arbitrarily Large	x	x	x	x	x	x
OUTPUT INFORMATION						
At Selected Times						
Energy/Work Type and Amount	x	x	x	x	x	x
Nodal Station Data						
Locations Y,Z	x	x	x	x	x	x
Displacements	–	–	x	x	x	x
Moment Resultant	x	x	x	x	x	x
Circum. Force Resultant	x	x	x	x	x	x
Circumferential Strains						
Inner Surface	x	x	x	x	x	x
Outer Surface	x	x	x	x	x	x
Location where Prescribed Value is Exceeded	–	x	x	x	x	x
At Certain Other Times						
Time of First Yielding	x	x	–	–	–	–
Time when Strain First Exceeds a Prescribed Value	–	x	x	x	x	x
Time, Location, and Value of Largest Strain Reached During Run	–	–	x	x	x	x
CAPACITY INFORMATION						
Maximum No. of Finite-Difference Stations*	100	100	–	–	–	–
Maximum No. of Finite Elements*	–	–	50	50	50	50

*These limits can be circumvented by altering the dimensions of appropriate program variables (see each source reference).

CAT-32